

**Discovery of putative prognostic and
therapeutic miRNA in uEVs
of Dent's Disease 1 patients
and characterisation
of cellular models of the disease**

Carla Burballa Tàrrega

TESI DOCTORAL UPF / 2020

THESIS SUPERVISORS

**Dr. Vivek
Malhotra**

**Dra. Anna
Meseguer**

**Dr. Gerard
Cantero**

Cell and Developmental
Biology

Renal Physiopathology Group

Centre for Genomic
Regulation (CRG)

Vall d'Hebrón Institut de Recerca (VHIR)



Health and life science

To my grandma, Maribel
To my parents, Ricard and Cristina
and my sister, Ares
To Sergi

*“Nothing in life is to be feared, it is only to be understood.
Now is the time to understand more and fear less”*

Marie Curie

In appreciation

After these three years, I am so grateful to so many people that it would probably take me another thesis to thank you all properly.

In short, thank you very much to all the people who patiently have taught me everything in the lab, from how to pipette to how to perform a high molecular weight protein western blot and even how to use some Word Office applications (yes, this as well).

I would like first and foremost to acknowledge my thesis supervisors Dr. Meseguer, Dr Malhotra and Dr. Cantero.

Anna, thank you for giving me this great opportunity and for allowing me to get hands-on basic research; for sure this experience has enormously widened my perspective; thank you for your support, your dedication, your ideas, our talks and for radiating passion for science. Thank you for trusting me and being so kind and caring. Thank you for making this project possible.

Vivek, thank you for giving me the chance to join your lab. It has been an unforgettable, highly constructive experience. Thank you for your example.

Gerard, I have no words to thank you enough. Thank you for the mentorship in each and every step of the process, thank you for your commitment, for the fair balance you manage between exigence and understanding, taking into account that I had no idea about many things. Thank you for your patience, your positiveness and your calmness. On the whole, thank you for being my mentor

and for your friendship (I hope some beers will help to express my thanks).

Particularly I wish to express my sincere gratitude to Dr. Gema Ariceta, for your counselling, for your enormous support and because this project would have not been possible without you.

To ASDENT, the Dent's Disease patients' association in Spain, thanks to Eva and David because without their effort and perseverance this investigation and others would not have been achieved. I would like to express my gratitude to all the patients and the families who participated in this study and to all the physicians, paediatric and adult nephrologist who contributed to this research project.

I would like to acknowledge the CRG and VHIR for granting me the opportunity to join the collaborative research training programme pHD4MD. To tell the truth it has been a tough road, as science is challenging and results do not come as straightforwardly as one would desire or they do not end up coming at all, sometimes. Even with everything, I would sincerely recommend this training to other medical doctors as I really think it is necessary to have the complete picture, from the more basic biology (and all the multiple steps, repetitions, disappointments, joys and efforts it takes) to patients' treatment, not only in order to become potential

physician scientists but most importantly to widen our tools and our point of view as medical doctors.

As such, I want to thank all the people at PRBB building who have accompanied me, shared coffee or hallway/culture room talks.

I want to express a very special thanks to Cristi, my lab-mum; without you teaching me patiently how to walk in the lab I would not have managed it, I tell you.

Thanks to all my mates and also teachers at CRG. Thank you, Nathalie, for all the tips you gave me, you master of PCR, thank you for all the conversations and the shared moments. Ombry thank you for your encouragement and thanks for the serenity you transmit. It is been enormously helpful. Ah! And for helping me to fight western blots. Mary thank you for taking care of me when I stepped into the lab, for being a great example of what perseverance and resilience means. Thanks to Amy for all the help and to Ishier, Ankit and Jose, for their support and to former members of the lab, for aiding me and training me. I would like to thank Aida for her counselling and talks. Also great thanks to all the people in the Advanced Light Microscopy Unit, for their patient explanations and helping me every time I launched a SOS.

As for my “battle buddies” in VHIR, what to say... Mónica D. thank you so much for all the time together, urine-centrifuge days would have been dreary without you, and for mentoring me and being so patient. Big big thanks to Mónica V. for everything; for leading the way and making mine much easier, thank you for your patience

and thanks that I am a little more organised now (I think). I wish to appreciate Edu, for his support, feed-back and funny moments in the lab. Irene for the talks and the tips, Jazz for all the shared moments and for being an example and Stephan for being a model of hard work. I appreciate Conxi and Ander for their inspiration and kindness.

I wish to express my gratitude to the Nephrology Department in Hospital del Mar. Thanks to Julio, Marta, Mariajo, Dolo, Pepa and Marta R. and all the people who have transmitted to me their passion for nephrology, science and knowledge and specially Laia, for her support and for encouraging me to explore beyond my comfort zone. Thanks to Carlos, Anna and Laura for their help and to the USR for being with me all the way. Many thanks to all my mates in Hospital del Mar, for their support and for allowing me to keep practicing medicine and being in contact with patients during these years.

My sincere appreciation goes to Alberto Tejedor, for making me fall in love with nephrology, in general and particularly with the renal tubule.

To all my friends, to the *Far West* and *Barçalanus*, thank you for being always there and filling with joy my leisure time. To the *Daines*, thank you so much for the laughter, the positive energy you give me and the mountain air shared.

I would like to thank Gorka, for being the best brother-flatmate ever, for his encouragement and for taking care of me. Also, thanks to Lidia, Anna and Mireia, for being beside me even being in fierce competition with cells, shifts and databases.

I wish to express my gratitude to my family, because even if they are far and in this difficult 2020 I have not seen them as much as I would have liked to they are always near. And thanks also to my family in Barcelona, thanks to Jose, Paco, Ferran and Cristina for your support; I have felt your warmth all the way.

To my parents and my sister, an enormous thank you for your unconditional love, for being my shelter and for always believing in me and encouraging me to go above and beyond.

And I want to thank you Sergi, for all you do and how you do it, for keeping everything simple and colourful, for being my home.

Abstract

Dent disease 1 (DD1) is a rare renal tubulopathy caused by *CLCN5* mutations and characterized by low molecular weight proteinuria, variable hypercalciuria, nephrocalcinosis and/or nephrolithiasis and progression to kidney failure.

The underlying mechanisms linking CIC-5 loss-of-function and endocytosis impairment in the renal proximal tubule (and other DD1 phenotypes) remain unknown. In this thesis we have followed three approaches to identify altered pathways by CIC-5 mutations: (1) conduct a European survey to analyse the prevalence and DD1 clinical features, (2) study miRNA expression profiles from DD1 patients' urinary exosome-like vesicles (uEVs) to get insight into DD1 pathophysiological mechanisms and (3) characterisation of a DD1 cell model. The European survey showed that DD1 has a variable presentation. Our study of uEVs miRNA identified new pathophysiological pathways, which may lead to identify putative diagnostic and prognostic biomarkers. Finally, our cell model with different mutations provides a valuable prototype for additional investigation of impaired pathways.

Resum

La malaltia de Dent 1 (DD1) és una tubulopatia renal rara causada per mutacions en el gen *CLCN5* i caracteritzada per proteinúria de baix pes molecular, hipercalciúria, nefrocalcinosi i/o litiasis renals així com progrés a insuficiència renal. Els mecanismes que causen la pèrdua de funció de ClC-5 i el defecte en l'endocitosi en el túbul proximal (entre d'altres fenotips de DD1) no es coneixen. En aquesta Tesi hem desenvolupat tres aproximacions per identificar vies alterades per mutacions en ClC-5. (1) hem fet una enquesta europea per analitzar la prevalença i les característiques clíniques de DD1, (2) hem estudiat l'expressió de miRNA en *exosome-like vesicles* (uEVs) per entendre els mecanismes fisiopatològics de la malaltia i (3) hem caracteritzat un model cel·lular de DD1. L'enquesta europea mostrà que DD1 té una presentació variable. El nostre estudi de miRNA en uEVs va permetre identificar nous mecanismes fisiopatològics que poden ser potencials biomarcadors diagnòstics i pronòstics de DD1. Finalment, el nostre model cel·lular amb diferents mutacions provà representar un prototip vàlid per investigacions addicionals dels mecanismes desregulats.

Preface

Dent's Disease type 1 (DD1) is a renal rare disease with heterogeneous symptom profiles and scarce tools for diagnosis and disease progression assessment, which probably makes it a misdiagnosed disorder. Furthermore, the limited understanding of the cellular pathways and molecular mechanisms causing the disease and progression to chronic kidney disease (CKD) complicates its management. Consequently, nowadays patients can only benefit from symptomatic treatment since no current targeted or curative therapy.

There is a growing body of evidence that miRNA are involved in the pathophysiology of several disorders and, together with other prototypes, such as cell models, constitute valuable means for unravelling processes involved in health and disease.

This Thesis Project provides a current picture of Dent's Disease type 1 in Europe, confirming the variability in clinical presentation and raises awareness of the need to improve diagnosis; identifies a uEVs miRNA signature for DD1 patients and provides insight into molecular processes potentially involved in the disease pathophysiology which might contribute to its different phenotypic manifestations. Finally, this study provides the characterisation of a cell model for further functional studies and future drug testing.

This Thesis project was developed under the framework of a collaborative research training programme between Vall d'Hebrón Research Institute (VHIR), and Centre for Genomic Regulation (CRG), pHD4MD. The project was carried out both in the Renal Physiopathology Group (VHIR) under the supervision of Dr. Meseguer and Dr. Cantero and in the Cell and Developmental Biology program (CRG) under the supervision of Dr. Malhotra.

Table of contents

| | |
|---|----|
| INTRODUCTION..... | 3 |
| 1. THE KIDNEYS: FUNDAMENTAL ROLE IN ORGANISM HOMEOSTASIS..... | 5 |
| 1.1. THE KIDNEYS. DEFINITION AND STRUCTURE | 5 |
| 1.2. THE KIDNEYS. FUNCTION AND URINE PRODUCTION. | 6 |
| 2. THE PROXIMAL TUBULE: THE HORSESHOE OF THE KIDNEY | 10 |
| 2.1. STRUCTURE OF THE PROXIMAL TUBULE | 10 |
| 2.2. FUNCTIONS OF THE PROXIMAL TUBULE | 11 |
| 2.3. PROTEINURIA AND DYSFUNCTION IN THE PROXIMAL TUBULE | 14 |
| 3. OTHER FUNCTIONS OF THE RENAL TUBULE SYSTEM..... | 15 |
| 3.1. SODIUM AND CHLORIDE REABSORPTION IN THE THICK ASCENDING LIMB (TAL) OF LOOP OF HENLE | 15 |
| 3.2. PHOSPHATE AND CALCIUM HANDLING BY THE TUBULE SYSTEM | 17 |
| 4. ENDOCYTOSIS. A TREK ALONG THE ENDOSOMAL-LYSOSOMAL PATHWAY .. | 19 |
| 4.1. ENDO-LYSOSOMAL SYSTEM..... | 20 |
| 4.1.1. <i>Early and late endosomes</i> | 20 |
| 4.1.2. <i>Lysosomes</i> | 21 |
| 4.1.3. <i>Recycling</i> | 21 |
| 4.1.4. <i>Other proteins involved</i> | 22 |
| 4.2. RECEPTOR-MEDIATED ENDOCYTOSIS..... | 22 |
| 4.2.1. <i>The receptor complex: Megalin and CUBAM.</i> | 22 |
| 4.2.2. <i>Acidification of endo-lysosomal pathway</i> | 28 |
| 4.2.3. <i>Lysosomal degradation</i> | 29 |
| 4.2.4. <i>Recycling</i> | 30 |
| 4.3. FLUID-PHASE ENDOCYTOSIS | 31 |
| 5. CLC-5: A CRITICAL PLAYER IN RENAL PROXIMAL TUBULE RECEPTOR MEDIATED ENDOCYTOSIS | 32 |
| 5.1. CLC ION CHANNEL AND ANTIPORTERS SUPERFAMILY..... | 32 |
| 5.2. CLC-5 CHLORIDE/PROTON ANTIPORTER..... | 33 |
| 5.2.1. <i>CLC-5: from gene to protein</i> | 34 |
| 5.2.2. <i>Structure of CLC-5</i> | 34 |
| 5.2.3. <i>Regulation of the Trafficking and Activity of CLC-5 by Protein-Protein Interactions</i> | 36 |
| 5.2.4. <i>Function of CLC-5 in the endocytic pathway</i> | 38 |
| 6. DENT'S DISEASE TYPE 1 | 40 |
| 6.1. EPIDEMIOLOGY | 41 |
| 6.2. HISTORY | 41 |
| 6.3. CLINICAL PRESENTATION | 42 |

| | |
|--|------------|
| 6.3.1. Hypothesized physiopathology of the different symptoms..... | 44 |
| 6.4. KIDNEY HISTOLOGICAL FEATURES IN DD1 PATIENTS | 51 |
| 6.5. DD1 MUTATIONS | 52 |
| 6.6. TREATMENT | 54 |
| 6.7. RESEARCH ON DD1: BIOLOGICAL MODELS | 55 |
| 6.7.1. Cellular models | 55 |
| 6.7.2. Murine models..... | 56 |
| 7. EXTRACELLULAR VESICLES..... | 58 |
| 7.1. EXOSOMES..... | 59 |
| 7.1.1. Biogenesis of exosomes | 60 |
| 7.1.2. Exosomes composition..... | 63 |
| 7.1.3. Exosomes secretion and internalization | 65 |
| 7.1.4. Function of exosomes | 67 |
| 7.1.5. Urinary exosomes in kidney physiology and pathology..... | 68 |
| 7.1.6. Isolation of exosomes | 70 |
| 7.1.7. Characterization of isolated exosomes | 72 |
| 8. MICRORNAS (MIRNA) | 73 |
| 8.1. MIRNA DEFINITION AND DISCOVERY | 73 |
| 8.2. BIOGENESIS OF MIRNA | 76 |
| 8.3. ANNOTATION OF MIRNA..... | 77 |
| 8.4. TECHNIQUES FOR QUANTIFICATION OF MIRNA | 79 |
| 8.5. MIRNA DATA PROCESSING AND MOLECULAR INTEGRATION | 81 |
| 8.6. IN VITRO VALIDATION OF MIRNA TARGET..... | 81 |
| 8.7. MIRNA AND THE KIDNEY..... | 83 |
| 8.8. USE IN DIAGNOSIS AND TREATMENT | 85 |
| HYPOTHESIS | 87 |
| OBJECTIVES | 91 |
| MATERIALS AND METHODS | 95 |
| 1. EUROPEAN SURVEY..... | 97 |
| 1.1. SURVEY SETTING AND STUDY DESIGN | 97 |
| 1.2. PATIENTS..... | 98 |
| 1.2.1. Patient's growth | 98 |
| 1.2.2. Kidney function..... | 99 |
| 1.2.3. Hypercalciuria, nephrocalcinosis and nephrolithiasis | 99 |
| 1.3. STATISTICAL ANALYSES FOR SURVEY RESPONSES | 99 |
| 2. MIRNA SIGNATURE IN UEVS FROM DD1 PATIENTS..... | 100 |
| 2.1. PATIENTS AND SAMPLES..... | 100 |
| 2.2. URINARY EXOSOME ISOLATION | 101 |
| 2.3. CHARACTERIZATION OF VEVs..... | 104 |
| 2.3.1. Nanoparticle tracking analysis (NTA) | 104 |
| 2.3.2. Cryogenic Transmission Electron Microscopy (Cryo-TEM)..... | 105 |

| | | |
|--|--|------------|
| 2.3.3. | <i>Immunoblotting</i> | 106 |
| 2.3.4. | <i>Exosome protein extraction</i> | 106 |
| 2.3.5. | <i>Western blotting</i> | 107 |
| 2.4. | RNA PROCESSING AND ANALYSIS | 108 |
| 2.4.1. | <i>RNA extraction and quantification</i> | 108 |
| 2.4.2. | <i>Reverse transcription and qPCR</i> | 109 |
| 2.5. | BIostatistical ANALYSIS | 111 |
| 2.5.1. | <i>Target gene prediction and integrated analysis by Ingenuity Pathway Analysis</i> | 115 |
| 3. | CHARACTERISATION OF A CELLULAR MODEL FOR DD1 | 115 |
| 3.1. | CELL CULTURE BASICS, MEDIA AND PROCEDURES | 115 |
| 3.1.1. | <i>RPTEC/hTERT1 cell line</i> | 116 |
| 3.1.2. | <i>Culture media</i> | 117 |
| 3.1.3. | <i>Trypsinisation</i> | 119 |
| 3.1.4. | <i>Cell counting</i> | 119 |
| 3.1.5. | <i>Cell cryopreservation</i> | 120 |
| 3.1.6. | <i>Cell thawing</i> | 121 |
| 3.2. | GENERATION OF A CELL MODEL FOR DENT'S DISEASE | 121 |
| 3.2.1 | <i>CLCN5 knockdown by shRNA</i> | 122 |
| 3.2.2 | <i>CLCN5 cloning by Gateway system, introducing rescue sequence and CLCN5 mutations by site-directed mutagenesis</i> | 123 |
| 3.3. | NUCLEIC ACID METHODS | 126 |
| 3.3.1 | <i>RNA isolation</i> | 126 |
| 3.3.2 | <i>Reverse transcription</i> | 127 |
| 3.3.3 | <i>PCR-polymerase chain reaction – Amplification</i> | 128 |
| 3.3.4 | <i>RT-qPCR</i> | 130 |
| 3.4. | PROTEIN ANALYSIS ASSAYS | 132 |
| 3.4.1 | <i>Protein extraction</i> | 132 |
| 3.4.2 | <i>Protein concentration determination-BCA assay</i> | 133 |
| 3.4.3 | <i>Protein detection by immunoblot</i> | 134 |
| 3.4.4. | <i>Immunocytochemistry and confocal microscopy</i> | 139 |
| 3.5. | FUNCTIONAL ASSAYS | 141 |
| 3.5.1. | <i>CIC-5 and mutant proteins half-life</i> | 141 |
| 3.5.2. | <i>Endocytosis quantification via fluorimetry of fluorescent albumin and dextran uptake</i> | 143 |
| 3.5.3. | <i>Confocal microscopy Endocytosis Assay</i> | 146 |
| 3.5.4. | <i>Endo-lysosomal pH measurement using a fluorescence dye</i> | 147 |
| 3.6. | STATISTICS | 149 |
| 3.7. | IMAGES | 149 |
| RESULTS | 151 | |
| 1. CHAPTER 1. DENT'S DISEASE TYPE 1: PICTURE OF THE CURRENT SITUATION IN EUROPE | 153 | |
| 1.1. SURVEY RESPONDENTS | 153 | |

| | |
|--|------------|
| 1.2. PRESENTATION AT DIAGNOSIS | 155 |
| 1.3. PHENOTYPIC CHARACTERISTICS | 156 |
| 1.4. RENAL FUNCTION | 158 |
| 1.5. PHENOTYPE ACCORDING TO AGE | 160 |
| 1.6. GENE MUTATION SPECTRUM | 162 |
| 1.7. PHENOTYPE ACCORDING TO MUTATION SEVERITY | 163 |
| 1.8. TREATMENT | 166 |
| 2. CHAPTER 2. MIRNA SIGNATURE IN UEVS FROM DD1 PATIENTS | 169 |
| 2.1. STUDY POPULATION | 169 |
| 2.1. ISOLATION AND CHARACTERIZATION OF URINARY EXOSOMES | 171 |
| 2.2. RNA EXTRACTION AND QUANTIFICATION | 173 |
| 2.3. MIRNA QUANTIFICATION BY OPENARRAYS QPCR | 174 |
| 2.3.1. <i>miRNA differentially expressed</i> | 175 |
| 3. CHAPTER 3: VALIDATION OF DD1 CELLULAR MODEL | 185 |
| 3.1. MRNA AND PROTEIN CLC-5 LEVELS IN RPTEC STABLE CELL LINES | 185 |
| 3.2. COMPARISON OF CLC-5 HALF-LIFE BETWEEN WT AND MUTANTS: V523DEL HAS A LONGER SPAN. | 188 |
| 3.3. CLC-5 WT AND MUTANTS' LOCALIZATION IN THE ENDO-LYSOSOMAL PATHWAY | 190 |
| 3.4. ASSESSMENT OF RECEPTOR-MEDIATED AND FLUID-PHASE ENDOCYTOSIS IN DD1 CELL MODEL. | 194 |
| 3.4.1. <i>Evaluation of receptor-mediated and fluid-phase endocytosis via fluorimetry</i> | 194 |
| 3.4.2. <i>Evaluation of receptor-mediated and fluid-phase endocytosis via confocal microscopy</i> | 198 |
| 3.4.3. <i>Endo-lysosomal pH measurement</i> | 204 |
| 3.4.4. <i>Endocytosis Receptor complex main components: Megalin and cubilin</i> | 205 |
| DISCUSSION | 209 |
| 1. DENT'S DISEASE TYPE 1: PICTURE OF THE CURRENT SITUATION IN EUROPE | 211 |
| 1.1 A SURVEY AS A SOURCE OF INFORMATION | 211 |
| 1.2 DIAGNOSIS | 212 |
| 1.3 PHENOTYPE | 215 |
| 1.3.1. <i>Different clinical spectrum Europe/US vs. Japan?</i> | 216 |
| 1.3.2. <i>Phenotype changes over time</i> | 216 |
| 1.3.3. <i>Unusual clinical presentation</i> | 217 |
| 1.4 RENAL FUNCTION | 218 |
| 1.5 MUTATIONS | 219 |
| 1.5.1. <i>Severity of mutations may impact on clinical phenotype</i> | 219 |
| 1.6 TREATMENT | 220 |
| 1.7 SUMMARY AND LIMITATIONS | 221 |
| 2. MIRNA SIGNATURE IN UEVS FROM DD1 PATIENTS | 223 |

| | |
|--|------------|
| 2.1.UEVs ISOLATION AND RNA EXTRACTION..... | 225 |
| 2.2.EXOSOME MIRNA IN DD1 PATIENTS. DYSREGULATED PATHWAYS..... | 229 |
| 2.3.DOWNREGULATED MIRNA IN DD1 UEVs | 234 |
| 2.3.1. <i>miR-145-5p and miR-143-3p</i> | 235 |
| 2.3.2. <i>miR-629-3p</i> | 237 |
| 2.4.UPREGULATED MIRNA IN DD1..... | 239 |
| 2.4.1. <i>miR-29 family</i> | 239 |
| 2.4.2. <i>miR-216b-5p</i> | 240 |
| 2.4.3. <i>miR-664a-3p</i> | 241 |
| 2.5.DIFFERENT MIRNA IN DD1 PATIENTS WITH DIFFERENT PHENOTYPE | 242 |
| 2.5.1. <i>miRNA in DD1 patients with CKD</i> | 242 |
| 2.5.2. <i>miRNA in DD1 patients with Fanconi Syndrome</i> | 244 |
| 2.5.3. <i>miRNA in DD1 patients with kidney stones</i> | 244 |
| 2.6.SUMMARY AND LIMITATIONS | 245 |
| 3. VALIDATION OF DD1 CELLULAR MODEL..... | 247 |
| 3.1.RPTEC/ hTERT1 CELLS AS A MODEL FOR DENT’S DISEASE | 247 |
| 3.2.CLC-5 MUTANTS | 249 |
| 3.2.1. <i>CLC-5 protein expression and half-life</i> | 250 |
| 3.2.2. <i>CLC-5 subcellular distribution</i> | 252 |
| 3.3.A CONSISTENT MODEL FOR ENDOCYTOSIS ASSESSMENT WITH SOME DRAWBACKS | 255 |
| 3.3.1. <i>Quantification by fluorimetry</i> | 255 |
| 3.3.2. <i>Assessment of endocytosis by immunofluorescence imaging.</i> .. | 258 |
| 3.3.3. <i>pH measurement</i> | 260 |
| 3.3.4. <i>Multi-ligand receptors in DD1 cell model</i> | 263 |
| 3.4.SUMMARY AND LIMITATIONS..... | 266 |
| CONCLUSIONS..... | 271 |
| REFERENCES | 277 |
| ANNEXES | 315 |
| 1. ANNEX I..... | 317 |
| 2. ANNEX II..... | 319 |
| 3. ANNEX III..... | 329 |
| 4. ANNEX IV | 337 |
| 5. ANNEX V | 339 |
| 7.ANNEX VII | 349 |

INTRODUCTION

1. The Kidneys: fundamental role in organism homeostasis

1.1. The kidneys. Definition and structure

The kidneys are the primary functional organ of the renal system together with the urinary bladder and the ureters. They are located on the left and right in the retroperitoneal space, and in adult humans their size can vary between 10 and 12 centimetres¹.

The renal cortex, medulla and pelvis are the three main internal regions found in a kidney. The outer region is the cortex, where the renal corpuscles and renal tubules (see below) except for parts of the loop of Henle (see below, section 1.2) are located. The medulla is the innermost region and is arranged into pyramid-like structures (renal pyramids) that consist of the bulk of nephron structure. Finally, the renal pelvis contains the hilum, where blood vessels and nerves enter and exit the kidney; it is also the point of exit for the ureters. The urine coming from the renal pyramids enters the renal pelvis through the renal calices² *Figure 1A*

The human kidney is composed of structural and functional units called nephrons. Nephrons have two lengths with different urine concentrating capacities: long juxtamedullary nephrons and short cortical nephrons. Each nephron consists of a filtrating unit, the glomerulus (Bowman's capsule, Bowman's space, and the glomerular capillary network) which is located in the cortex, followed by a secreting and reabsorbing tubular system, formed by

the proximal (convoluted) tubule, the loop of Henle which has a descending and an ascending pars, the distal convoluted tubule and the collecting tubule¹ *Figure 1B*

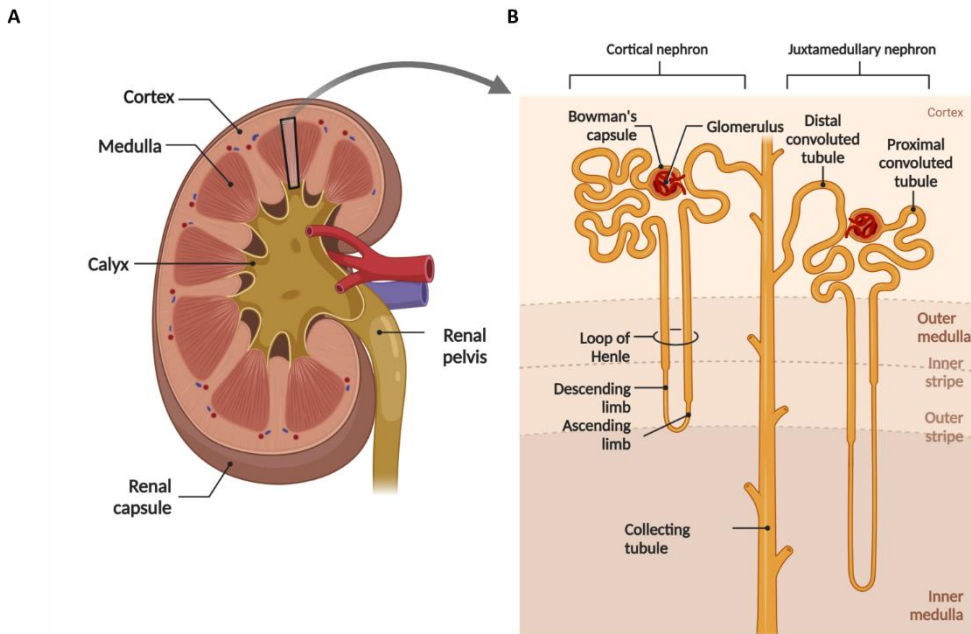


Figure 1 Kidney anatomy and nephron structure A. Frontal section of the kidney showing the renal cortex, renal medulla and renal pelvis. B. Different segments within the nephron: Glomerulus and tubular system with proximal tubule, loop of Henle, distal convoluted tubule and the collecting duct.

1.2. The kidneys. Function and urine production.

The kidneys perform vital functions for optimal body homeostasis such as the regulation of electrolytes, maintenance of body fluid and acid–base balance¹. These processes involve mainly three mechanisms: filtration, reabsorption and secretion.

Kidneys are responsible for blood filtering; they secrete solutes and remove wastes to be excreted with the urine (e.g. creatinine, urea nitrogen, etc.) and reabsorb water and many solutes such as bicarbonate, phosphate, calcium, magnesium and others that are essential for the organism. In addition, the kidneys produce hormones including calcitriol involved in phosphate-calcium homeostasis, erythropoietin that stimulates red blood cell production and the enzyme renin, which is involved among other functions in blood pressure regulation³.

The kidneys receive roughly 20% of the cardiac output (approximately 1 litre of blood) per minute. The blood enters individual glomerular tufts via the afferent arteriole and, from this renal blood flow, only the plasma crosses the glomerular filtration barrier (GFB) producing the ultrafiltrate in a process called glomerular filtrate; the rest exits the glomerulus through the efferent arteriole. The GFB prevents many solutes to pass through it, especially those with higher molecular weight (>70 kDa), and negatively charged¹, yet other organic and inorganic solutes together with water reach the tubule system with the ultrafiltrate. Kidneys produce around 150-180 litres of ultrafiltrate every 24 hours, still urine output averages only about 1.5-2 L daily⁴. Thus, reabsorption of 178.5 L is accomplished by the tubule system in a process called tubular reabsorption, which allows recovery of 99% of filtered glucose, amino acids, proteins and other essential nutrients that would be otherwise lost with the urine. In brief, the proximal tubule reabsorbs most of the ultrafiltrate (80%), mostly

organic ions (e.g. glucose, phosphate and amino acids), salt, bicarbonate and water; the descending limb of Henle's loop is freely permeable to water so it reabsorbs it and creates osmotic hypertonicity inside the tubule lumen for salt to be reabsorbed in the thick ascending limb (TAL) of Henle's loop where also magnesium, calcium and bicarbonate are reabsorbed; the distal convoluted tubule handles calcium homeostasis and finally the collecting duct, which is divided in cortical segment, where pH and potassium are adjusted and sodium is reabsorbed, and the connecting duct where final urine volume is adjusted. (*Figure 2*)

Thus, waste ions and other metabolic waste products (e.g. hydrogen, urea, creatinine) pass from the capillaries into the renal tubule and are secreted together with sparing water and become urine.¹

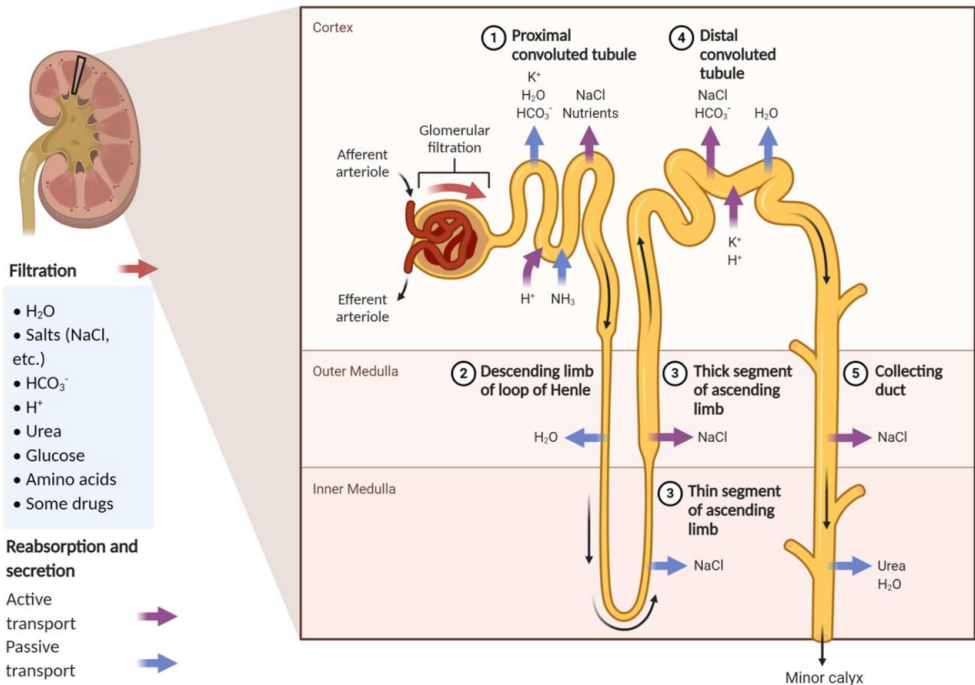


Figure 2 Urine formation. After blood filtration through the glomerulus (red arrow), the ultrafiltrate enters the tubule system where reabsorption and secretion processes by active (purple arrows) and passive (blue arrows) transport take place.

Despite the essential functions developed by every part of the tubule system, given its high complexity, for the scope of this project proximal tubule will be more thoroughly reviewed. As for the TAL of Hendel’s loop we will go into further details for better comprehension of some parts of this work.

2. The proximal tubule: the horseshoe of the kidney

The proximal tubule (PT), the first part of the tubule system after the glomerulus, is responsible for reabsorption of 55-60 % of a daily filtration rate of 180 L including almost all the glucose and amino acids, 90% of HCO_3^- , 65% of Na^+ and 55% of Cl^- owing to a complex endocytic machinery detailed hereinafter^{5,6}.

2.1. Structure of the proximal tubule

The proximal tubule is divided into two major anatomic sections, pars convolute (PCT) and pars recta (PR). Based on differences in cell ultrastructure, the proximal tubule is also divided into three segments S_1 , S_2 , and S_3 . S_1 cells have, within the PCT, a tall brush border in the apical membrane and an interdigitated basolateral membrane in addition to a well-developed endosomal-lysosomal system and many mitochondria suggesting these cells have high energy requirements. In fact, this high metabolic rate makes these cells particularly susceptible to ischemic damage⁷. S_1 cells play a more important role in Na^+ and HCO_3^- reabsorption, than the other two segments. S_2 cells have a shorter brush border and less mitochondria while S_3 cells are low complex cells, with almost no mitochondria and no transport

system but with a high proliferative and dedifferentiation capacity⁴. *Figure 4A*

2.2. Functions of the proximal tubule

On the one hand, the main function of the PT is reabsorption by polarised transport. Glucose, amino acids, phosphate and other organic acids are reabsorbed via sodium (Na^+)-dependent cotransporters (e.g. SGLT1 or GLUT2 for glucose⁸, NaP2a for phosphate⁴ or B0AT1 for amino acids⁹) that are expressed in the apical membrane, together with the Na^+/H^+ Exchanger 3 (NHE3)^{10,11} (which is regulated by PTH¹²). For this transport to normally occur, the basolateral Na^+-K^+ -ATPase pump (pumps 3 Na^+ out of the cell to the interstitium and 2 K^+ into the cell) is essential as it promotes a transcellular osmotic gradient that enhances the passive reabsorption of more sodium, chloride, potassium, calcium and water through the tight junctions. Water is also reabsorbed via aquaporin-1 (AQP1). Potassium (K^+) is additionally pumped into the cell from the peritubular capillary by the Na^+-K^+ -ATPase and it is diffuse back into the peritubular capillaries by ATP-sensitive K^+ channel (KCC4), in the basolateral membrane. Likewise, by the action of a carbonic anhydrase and a $\text{Na}^+-\text{HCO}_3^-$ cotransporter (NBCe1A) in the basolateral membrane, HCO_3^- is mostly reabsorbed in the proximal tubule⁴. *Figure 3*.

Proximal tubule also mediate calcium reabsorption⁴ (see section 3.1)

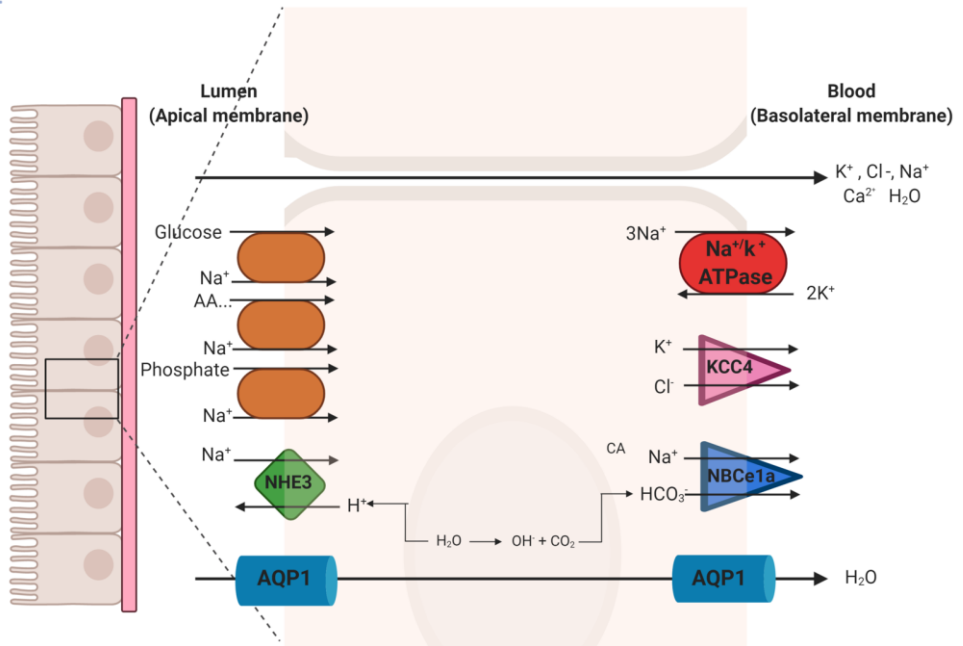


Figure 3 Ion and solute absorption and secretion in the proximal tubule. Na^+ is reabsorbed together with glucose, phosphate and amino acid through specific sodium-dependent co-transporters and through the Na^+/H^+ Exchanger 3 (NHE3) and is pumped into the interstitium by the Na^+/K^+ -ATPase and by NBCe1a. The increase of Na^+ into the interstitium allows passive reabsorption of more Na^+ , K^+ and Cl^- together with Ca^{2+} and water through the tight junctions. CA. Carbonic Anhydrase

On the other hand, a significant amount of albumin (estimated 3.2 g/day) and low-molecular-weight (LMW) proteins (estimated 9.6 g/day)¹³ escapes the GBM filter and are reabsorbed by proximal tubule cells¹⁴. These LMWP include transferrin, hormones (parathyroid hormone, insulin and growth hormone), carrier proteins (retinol, vitamin D and folate), enzymes (cytochrome c and lysozyme), cell surface antigen components (β 2-microglobulin) and immunoglobulin light chains. In physiological conditions

human urine is almost devoid of proteins (protein/creatinine ratio of $< 180 \text{ mg/g}$) as a result of their massive uptake by the proximal tubule¹⁵. Especially in S_1 , proximal tubular cells (PTCs) have two mechanisms for reabsorbing and processing proteins: the principal, receptor-mediated clathrin-dependent endocytosis and fluid-phase endocytosis. Standard fluid-phase endocytosis markers are dextran or inulin, while transferrin and albumin are usually used as receptor-mediated endocytosis markers^{16,17} (Figure 4C)

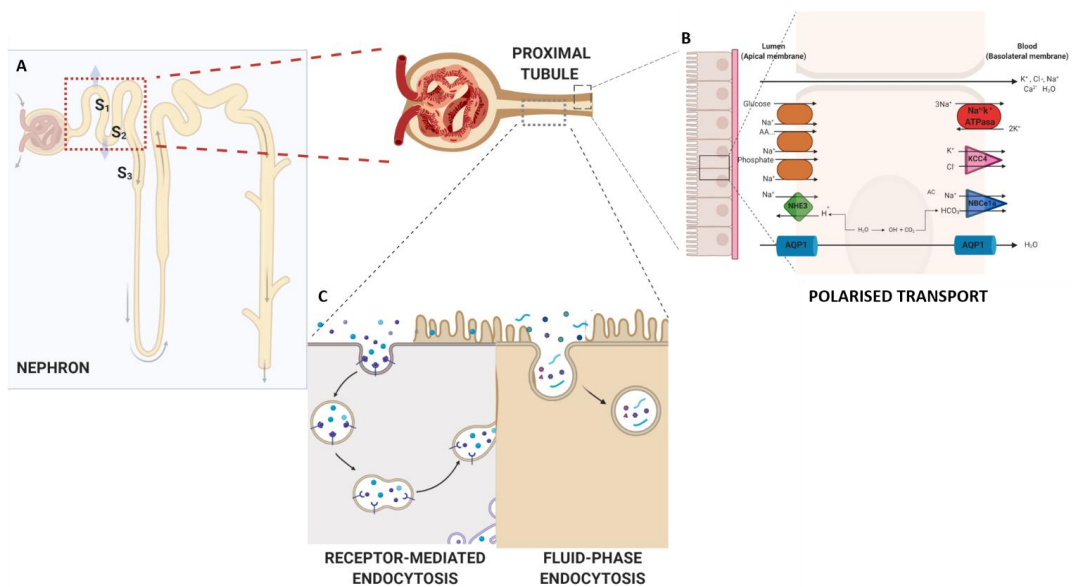


Figure 4 Proximal tubule structure and functions. A The proximal tubule (PT) is functionally divided in three segments, S_1 , S_2 and S_3 . B. The PT retrieves 80% of ions in the ultrafiltrate. Phosphate, citrate, glucose and amino acids are reabsorbed via sodium-dependent cotransporters. C. Uptake of proteins and other solutes occur via receptor-mediated endocytosis or fluid-phase endocytosis.)

2.3. Proteinuria and dysfunction in the proximal tubule

The causes underlying proteinuria (both from glomerular and tubular origin) as well as the causes for PT dysfunction are multiple and beyond the scope of this project. Nonetheless, some concepts related should be review before moving forward.

On the one hand, an excessive loss of protein with urine is called proteinuria and it has been demonstrated as an independent risk factor for many conditions such as cardiovascular disease^{18,19} and associated with higher mortality²⁰. Classically, proteinuria had been considered a consequence of GFB excessive permeability due to the highly restrictive nature attributed to the GFB. Nonetheless, not without controversy, proximal tubule fundamental role in protein reabsorption is nowadays well recognized and key to prevent proteinuria²¹. While nephrotic range proteinuria (>3.5 g/24h) would be associated to glomerular disease, there is considerable overlap with non-glomerular disease which can also cause large proteinuria and albuminuria²². Nonetheless, proteinuria due to a tubular defect in endocytosis would hardly ever (or never) cause pure albuminuria but mixed tubular proteinuria (LMWP) including retinol-binding protein (RBP), α 1-microglobulin (α 1M), and β 2-microglobulin (β 2M), typically in excess of 10 times normal^{23,24}.

On the other hand, defective sodium (Na^+)-dependent co-transporters can cause specific deficiencies depending on the

solute co-transported. Thus, defects in SGLT1 or GLUT2 cause loss of urinary glucose (glucosuria), in physiological conditions no glucose is found in urine; defects in NaPi2a would cause loss of phosphate with urine (phosphaturia) and defects in co-transporters of amino acids would cause aminoaciduria. Thus, excessive urinary excretion of amino acids, glucose, phosphate, bicarbonate, uric acid and all the solutes reabsorbed in the PT is known as Complete Fanconi Syndrome, while loss of just some of the is known as Incomplete Fanconi Syndrome²⁵.

3. Other functions of the renal tubule system

As stated before, detailed explanation of the functions of other nephron segments are out-of-scope, however some notions are necessary for the further interpretation of the some of the results here exposed.

3.1. Sodium and chloride reabsorption in the thick ascending limb (TAL) of loop of Henle

The thick ascending limb (TAL) of the loop of Henle mediates salt and other cations' reabsorption. This process takes place via two pathways: (1) transcellularly, via the apical electroneutral $\text{Na}^+\text{-K}^+\text{-2Cl}^-$ cotransporter (NKCC2), together with the Na^+/H^+ exchanger (NHE3) also in this part of the nephron. Once reabsorbed from the lumen, Na^+ exits the cell via the Na^+/K^+ ATPase pump. After entry

via NKCC2, Cl^- ions exit the cells via ClC-Ka and ClC-Kb channels, which are both regulated by the Barttin subunit. Finally, K^+ ions are delivered back to the lumen through the apical renal outer medulla K^+ channel (ROMK), which ensures K^+ recycling to the lumen that is essential for Na^+ and Cl^- reabsorption and sets a positive transepithelial voltage. This voltage gradient is essential for (2) the paracellular reabsorption of Na^+ and also other cations like Ca^{2+} and Mg^{2+} , which is tightly regulated by claudin16/19²⁶. (Figure 5)

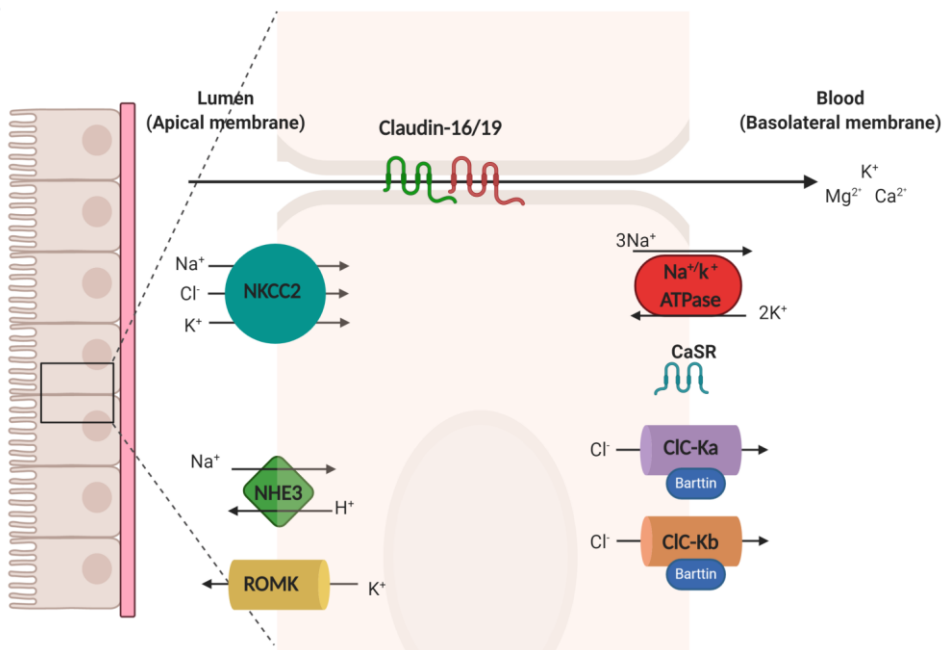


Figure 5 Ion absorption and secretion within TAL of the Henle's loop. At the thick ascending limb (TAL) of Henle's loop, Na^+ is reabsorbed through NHE3 and importantly through NKCC2 together with Cl^- and K^+ . Na^+ is bumped into the interstitium by the Na^+/K^+ -ATPase. K^+ is delivered back to the lumen via ROMK and Cl^- exits the cells via ClC-Ka and ClC-Kb channels, which are both regulated by the Barttin subunit. This sets a

positive transepithelial voltage that allows paracellular reabsorption of Ca^{2+} and Mg^{2+} through claudin16/19.

3.2. Phosphate and calcium handling by the tubule system

Phosphate and calcium homeostasis are maintained by counterbalance between dietary P_i and Ca^{2+} absorption by the gut, mobilisation from bone and renal excretion.

Approximately 80% of filtered phosphate is reabsorbed from the urine via PT transporters (electroneutral $\text{NaPi}2\text{a}$ is the most important in humans). The amount of phosphate reabsorbed is dependent on the abundance of sodium phosphate cotransporters²⁷. $\text{NaPi}2\text{a}$ is negatively regulated by PTH, endocytic membrane retrieval and degradation. The scaffolding protein Na^+/H^+ exchanger regulatory factor (NHERF1) is necessary for this PTH-induced internalization of $\text{NaPi}2\text{a}$, as well as a PTC membrane receptor called megalin²⁸, referred more extensively afterwards²⁹.

About 98% of filtered calcium is reabsorbed along the nephron. In the PT it is mainly reabsorbed paracellularly, partially driven by the activity of NHE3, which creates a concentration gradient that drags Ca^{2+} in. NHE3 is negatively regulated by PTH¹⁰. In TAL of the Henle's loop, calcium is reabsorbed by specialized paracellular pathways that include claudin14, 16 and 19.³⁰ The driving force for calcium is produced by the combined action of the basolateral $\text{Na}^+-\text{K}^+-\text{ATPase}$, the $\text{Na}^+-\text{K}^+-\text{Cl}^-$ cotransporter (NKCC2) and the

outward rectifying ROMK channel on the apical membrane. Finally, a small proportion, is reabsorbed transcellularly in the distal convoluted tubule and connecting tubule through TRPV5 channels and exits the cell at the basolateral side by the Na^+ - Ca^{2+} exchanger 1 (NCX1) and the Ca-ATPase PMCA4³⁰. Any calcium delivered to the collecting duct is subjected to precipitation depending importantly upon the tubular pH³¹.

PTH and Vitamin D are the two major regulators of mineral metabolism, including calcium and phosphate handling, together with the calcium-sensing receptor (CaSR).

On the one hand, PTH, synthesised in the parathyroid gland in response to low calcium levels as sensed by CaSR, exerts its effect on gut, bone and kidney to maintain serum calcium within a tight range. In the kidney, it is freely filtered by the glomerulus, reaches the luminal surface of PTCs and it either binds the PTH receptor or is uptaken via megalin-mediated endocytosis. As said, it positively regulates NHE3 enhancing calcium reabsorption in the PT and also, positively regulates the calcium channel TRPV5 in the distal convoluted tubule³². As for phosphate, as stated, it enhances its excretion with urine by negatively regulating its receptor, NaPi2a, in PTCs.

On the other hand, proximal tubule cells are the only site for $1\alpha,25$ -dihydroxyvitamin D₃ [$1,25(\text{OH})_2\text{D}_3$] production³³ after $25(\text{OH})$ vit D is uptaken via endocytosis and processed. This requires the action of mitochondrial 1α -hydroxylase, only present in the PTCs and positively regulated by PTH. The vitamin D receptor

(VDR) senses the circulating 1,25(OH)₂D₃ and their interaction blocks the activity of the 1 α -hydroxylase and promotes the 24-hydroxylase which inactivates 1,25(OH)₂D₃³⁴. The main function of 1,25(OH)₂D₃ is to increase calcium and phosphate absorption in the gut and negatively regulate PTH production by the parathyroid glandule³⁵.

4. Endocytosis. A trek along the endosomal-lysosomal pathway

As indicated before, uptake of molecules across the PT cell membrane occurs either via specific receptor-mediated endocytosis (RME) or nonspecific fluid-phase endocytosis (FPE). As recent investigations establish, while FPE occurs along the entire PT, early segment S₁ is highly specialized to perform protein reabsorption, and so S₁ cells have a well-developed endo-lysosomal system³⁶.

Endocytosis is the cellular process by which fluid, solutes, macromolecules, plasma membrane components, and particles are internalised by the cell. It occurs at the cell surface involving internalization of the plasma membrane (PM) along with its constituent membrane proteins and lipids³⁷. There are several different ways to entry into the cell: phagocytosis, micropinocytosis, clathrin-mediated endocytosis and caveolae-mediated.

4.1. Endo-lysosomal system

After molecules have been internalized through one of these different endocytic pathways they are trafficked through the endo-lysosomal pathway composed by tubulovesicular compartments, called endosomes. Internalized macromolecules may have different fates: they can be recycled back to the plasma membrane, delivered to the lysosomes for degradation, or sent across the cell through a process called transcytosis.

4.1.1. Early and late endosomes

After endocytosis, internalized vesicles undergo fusion to form early endosomes (EE) which contain cell-surface proteins and soluble proteins associated with the extracellular milieu³⁸. The trans-Golgi network and endoplasmic reticulum can also contribute to the formation and the content of the EE. EE have a mildly acidic pH (6-6.5) that triggers the dissociation of some ligands from their receptors. These ligands are recycled back to the cell membrane through recycling endosomes³⁹. Meanwhile, the EE, by altering key phosphatidylinositol lipids through regulation by lipid kinases and phosphatases, by drop in internal pH and by differential recruitment and activation of Rab-family GTPases, mature into late-sorting endosomes (LSE). These LSEs can eventually give rise to multivesicular bodies, MVBs (also called multivesicular endosomes) with intraluminal vesicles (ILVs), which develop from

the inward invagination of the endosomal limiting membrane (which comes from double invagination of the PM)⁴⁰.

4.1.2. Lysosomes

Thus, degradation starts in MBVs or late endosomes and continues in the lysosome. Late endosomes/MVBs develop into lysosomes by multiple fusion and scission cycles^{41,42}. After degradation of the lysosomal content, transporter molecules translocate sugars, amino acids and lipids across the limiting lysosomal membranes into the cytosol where they exert their function.

4.1.3. Recycling

Most of the membrane components and receptors involved in endocytosis are not fated for degradation and so they are returned to the cell membrane by recycling. Recycling can occur directly from peripheral early endosomes within the process called fast recycling⁴³ or via the slow recycling pathway, so that once the receptors are detached from their ligands due to more acid pH, these receptors are retrieved back to the cell membrane by a distinct subpopulation of endosomes, the recycling endosomes³⁹, that have a slightly higher pH (~6.4) and travel to the cell membrane where display exocytosis⁴⁴.

4.1.4. Other proteins involved

It is essential mentioning that, during maturation, small GTP-binding proteins termed Rabs are sequentially recruited into the endosomes and they mediate changes in the membrane composition and recruit motors and other cytosolic proteins that allows the forwards movement along the endo-lysosomal pathway. In fact these GTP-binding are also used to characterise each of the compartments. Thus, e.g. Rab5 helps form and identifies the early endosomes⁴⁵; Rab7 regulates formation and identified the late endosome⁴⁶ and Rab11 regulates the transport and sorting in recycling endosomes.⁴⁷

4.2. Receptor-mediated Endocytosis

Receptor-mediated endocytosis (RME) is the main mode of endocytosis in the PTCs and it is essential for uptake of proteins from the ultrafiltrate but also to conserve a variety of essential substances such as vitamins and trace elements carried by plasma proteins⁴⁸ (*see Annex 1*).

4.2.1. The receptor complex: Megalin and CUBAM.

RME of protein ligands relies on the formation of a macromolecular endocytic complex at the brush border. This complex consists of the multi-ligand receptors megalin and cubilin together with amnionless (AMN) (complex known as CUBAM), the

vacuolar H⁺ ATPase (V-ATPase), the NHE3 and the Cl⁻/H⁺ antiporter 5 (CIC-5). Due to the relevance of CIC-5 for the purpose of this Thesis, it will be described in detail in section 5.

As indicated previously, receptor-mediated endocytosis is mediated by a receptor complex with megalin and cubilin as key players. This complex is highly conserved across species⁴⁹ revealing its essential role in the maintenance of kidney function. These two receptors are structurally very different, have different affinity for the ligands (and, indeed, they can bind different ligands) that escape the glomerular filtration barrier. These receptors were initially thought to be co-expressed and just function together, yet it has been shown that they can be expressed and function separately⁵⁰.

4.2.1.1. Megalin

Megalin (also called gp330 or LRP2) is a 600 kDa protein (4600 aa) belonging to the Low-Density Lipoprotein Receptor (LDLR) family. Structurally, it has a large aminoterminal extracellular domain (ectodomain), a single transmembrane domain and a short carboxyterminal cytoplasmatic tail (213 aa)⁵. The ectodomain is composed by four cysteine-rich clusters, separated by 17 epidermal-growth factor-like (EGF) repeats and eight cysteine-poor spacer regions with YWTD (Tyr-Trp-Thr-Asp) repeats, four-stranded beta-propeller repeats found in LDLR, that are involved in the pH-dependent release of ligands in endosomal vesicles⁵¹. The single transmembrane domain (22 aa) is followed by the cytoplasmatic

tail that contains two NPXY (Asn-Pro-x-Tyr) motifs that might also be involved in signal transduction⁵². Within the kidney, megalin is found primarily at the apical surface and in apical endosomes of epithelial cells in the S₁ segment of the PT, with decreasing expression in the S₂ and S₃ segments of the PT³⁶. Megalin is also expressed in podocytes⁵³.

Megalin mediates the endocytosis of a large group of ligands, including plasma proteins, peptides, enzymes, vitamin-binding proteins, hormones, and hormone-binding proteins, as well as drugs and toxins. Some of the ligands are shared with cubilin, whereas others are specific for either megalin or cubilin (Figure 6A). See Annex 1 for the complete list of ligands for megalin and cubilin.

4.2.1.2. Cubilin and amnionless (CUBAM)

Cubilin, also known as intestinal intrinsic factor–vitamin B12 receptor, is a 460 kDa (3600 aa) peripheral membrane glycoprotein mainly composed by 27 CUB (complement subcomponents C1r/C1s, EGF-related sea urchin protein and bone morphogenic protein-1) domains, which name the protein and mediate the interaction with several other proteins and cargos⁵⁴. These CUB domains are preceded by an initial amino-terminal stretch of 110 aa and followed by eight EGF-like repeats. Cubilin has no transmembrane domain and depends on the single transmembrane protein named amnionless (together they form

the so called CUBAM complex) for its proper anchorage to the plasma membrane and later recycling^{55,56}.

Amnionless (AMN) is a 38–50 kDa protein and contains cytoplasmic NPXY (Asn-Pro-x-Tyr) motifs that direct cubilin internalization. In fact, cubilin has been shown retained intracellularly in PT cells of amnionless knockout mice⁵⁷, confirming the importance of AMN for the correct localization of cubilin at the apical plasma membrane.

Main ligands for CUBAM complex are albumin, transferrin, or apolipoprotein A⁵⁸. (Figure 6B)

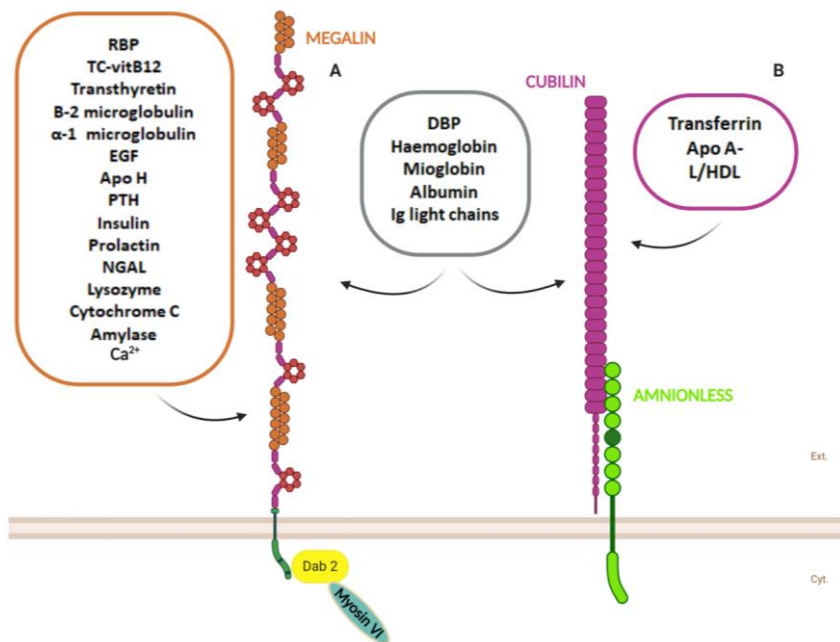


Figure 6 Receptor complex Megalin and CUBAM (Cubilin-Amnionless). A. Megalin. (For structure see the text) Ligands for megalin (orange box). For megalin to endocytose correctly its interaction with Dab2 and Myosin VI is essential. B. Cubilin (purple) and Amnionless (green) (For structure see the text). Ligands for cubilin (purple box). Ligands shared by megalin and cubilin (grey box). Abbreviations: Cyt. Cytoplasm. Ext. Extracellular RBP.

Retinol Binding Protein; TC-vitB12 Transcobalamin-vitamin B12. EGF Epithelial growth factor; PTH. Parathyroid Hormone; NGAL neutrophil gelatinase-associated lipocalin, DBP. Vitamin D Binding Protein

4.2.1.3. Megalin-CUBAM functioning

After binding to respective ligands, both receptors, megalin by the NPXY motifs and cubilin by AMN, engage the clathrin adaptor disabled-2 (Dab2) that together with Myosin VI help to mediate endocytosis of the receptors into the apical endocytic compartments. The megalin-cubilin receptor role in endocytosis has been extensively studied^{50,59-61}; they are scavenger receptors and, as said, it is known they have own and shared ligands like albumin (*Figure 6*).

Special remark on albumin reabsorption in the PT should be made for the understudying of some results here exposed. Albumin uptake by the PT is concentration-dependent and can be endocytosed by two main ways: 1. Saturable receptor-mediated endocytosis: 1a. by CUBAM high-affinity site; 1b. by megalin low-affinity and 2. by non-saturable fluid-phase endocytosis. A recent study assessed albumin endocytosis in opossum kidney cell culture model of the PT cells and by examining the effects of different doses albumin uptake they concluded that, on the one hand, normally-filtered albumin would be dependent on CUBAM receptor high affinity site, as already reported in mice and cell knockdown for cubilin^{58,62} and less on low affinity site in megalin; in fact, the primary function of megalin would be to maintain

cubilin-dependent uptake under normal conditions^{63,50}. On the other hand, under nephrotic conditions when receptor-mediated endocytosis saturates, albumin would be uptaken via non-saturable fluid-phase pathway. Interestingly, *Ren et al.* assessed this pathway by using labelled dextran in Dab2 and megalin knockdown cells and found dextran uptake dramatically reduced, which implies both Dab2 and megalin, not by direct binding to the receptor but by mechanisms still not understood (maybe by disrupting the formation of fluid phase vesicles), are necessary also for fluid-phase endocytosis⁶⁴. Recent studies suggest that a pH-dependent receptor named Neonatal Fc receptor (FcRn) may also play a role in endocytosis. Whether it participates in luminal albumin binding is not known, probably not because of luminal more basic pH. Yet, once inside the cell, as the pH in the clathrin-coated pits and fluid-phase endocytosis vesicles decreases to approximately 5.0, albumin dissociates from the receptor and binds to FcRn, whose affinity dramatically increases. Thus, albumin is capable of moving to a high-capacity pathway of transcytosis and be recycled¹⁵

Another major function was demonstrated for megalin in supplying active lysosomal enzymes to PT cells via their uptake from the tubular lumen⁶⁵.

4.2.2. Acidification of endo-lysosomal pathway

After ligand binding, the endocytic complex is internalized via clathrin-coated pits and progresses along the endocytic pathway. This progression requires maturation of the endosomal vesicles, from early to late endosomes and trafficking to lysosomes. A fundamental step in endosomal maturation is the successive acidification of each compartment (from pH=6-6.5 in early endosomes to pH<5 in lysosomes) mainly by the vacuolar H⁺-ATPase (V-ATPase)⁶⁶, which functions by pumping H⁺ in the lumen of endosomes or lysosomes by consuming ATP⁶⁷. NHE3, however, is thought to initiate acidification by dissipating the endosomal Na⁺ gradient in exchange for cytosolic H⁺⁶⁸. Then again, the translocation of H⁺ from the cytoplasm into the endosomes generates a transmembrane electrical potential, which would cause rapid inhibition of V-ATPase activity⁶⁹. The V-ATPase activity thus hangs on the dissipation of the potential either by cation retrieval or by intravesicular increase of [Cl⁻], which in fact physiologically increases progressively from early endosomes (20–40 mM) to lysosomes (>80 mM)⁷⁰. The reduction of pH and increase in [Cl⁻] in early endosomes is basically induced by ClC-5⁷¹, while ClC-7 is the main player in lysosomes⁷²(*Figure 7*).

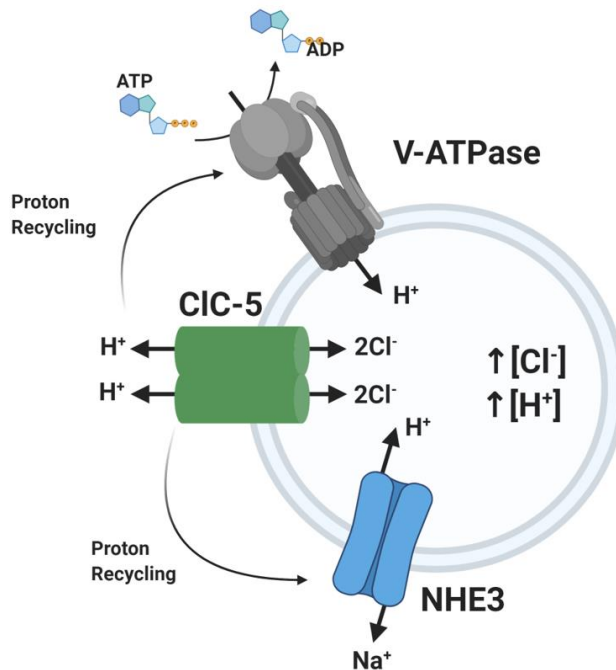


Figure 7 Potential role of CIC-5, V-ATPase and NHE3 in endosome acidification. CIC-5 mediates translocation of 2 Cl⁻ ions into the endosomal lumen and 1 H⁺ toward the cytosol. The H⁺ bumped into the cytosol either by V-ATPase or by exchange with a Na⁺ ion by NHE3.

As specified before (see section 4.2.3) acidification of endosomes allows both receptor recycling to the cell membrane and maturation of endosomal vesicles along the endo-lysosomal pathway.

4.2.3. Lysosomal degradation

Most endocytosed proteins are targeted to lysosomes for degradation¹⁵ by hydrolytic enzymes that need to be transported from the trans-golgi network. An alternative pathway for protein degradation is occasionally active, specially to degrade misfolded

proteins, and it involves proteasome and autophagosome system. After degradation, the resulting amino acids, as well as other reabsorbed substances, are transported through the basolateral cell surface and back to the renal capillaries⁵⁹. It has been calculated that recycle of receptors to the cell membrane occurs in 43 seconds, while it takes approximately 23 minutes for a ligand to reach the lysosomes⁶³. A scheme of all this process is depicted in *Figure 8*.

4.2.4. Recycling

On the other hand, some ligands such as albumin and IgG are thought to switch receptors at more acidic pH and bind to the Neonatal Fc receptor (FcRN), which, by transcytosis through the basolateral membrane, avoids default delivery to lysosomes⁷³.

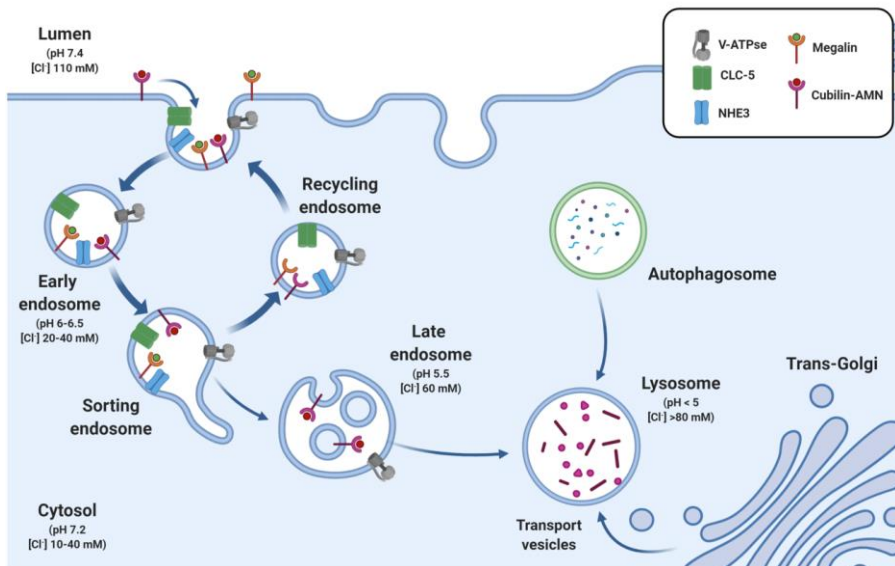


Figure 8 Receptor-mediated endocytosis in PT. The endo-lysosomal pathway. Upon ligands attach to their receptors, Megalin and Cubilin-amnionless (AMN) (CUBAM), the endocytic complex at the apical membranes is internalized via clathrin-coated pits. The vacuolar ATP (V-ATPase), the sodium-proton exchanger isoform 3 (NHE3) and the chloride-proton antiporter CLC-5 allow for the intravesicular pH to decrease and the $[Cl^-]$ to increase. Progressive acidification of each endocytic compartment facilitates release of ligands from their receptors; receptors are recycled back to the plasma membrane and protein ligands are processed and degraded in the lysosomes.

4.3. Fluid-Phase endocytosis

Fluid-phase endocytosis is the process by which small amounts of extracellular fluid and solute molecules are taken up by the cells in a non-specific manner and, in most cells through a clathrin-independent mechanism⁷⁴. So, it is not preceded by specific binding to the plasma membrane or concentration of molecules, but to a continuous process that allows the cell to check the

environment and maintain the cell volume, preventing shrinking or swelling ⁷⁵.

The molecules once inside the cells form vesicles which are then fused with the endosomes for the metabolic processes.

As already indicated, fluid-phase endocytosis also takes place in PTCs. Although most of solute endocytosis in this segment of the nephron occur via receptor-mediate uptake, fluid-phase may play a major role in pathological conditions, as explained before (*see section 4.2.1.3*) in nephrotic conditions, where the reabsorb bulk of proteins that are filtered through the glomerulus.

5. ClC-5: a critical player in renal proximal tubule receptor mediated endocytosis

5.1. ClC ion channel and antiporters superfamily

Chloride channels, ClC, are expressed in the prokaryote and eukaryotic cells and they participate in many physiological functions such as cellular volume regulation, transepithelial transport and membrane excitability. Despite being referred to as chloride channel, the family of ClC proteins includes both selective chloride ion channels and chloride-proton antiporters⁷⁶. The human family of ClC chloride channels and transporters is divided into two subfamilies based on sequence homology and mode of ion transport. (1) The chloride ion channels, ClC-1, ClC-2, ClC-Ka and ClC-Kb, located in the plasma membranes where they maintain

the membrane potential and ion homeostasis, (2) the chloride-proton transporters, or antiporters divided in two according to the homology (2a) ClC-3, ClC-4 and ClC-5 and (2b) ClC-6 and ClC-7. They are mainly expressed in intracellular membranes of the endosomal-lysosomal pathway, where they are involved in protein endocytosis and degradation⁷⁷.

These abundant Cl⁻ channels are involved in a huge variety of physiological functions and, if deficient, they cause a variety of pathologies such as Bartter Syndrome⁷⁸, a renal salt wasting tubulopathy associated to hypokalaemia and metabolic alkalosis, epilepsy⁷⁹, myotonia⁸⁰ or osteopetrosis⁸¹.

Due to its importance in Dent Disease type 1, Cl⁻/H⁺ antiporter ClC-5 will be described in more detail.

5.2. ClC-5 chloride/proton antiporter

The Cl⁻/H⁺ antiporter ClC-5 is mainly located in intracellular vesicles, however, it is also expressed at low levels in plasma membranes⁷⁶. As has already been mentioned, ClC-5 is expressed in apical endosomes of proximal tubular cells⁸² where it co-distributes with the V-ATPase⁸³.

Aside from its location in the PT, where its effects have been thoroughly investigated, ClC-5 expression has also been reported in thick ascending limb of Henle's loop and in the α - and β -intercalated cells of the collecting duct where its role remains speculative^{84,85}. Remarkably, a physiological role for ClC-5 in

podocytes as mediator of endocytosis has also been proposed^{86,87}. In addition, CIC-5 has recently been associated with Barttin, a small protein that is necessary for proper function of CIC-K channels⁸⁸. It is also expressed in minor to moderate levels in liver, brain and intestine⁸⁹⁻⁹¹, where it is suggested CIC-5 also have a role in endocytosis but is still to be confirmed.

5.2.1. CIC-5: from gene to protein

CIC-5 protein is encoded by *CLCN5* gene, which was described 25 years ago⁹². It is located at Xp11.22-p11.23 and has a coding region of 2.238 bp, consists of 17 exons, including 11 protein-coding exons (from 2 to 12) and a large UTR. The *CLCN5* gene has five different transcripts, two of them (transcript variants 3 [NM_000084.5] and 4 [NM_001282163.1]) encode for the canonical 746 amino acid protein, other two (transcript variants 1 [NM_001127899.3] and 2 [NM_001127898.3]) encode for the NH₂-terminal extended 816 amino acid protein and the last one does not encode for any protein (transcript variant 5, NM_001272102.2) (<http://grch37.ensembl.org/>).

5.2.2. Structure of CIC-5

CIC-5 forms a dimer with two identical units that span the membrane in opposite orientations. Each subunit contains a pore responsible for the selective coupling of the Cl⁻ flux to H⁺ counter transport⁹³. One unit of the canonical isoform of CIC-5 consists of 746 aa distributed in 18 α -helices (named from A to R) with two

phosphorylation and a main N-glycosylation site⁹⁴. Different molecular weights have been established for the protein; 90-kDa if it is core-glycosylated or 100-kDa if it received complex glycosylation⁹⁵. In the tertiary structure, helices B, H, I, O, P, Q are mainly involved in the dimer interface formation and are basic for proper pore establishment⁹⁶, while helices D, F, N and R mainly provide the Cl⁻ selectivity. The function of E helix is still unclear. Two amino acids that are key for ClC-5 function are the so-called “proton glutamate” (Glu 268) and the “gating glutamate” (Glu 211). The “proton glutamate” acts as a H⁺ transfer site, being crucial to the H⁺ transport⁹⁷; whereas the “gating glutamate” is necessary for Cl⁻ voltage dependence⁹⁸. Likewise, the cytoplasmatic carboxy-terminus domain contains two cystathionine beta-synthase (CBS) domains that combine with ATP to facilitate Cl⁻/H⁺ exchange and have also been implicated in intracellular targeting and trafficking as well as protein–protein interactions⁹⁹. There are, as well, a proline-rich domain (PY), a sorting signal which modulates ClC-5 retention at the cellular membranes¹⁰⁰, and a potential PDZ protein-binding module in the C-terminal¹⁰¹ (Figure 9).

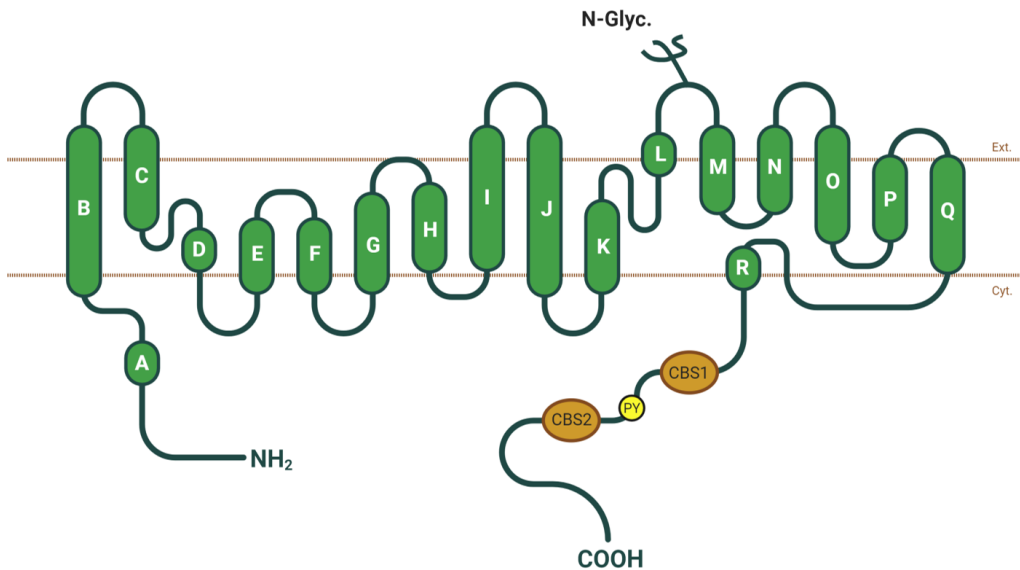


Figure 9 Schematic topology diagram of a single CIC-5 protein subunit A 746-aa protein that consists of 18 α -helices with the NH_2 and COOH terminus domains being cytoplasmic (membrane boundaries indicated by dashed lines). The C-terminal domain contains two cystathionine beta-synthase (CBS) domains and one proline-rich domain (PY) domain. Abbreviations, Cyt. Cytoplasm. Ext. Extracellular

5.2.3. Regulation of the Trafficking and Activity of CIC-5 by Protein-Protein Interactions

The trafficking and functions of CIC-5 are regulated by its interactions with other proteins.

To date, four proteins have been proved to direct interact with the C-terminus region of CIC-5, rich in binding motifs: Nedd4.2, cofilin, kinesin family member 3B (KIF3B), and NHERF2. Nedd4.2, NHERF2 and cofilin are cytosolic proteins which modulate the level of CIC-5 at the plasma membrane; KIF3B is a motor protein that mediates

the interaction with the cytoskeleton to regulate CIC-5 subcellular trafficking.

5.2.3.1. *Nedd4.2*

The ubiquitin ligase Nedd4.2 was identified to interact with the PY motif to promote mono-ubiquitination and shunting of CIC-5 into the endocytic pathway. This happens, for example in the presence of albumin in the lumen; Nedd4.2 is recruited to the endocytosis complex in the plasma membrane and ubiquitinates CIC-5 which is removed into the albumin endocytic pathway. This was illustrated by down-regulation of Nedd4.2 activity using silencing RNA which resulted in a moderate decrease in endocytosis¹⁰². Some years later though, in a mouse model with a mutation in the PY motive, Y672E, (which impaired the interaction with Nedd4.2) did not show reduction of CIC-5 or proteinuria, so the role of Nedd4.2 in endocytosis by interacting with CIC-5 was called to question¹⁰³.

5.2.3.2. *NHERF2*

CIC-5 also interacts with Na⁺-H⁺ exchanger regulatory factor 2 (NHERF2), by a PDZ binding motif residing in the CBS domain linker. NHERF2 is a scaffold protein, which has been shown to mediate the cell surface recruitment of CIC-5 in response to luminal albumin where it could initiate or promote endocytosis. Silencing NHERF2 protein in kidney epithelial cells resulted in a dramatic reduction of CIC-5 in cell surface and a reduction in the uptake of albumin⁶⁶.

5.2.3.3. Cofilin

Although the binding site remains unknown, CIC-5 C-terminus directly interacts with cofilin, an actin depolymerizing protein that allows dissolution of the actin cytoskeleton to mediate budding of nascent endosomes. Inhibition of the cofilin-CIC-5 protein interaction dramatically reduced albumin uptake in a model of the proximal tubule¹⁰⁴.

5.2.3.4. KIF3B

Kinesin family member 3B (KIF3B) interacts with CIC-5- containing endosomes and promotes their trafficking along microtubules away from the plasma membrane¹⁰⁵. Over-expression of KIF3B in polarized epithelial cells reduced the population of CIC-5 at the cell surface and subsequently decreased endocytosis of albumin¹⁰⁶. These results support the idea that the amount of CIC-5 at the plasma membrane is a rate-limiting step in renal endocytosis, and implicates the kinesin motor complex as a major regulatory factor of CIC-5's subcellular trafficking¹⁰⁵.

5.2.4. Function of CIC-5 in the endocytic pathway

The most well studied functions of CIC-5 are those implemented in the proximal tubule, where three main roles are attributed to this Cl⁻/H⁺ antiporter.

- I. Regulation of endosomal acidification by providing an electric shunt for vacuolar H⁺-ATPase. Efficient endosomal acidification is essential for endosomal maturation and trafficking along the endo-lysosomal pathway (see section 4.2.2). Loss-of-function of CIC-5 have demonstrated impairment of acidification in some cases^{83,89}.
- II. CIC-5 is required for the recycling to the cell membrane of megalin and cubilin but also for their trafficking in the PTCs although the mechanisms remain unknown. CIC-5 disruption has been demonstrated to lead to a trafficking defect of megalin and its co-receptor cubilin^{107,108}
- III. By its interactions with other proteins through its Ct binding motifs (see section 5.2.3), it is involved in tethering the endocytosis complex, playing a role in maintaining the integrity of this complex. By its interactions it also mediates the vesicles intracellular trafficking.

Even less understood are CIC-5 functions in other segments of the nephron where it is also located.

- IV. In the thick ascending limb of Henle's loop, although it is still to be confirm, CIC-5 would putatively be involved in endocytosis and recycling of membrane receptors

which would allow the physiological function of this segment of the nephron (see section 3.1)^{84,109}

- V. In the α - and β -intercalated cells of the collecting duct, ClC-5 role is not still understood yet its dysfunction in this segment has been hypothetically related to calcium crystal and resulting stones formation¹¹⁰.
- VI. ClC-5 has also been located in the podocytes, where it is hypothesized it plays a role in clathrin-mediated endocytosis. It was found overexpressed in biopsies of patients with proteinuria suggesting a key role in albumin handling in proteinuric states in the glomeruli⁸⁶.
- VII. They may play a role in the distribution of V-ATPase as its endosomal distribution has been shown to be significantly altered in patients with DD1¹¹¹

6. Dent's disease type 1

Dent's Disease is a rare X-linked renal disease characterized by manifestations of proximal tubule dysfunction. The disease is caused by mutations in either the *CLCN5* (Dent disease 1 (OMIM #300009)) accounting for 65% of cases or *OCRL1* (Dent disease 2 (OMIM # 300535)) in 15% of cases. Mutations are not found in these 2 genes in 25% of patients with the Dent's phenotype. The possibility that other genes may encode some of the proteins that

interact with CIC-5 has been investigated but no mutations in cofilin or CIC-4 were identified^{29,112,113}.

Although we will refer occasionally to Dent's Disease type 2, for the scope of this Thesis project we will focus on Dent's Disease type 1, caused by mutations in the *CLCN5* gene, which encodes for the CIC-5 Cl^-/H^+ antiporter.

6.1. Epidemiology

The prevalence of DD1 is unknown although with a possible great proportion of misdiagnosis. It is estimated that around 400 families are affected worldwide¹¹⁴. In any case, DD1 is considered a rare disease, according to the European Union, as it affects less than 1 in 2000 citizens^{115,116}.

6.2. History

Dent's disease was first described in 1964 by Dent and Friedman in two unrelated cases presenting with rickets and hypercalciuria, together with urinary loss of amino acids and phosphate and a noticeable fail to thrive¹¹⁷. At the beginning of the eighties, the case of a male with hypercalciuric rickets and loss of tubular proteinuria within the urine was described¹¹⁸. Meanwhile, in Japan two groups described several male patients presenting with tubular proteinuria but no other sign or symptom^{119,120}.

In 1990, the group of *Wrong et al*, at the University College Hospital in London described a family with 23 members showing tubular proteinuria, and named the disease after Wrong's mentor, *Charles Enrique Dent, the doctor born in Burgos who first described it*¹²¹. The same group determined four years later that Dent's Disease was X-linked hereditary¹²². The gene causing DD1 was isolated and cloned in 1995 by Fisher et al⁹².

It is not surprising that, although today they are known to share the same aetiology, several entities arose in different parts of the globe, with different names as different affected families were described^{123–125} : X-linked recessive nephrolithiasis (XRN) (OMIM #310468), X-linked recessive hypercalciuric hypophosphatemic rickets (XLRH) (OMIM #300554), Low-molecular-weight proteinuria with hypercalciuria and nephrocalcinosis of Japanese children (JILMWP) (OMIM #308990). It was *Lloyd et al* who concluded they were all the same disease with phenotype variations and shared aetiology, *CLCN5* mutations¹²⁶.

6.3. Clinical presentation

Low molecular weight proteinuria (LMWP) is the hallmark of the disease and it is classically associated with hypercalciuria and nephrocalcinosis/nephrolithiasis. Besides, patients may show an incomplete or complete Fanconi Syndrome (FS) with defective reabsorption of one or several other solutes, which are cargos for proximal tubular cells, as amino acids, glucose, phosphate or uric

acid^{127,128}. Further manifestations such as hypophosphatemic ricket, growth restriction and short stature are occasionally present^{129,130}. Remarkably, few patients manifest with significant albuminuria, glomerulosclerosis and hardly no features of tubular disease^{131,132} and other few cases show additional atypical hypokalemic metabolic alkalosis and hyperaldosteronism, symptoms usually associated with another tubulopathy affecting the thick ascending part of Henle's loop, Bartter syndrome (BS)¹³³⁻¹³⁶.

The disease progresses to chronic kidney disease (CKD) between the thirties and the fifties in up to 80% of patients and finally to renal failure requiring renal replacement therapy (RRT)^{114,137}.

Although the disease affects almost exclusively hemizygous males, female carriers may have a mild phenotype, including LMWP or even hypercalciuria, yet very few carriers have been studied^{122,123}. CKD has only been reported once in a female carrier in 1994¹²². In fact, in 2019 the first case of successful kidney transplantation from a carrier female donor to his affected son was described¹³⁸, though there is no information about the outcomes after two-months post-transplantation.

Japanese studies revealed that despite similarity in genetic background, there are several phenotypic differences in clinical presentation in comparison to patients from Europe and USA. So Japanese DD1 patients present with less hypercalciuria, less proportion of rickets or nephrocalcinosis and even less proportion of CKD, but nonetheless a higher proportion of renal dysfunction at

younger ages, the reason for these differences has not been fully elucidated¹³⁹.

6.3.1. Hypothesized physiopathology of the different symptoms

The mechanisms whereby a functional loss of this renal chloride channel leads to Dent's Disease type 1 are not completely understood. As stated before, CLC-5 is involved in many functions that, if impaired, could explain the physiopathology of Dent's Disease. First hypothesis was that CLC-5 defect does not allow proper acidification of early endosomes blocking endocytosis given that progressive acidification is necessary for proper sorting and function along the endo-lysosomal pathway^{82,83,89}. Later, though, Jentsch's group provided evidence that chloride concentration played a crucial role in endocytosis, rather than endosomal acidification⁹⁸. Nowadays, to what measure exactly the change in endosomal pH or $[Cl^-]$ contribute to the disease pathology remains unclear.

What is more, as already mention in section 5.2.3, CLC-5 entails many protein-to-protein interactions that are essential for endocytosis, so its decreased presence in the plasma membrane could also be a factor for endocytosis deficiency¹⁴⁰. As a result of defective CLC-5, it has also been seen that levels of the main actors of the receptor complex (i.e. megalin and CUBAM) are reduced, probably due to a disturbed intracellular trafficking and an

impaired recycling, and so, without the main effectors of ligand uptake, endocytosis cannot take place^{50,137}.

If we considered every clinical manifestation separately:

6.3.1.1. Low molecular weight proteinuria

Assessed by the quantification of β 2-microglobulin, retinol-binding protein or α 1-microglobulin in urine and found elevated from 10-fold to 1000-fold¹⁴¹ normal as compared to physiological amount¹⁴². It is the hallmark of the disease, present in all patients, and is suggested to be caused by a defect in receptor-mediated endocytosis, either because of impaired endosomal acidification/ Cl^- concentration or because there is a decrease in multi-ligand receptors due to impaired recycling, as it has been demonstrated both in mouse models^{143,144} and in humans¹⁴⁵ that loss of CIC-5 causes defective PTC trafficking of megalin and cubilin.

6.3.1.2. Hipercalciuria

Although hypercalciuria has been reported with lower prevalence among Japanese DD1 patients (51%)¹³⁹, in European-US cohorts almost all patients are affected (80-100%)^{113,129,146}. Loss of urinary calcium decreases in parallel to renal function and so, calcium excretion was described normal in 85% of patients over 30 years¹³⁰.

On the one hand, the initial hypothesis for hypercalciuria was that increased tubular PTH concentrations due to a lack of ClC-5-related endocytosis would stimulate the PTH receptor and induce up-regulation of 1- α -hydroxylase. Thus 1,25-dihydroxivitamin D (1,25-(OH)₂-vitamin D₃) would rise and promote intestinal absorption of calcium and excessive calcium would get to the tubule to be excreted, leading to clinical symptoms of hypercalciuria and renal calcification. In fact, *Blanchard et al.*, in a numerous cohort of 109 DD1 and 9 DD2 found that levels of 1,25-(OH)₂-vitamin D₃ were normal or in the upper range of normality and remained normal even in the late stages of CKD¹³⁰ (when normally it decreases together with glomerular filtration rate¹⁴⁷. However, it is to be considered that the inactive vitamin D precursor 25(OH)-VitD₃ and its binding protein, substrate for 1.25 (OH)₂D₃, are also less endocytosed, so its production would not be as high as expected despite the PTH stimulation.

On the other hand, there is another hypothesis considering ClC-5 localisation in the thick ascending limb of Henle's loop. Although it is still not well established, this theory suggests that ClC-5 dysfunction would impair the recycling and activities of the surface transporters¹⁴⁸, e.g., the sodium-potassium-chloride cotransporter (NKCC2), the chloride channel (ClC-Kb), and the renal outer medullary potassium channel (ROMK) (see section 3.2), which are involved in generating the transepithelial potential difference that is necessary for paracellular calcium uptake. Thus, this

transepithelial gradient would not be efficiently produced and calcium would not be reabsorbed and hence lost with the urine¹⁴⁹.

6.3.1.3. Nephrocalcinosis

Nephrocalcinosis stands for the deposition of calcium salts in the renal parenchyma and affects approximately 40% of DD1 patients¹²⁹. If the degree of nephrocalcinosis is from moderate to severe, it can be easily seen through X-ray imaging as kidney appear white.

Several hypotheses have been proposed for this sign; the most plausible has to do with the still speculative role of CIC-5 in the α -intercalated cells of the collecting duct. In a collecting duct cell model (Mimcd.3), the silencing of CIC-5 expression caused the endocytosis to be arrested and calcium oxalate crystals agglomerated on the CIC-5 silenced cells^{85,110}.

6.3.1.4. Nephrolithiasis

Approximately 25% of DD1 patients present at least one event of kidney stone (calcium oxalate and/or phosphate)^{113,129,130}. This condition seems to result from the association of hypercalciuria and an impaired handling of calcium phosphate and calcium oxalate crystals in the collecting duct (see section 6.3.1.3).

6.3.1.5. Hypophosphatemic rickets and hyperphosphaturia

This disorder of bone mineral formation is characterised by bone pain, fractures and growth abnormalities. The prevalence of rickets is very variable according to the different cohorts described in the literature and it varies between 2% in Japanese cohorts¹³⁹, 48% in Italian cohorts¹¹³ and 60% in Spanish cohorts¹²⁹.

Loss of phosphate within the urine and consequent hypophosphatemia and development of rickets has been deemed secondary to defective reabsorption of PTH. PTH is a ligand for megalin, so CIC-5 defect, by impairing endocytosis and decreasing megalin, causes PTH to accumulate in the lumen of the tubule stimulating PTH receptors and triggering the internalization and degradation of NaPi2a (see section 3.2). Thus, phosphorus cannot be reabsorbed and is lost within urine. It can also be attributed to a loss of PT cells differentiation, by which the expression of apical NaPi2a is decreased. Likewise, a potential link between CIC-5 and the scaffold protein Na⁺-H⁺ exchanger regulatory factor 1 (NHERF1) whereby CIC-5 influences PT apical NaPi2a expression has been proposed, but not confirmed¹⁵⁰ Further, vitamin D is involved in bone formation and the urinary loss of vitamin D binding protein, which carries most of the circulating vitamin D in the plasma, may also lead to bone defects¹⁵¹.

6.3.1.6. Fanconi Syndrome

Complete Fanconi Syndrome (FS) accounts for impairment of proximal tubule reabsorption of sodium, bicarbonate, potassium, phosphate, glucose, amino acids, uric acid, LMWP, peptides, as well as other organic solutes. The complete form of the condition has low prevalence among DD1 patients^{134,146}. Nonetheless, the loss of determined cargoes, incomplete Fanconi Syndrome, is more frequent and has been seen in approximately 70% of patients with DD1^{129,152}. The pathophysiological mechanisms underlying these conditions are not completely understood, especially because they affect some patients and not others. The most plausible explanation is the reduction of specific transported in the apical membrane of the cell due to defective recycling or dedifferentiation of the proximal tubular cells¹⁵³.

6.3.1.7. Atypical phenotypes. Hypokalaemia, metabolic alkalosis

As previously reported by some authors^{114,130}, some cases show progressive hypokalaemia and normochloremic alkalosis. Though they are not common symptoms, *Blanchard et al* reported hypokalaemia in 29% of patients, especially in those older than 18 years old¹³⁰. They studied thoroughly some of these patients and found kaliuresis was inappropriately increased as well as plasma renin in all of them. Serum aldosterone was variable amongst these patients; it was found elevated in some and normal in some

others. The fact that this presentation is typical of Bartter Syndrome, a salt-wasting tubulopathy caused by mutations of genes encoding proteins that transport in the ascending loop of Henle (see section 3.1), where CIC-5 is also located, invites to postulate that CIC-5 plays also a role in this part of the nephron. No mutations in genes encoding for proteins linked to Bartter-like symptoms (specifically, NCCT, CIC-Kb, Kir1.1, and NKCC2) have been discovered so far in DD1 patients^{133–135}

Barttin, codified by *BSND*, serves as an accessory subunit regulating the function and subcellular localization of the CIC-k channels in the TAL of the Henle's loop (see section 3.1). *Wojciechowski et al.*¹³⁶ assessed its potential interaction with CIC-5 by studying WT and mutated Barttin co-expressed with WT and mutated CIC-5 in HEK293 cells. They concluded that Barttin (1) regulates the complex glycosylation of CIC-5 in a concentration dependent manner, (2) it also changed CIC-5 localization, by reducing its presence in the membrane and (3) modified the ionic transport mediated by CIC-5 as measured by cell patch clamp. All in all, these findings suggest that barttin-dependent regulation of CIC-5 trafficking and processing might be altered in DD1 patients contributing to this Bartter-like presentation showed by some patients.

6.3.1.1. CKD in DD1

The mechanisms by which DD1 leads to chronic kidney disease in 30-80% of affected males between the third and fifth decade of life

¹⁵⁴ still remains elusive. It has been hypothesised that the cellular consequences of CIC-5 dysfunction may cause a chronic activation of apoptotic and inflammatory pathways, that, in combination with calcification terminates in kidney failure, as in other kidney diseases, but it has not been proved. Interestingly, the effect of CIC-5 in glomeruli may also play a role in progression of CKD. (see next section 6.4)

6.4. Kidney histological features in DD1 patients

Initially Dent's Disease 1 was considered limited to the tubule, as its location was considered to be restricted to this part of the nephron⁸². Nonetheless, few years ago it was first demonstrated that CIC-5 is also in the glomeruli⁸⁶ and in fact, some reports of glomerular lesions in DD1 patients had already been published by that time¹³². In a study by the Rare Kidney Stone Consortium, *Wang et al.* examined the histopathology of 30 DD patients (26 DD1, 2 DD2 and 2 with clinical criteria of DD but no genetic confirmation). The median age at biopsy of the cohort was 7.5 (5, 19) years with an eGFR of 69 (44, 94) ml/min. They found that 83% of patients presented with focal global glomerulosclerosis (FGGS), focal segmental glomerulosclerosis in 6.6% of cases and in 57% of cases foot processes were found effaced, though mild and segmentally. More expectedly 60% showed interstitial fibrosis and 70% tubular damage. The authors concluded that a higher percentages of globally sclerotic glomeruli, foot process

effacement, and interstitial inflammation were associated with lower eGFR at biopsy, whereas foot process effacement was associated with steeper annual eGFR decline¹³¹

The appearance of glomerulosclerosis in patients with DD1 has been generally regarded as a consequence of tubular damage^{155–157} yet *Solanki et al*, by assessing transferrin endocytosis in a CIC-5 knock down cell model, suggested that CIC-5 plays a critical role in podocytes function by participating in protein endocytosis⁸⁷.

In fact, glomerulosclerosis lesions have been also reported in other tubulopathies such as nephronophthisis^{158,159} and Bartter Syndrome¹⁶⁰.

6.5. DD1 mutations

As said, DD1 is caused by mutations in the *CLCN5* gene and accounts for 60% of patients showing Dent's disease phenotype.

Up to July 2020, 265 different *CLCN5* pathogenic variants had been described in literature associated to DD1^{113,114,154}. Mutations are found scattered along all the gene sequence, with no evidence for mutational hot spots. The proportion of each type of mutation depends on the series of patients described. Taking into account all those mutations already described, 35% are missense, 31% frameshift, 16% nonsense, 10% splicing, 4% large deletion, 2% in-frame and 2% other types¹⁵⁴. Most of them are predicted to generate a truncated, miss-functional or absent protein although

only few of them have been functionally characterised *in vitro* or *in vivo*^{161,162}. Similar to other X-linked disorders, the number of *de novo* mutations is estimated around 8-10%^{138,163}.

Several classifications have been coined according to different factors, but no clear correlation between genotype and phenotype has been established. Taking into account their severity, Blanchard et al¹³⁰ classified mutations as severe (nonsense, frameshift, large deletion, or splice-site mutations) or less severe (missense and in-frame mutations). Another classification by *Grand et al.* divided mutations in a) Type I (with depressed chloride currents but present in plasma membrane and correct complex glycosilation) and b) Type II (including mutants that could not traffic to the membrane and showed defective N-glycosilation, resulting in endoplasmic reticulum retention)⁹⁵.

Nowadays, the most used classification is based on functional data. Thus, mutations are classified into the following groups^{95,161,164}:

- I. Class 1. This group includes those mutations that generate a protein with impaired processing and folding that causes its endoplasmic reticulum (ER) retention and degradation by the proteasome. These mutations are associated with reduced protein expression and impaired N-glycosylation. Class 1 ClC-5 mutants do not present electric activity. Endosomal pH has not been tested. E.g., I524K, S270R, G513E, R516W
- II. Class 2. These mutations appear to have little effect on subcellular distribution and, therefore, are present at the

cell surface and in early endosomes. Nonetheless, they are functionally impaired so that they are devoid of electrical activity and fail to enhance endosomal acidification. E.g., E527D.

- III. Class 3. These mutations cause variable effects on localization as some present abnormal subcellular location with reduction of plasma membrane expression and alteration in endosomal targeting and other do not. They are associated with reduction of currents at the cell surface but proper endosomal acidification E.g., G57V, R280P.

6.6. Treatment

There is no direct therapy for DD1, so the treatment given intends to reduce hypercalciuria or rickets, to prevent nephrolithiasis and nephrocalcinosis, or to supplement the ion deficiencies.

In order to reduce hypercalciuria, thiazides proved effective in a randomised trial¹⁶⁵ that nonetheless was stopped because of the side effects generated by the treatment in children¹³⁰. Though not approved by clinical trial, experimental data showed *CLCN5* knockout mice treated with citrate reduced hypercalciuria and, so, DD1 patients are often treated with citrate (usually potassium citrate) to prevent nephrolithiasis and reduce acidosis¹⁶⁶. On the other hand, some patients are supplemented with vitamin D to prevent bone disease, yet close surveillance needs to be guaranteed on calcemia and calciuria so they do not increase. In

this regard, some patients with hypophosphatemia or bone disease are supplemented with phosphate.

Although angiotensin-converting enzyme inhibitors (ACEi) or angiotensin II receptor blockers (ARBs) therapy is not effective for tubular proteinuria, it has showed good results in those few patients with glomerular damage¹⁶⁷.

Thus, it is necessary to provide new directed therapies that can really stop the progression of the disease or even cure it.

6.7. Research on DD1: Biological models

6.7.1. Cellular models

Functional investigations have been performed in a variety of cell types like *Xenopus Laevis* oocytes, especially used for electrophysiological studies by performing voltage-clamp recordings^{168–170}, Opossum Kidney (OK)¹⁰², among others, human embryonic kidney cells (HEK293) have been used to document the subcellular localization of CIC-5^{161,162,171} or conditionally immortalized proximal-tubular epithelial cell lines (ciPTEC) from patients with DD1¹⁷². Nonetheless, either the degree of differentiation and polarization of most of these models is far from resembling the human proximal tubule cells, like the *Xenopus Laevis* oocytes or the Opossum Kidney cells or are difficult to grow and maintain stable like ciPTECs.

Hence, new models are needed to reproduce more accurately the features of human PTCs.

6.7.2. Murine models

Likewise, mainly two murine *CLCN5* knock-out models have been created, Guggino's and Jench's models^{109,173}. Both models showed LMWP, phosphaturia, and normal serum PTH; the Guggino's model also revealed hypercalciuria, nephrocalcinosis, and an increase in serum of 1,25(OH)2D. Later, *Novarino et al.* generated a Knock-in mouse model with a novel mutation in *CLC-5* (E211A), not yet found in a patient, that uncoupled Cl^-/H^+ transport reproducing Dent's disease with low molecular weight proteinuria, hypophosphaturia, and hypercalciuria, but without impaired endosomal acidification⁹⁸. Table 1 summarizes the features of the three mouse models. On-going research is aimed to create new mouse models, but results have not been published.

Table 1. Mouse models currently existing for DD1

| | Jentsch model 107 | Guggino model 109 | Novarino model 98 |
|--|---|---|---|
| CIC-5 KO method | Targeting part of exon 5 and 6: C57BL/6 strain | Targeting exon 6 C57BL/6 strain | Knock -in insertion E211 mutation |
| Renal phenotype | | | |
| Low molecular weight proteinuria | Vitamin D-binding protein, retinol-binding protein, β 2-microglobulin, lactoglobuli | Vitamin D-binding protein, clara cell protein, transferrin, β 2-microglobulin | Vitamin D-binding protein, retinol-binding protein, β 2-microglobulin, lactoglobuli |
| Megalyn | Not tested | Defective trafficking | Defective trafficking |
| Cubilin | Not tested | Defective trafficking | Defective trafficking |
| Defective fluid-phase endocytosis | Fluorescein isothiocyanate-dextran, horseradish peroxidase. Yes | Fluorescein isothiocyanate-dextran, horseradish peroxidase. Yes | Labelled-dextran. Reduced |
| Natriuria | Not tested | Increased | Absent |
| NHE3 | Decrease apical exposure | Decrease protein abundance | Not tested |
| Phosphaturia | Present (decreased NaPi2A) | Present | Present |
| Hypercalciuria | Absent | Present | Present |
| Aminoaciduria | Not reported | Present | Not tested |
| Glycosuria | Not reported | Present | Present |
| Nephrocalcinosis | Abscent | Intrarenal calcium deposits | Not tested |
| Serum 1,25(OH)2D | Reduced | Increased | Not tested |
| Serum 25(OH)D | Reduced | Not tested | Not tested |
| Serum PTH | Normal | Normal | Not tested |
| Urine 1,25(OH)2D | Increased | Not tested | Not tested |
| Urine 25(OH)D | Increased | Not tested | Not tested |
| Urine PTH | Increased | Not tested | Not tested |
| Bone turnover markers | Not tested | Increased | Not tested |

7. Extracellular vesicles

Extracellular vesicles (EV) are a heterogeneous group of particles released by almost any prokaryotic or eukaryotic cell and thought to mediate cell-to-cell communications by transporting different cargoes including bioactive molecules as proteins, membrane receptors, nucleic acids and lipids, which in turn can be transferred to target cells¹⁷⁴.

The study of EVs is a very active area of research nowadays. The fact that they are found in all biological fluids and that they provide valuable information about the cells they are secreted by, make them attractive as diagnostic minimally invasive liquid biopsies. Upmost, the efficient exchange of cellular components through EVs allows their engineering to deliver diverse therapeutic payloads, so they have a promising future as therapeutic tools.

However, besides the intense investigation due to their diagnostic and therapeutic potential, there is still no standardized terminology for exosomes and extracellular vesicles¹⁷⁵. At present, although there are several continuously-evolving classifications of EVs¹⁷⁶, 3 main subgroups have been defined according to their size, origin and composition:

- I. Apoptotic bodies: These 50-5000 nm sized particles are released during apoptosis when plasma membrane blebbing occurs¹⁷⁷.

II. Ectosomes: Also called microvesicles or microparticles, they are generated directly from the plasma membrane by its outward budding producing vesicles in the size range 100–1000 nm in diameter¹⁷⁸.

III. Exosomes: These particles, originated from endosomal system, are the smallest EVs (40–200 nm, ~100 nm on average). Exosomes are formed by the fusion of intracellular multivesicular bodies (MVBs or also called late endosomes) with the plasma membrane, leading to the release of their content into the extracellular space¹⁷⁸.

Ectosomes are beyond the scope of this project and in this Thesis we are considering only exosomes. Nonetheless, isolation techniques allow to obtain a mixture of extracellular vesicles enriched in exosomes, so for simplicity, we will use the terms exosome and uEVs (urinary exosome-like vesicles) indistinctively (*Figure 10*).

7.1. Exosomes

Exosomes are lipid-enclosed vesicles and can contain membrane and cytosolic proteins (proteins from the nucleus, mitochondria, ER or Golgi are mostly absent) extracellular matrix proteins, metabolites and nucleic acids.

The presence of membrane-enclosed vesicles outside the cells, in tissues or in biological fluids has been described for decades. The

first report is found in 1946 by Chargaff and West, when EVs were observed as procoagulant platelet-derived particles in normal plasma¹⁷⁹. They were also early observed in cartilage¹⁸⁰ and later described as budding from tumoral cells¹⁸¹ and in semen, later termed proteasomes¹⁸². In 1981, *Trams et al.* proposed the term 'exosomes' for exfoliated membrane vesicles, appearing as large (500–1000 nm) and small (approximately 40nm) vesicles, which they identified to be secreted by a variety of cell types. These vesicles were first assumed to be released by direct budding of the plasma membrane, yet in 1983, by ultrastructural studies in differentiating immature red blood cells, a more complex secretion pathway was depicted in which vesicles formed intracellularly within multivesicular bodies and were subsequently released^{183,184}. From then onwards, an exponentially increasing interest in exosomes has arisen with 25 publication on exosomes in the year 2000 and 3767, so far, in 2020. (pubmed)

7.1.1. Biogenesis of exosomes

As explained elsewhere (see section 4.1), the fate of most multivesicular bodies (MVBs) is to fuse with lysosomes for their content degradation. Nonetheless, some sorted intraluminal vesicles (ILVs) inside MVBs fuse with the plasma membrane (PM) instead, releasing their content to the extracellular milieu, these are exosomes. The sorting signals are not fully understood, but for some cases MVBs content indicates its destiny; cholesterol-positive

MVBs for example fuse with PM¹⁸⁵ and contrarily, those enriched LBPA (lysobisphosphatic acid) are fated for degradation¹⁸⁶.

For EVs formation, the most well-known mechanism is that involving the components of the endosomal sorting complex required for transport (ESCRT). ESCRTs consist of approximately twenty proteins that assemble into four complexes (ESCRT-0, -I, -II and -III) with associated proteins (VPS4, VTA1, ALIX), The ESCRT-0 complex recognizes and sequesters ubiquitylated proteins in the endosomal membrane¹⁸⁷, whereas the ESCRT-I and -II complexes are in charge of membrane deformation into buds with cargo inside, and ESCRT-III components subsequently drive vesicle scission^{188,189}.

However, *Stuffers et al.* generated evidence that MVBs can form in the absence of ESCRTs by concomitantly inactivating proteins essential for the four different ESCRT complexes, thus an ESCRT-independent mechanism was suggested¹⁹⁰. For inward budding in these conditions, two lipid metabolism enzymes seem essential: neutral sphingomyelinase (nSMase) allowing hydrolysis of sphingomyelin into ceramide¹⁹¹, and phospholipase D2 allowing hydrolysis of phosphatidylcholine into phosphatidic acid¹⁹², although their exact role has not been fully elucidated.

Other proteins involved in this process are Rab GTPases, tetraspanins (CD9, CD81, CD63), integrins, lipids and immunomodulatory proteins^{193–195} (*Figure 10*). Different proteins, lipids, and cytosol are specifically sorted to the ILVs, though the sorting mechanism remains unknown. Some post- translational

modifications specifically reflect the vesicle localization, cellular origin and mechanism of secretion^{196–199}. Actually, ISGylation (it is a post-translational modification) of the MVB proteins such as TSG101 induces its aggregation and degradation, impairing exosome secretion²⁰⁰.

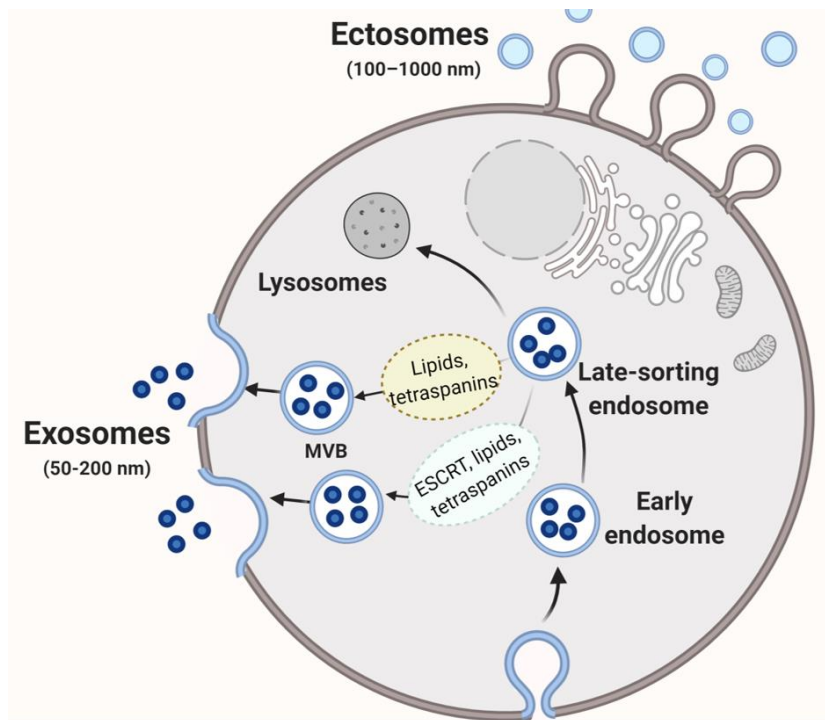


Figure 10 Extracellular vesicles. Schematic representation of the different types of membrane vesicles released by eukaryotic cells, either by direct budding from the PM, forming ectosomes or by fusion of internal MVBs with the PM, forming exosomes. The two main mechanisms of exosomes formation are shown: ESCRT- dependent and ESCRT- independent. Abbreviations: PM plasma membrane MVBs multivesicular bodies. ESCRT endosomal sorting complexes required for transport.

7.1.2. Exosomes composition

Exosomes present high variations in size, content, cell of origin and topography (e.g. from basolateral or apical cell surfaces), environmental factors, activating stimulus and functional impact on recipient cells^{201,202}, giving rise to complex heterogeneity. Their content (except for a proportion which is supposed to be randomly taken) has been suggested selectively incorporated into exosomes^{203,204} by a regulatory process that is still not clarified, so that they target to a determined cell or tissue and perform their expected function²⁰⁵.

Most studies of biochemical composition of EVs involve a bulk group of vesicles because most isolation methods give heterogeneous population (or even eliminate some subpopulations), and there are not specific exosome markers. So, the exact composition of exosomes remains unclear but in general the main cargoes include proteins, nucleic acids and lipids (*Figure 11*).

- **Proteins.** Latest studies using proteomic analysis techniques have allowed large-scales protein identification and the results are assembled in a database named *Vesiclepedia*²⁰⁶ (<http://microvesicles.org>). In a nutshell, exosomes contain two subsets of proteins, 1) dependent on cell type of origin and 2) independent of cell type (found in most exosomes and involved in EVs biogenesis) that can be used as markers (e.g. Adhesion molecules like tetraspanins -CD81 (*Cluster of Differentiation*

- 81), CD63 (*Cluster of Differentiation 63*); and CD9 (cluster of dedifferentiation 9)- or other proteins as ALIX or TGS101)^{201,207}
- **Nucleic acids.** As described before, other important exosome cargoes are nucleic acids; indeed, a wide variety of molecules may be found as mRNA, Pre-miRNA, miRNA, Y-RNA, CircRNA, mtRNA, tRNA, tsRNA, snRNA, snoRNA and piRNA. DNA strands are also potential payloads for exosomes in the form of mtDNA, dsDNA ssDNA or viral DNA²⁰⁸⁻²¹². Of note, a major breakthrough in the field of exosomes was made when it was discovered that they carry nucleic acids, in the form of miRNA and mRNA. In 2006, the presence of functional miRNA was described in murine stem cell-derived EVs and in 2007, these murine mast cell-derived EVs and RNA within them were taken up by human mast cells, proving that miRNA are exported outside the cell and can affect expression in distant cells^{213,214}.
 - **Lipids.** Regarding lipidic content, although studies are scarcer than for other components, EVs are generally enriched in sphingomyelin, cholesterol, phosphatidylserine and glycosphingolipids compared to their parent cells. In fact, exosomes present a unique sphingomyelin/phosphatidylcholine reversal ratio (3:1) compared to that normally found in human cells or plasma, which probably confers the special stability these vesicles maintain in different extracellular environments. They present lipid-rafts like subdomains with different levels of ceramide and cholesterol together with GPI-anchored proteins and flotillins

(detergent-resistant subdomains as found in the plasma membrane) that confers still more stability and could be key for improve liposomal drug delivery systems^{186,215}.

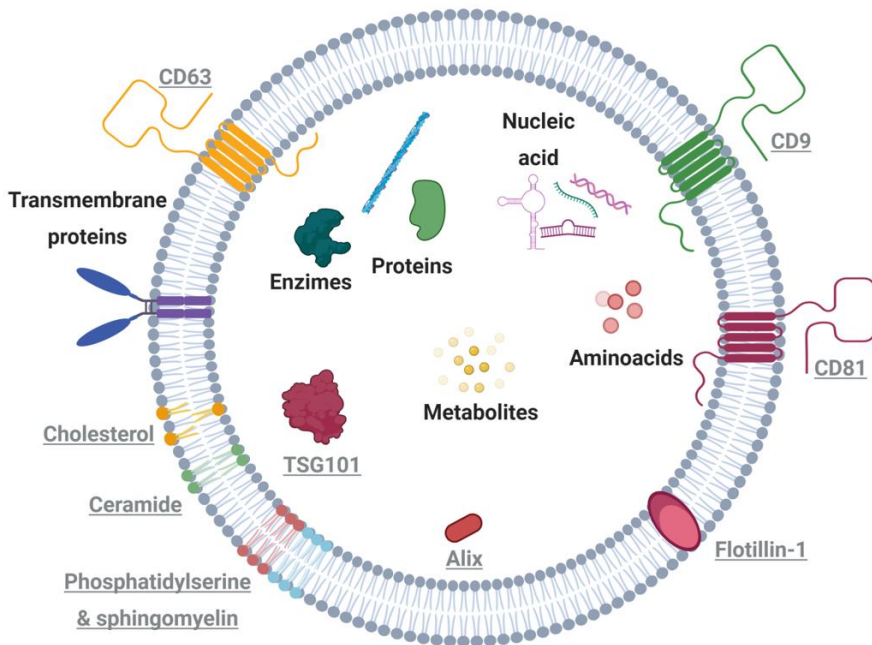


Figure 11 Exosomes' content and biomarkers. Exosome can contain different types of cell surface proteins, intracellular proteins, DNA, RNA, amino acids and metabolites. They also include proteins that are involved in their biogenesis and can be used as markers (CD81, CD9, CD63, TSG101, Alix and others)

This Thesis project, as further explained later, focus on the analysis of human urinary exosome miRNA content.

7.1.3. Exosomes secretion and internalization

Exosomes are released to the extracellular milieu by a process involving MVBs intracellular transport and posterior fusion with

the plasma membrane. Similar to the endo-lysosomal pathway (as described in section 4.1.4), Rab-GTPase proteins have been identified in this process (Rab7, Rab11, Rab27a/b, Rab35)²¹⁶, as well as several SNARE proteins (VAMP7, YKT6, SNAP23)²¹⁷.

Exosomes are found in most body fluids as blood²¹⁸, urine²¹⁹, cerebrospinal fluid²²⁰, saliva²²¹, pleural effusion²²², ascites fluid²²³, amniotic fluid, breast milk²²⁴, and bronchoalveolar lavage fluid (BALF)²²⁵. In this Thesis project we will focus on urinary extracellular vesicles, named urinary exosome-like vesicles (uEVs) (as although variable vesicles are isolated, most are exosomes) because of their potential as diagnostic biomarkers and because they can provide hints on the pathophysiology of kidney diseases, in particular Dent's Disease type 1, the focus of this Thesis project.

Once in the body fluids or extracellular medium, they travel until reaching the target cell where they will induce changes in its physiology. Surface-exposed adhesion molecules are responsible for biodistribution²²⁶. The interaction between EVs and the target cell can (1) entail a direct stimulation of downstream signalling pathways by direct interaction (without membrane fusion) of adhesion molecules and (2) exosomes can transfer their content by direct fusion with target cells¹⁷⁴ or (3) after endocytosis, cargoes are incorporated into the endo-lysosomal pathway for processing²⁰⁸. Entry of intact exosomes in the target cells can involve phagocytosis²²⁷, micropinocytosis²²⁸ and receptor-mediated endocytosis. Indeed, several classical ligand/receptor pairs have

been described each one specific to a given cellular source of EVs and a given recipient cell type^{229,230}. Endocytosis can also involve clathrin-coated pits as exemplified in neurons²³¹, cholesterol and lipid rafts in some tumoral cells²³² or caveolae-dependent endocytosis described in epithelial cells²³³. The uptake process appears to depend upon the type of recipient cell and the size of the EV²²⁶. It is unknown though whether a different mode of exosome uptake by recipient cells results in distinct localization, degradation, and/or functional outcomes of the exosome constituents once inside the cell²³⁴.

7.1.4. Function of exosomes

The physiological purpose of exosomes remains largely unknown. The first attributed purpose was to remove excess or unnecessary senescent constituents (lipids, proteins) from cells to maintain cellular homeostasis^{183,184}.

However, there is an important body of evidence that exosomes protect their content from degradation and, indeed, they carry intact nucleic acids, proteins, lipids and metabolites over distance²³⁵, so they have been suggested to have roles in intercellular signalling in a cell-selective manner²³⁶. Exosomes, as said, may directly stimulate target cells by receptor-mediated interactions or may transfer from the cell of origin to the target cells various bioactive molecules. Thus, they can affect various aspects of target cell biology, selectively inducing specific signals in recipient cells to regulate global processes such as development or

immune responses, and therefore having an important role in different pathologies. To set some examples, exosomes may play a role in mammalian reproduction and development as semen, amniotic fluid, blood, and breast milk all contain exosomes with putative function in sperm maturation, genitalia-resident immunity, and breast milk–derived immunity²³⁷. Exosomes can also influence the proliferation and activity of recipient cells of both the innate and adaptive immune system²³⁸. They have been widely studied in the context of cancer²³⁹, in metabolic and cardiovascular diseases²⁴⁰ and also in neurodegeneration²⁴¹. Altogether, currently exosomes are considered to have a more relevant role in health and disease by regulating near and long-distance intercellular communication.

7.1.5. Urinary exosomes in kidney physiology and pathology

On the basis of protein mass spectrometry (MS), urinary exosomes appear to derive from each of the epithelial cell types facing the renal tubule lumen²¹⁹ and so they can give valuable information to monitor physiological and pathological changes throughout the nephron via urine collection and analysis, which is a non-invasive procedure. Indeed, *Gonzales et al*, in an important effort, by liquid chromatography–MS/MS-based protein, accomplished a large-scale profiling of proteins present in urinary exosomes from healthy human individuals which is now publicly available

(<http://dir.nhlbi.nih.gov/papers/lkem/exosome/>) with 1160 exosome proteins¹⁹⁷. An in vitro study has shown that exosome content may transfer from renal proximal tubule cells to human distal tubule and collecting duct cells²⁴² and again, MS analysis showed that normal human urinary exosomes are enriched with innate immune proteins, including antimicrobial proteins, which potently inhibited bacterial growth and induced their lysis²⁴³.

Urinary exosomes have been already applied as diagnostic instruments in renal pathology and are being studied as therapeutic tools specially their content in miRNA, as explained below. Their protein content has also been described in some nephropathies and have given important hints on pathophysiologic processes: in polycystic kidney disease, for example, exosomes were found to cell-communicate among cilia²⁴⁴; proteomic analysis of urinary exosomes proved effective in distinguishing autosomal dominant polycystic kidney disease and medullary sponge kidney²⁴⁵.

Exosome role as therapeutic tools relies on their potential as efficient vehicles, owing to its nanosized vesicles, high permeability, less immunogenicity, non-cytotoxicity and characteristic stability. Studies to date have explored small RNAs, mRNAs, proteins, drugs and small molecules as therapeutic cargo to be loaded in EVs. None is being currently used to treat kidney pathology, yet as pointed, clinical trials are ongoing (clinicaltrials.gov)

7.1.6. Isolation of exosomes

There are various approaches available for exosomes isolation, although there is no consensus regarding which is the best methodology^{246–249}. Different isolation methodologies currently used are described below (*Figure 12*):

- I. Differential centrifugation is one of the most universally used methods. In this case, separation is based on size so large EVs collect earlier at the bottom and at lower g forces than small EVs. Therefore, sequentially increasing the centrifugal force, cells and debris are discarded after the first centrifugation steps. To get rid of possible protein aggregates, many differential centrifugation steps should be taken²⁵⁰. This method is time-consuming and so, its application in daily clinical practice is debatable.
- II. Density gradient centrifugation, where separation depends on the size and mass density. Sucrose and iodixanol are the density media most used to isolate EVs. The soluble components with a high density relative to the gradient will collect at the bottom of the tube²⁵¹. It is also a very laborious method thus unused.
- III. Size exclusion chromatography that uses a porous matrix which separates solutes according to size²⁵². This is an effective, time saving method.

- IV. Ultrafiltration, where soluble proteins and particles smaller than the size cutoff ($\approx 10^5$ kDa) are pushed through the filter and the EVs are collected at the filter²⁵³. Both methods are timesaving and could be used in every day clinical practice.
- V. Immunocapture assays use monoclonal antibodies immobilized on the surface of a plate, bead or chip to capture EVs that expose a specific ligand²⁵⁴.
- VI. Finally, precipitation is based on addition of a precipitating agent that induces clattering of EVs, non-EV particles, and soluble proteins. The clumps will sediment, a process that can be accelerated by centrifugation.²⁵⁵

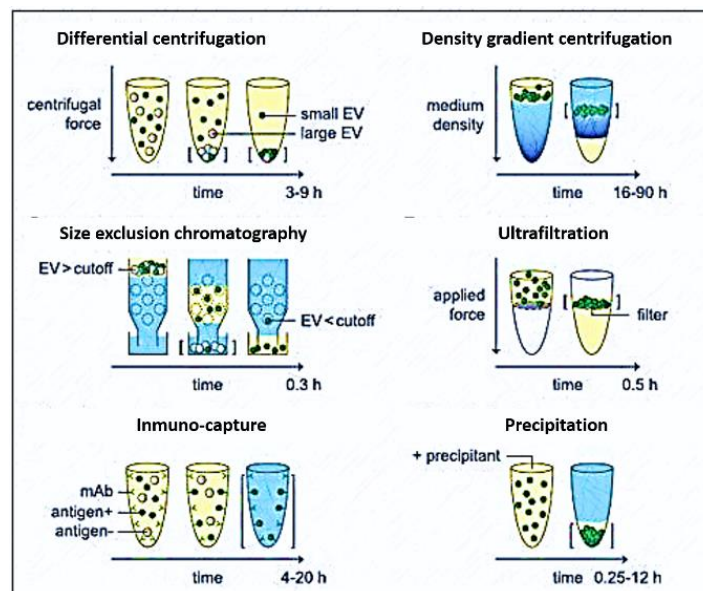


Figure 12 Different techniques for miRNA isolation. Modified from A.W. et al. 2017.

As for urinary exosomes, some considerations need to be thought before choosing the isolation method^{246,248}: 1) the concentration of

the urinary sample, as low concentration may result in reduced quantity of exosomes; 2) the amount of Tamm Horsfall (THF) protein, the most abundant protein in urine, or other type of proteinuria capable of entrapping uEVs²⁵⁶ and 3) the normalization factor, as many studies use urinary creatinine for normalisation of the exosome quantification to overcome the logistic aspect of timed urine collection, yet urinary creatinine is not a stable parameter in kidney injury^{257,258}.

7.1.7. Characterization of isolated exosomes

Regardless of the protocol used, each technique must be validated in order to confirm the identity of the purified vesicles. This requires the use of a combination of some methods to determine exosomes morphological, biochemical, and physical features as described below:

1) Shape. Exosomes shape is frequently checked by cryo-Electron microscopy (cryo-EM). By using this technique samples are vitrified in liquid ethane to prevent the formation of ice crystals that can alter the ultrastructure of cells and membranes. EVs as observed by cryo-EM have a round shape^{259,260} 2) Size. Nanoparticle Tracking Analysis (NTA) has been designed to measure the size, distribution and concentration of nanoparticles²⁶¹. It tracks the movement of laser-illuminated individual particles under Brownian motion and then calculates their diameter using statistical methods.

3) Markers. Exosomes may be identified by detecting EVs-specific markers (see Figure 12). Only a few membrane proteins, CD81 and TSG101, are deemed to be specific of smaller EVs (so they can more specifically detect exosomes, but not exclusively). Other markers, previously thought to be exosome specific, such as membrane proteins CD9 and apoptosis-linked gene 2-interacting protein X (ALIX) might also be found on larger EVs. Other proteins are often used as markers, although not specific either, like tetraspanins (CD9, CD63 and CD82), major histocompatibility complex (MHC) molecules and cytosolic proteins such as specific stress proteins (e.g. heat shock proteins; HSPs) and the Endosomal Sorting Complex Required for Transport (ESCRT)^{246,262}.

8. MicroRNAs (miRNA)

8.1. MiRNA definition and discovery

MicroRNAs (miRNA) are small non-coding, endogenous, single-stranded RNA molecules (19–25 nucleotides in length) that regulate gene expression by blocking the translation of mRNAs into proteins.

miRNA were first discovered in *C. elegans*, almost three decades ago^{123,263,264}. In 2006, the Nobel Prize in Physiology or Medicine was jointly given to Dr. Fire and Dr. Mello for their discovery, in 1998, of the mRNA expression silencing mechanism by small interfering RNA molecules (today known as the action mechanism of miRNA)²⁶⁵. The first evidence for miRNA involvement in disease

arose in 2002 when studies by Dr. Croce's group discovered that mutations in a region of the Chromosome 13, which encodes two miRNA, miR-15a/16-1 c, were involved in chronic lymphocytic leukemia²⁶⁶

According to miRbase (the first and largest database of miRNA) latest version (v22, <http://www.mirbase.org>), 2654 mature miRNA have been identified so far, composing the human miRNAome.

In the cell, miRNA regulate gene expression at the post-transcriptional level through specific recognition of short sequences of the target mRNAs leading to their degradation or translation repression^{267,268}. The complementarity between miRNA and mRNA does not need to be perfect for translational inhibition, in fact one miRNA regulates several hundred mRNAs and one mRNA is regulated by several miRNA²⁶⁹. Significantly, it is estimated that over 50% of all protein coding genes are regulated by miRNA in mammals²⁷⁰ revealing their overall involvement in diverse physiological as well as pathological processes²⁷¹⁻²⁷³ miRNA can also be actively secreted into the extracellular microenvironment or into body fluids and either be transported by RNA-binding proteins (Argonaute 3, nucleophosmin 1)²⁷⁴ or imbedded in EVs and transported to their targeted tissue or cells, protected from RNAases²⁷⁵. miRNA can be found in at least twelve different body fluids including serum/plasma, milk, colostrum, saliva, seminal fluid, tears, urine, amniotic fluid, bronchial lavage, cerebrospinal fluid, pleural fluid, and peritoneal fluid²⁷⁶. The abundance of miRNA might be different between fluids; for

example, in serum there is a higher abundance than in urine, probably because of a higher RNAase activity in the urine²⁷⁷. Extracellular miRNA are very stable and resistant to degradation even with long-time storage at room temperature, pH variability and multiple freeze-thaw cycles²⁷⁸.

As extensively reviewed, miRNA are involved in many biological processes including cell proliferation, cell differentiation and apoptosis^{279,280}. They are known as important players in development and growth^{281,282} as well as in other physiological functions such as immune system regulation²⁸³, angiogenesis²⁸⁴, pregnancy²⁸⁵ or senescence²⁸⁶. In addition, miRNA exhibit tissue and cell-type specific expression patterns²⁸⁷, which can be altered in disease, malignancy and cell stress²⁸⁸. Thus, aberrant expression of miRNA is causally related to a variety of diseases such as cancer, diabetic nephropathy and heart failure^{289–293}. As their profiles reflect pathological processes, miRNA have been proved valuable as diagnostic as well as prognostic biomarkers in several diseases^{294,295}. Though not still implemented in current clinical practice, research efforts are trying to identify and make their isolation, analysis and interpretation simpler and cheaper for them to be used in daily medical exercise^{296,297} as extensively explained below.

8.2. Biogenesis of miRNA

Genes encoding miRNA are located in non-coding DNA regions, frequently organized in clusters (canonical pathway) or in introns of protein-coding genes (miRtrons) and are co-transcribed with the host gene (mirtron pathway)²⁹⁸. In the nucleus, miRNA are transcribed by RNA polymerase II as primary miRNA (pri-miRNA), long capped and polyadenylated hairpin transcripts. The ribonuclease III (RNase III) enzyme Drosha together with DGR8, which guides the position of Drosha (Drosha/DGCR8 complex), form the precursor miRNA (pre-miRNA) by cleaving the flanks of pri-miRNA to liberate ~70 nucleotide stem-loop structures, known as pre-miRNA. pre-miRNA are then moved from the nucleus to the cytoplasm by the protein Exportin 5 in a Ran-GTP dependent manner. In the cytoplasm the protein DICER together with the RNA-binding protein TRBP²⁹⁹ cleaves the pre-miRNA and produces a double stranded RNA molecule of approximately 22 nucleotides. One strand will serve as the mature miRNA (18 - 22 nt length), while the other (called minor, passenger or depicted with a star symbol (miRNA*)), in most cases, is degraded. Mature miRNA then binds to a protein complex including Argonaut 2 (AGO2), forming the so-called RNA-induced silencing complex RISC. RISC complex, together with other regulating factors, leads the miRNA to the mRNA target. Nucleotides in positions 2-8, called the seed sequence, are essential for pairing with the target mRNA. If miRNA bind perfectly to the mRNAs, they induce degradation of the

mRNA. If the binding is imperfect, the miRNA represses translation of the mRNA (Figure 13).^{267,300}.

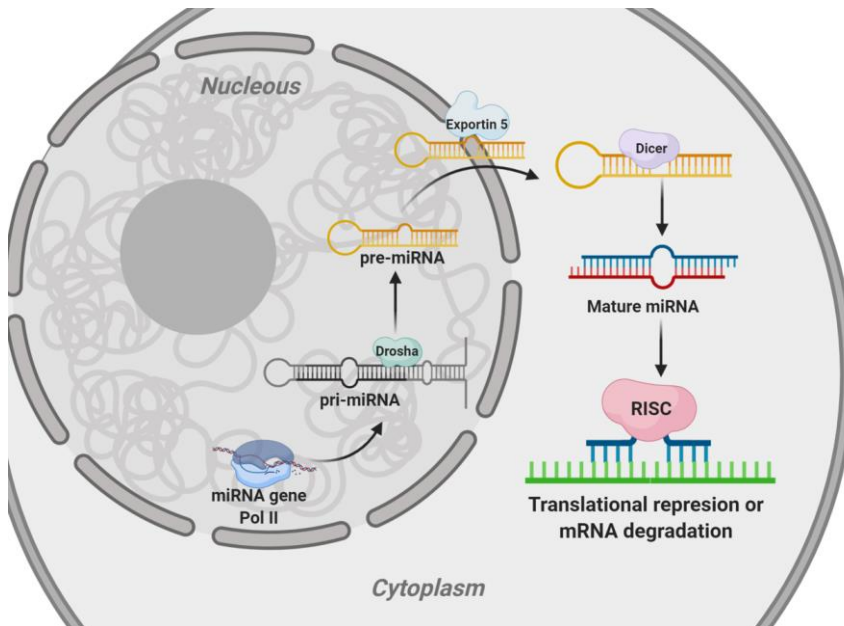


Figure 13 miRNA biogenesis. In the nucleus, miRNA are transcribed by RNA polymerase II as primary miRNA (pri-miRNA). Pri-miRNA is processed by the RNase III endonuclease, Drosha, and its cofactor, Dgcr8 into smaller stem-looped structures known as precursor miRNA (pre-miRNA). Pre-miRNA are exported out of the nucleus by Exportin 5 into the cytosol, where a second RNase III enzyme, Dicer, leads to the generation of mature miRNA. The mature miRNA associates with the miRNA-induced silencing complex (RISC) which leads the miRNA to the mRNA target, so that miRNA can degrade mRNA.

8.3. Annotation of miRNA

miRNA are designated as miR followed by a sequentially assigned number, and similar sequences are usually given suffixes, letters and numbers. Lin-4 and let-7 (lethal-7) are an exception for historical reasons and maintain their original names³⁰¹ (Figure 14).

miRNA annotation follow these rules:

- The three letters in front of the miR represents the species in which a particular miRNA is observed; e.g. hsa (homo-sapiens).
- mir and miR: a small (r) represents the pre- miRNA while the (R) represents the mature miRNA, e.g. mir-29 is the precursor miRNA-29 and miR-200 the mature of miRNA-200.
- If the miRNA share the same seed, sequence of 2-8 nucleotides, they are derived from the same precursor and belong to the same cluster generating a miRNA family; e.g. the mir-15 family consists of miR-15a and miR-15b sequences.
- The same miRNA in different species receives the same number to preserve homology e.g. hsa-miR-16-5p (human) is the ortholog of mmu- miR-16-5p (mouse).
- Mature miRNA can derive from either arm of the pre-miRNA and so the suffix -5p or -3p is added to define from which arm of the pre-miRNA the mature miRNA is originating.
- Sequences with one or 2 different nucleotides are assigned with the same number but an additional letter to distinguish, e.g. hsa-miR-200a and hsa-miR-200b.
- The accession number of each miRNA is the only unique identifier.

- If the same miRNA is found in different loci of a chromosome, the difference is indicated from the pre-miRNA level, a number is added to distinguish them; e.g. hsa-mir-200-1 and hsa- mir-200-2.

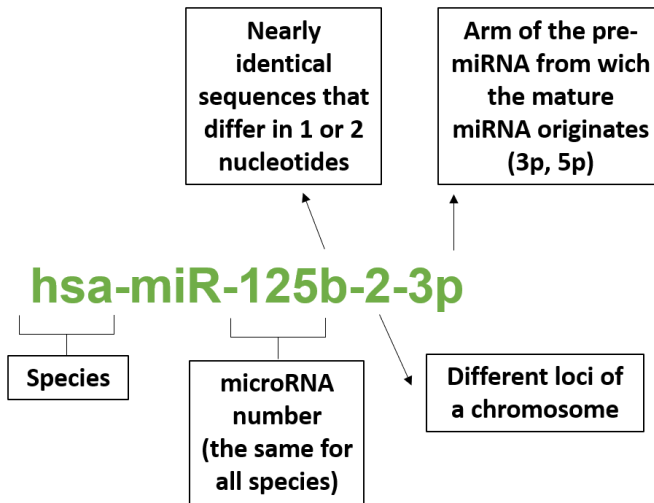


Figure 14 miRNA annotation

8.4. Techniques for quantification of miRNA

Several techniques are used to detect and quantify miRNA expression and can be mainly classified according to the platform used. Northern blotting was the technique used to identify the very first miRNA³⁰² while many more techniques have been developed and used afterwards (Table 2)^{302,303}.

Several parameters are to be considered when choosing the method of detection: sensitivity, amount of RNA needed, the number of initial samples, cost, time to results and data

processing. These techniques must overcome some challenges inherent to miRNA: short sequence length, low abundance of target molecules (mature miRNA molecules are very short and their prevalence in total RNA is also very low), and sequence homology between miRNA (many different miRNA belong to families sharing similar sequences differing by as little as a single nucleotide).

Table 2 miRNA quantification techniques

| | Methods | Advantatges | Disadvantatgees | Detection range |
|-----------------------------------|---|--|--|-----------------|
| Northern blotting | Visualisation of miRNA with fluorescent/ radiolabeled probes complementary to the target miRNA | -Widely used method -Good specificity -Quantitative detection of mature miRNA, primary miRNA and precursor miRNA and miRNA complexes with Drosha, DICER and RISC | -Poor sensitivity -Time-consuming -Large amount of RNA sample required -Multiple handling steps -Low throughput | Nano- molar |
| RT-qPCR | miRNA are converted to complementary DNAs generating cDNA followed by PCR amplification with specific primers to target miRNA of interest. | -Sensitivity, - Specificity -Quantitative High accuracy -Reproducibility -Simplicity -Fast -Small amount of RNA sample needed | -Lack of standardized normalization molecules, -Depends on purity and quality of RNA input, -Demanding design of the primers to deal with the small miRNA size | Femto- molar |
| Microarray | Based on nucleic acid hybridization between target molecules and their corresponding complementary probe immobilized on to miRNA microarray chip and detection via fluorescence | -Suitable for comparison between two conditions -High-throughput miRNA profiling -Test multiple samples simultaneously -Easy, straightforward | -Prefixed probes - Not possible to detect new molecules, -Hybridization bias, -Semi-quantitative method -Low sensitivity -Low specificity | Femto- molar |
| Next generation sequencing | Direct detection and identification of miRNA in total RNA from tissue and cells High-throughput miRNA profiling | -Transcriptome-wide profile of microRNAs in any species, of any size, known and unknown -Highly sensitive and specific | -Costly -Time consuming -Complicated analysis of data | Femto- molar |
| Electrochemical detection | Oxidation of miRNA-ligated nanoparticles | -High-sensitivity -Quantitative -Direct detection of miRNA in total | -Detection of miRNA in vivo -Requirement of sophisticated instruments | Femto- molar |
| Biosensor Techniques | A bio-recognition element (a DNA probe complementary to the miRNA of interest) is in direct contact with a transduction element | -High sensitivity, -Very fast, | -Hybridization bias -Not useful for multiplexing -Mass transfer challenge -Reliability of measurements | Pico- molar |
| Surface plasmon resonance imaging | Combination of surface poly-(A) enzyme chemistry and gold nanoparticle-amplified SPR measurements to detect multiple miRNAs | -Excellent sensitivity -High-throughput quantification -Suitable for expression profiling | -Costly -Requires sophisticated readout system Elaborated analysis | Atto- molar |

8.5. miRNA data processing and molecular integration

One of the most challenging issues to face when studying miRNA for clinical and other applications is the fact that miRNA can control up to hundreds of mRNA, both in physiological and pathological conditions³⁰⁴. It is essential to identify the targets of miRNA and restrict the options to the most relevant to a specific aim. Various bioinformatics approaches have been taken to create web-tools that predict possible miRNA targets through different algorithms. The parameters these web-tools consider are: 1) complementarity of the first 2-8 nucleotides of a miRNA in the 5'-end to the 3'-UTR (seed region) of the mRNA target, 2) seed region conservation through species, 3) thermodynamic stability, the higher the free energy (Gibbs energy) of mRNA the more stable the complex and more possible the binding of miRNA, and 4) the number of possible binding sites a mRNA has for a specific miRNA³⁰⁵⁻³⁰⁷.

Complementary to the prediction tools are the databases that contain information on experimentally validated miRNA targets³⁰⁸⁻³¹⁰.

8.6. In vitro validation of miRNA target.

Currently, in vitro studies are the gold standard for validating predicted miRNA targets. The aim of the in vitro studies is to monitor any changes of the target gene's expression in response to

loss or gain of function of the specific miRNA. This is accomplished mainly through artificial manipulation of the miRNA concentration with either the use of double stranded miRNA mimics or miRNA inhibitors (antagomirs). miRNA mimics are artificial, chemically modified miRNA-like small RNAs with the ability to mimic the function of a miRNA guide strand while bypassing the maturation steps of Drosha and DICER and causing a rapid decrease in the expression of the potential target mRNA³¹¹. On the other hand, antagomirs act by binding to mature miRNA, blocking their activity, hence leading to the increased expression of the mRNA target³¹². The interactions of miRNA with their target genes are depicted in figure 15³¹³.

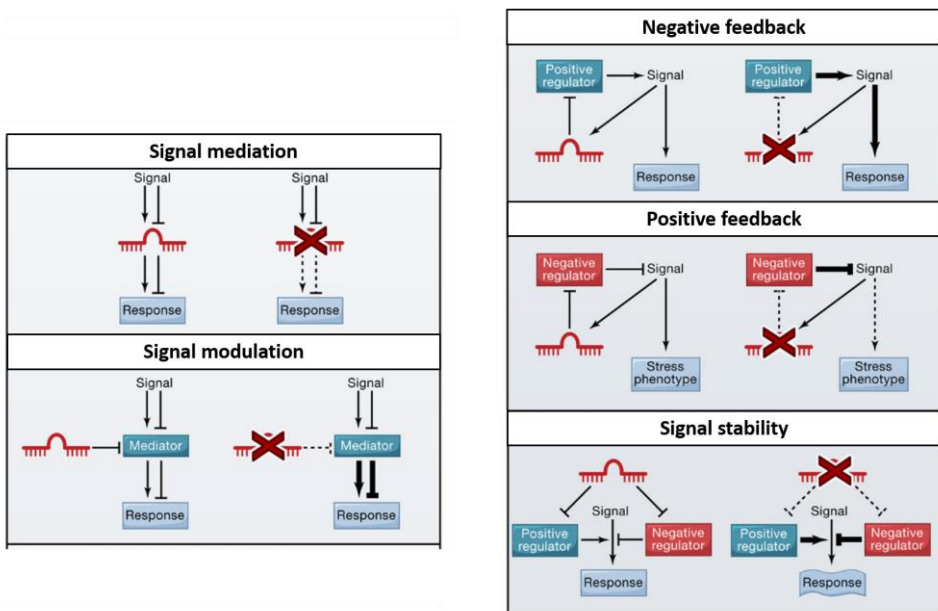


Figure 15 Different responses from the interaction of miRNA with their target mRNA. mRNA are depicted as a red strand, miRNA as a red cross. Adapted from Mendell et al.

8.7. miRNA and the kidney

Several studies have demonstrated miRNA involvement in kidney development, physiology and pathology²³⁴. In summary, these studies indicate that miR-146a, miR-886, miR-192, miR-194, miR204, miR-215 and miR-216 are renal-specific microRNAs³¹⁴. In addition, let-7a-g, miR-196a/b, miR-10a/b, miR-130, miR146, miR-21, miR-200a, miR-30a-e and miR-872 are highly expressed in renal tissue^{315–317}.

miRNA are important for kidney from early development. As shown by *Nagalakshmi et al.*, a selective ablation of DICER within nephron progenitors (model with no mature miRNA formation) results in apoptosis and early termination of nephrogenesis³¹⁸. For instance, miR-30 and mir-200 families are involved in the nephron development and glomerular integrity^{225,319}.

Besides, miRNA are key for renal normal function and homeostasis. Some kidney functions such as electrolyte balance, ion transport, acid-base homeostasis and blood pressure regulation may be controlled by miRNA; for example regulation of water re-absorption, mediated by aquaporins³²⁰ is predicted to be highly influenced by miRNA, yet only miR-320 has been experimentally validated^{321,322}; miR-200 and miR-717 have been experimentally connected to tonicity, so that exposure of kidney cells to high NaCl causes their downregulation allowing cells to adapt³²³. As for fluid and electrolyte balance, miR-192 has been shown to target the $\beta 1$ subunit of the Na^+/K^+ -ATPase so it negatively affects the enzyme

activity, contributing to renal handling of fluid unbalance³¹⁹. Control of blood pressure, mediated by the renin-angiotensin-aldosterone system (RAS), is another of Kidney key functions. The important role of miRNA in this process was demonstrated by a recent study in which *Sequeria-Lopez et al.*, by applying a conditional deletion of DICER, caused a downregulation of the renin genes, a decrease in renin production and consequently a drop in mice blood pressure³²⁴.

Regarding miRNA involved in nephropathologies, significant variations in urinary miRNA have been associated to different chronic kidney disease (CKD) etiologies including diabetic glomerulosclerosis (decrease of miR-15), IgA nephropathy (increase in miR-17 levels) and hypertensive nephrosclerosis (increase of miR-21 and miR-216a)³²⁵. Interestingly, miRNA known to be associated to renal fibrosis, including miR-192, miR-29a, miR-29b, miR-29c, miR-200a, miR-200b and miR-200c, displayed reduced in urine of CKD patient³²⁵. In contrast, miR-21 is considered as a pro-fibrotic miRNA with increased urinary abundance in renal fibrosis³²⁶.

Figure 16 shows a summary of some of those miRNA experimentally assessed so far³¹⁴.

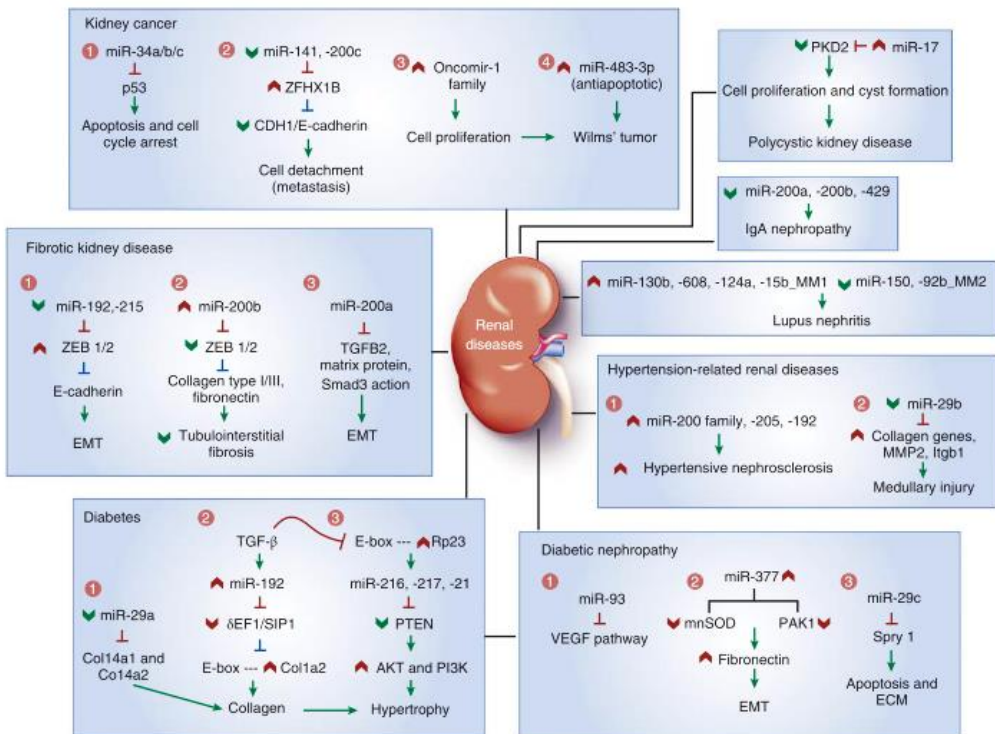


Figure 16 miRNA in kidney disease. MicroRNAs (miR) in renal diseases. Possible miRNA-regulatory networks involved in renal pathophysiology as described in text are shown. Col1, collagen type 1; ECM, extracellular matrix; δ EF1, delta 1–crystallin enhancer binding; EMT, epithelial–mesenchymal transition; Ig, immunoglobulin; Itgb1, integrin beta 1; miRNA, microRNA; MMP2, matrix metalloproteinase 2; mnSOD, manganese superoxide dismutase; PI3K, phosphoinositide kinase-3; PKD, polycystic kidney disease; PTEN, phosphatase and tensin homolog; SIP1, smad-interacting protein; TGF- β , transforming growth factor beta; VEGF, vascular endothelial growth factor; ZEB, zinc finger E-box-binding homeobox. Adapted from Chandrasekaran et al.,2012

8.8. Use in diagnosis and treatment

Referring to the FDA’s description of an ideal biomarker, extracellular miRNA fit all the criteria: 1) easy accessibility in diverse body fluids, 2) stability, 3) conservation across species, 4) association with particular tissues or pathological states and 5) a

sensitive measurement method.³²⁷ Due to these unique features, miRNA have shown great potential as non-invasive biomarkers. Several lines of research aimed at improving common CKD diagnostic tools and avoiding invasive kidney biopsies; thus, circulating miRNA have been identified as possible diagnostic and even prognostic biomarkers of kidney disease^{328,329}.

To date, there are 670 on-going clinical trials studying miRNA as biomarkers (clinicaltrials.gov, 2020); several of these miRNA being also associated with kidney diseases like autosomal dominant polycystic kidney disease (ADPKD), renal transplantation, renal cell carcinoma and acute kidney injury (AKI) after cardiac surgery, yet none of them is being used in daily basis clinicaltrials.gov, 2020.

As for therapeutics, it is based on two main kinds of molecules: miRNA mimics and antagomir; miRNA inhibition or delivery may provide a highly potent means to modulate a disease process while avoiding unwanted toxic effects in normal tissues. On the basis of the increasing interest in miRNA therapeutics, it is a promising future tool. Importantly, there is an on-going clinical trial of a new molecule aimed to inhibit miR-21 in Alport Syndrome³³⁰.

HYPOTHESIS

We hypothesize that understanding the molecular processes involved in Dent's Disease type 1 physiopathology that contribute to its different phenotypic manifestations, together with analysing uEVs miRNAs of DD1 patients, will provide novel diagnostic biomarkers of the disease and its different clinical expression.

OBJECTIVES

General objective

The main objective of this thesis is to identify new prognostic biomarkers for DD1 and to generate a good cellular model of the disease to understand the molecular and cellular processes underlying CIC-5 mutations and leading to disease.

Specific objectives

Herein specific aims of this doctoral thesis are:

1. To study a large European cohort of DD1 patients in order to estimate the prevalence of the disease, to evaluate the gene mutation spectrum and different clinical features, and to review the different management strategies in our country.
2. To establish a uEVs microRNA signature for Dent's Disease type 1. We expect these miRNA to lead to the identification of novel processes participating in the disease. Moreover, these miRNA could be used as potential biomarkers related to different phenotypes of the disease and its progression.
3. To characterise novel DD1 cellular models of the disease for *in vitro* testing of the pathways involved in DD1 pathophysiology and potential future drugs.

MATERIALS AND METHODS



1. European survey

1.1. Survey setting and study design

We developed a 46-item web-based cross-sectional survey using the online tool SurveyMonkey (SurveyMonkey.com). The survey contained multiple-choice and open-ended, non-mandatory questions, divided into five sections: patients' socio-demographic and anthropometric data; diagnosis; patients' current clinical evaluation; patients' current blood/urinary biochemistry parameters and management. A list of all questions is provided in *Annex 2*.

The sampling frame was the membership list of ERKnet (Rare Kidney Disease Reference Network), the groups on inherited kidney diseases and inherited renal disorders from the ERA-EDTA (European Renal Association-European Dialysis and Transplant Association), the ESPN (European Society for Paediatric Nephrology), the AENP (Asociación Española de Nefrología Pediátrica) and the SEN (Sociedad Española de Nefrología) together with data was occasionally obtained from RenalTube, a research platform aimed to gather clinical and molecular information of patients with a rare tubulopathy³³¹. Most of the potential respondents received an initial email and eight weeks later, a subsequent reminder including an electronic link to the questionnaire that was available online from July 2019 to May

2020. Survey responses were anonymously collected and stored electronically by the survey service until further analysis. Few possible respondents received the form by regular mail. Data were deemed adequate for analysis if more than 50% of the items were completed.

1.2. Patients

One hundred thirty-five patients with DD1 were reported. Those patients without a documented *CLCN5* mutation were excluded. We also exclude those patients for whom the registers were incomplete.

Clinical and biochemical data both at diagnosis and at last follow-up were collected. Regarding the last follow-up data, only patients who did not need renal replacement therapy were considered. Data of some patients had been previously reported^{332,333}.

1.2.1. Patient's growth

We assessed patient growth by adjusted Z-score estimation using reference growth data from the World Health Organization³³⁴. Cut-off values of ± 2 standard deviations, which correspond to 2.5nd and 97.5th percentile were used to define abnormal growth or failure to thrive considering insufficient weight-for-age and length/height-for-age.

1.2.2. Kidney function

Estimated glomerular filtration rate (eGFR) was calculated using the modified Schwartz formula for children³³⁵ and the Chronic Kidney Disease-Epidemiology Collaboration (CKD-EPI) formula for adults (>18 years)³³⁶. Last eGFR value was imputed for 8 patients after starting renal replacement therapy.

1.2.3. Hypercalciuria, nephrocalcinosis and nephrolithiasis

Hypercalciuria was defined as a urinary calcium/creatinine ratio result above upper limit of normality for age range³³⁷. Data on nephrocalcinosis and nephrolithiasis were provided by the clinicians in charge and reflect the local imaging protocols and interpretation. Calcemia and phosphoremia values were considered according to age rang^{338,339}.

1.3 Statistical analyses for survey responses

Data are shown as frequencies (percentages) for categorical variables. Continuous variables are presented as means \pm standard deviations (SD) for normally distributed variables, according to Kolmogorov-Smirnov/ Shapiro-Wilk test and as median (interquartile range (IQR)) if non-normally distributed. Continuous variables were analysed by t-test or U-Mann Whitman; binary and

categorical variables by chi-square or Fisher exact test, depending on group size.

Because the participant did not answer all questions, the percentage of respondents providing a given answer was calculated individually for each question, using the number of respondents to that question in the denominator. A p value <0.05 was considered statistically significant. Statistical analysis was performed using SPSS V 21.0 (SPSS Inc., Chicago, IL) and graphs were performed using GraphPad Prism v 8.0 (GraphPad Software, San Diego, California USA).

2. miRNA signature in uEVs from DD1 patients

2.1. Patients and samples

The Spanish nephrologists responding to the European survey were further contacted to participate in this part of the study (*see Annex 3*) Thus, urine samples from 25 male patients with DD1 were collected at different hospitals in Spain to be individually processed at Hospital Universitari Vall d'Hebrón (Barcelona, Spain). Clinical and genetic data from these patients was either provided by their nephrologist from clinical records or from the RENALTUBE Spanish Registry (www.renal-tube.com) were most of the patients are included. Healthy donors were used as controls (n = 10).

The study was ethically approved by Vall d'Hebrón Hospital Ethics Committee and all patients or their parents provided written

informed consent prior inclusion (*see Annex 4*) after receiving descriptive information of the project. (*see Annex 5*)

Estimated glomerular filtration rate (eGFR) was calculated using the chronic kidney disease epidemiology collaboration (CKD-EPI) formula³⁴⁰

Urine samples were collected in sterile recipients and stored at 4°C for a maximum of 36 hours until processing. A urinalysis using a dipstick was performed to every sample to exclude urinary tract infection.

2.2. Urinary exosome isolation

Urinary exosome isolation was performed according to the protocol detailed below:

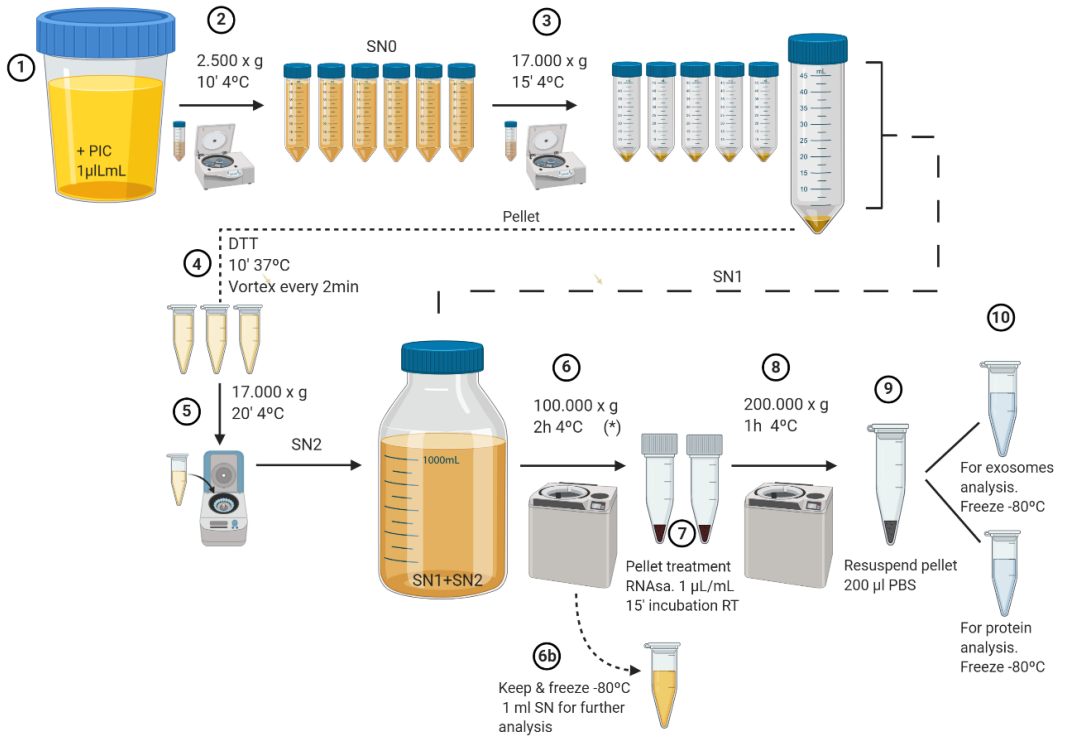


Figure 17 uEVs extraction by differential ultracentrifugation

1. Urine sample (400 mL) was transferred from sterile recipients into falcon tubes and protease inhibitor cocktail (PIC) (#S8820 Sigma-Aldrich, Darmstadt, DE) was added to the sample at concentration [1 µL/mL].
2. Samples were centrifuged for 10 min at 2,500 × g at 4°C to remove cell debris. Collection and mixture of all samples' supernatants were performed. Supernatants mixture was transferred to a bottle on ice (SN0) (not shown in the picture) and pellets were removed.
3. SN0 was transferred into tubes and centrifuged 15 min at 17,000 x g (4°C) to pull down cell fragments. Supernatant (SN1)

was transferred to a bottle on ice. Pellets were transferred to tubes and treated with DTT (#A2948 AppliChem, Barcelona, ES) [200 mg/ mL] at 37 °C for 10 min and vortexed every 2 min. This step was meant to depolymerase the Tamm Horsfall protein network.

4. Tubes containing the pellets were centrifuged 20 min at 16,000 x g at 4°C. Pellets were removed and SN2 obtained. SN1 and SN2 were mixed in a bottle on ice.

5. SN1+SN2 was transferred to ultracentrifuge tubes (36 mL). Ultracentrifugation for 2 hours at 100,000 x g at 4°C was performed; this step was repeated to have all the urine ultracentrifuged.

6. To discard the extravesicular RNA, pellets were treated with RNAase 1µL/mL (#158924, Qiagen) and incubated at room temperature (RT) for 15 minutes.

6b. 1mL of the exosome-depleted supernatant was kept for further analysis.

7. After resuspending the pellets with the remaining supernatant, they underwent the last ultracentrifugation at 200,000 × g for 1 h at 4°C.

8. Supernatant was removed and pellet was resuspended with 200 µL cold pre-filtered PBS (0.22 µm pore size).

9. We kept the processed sample at -80°C in two tubes: 30 µL for protein analysis, 170 µL for exosome analysis.

2.3. Characterization of uEVs

To validate the exosome purification protocol, urinary exosome morphology, shape and size were characterized by three methods²⁴⁶: Nanoparticle Tracking Analysis (NTA), Cryogenic Transmission Electron Microscopy (cryo-TEM) and immunoblotting techniques.

2.3.1. Nanoparticle tracking analysis (NTA)

Nanoparticle tracking analysis (NTA) combines the properties of both laser light scattering microscopy and Brownian motion to quantify and obtain size distributions – within limit range 10 - 2.000 nm - of particles in liquid suspension. The NTA software enables sizing of single particles by tracking their mean squared displacement and thereby calculating their theoretical hydrodynamic diameter using the Stokes Einstein equation³⁴¹. NTA also allows for an estimation of particle concentration knowing the analysed sample volume.

NTA was performed using NanoSight NS300 (Malvern Instruments, UK), registered using high sensitivity camera and analysed using NTA software v3.1 (NanoSight Ltd., Malvern Instruments, UK) at ICMAB-CSIC (Institut de Ciència de Materials de Barcelona) at Universitat Autònoma de Barcelona, Spain. Five microliters of 12 uEVs samples were randomly taken for further analysis. They were diluted in PBS 1x to optimal concentrations according to manufacturer's protocol. Other settings, such as blur, minimum track length and minimum expected size were set to automatic.

Each measure was carried out in triplicates of 60 s recordings at 25 frames per second at room temperature; the triplicate measures were averaged³⁴². As said, uEVs quantification was normalised to the total initial urine volume.

2.3.2. Cryogenic Transmission Electron Microscopy (Cryo-TEM)

Cryogenic Transmission Electron Microscopy (Cryo-TEM) was performed at the Microscopy Facility of Universitat Autònoma de Barcelona, Spain. The cryo-electron microscope *JEOL JEM-2011* (JEOL Ltd. Tokyo, Japan) together with Leica EM CPC Cryoworkstation (Leica Biosystems. Nussloch· Germany) were used. Cryo-TEM is used for direct visualization of vesicles without the addition of any heavy metals or fixatives, which might cause artefacts. The sample is frozen so rapidly that the water vitrifies forming no ordered crystals, and the native structure of the sample is preserved.

Ten microliters of uEVs diluted in PBS 1x were applied on to the carbon side of *QUANTIFOIL® Holey Carbon 400* (Electron Microscopy Science, ^{Hatfield, PA. USA}) EM grids. The preparation was placed inside the cry workstation Leica *EM CPC* and plunge-frozen into the precooled liquid ethane at -179 °C to vitrify the sample. Samples were visualized and analysed on the transmission electron microscope at an accelerating voltage of 200 kV.

2.3.3. Immunoblotting

For more detailed explanation see section 3.4, Materials and Methods)

2.3.4. Exosome protein extraction

Thirty microliters of uEVs suspensions were treated with lysis buffer RIPA (*Radioimmunoprecipitation assay buffer, table 3*) 2x. PIC (*protease inhibitor cocktail*) (1:100) (#S8820 Sigma-Aldrich, St Louis, Missouri, US), Na₃Vo₄ (1:100) (#S6508, Sigma-Aldrich) and NaF (#S7920, Sigma-Aldrich) (1:500) were also added. The samples mixed with the lysis buffer were shaking for 1h at 4 °C, sonicated at maximum amplitude 5 cycles of 10 s and finally centrifuged at 13,000 × g for 15 min at 4 °C. Supernatants were collected.

Table 3 Components of RIPA lysis buffer

| Component | Final concentration |
|---------------------------------------|----------------------------|
| NaCl (#PA146994, Panreac) | 300 mM |
| EDTA (#ED2SS, Sigma-Aldrich) pH 8,0 | 2 mM |
| Tris-HCl pH 7,5 (#A2264, Panreac) | 100 mM |
| NP-40 (#74385, Sigma-Aldrich), | 2% |
| Sodium deoxycholate (#106504, Merck), | 1% |
| SDS (#A2572, Panreac). | 0.2% |

2.3.5. Western blotting

Thirty microliters of uEVs lysates were mixed with Laemmli sample buffer 1:1 (Tris–HCl pH 6.8 0.3 M, SDS 10%, glycerol 5%, β -mercaptoethanol 2%, bromophenol blue 0.01%) and loaded onto 10% and 15% acrylamide gel (for composition see table 10 in section 3.4.3 of Materials and Methods) together with the molecular weight marker and ran at 100–150 V for 1-2 h. Proteins were transferred to a PVDF 0.2 μ m membrane (Immobilon-PSQ) (#ISEQ00010 Millipore, Darmstadt, DE) at 100 V for 1 h. Membranes were blocked using 5% non-fat dry milk diluted in PBS-T (PBS 1 \times , Tween-20) for one hour and incubated overnight with specific primary antibodies, against the target protein (see table 4 below) and finally incubate for 1 hour at room temperature with secondary antibodies coupled with a horseradish peroxidase (HRP) (see table 4).

Table 4 Primary and secondary antibodies used for exosome and non-exosome protein detection

| Antibody | Species | Epitop | Solution | Dilution factor | Reference |
|---------------------------|-------------------|---------------|--------------------------------------|------------------------|---|
| Primary antibodies | | | | | |
| Anti-TSG101 | Mouse monoclonal | 167-374 | 5% non-fat dry milk diluted in PBS-T | 1:500 | #Ab83 (Abcam Cambridge, UK) |
| Anti-CD81 | Rabbit monoclonal | 90-210 | | 1:1000 | #sc-166028; (Santa Cruz, Dallas, Texas, US) |

| | | | | |
|-----------------------------|----------------------------------|--------|--------|--|
| Anti-GRP78 | Rabbit polyclonal | C-term | 1:1000 | #Ab21685 (Abcam Cambridge, UK) |
| Secondary antibodies | | | | |
| Anti-Mouse | Rabbit Anti-Mouse Antibody | Ig/HRP | 1:5000 | #P0260; Dako, Agilent (Santa Clara, US) |
| Anti-Rabbit | Goat Anti-Rabbit Ig/HRP Antibody | | 1:5000 | #P0448; Dako,, Agilent (Santa Clara, US) |

After these processes, 3-5 washes with PBS -Tween were made. Membranes were incubated with *HRP Immobilon Forte* (#WBLUF0100, Merck™) for 5 minutes and imaged using *Odyssey® Fc Imaging System* (LI-COR Biosciences).

Supernatants from uEVs precipitation step, were included as control to demonstrate that no exosome particles remained in those supernatants.

2.4. RNA processing and analysis

2.4.1. RNA extraction and quantification

One hundred microliters of exosome suspension from each sample in the study cohort were used for RNA extraction. RNA was isolated using *miRNeasy Mini kit* (#217004, Qiagen, Hilden, Germany) according to the manufacturer's instructions.

RNA quantification was performed with the device *BioAnalyzer 2100* (#G2939BA, Agilent Technologies, Santa Clara, CA, USA) in conjunction with a chip for RNA quantification and size assessment. This bio-analytical device is based on a combination of microfluidic chips, voltage-induced size separation in gel filled channels and laser-induced fluorescence detection. Fluorescence correlates with the amount of RNA of a given size. The chip used was RNA 6000 Pico LabChip kit (#5067- 1513, Agilent Technologies, Santa Clara, CA, USA), which is used for analysis of RNA samples of limited abundance down to 50 pg/ μ L of total RNA.

One microliter per sample was analysed by each chip and the results were obtained with the *2100 Expert Software* and plotted in electropherogram.

2.4.2. Reverse transcription and qPCR

After exosome RNA extraction, total RNA was reverse transcribed using the TaqMan[®] Advanced miRNA cDNA Synthesis Kit (A28007 Thermo Fischer Scientific, Waltham, MA, USA) according to the instructions of the manufacturer. This process includes several steps: (1) Poly(A) tailing, extending the 3' end of the mature transcript through poly(A) addition (2) 5' adapter ligation, lengthening the 5' end by adaptor ligation (3) Reverse transcription and (4) Amplification to increase uniformly the amount of cDNA for all miRNA. From 3.7 μ L of exosome RNA from each individual, by

following the aforementioned steps, amplified cDNA was produced and stored at -20°C until use.

Real-time PCR is usually conducted to quantify the absolute amount of a target sequence or to compare relative amounts of a target sequence between samples.

Real-time PCR was performed using OpenArray plates at Universitat Pompeu Fabra (UPF) Genomics core facility (Barcelona, Spain) The pre-amplified cDNA (diluted 1:20) was mixed with 2X TaqMan OpenArray Real-Time Master Mix (4462159 Thermo Fischer Scientific, Waltham, MA, USA). Five microliters of each sample cDNA/master mix were distributed into each well of 384-well plate; 16 replicates were plated per sample. From the 384-well plate, samples were loaded onto the OpenArray plate OpenArray™ Human Advanced MicroRNA Panel, QuantStudio™ 12K Flex (Thermo Fischer Scientific, Waltham, MA, USA) using the OpenArray™ AccuFill™ System (Thermo Fischer Scientific, Waltham, MA, USA) so that 33 nL of mixture was transferred into each through-hole. Each TaqMan Open Array plate contains 3075 through-holes arranged in 48 subarrays of 64 through-holes each. Each through-hole is 300 µm in diameter and 300 µm deep. Through-holes are treated with hydrophilic coatings as well as the plate surface so that samples are retained by surface tension. Finally, real-time PCR was run on the QuantStudio™ 12K Flex Real-Time PCR System (Thermo Fischer Scientific, Waltham, MA, USA).

Each panel enables the quantification of miRNA expression in 3 samples and up to 4 panels can be cycled simultaneously, allowing for the analysis of 12 samples on a QuantStudio 12K Flex Real-Time PCR system at the same time.

2.5. Biostatistical analysis

Data analysis was performed at MARGenomics, IMIM, Barcelona, Spain.

Data analysis associated with qPCR depends upon the concept of cycle quantification (Cq), the cycle at which the level of fluorescence from accumulating amplicons crosses a defined threshold; the higher Cq, the lower amount of the evaluated miRNA because you need more cycles of amplification to detect the fluorescence. There are two methods used for Cq obtention: the Ct (threshold cycle) or “baseline threshold” method and the Crt (relative threshold cycle) or “relative threshold” method. Unlike the Ct method, which considers all the curves for a specific target to determine the threshold, the Crt method sets a threshold for each curve individually, based on the shape of the amplification curve, regardless of the height or variability of the curve in its early baseline fluorescence. Both methods come down with analogous results ³⁴³ however Crt is selected for low initial volume cDNA samples, which show fluorescence variability. This variability can be discarded by analysing the amplification curves for each through-hole individually.

Hence, raw data was obtained by the aforementioned relative threshold method (Crt) and processed using the Thermo Fisher Cloud™ solutions. Crt values were obtained for the 754 miRNA included for each subject. Two control indicators were considered: (1) the amplification score (AmpScore) value, which is a quality measurement indicating a low signal in the amplification curve linear phase (range between 0 and 2), and (2) the cycle confidence (Cqconf), a quality flag that highlights when the calculated confidence for the Cq value of the well is less than the minimum confidence value defined in the analysis settings.

miRNA with a Crt value > 28, AmpScore < 1.24 or Cqconf < 0.8 were considered unamplified for further analysis. Filtered Crts were exported to be processed in R (v 3.6.3, (R Core Team 2018)) using in-house built functions.

Global mean method was used to normalize raw Crts for each miRNA. The global mean normalization method is an endogenous miRNA-based normalization strategy that uses the averaged Crt values of all the analysed miRNA (global mean) per each sample separately, a strategy commonly used in experiments assaying large numbers of miRNA and/or in experiments in which stable reference genes are unknown³⁴⁴.

Example. Global normalisation of miRNA1:

$Ct \text{ normalized (miRNA1, sample3)} = Ct \text{ (miRNA1, sample3)} - Ct \text{ (mean all miRNA of sample3)}$

Per each miRNA, mean of the global normalized Ct values for controls (ΔCtr controls) and mean of the global normalized Ct values for patients (ΔCtr patients) was calculated.

Normalized values were compared between conditions using a Student's t-test. p-values were corrected for multiple comparisons using the FDR (False discovery rate) method³⁴⁵⁾ to obtain an adjusted p-value.

Finally, $\Delta\Delta Ct$ was calculated as:

$\Delta\Delta Ct = \text{mean global normalized Ct patients } (\Delta Crt \text{ patients}) - \text{mean global normalized Ct controls } (\Delta Crt \text{ controls}).$

To calculate the relative miRNA expression levels between patients and controls the

$2^{\Delta\Delta Ct}$ method was used:

$RQ = \text{Relative quantification} = 2^{\Delta\Delta Ct}$

The RQ is the fold change compared to the reference sample (control sample in this case). The reference sample has a RQ value of 1. So, if $RQ=1$ there are no differences between patients and controls. A RQ of 10 means that this miRNA is 10 times more expressed in patients than in the control samples. A RQ of 0,1 means that the miRNA is 10 times less expressed.

Once established the criterion for statistical significance, we proceed to establish comparison of miRNA expression levels between groups in three different approached:

- (1) Differential expression analysis by considering all those miRNA that were significantly dysregulated in patients compared to controls (adj. p-value < 0.05).
- (2) A second more restrictive approach was to consider those miRNA particularly differentially expressed between patients and controls, the top downregulated and the top upregulates miRNA. So, we arbitrary studied those miRNA with adj. p-value < 0.05 and RQ > 2 or < 0.15
- (3) Finally, comparisons between miRNA of patients with different DD1 phenotypes were established. The comparison groups are listed below:
 - Patients with no CKD (FGe>90 mL/min) vs patients with CKD (FGe<90 mL/min).
 - Patients with history of lithiasis vs. patients with no history of lithiasis.
 - Patients with nephrocalcinosis vs. patients without nephrocalcinosis..
 - Patients with incomplete Fanconi Syndrome (glucosuria and/or aminoaciduria) vs. patients without these findings.

- Patients with history of rickets vs. patients without history of rickets.

2.5.1. Target gene prediction and integrated analysis by Ingenuity Pathway Analysis

Differentially expressed miRNA were further analysed to gain insight into the functions, pathways and networks of miRNA target genes by using the web-based bioinformatics tool IPA (Ingenuity pathway analysis) (Ingenuity Systems, <http://www.INGENUITY.com> QIAGEN's). Results obtained (miRNA with an adjusted p.value <0.05) were uploaded to IPA. Using miRNA Target filter tool, the experimentally observed target genes were retrieved and a subsequent Core analysis was performed for all the differentially expressed miRNA.

To obtain the targets, IPA has several sources of experimentally determined miRNA targeting information, namely miRecords, TarBase v.8.0³⁴⁶, and direct acquisition from the literature (Ingenuity Expert Findings). For the six top differentially expressed miRNA, aside from those experimentally observed targets, those highly predicted were also considered. An interaction network was constructed using miRNet³¹⁰.

3. Characterisation of a cellular model for DD1

3.1. Cell culture basics, media and procedures

3.1.1. RPTEC/hTERT1 cell line

The development of this part of the project was based on the use of the RPTEC/hTERT1 cell line (CRL-4031) (ATCC American Type Culture Collection, Rockville, MD, USA).

This cell line derives from the renal proximal tubule epithelial cells (RPTEC) of a healthy human male donor and shows no chromosomal abnormalities. They were immortalized (Evercyte Laboratories, Vienna, Austria) with expression of catalytic subunit of the human telomerase reverse transcriptase (hTERT). This cell line exhibits the characteristic morphology and functional properties of normal well-polarized proximal tubular epithelial cells, including preserved cilia, parathyroid hormone receptors and transporters such organic cation transporter (OCT) and organic anion transporter (OAT), multidrug and toxin extrusion protein 1 (MATE), sodium dependent uptake of phosphate and intact functionality of the endocytic receptor complex. Differentiation in these cells is attained when the cells are fully polarized, as shown by (1) microvilli formation and (2) the presence of Na⁺/K⁺-ATPase in the basolateral membrane, and when there is increased mRNA expression of transporters such as OCTs and MATEs ³⁴⁷.

This cell line also preserves metabolic and genomic stability when fully differentiated (describe the process of differentiation) in culture enhancing suitability for metabolomic, proteomic and transcriptomic investigations *in vitro* ^{348,349}

3.1.2. Culture media

Cells were cultured at 37°C in the incubator supplied with 5% CO₂. The culture medium used was DMEM/F-12, GlutaMAX™ (*Thermo Fisher Scientific, Inc* Waltham, Gibco, #31331-093) supplemented as listed in the table (*Table 5*). The silencing vector with the shRNA (see section Cell model creation) contains the puromycin resistance gene (*Thermo Fisher Scientific, Inc* Waltham, MA, USA., #A11138-03) which was included in the medium at a concentration of [8µg/mL]. The expression vector contains the hygromycin resistance gene for selection so hygromycin (Formedium™, Norkfolk, UK, #HYG1000) was introduced into the medium at a concentration of [400 µg/mL].

Table 5 Cell culture media composition

| Product | Reference | Use | Store | [Stock] | [Final] |
|--|---------------------------------|---|--------|---------|---------|
| DMEM/F-12, GlutaMAX™ Supplement | Life Technologies #31331-093 | L-glutamine: energy production, protein & nucleic acid synthesis. | 4 °C | - | - |
| HEPES buffer | “Homemade”: adjusted pH to 7.3. | Zwitterionic organic chemical buffering agent. | 4 °C | 1M | 20 mM |
| Apo-Transferrin | Sigma Aldrich #T1428 | Uptake and transport of iron from culture medium to the cells, allowing proper oxygen uptake, also stimulates growth-related enzyme activation. | -20 °C | 5 mg/mL | 5 µg/mL |
| Human Insulin solution | Sigma Aldrich #I9278 | Growth factor, with anti-apoptotic and mitogenic effects. | 4 °C | 4 mg/mL | 5 µg/mL |

| | | | | | |
|--|-------------------------------------|--|--------|---------------------|----------|
| Dexamethasone | Sigma Aldrich #D8893 | Glucocorticoid anti-inflammatory agent, with effects on cell survival, cell signalling, and gene expression. | 4 °C | 2.5 mM | 50 nM |
| 3,3',5-Triiodo-L-thyronine sodium salt (T3) | Sigma Aldrich #T5516 | Regulates cell differentiation and protein expression. | -20 °C | 30 µM (20µg/mL) | 3 nM |
| EGF (Epidermal Growth Factor) | Sigma Aldrich #E4127 | Stimulation of ion fluxes, glucose transport, glycolysis, and synthesis of DNA, RNA and proteins. | -20 °C | 100 µg/mL | 10 ng/mL |
| Selenium | Sigma Aldrich #S9133 | It is incorporated into enzymes that protect cells by reducing ROS to non-harmful species. | 4 °C | ≈300 µM (289 µM) | 60 nM |
| FBS (Fetal Bovine Serum) | Biological Industries #04-007-1A | Supplement to provide an optimal culture medium (source for amino acids, proteins, vitamins). | -20 °C | 100 % | 2 % |
| Antibiotic/Antimicotic | Life Technologies #15240-062 | Controls the growth of bacterial and fungal contaminants. | -20 °C | 100x | 1x |

Cells were grown under sterile conditions using T75 EasYFlask, TC Surface with filter Cap (Thermo Fisher Scientific, Inc Waltham, MA, USA #156499) for adherent cells. For experiment plating, different well plates Nunc™ treated with polystyrene were used (Thermo Fisher Scientific, Inc Waltham, MA, USA. #142475, #150628, #140675). Likewise, µ-Dish 35 mm plates, high Glass Bottom (Ibidi, Gräfelfing, Germany, # 81156), were used. Cell cultures were maintained at 37°C in a humidified atmosphere of 95% air and 5% CO₂.

Mycoplasma detection test were run regularly in all the samples to assess negativity.

3.1.3. Trypsinisation

Cells were regularly trypsinised when reaching 80-90% confluency using Trypsin-EDTA 0.05% (Thermo Fisher Scientific, Inc Waltham, MA, USA #25300062) 1.5 mL/75 cm² and incubated for 3-5 min at 37°C. After cell detachment, trypsin was inactivated with 1:3 (4.5 mL/75 cm²) of culture media with FBS. Cells were afterwards plated at the desired concentration.

3.1.4. Cell counting

Almost before every procedure, it is necessary to quantify and use a consistent number of cells. This will help maintaining optimum growth and standardising procedures for results with better reproducibility. In order to plate cells at the required concentration, the number of viable cells was counted with the haemocytometer chamber of Neubauer via dilution. The haemocytometer with its slid was filled with cell suspension (diluted 1:10 in culture media) approximately 10 µL and viewed under an inverted phase contrast microscope using 20X magnification.

Cells in the four big squares were counted and cell concentration calculated according to the following equation:

$$\text{Viable Cell Count (live cells per millilitre)} = \frac{\text{Number of live cells counted}}{\text{Number of large corner squares counted}} \times \text{Dilution factor (in our case 10) x 10,000}$$

The central area of the counting chamber is 1 mm². This area is subdivided into 25 smaller squares (1/25 mm²). Each of these is surrounded by triple lines and is then further divided into 16 (1/400 mm²). The depth of the chamber is 0.1 mm. The correction factor of 10⁴ converts 0.1 mm³ to 1 mL (0.1 mm³ = 1 mm² x 0.1 mm). Cells were then seeded at the desired concentration, specified per platform used (*table 6*).

Table 6 Cells seeding density according to the platform used

| Seeding density | |
|-----------------------|------------------------|
| Culture plates | |
| 6-well | 0.3 x 10 ⁶ |
| 12-well | 0.1 x 10 ⁶ |
| 24-well | 0.05 x 10 ⁶ |
| Flasks | |
| T-75 | 2.1 x 10 ⁶ |
| Dishes | |
| 35 mm | 0.3 x 10 ⁶ |

3.1.5. Cell cryopreservation

Cells were periodically cryopreserved to keep a low passage number. Freezing was performed when cells reached a high concentration 90-100%. After being gently detached from flasks and counted using the Neubauer chamber as specified above, cells were centrifuged at 150 x g for 5 min. The supernatant was

decanted, and the cell pellet was resuspended using cold freezing medium (10% DMSO (Dimethyl Sulfoxide, Sigma Aldrich, St Louis, Missouri, US. #D2650), in culture medium). Cell suspension was aliquoted into cryogenic storage Nunc sterile CryoTube Vials (Thermo Fisher Scientific, Inc Waltham, MA, US #377267) that were placed in an isopropanol chamber (Mr.Frosty™, Thermo Fisher Scientific, Inc Waltham, MA, US #5100-0001) and stored first at – 80°C and then were transferred to liquid nitrogen, and stored until use.

3.1.6. Cell thawing

Cryovial containing the frozen cells were removed from liquid nitrogen and as soon as possible placed into a 37°C water bath where cells were thawed rapidly (< 1 minute) and diluted in pre-warmed growth medium. Cell suspension was centrifuged at approximately 200 × g for 5 minutes. After supernatant decantation, pellet was resuspended with culture medium and cells were plated at a high density to optimize recovery.

3.2. Generation of a cell model for Dent's Disease

In order to explore potential unknown physiopathological mechanisms causative of DD1, to validate the miRNA found differentially expressed in patients vs. controls and to test potential future drugs with a reliable *in vitro* prototype, models of proximal tubular cells carrying DD1 mutations were previously generated in our group (Renal Physiopathology Group, Vall

d'Hebrón Research Institute, by (Monica Durán Ph.D. Thesis and manuscript submitted). In this section we will recap how these cell models were previously created by Dr. Duran, to understand the next steps in the study.

To summarize, the endogenous *CLCN5* gene was silenced by using a short hairpin RNA (shRNA). Over this knockdown an exogenous *CLCN5* gene (WT) was overexpressed. Equally, *CLCN5* sequences carrying three different mutations causative of the disease (E527D, I524K, V523del) were overexpressed to create three different cell models.

3.2.1 *CLCN5* knockdown by shRNA

Several methods have been used to silence individual gene expression post-transcriptionally; one of the most widely used is RNA interference (RNAi) that allows post-translational silencing of gene expression by introducing a double-stranded RNA (dsRNA) into a cell³⁵⁰ RNAi is achieved either transiently by transfection of small interfering (si) RNA oligonucleotides or stably using short hairpin (sh) RNA expressed from a DNA vector or virus. shRNAs consist of two complementary 19–22 bp RNA sequences linked by a short loop of 4–11 nt similar to the hairpin found in naturally occurring miRNA. Like miRNA or exogenously delivered synthetic siRNA oligonucleotides, shRNA binds to the target mRNA and is incorporated into the RISC complex for targeting specific mRNA degradation. Introduction of shRNA into cells allows for stable long-term knockdown of the targeted gene³⁵¹. The first step in the

creation of Dent's Disease cell model was to silence the endogenous *CLCN5* by introducing the shRNA. Five different shRNA homologous to different regions of the gene mRNA were cloned into the pLKO.1-puro lentiviral vector (MISSION® Sigma Aldrich, St.Louis, Missouri, US.).

The most efficient shRNA, as established by qPCR with highest silencing, was used to perform the gene knockdown.

The sequence of this shRNA was :

| <i>ID</i> | <i>Sequence</i> |
|-----------------------|--|
| TRCN0000043904 | CCGGGCACCGAGAGATTACCAATAACTCGAG TTATTGGTAATCTCTCGGTGCTTTTTG |

3.2.2 CLCN5 cloning by Gateway system, introducing rescue sequence and CLCN5 mutations by site-directed mutagenesis

CLCN5 was cloned via Gateway system³⁵² into a pENTRY vector. The cDNA sequence for the canonical form of *CLCN5* (2238bp, transcript variant 3 [NM_000084.5]) was acquired from Harvard PlasmID (PlasmID; #HsCD00399904). Once cloned, silent mutations (change in the nucleotide bases without a subsequent change in the amino acid) were introduced into the sequence recognized by the shRNA to skip degradation. In one of the serial PCRs of this process, an HA tag was introduced in the C-terminus of *CLCN5*

sequence to further localize the protein. This mould was then used to introduce DD1 mutations (E527D; c.1581A>T, I524K; C.1571T>A and V523del;c-1566-1568del) by site-directed mutagenesis³⁵³. Finally, these inserts, either with the wildtype (WT) sequence or with one of the mutated sequences, were subcloned into the final expression vector pLenti CMV hygro DEST (Addgene, Watertown, Massachusetts, US #17454). A scheme showing the construction of the cells is depicted in *Figure 17*.

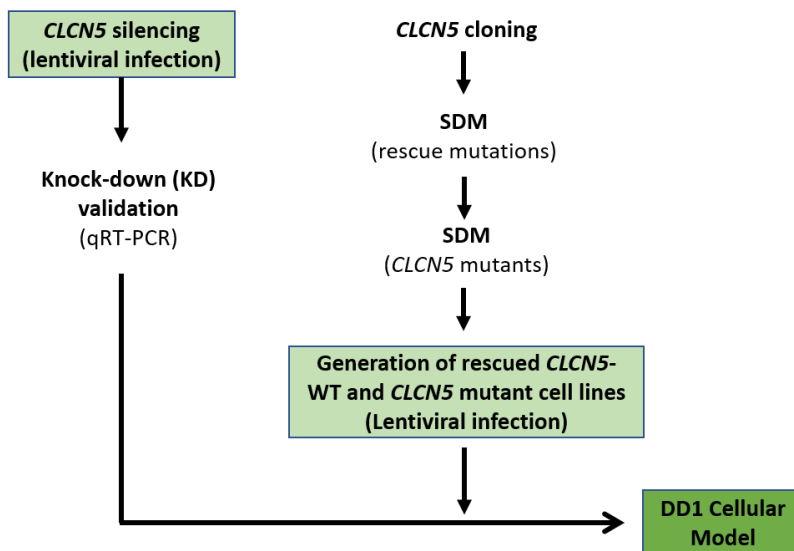


Figure 18 Strategy for cell models generation

SD: Site-directed mutagenesis. WT: Wild type. DD1: Dents' Disease type 1

The three mutations introduced were chosen because (1) they affect the same region of the protein, the P helix, and (2) each one of them belongs to a different class of the protein-effect classification (I524K class 1, E527D class 2¹⁶¹ V523del to be determined).

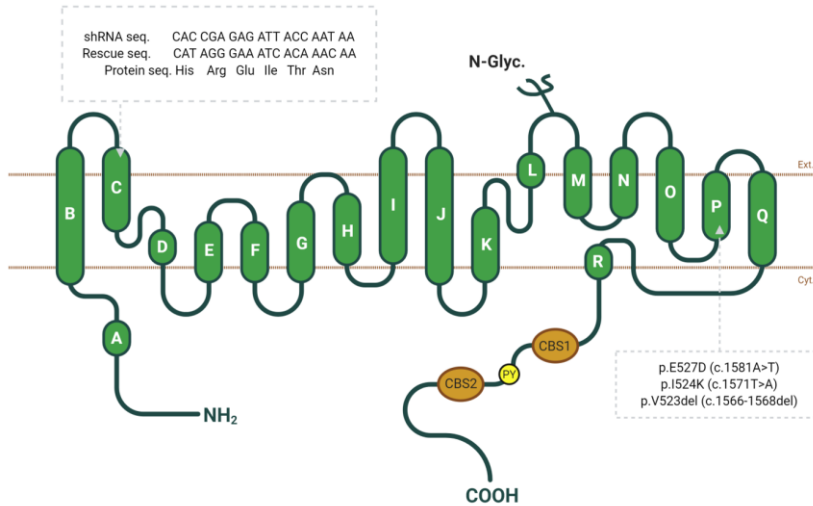


Figure 19 CLC-5 structure with location of shRNA sequence, rescue sequence and the three different mutations introduced.

After construction, PCR products of the whole *CLCN5* gene region were sent to Eurofins Genomics (Nazareth, Belgium) for complete sequencing.

All in all, the final cell lines the project are based on are:

| RPTEC | ENDO | EXO |
|------------------------------|------|-----|
| sh \emptyset + \emptyset | ✓ | ✓ |
| shCLCN5 + \emptyset | ✗ | ✓ |
| shCLCN5 + R + CLCN5 | ✗ | ✓ |
| shCLCN5 + R + I524K | ✗ | ✓ |
| shCLCN5 + R + E527D | ✗ | ✓ |
| shCLCN5 + R + V523del | ✗ | ✓ |

Figure 20 Cell lines udes for cell model characterisation. In red the vector pLKO.1.puro. If it contains the shRNA for CLCN5 is written as shCLCN5. If it is empty is \emptyset . R is the rescue sequence with synonym mutations for the expression vector not to be recognized by the shRNA V show if the cell line contains the endogenous CLCN5 or the exogenous CLCN5. In blue, the expression vector containing either the WT CLCN5 sequence or CLCN5 with one of the mutations of interest.

3.3. Nucleic acid methods

3.3.1 RNA isolation

Before every qPCR or RT-PCR performed (described in results), RNA was extracted directly from cell cultures 7-9 days after confluence from a 12 well-plate where the samples had been plated in triplicates per cell line. The RNA extraction procedure was performed by using RNeasy Mini Kit (Qiagen, Hilden, GE. #74106). Briefly, cells were washed with 1X PBS 3 times and lysed using 350 μ L RLT buffer for 15 minutes. After, 350 μ L of 70% ethanol were added to the lysate and gently resuspended twice for precipitation. Samples were then transferred to RNeasy columns in 2 mL tubes and centrifuged 15 seconds at 8,000 x g. Flowthroughs were discarded. The columns were then washed with 700 μ L of RW1

buffer and centrifuged at 8,000 x g for 15 seconds. Flowthroughs were again discarded. To each column, 500 μ L of RPE buffer were added and then centrifuged at 8,000 x g for 15 seconds at room temperature. This RPE wash and centrifuge was repeated once more. Then the column was spun at full speed for 2 minutes to remove any remaining buffer. The columns were placed in a new 1.5 mL RNase-free tubes. Thirty microliters of RNase-free water were added to the centre of the column and left at room temperature for 2-5 minutes. Tubes with columns were finally centrifuged at 8,000 x g to elute the RNA and samples stored at -80°C.

RNA concentrations and sample purity were assessed by Nanodrop Spectrophotometer (NanoDrop 2000, Thermo Fisher Scientific, Inc Waltham, MA, USA). Samples were considered as pure RNA if the ratio between absorbances 260nm / 280nm was >2.

3.3.2 Reverse transcription

For further analysis, the RNA samples needed to be first converted to cDNA by reverse transcription (RT), and then the cDNA was amplified by the polymerase chain reaction (PCR).

cDNA was synthesized using 2-step procedure and the SuperScript™ III Reverse Transcriptase (#18080-044). For reverse transcription, all RNA samples were arranged to the same concentration (1 μ g/ μ L). Negative controls (RT-) were also prepared with 3.3 μ L from each replicate and in absence of

SuperScript III Reverse Transcriptase. For RNA denaturation step, samples were mixed with dNTP mixture (1 μ L 10 mM dNTP, 0.5 μ L OligoDT, 0.5 μ L Random Hexamers (1:30)). The mixture was heated at 65° for 5 minutes.

The cDNA synthesis mix was then prepared for each sample, with the following composition: 4 μ L 5X First-Strand Buffer, 2 μ L 0.1 M DTT, 1 μ L RNase-free water, 1 μ L of SuperScript™ III RT (200 units/ μ L, except RT- samples were it was substituted with RNase-free water). The cDNA synthesis mix was added to the RNA-dNTP mix from the first step and was incubated at 50°C for 60 minutes. The reaction was inactivated by heating at 70°C for 15 minutes. cDNA synthesis reaction samples were either stored at -20°C or used for PCR immediately.

3.3.3 PCR-polymerase chain reaction – Amplification

All PCR reactions were performed using Phusion HighFidelity DNA Polymerase (# F549L, Thermo Fisher Scientific, Inc Waltha, MA, USA). All reactions and cycling parameters for the PCR were followed according to recommendations of the manufacturer. A mixture composed of 2.5 μ L 10x PCR Buffer, 0.8 μ L forwards primer 10 μ M, 0.8 μ L reverse primer 10 μ M, 0.8 μ L dNTP, 0.2 μ L taq DNA polymerase and 32.4 μ L of RNase-free water was added to the template cDNA synthesis reaction (1 μ L) from previous steps.

The parameters for the cycles, optimal annealing and extension temperature varied according to the primers.

In short, in PCR the amplification is based on three phases, denaturation, in which the two strands of DNA are detached, a hybridization phase in which the primers anneal to the ends of the target sequences, and elongation phase in which the polymerase adds nucleotides complementary to the target sequences following the two primers. So, temperature cycles are repeated several tens of times in the heating block and thus exponential amplification is achieved.

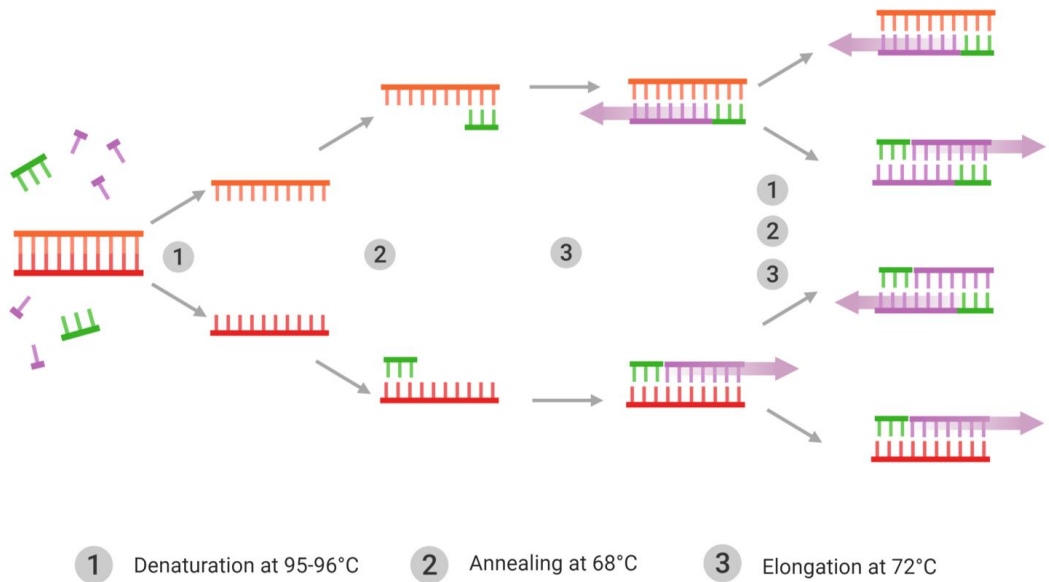


Figure 21 Basic steps in PCR

Primers used during the project are listed below:

Table 7 Primers used for cell model characterisation

| Gene | Forward Primer | Reverse Primer |
|--------------------------|--------------------------|-------------------------|
| <i>CLCN5</i> endogen | GGGATAGGCACCGAGAGAT | GGTTAAACCAGAATCCCCCTGT |
| HA | GGTTACACACAACGGGCGAT | CGTAATCTGGAACATCGTA |
| <i>LRP2</i> (Megalin) | TGGGTTGACTCTCGGTTTGA | CACGGCCATCTTTGTCCAAT |
| | AAGCTCATGTCTGACAAGCGGACT | TACAATCTCTTCTACTCGGTC |
| | AAATTGAGCACAGCACCTTTGA | CTGCTTTCCTGACTCGAATAATG |
| CUBN (Cubilin) | CCGCCATCCAAAATTTCTACA | GGTCCCTGCCAATTATCCAA |

The results of the PCR reaction were visualized by 2% agarose-gel electrophoresis, which separates DNA fragments according to size, determined by a DNA ladder.

3.3.4 RT-qPCR

To quantify DNA, quantitative polymerase chain reaction was performed (qPCR). Xpert Fast SYBR (Fluorescein) 2X mastermix (Grisp Research Solutions, Porto, Portugal #GE21.0100) was used for all procedures. Starting from biological triplicates per cell line, each replicate was divided in technical triplicates. Thus, 1.75 μ L of template cDNA/biological replicate were mixed with 17.5 μ L of 2x buffer (which includes the polymerase, the dNTP's and the SYBR dye), 0.12 μ L of forward primer and 0.12 μ L of reverse primer and 0.12 μ L water. A negative control for detection of possible contaminants was included per sample; in those controls, instead of cDNA, water was included. For quantification thermocycler

LightCycler® 480 Instrument II (Roche Diagnostics Penzberg, Alemania) was used.

In a nutshell, qPCR determines the actual amount of PCR product present at a given cycle, by using a fluorescence report in the PCR reaction. In the template, we have the target sequence we are interested in and forward and reverse primers are added to recognize this target sequence. The mixture 2x contains the polymerase and the SYBR I dye. After denaturation, the primers attach to the appropriate ends of the target sequence and the polymerase extends the sequence by adding nucleotides that are complementary to the DNA template. SYBR attaches all newly synthesized double stranded DNA complexes and fluoresces. The fluorescence accumulates and is measured at the end of each PCR cycle. The cycle at which the intensity of fluorescence generated by SYBR is above the background, is called the threshold cycle (Ct). The amount of target cDNA produced during amplification was compared to the amount of a normalizing/housekeeping sequence. For every qPCR reaction two housekeeping genes were used: GAPDH (Glyceraldehyde-3-Phosphate Dehydrogenase) and HPRT1 (Hypoxanthine Phosphoribosyltransferase 1).

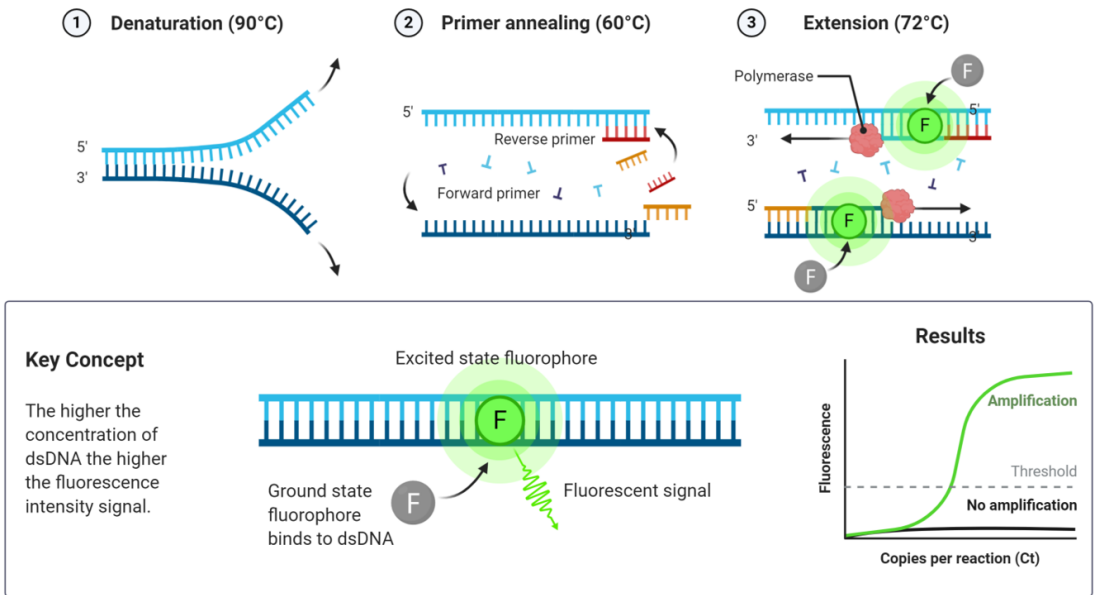


Figure 22 Basic steps of RT-Qpcr

3.4. Protein analysis assays

3.4.1 Protein extraction

Protein extraction was performed after cells had reached 7-9 days confluence from a 6-well plate. The whole procedure was performed on ice. After discarding the medium, cells were washed once with ice-cold PBS-1x. Lysis buffer (composition specified in table 8 with “homemade compounds” and protease inhibitors, final pH 7.4) was added (200 μ L/well). After 30 min on ice, cells were scraped using a cold plastic cell scraper and the lysates were collected in tubes.

Table 8 Lysis buffer composition

| <i>Solution</i> | <i>Stock Concentration</i> | <i>Final Concentration</i> | <i>Volume</i> |
|-----------------|----------------------------|----------------------------|---------------|
| TrisHCL | 1 M | 10 mM | 200 μ L |
| NaCl | 5 M | 150 mM | 600 μ L |
| EDTA | 0.5 M | 1mM | 40 μ L |
| SDS | 10 % | 1 % | 2000 μ L |

Samples were sonicated using the Bioruptor UCD 200 sonicator (Diagenode, Liège, Belgium) for 5 cycles of 15 seconds each to reduce the viscosity of the samples due to the presence of large genomic DNA strands. Samples were then centrifuged at 16,000 x g for 30 min at 4°C, the supernatant was collected in fresh tubes and stored frozen at -20°C.

3.4.2 Protein concentration determination-BCA assay

For protein quantification the bicinchoninic acid assay (BCA) was used (Pierce BCA protein kit, *Thermo Fisher Scientific, Inc* Waltham, MA, USA #23225). It is based on the well-known biuret reaction, the reduction of Cu^{2+} to Cu^+ by protein in an alkaline medium at a given temperature which forms a chelate complex with cupric. When adding a colorimetric detection reagent this complex turns into dark blue/purple and absorbs light at 540 nm. The amount of Cu^{2+} reduced and so the intensity of the colour produced is proportional to the number of peptide bonds participating in the reaction, and so, to the amount of protein in the sample. By building a calibration curve with a known protein concentration,

the protein concentration of any sample can be determined. So, reagent A, a carbonate buffer containing BCA reagent, was added to the samples and to the solutions of known BSA (bovine serum albumin) concentration. Reagent B, a cupric sulphate solution, was also added. After 30 min at 37°C in the dark, absorbance was measured using Tecan absorbance reader and compared to the calibration curve, we determined the concentration of our samples.

The same concentration of all samples was prepared for electrophoresis and Laemmli sample buffer 6x (Tris-HCl pH 6.8 0.3 M, SDS 10%, glycerol 5%, β -mercaptoethanol 2%, bromophenol blue 0.01%) was added to a final concentration of 1x. After, samples were heated at 75°C.

3.4.3 Protein detection by immunoblot

Western blotting (or immunoblotting) is one of the most common analytical techniques used for the detection of proteins in a sample by means of specific antibodies for the target protein. Firstly, the proteins must be separated by SDS-PAGE (Sodium Dodecyl Sulfate Polyacrylamide Gel Electrophoresis) and transferred afterwards to a membrane (nitrocellulose or PVDF) with the help of an electric field. This process allows the proteins to be accessible for antibody detection.

3.4.3.1. Protein electrophoresis

Table 9 Percentage of polyacrylamide gel according to the molecular weight of the protein of interest

| <i>Target protein molecular weight (kDa)</i> | <i>Polyacrylamide gel (%)</i> |
|--|-------------------------------|
| 10-30 | 15 |
| 30-70 | 12 |
| 70-100 | 10 |
| >100 | 6 |

Polyacrylamide gel electrophoresis (PAGE) is a common technique universally used to separate proteins according to their molecular weight, charge and conformation. When adding SDS (Sodium Dodecyl Sulfate) technique known as SDS-PAGE, this anionic detergent denatures the protein and eliminates the influence of structure and charge so that proteins are separated according to their molecular weight. The medium is a gel consisting of acrylamide in different concentrations (5-25% according to the target protein molecular weight, see *table 9*), buffers to adjust the pH, ammonium persulfate (APS) and TEMED in order to start the polymerization process and SDS. For the experiments performed, 6-15% gels were used, and their composition is detailed in *table 10*. The samples were loaded into the gel and the gel was run at a constant voltage of 100 V to migrate the proteins starting from the negative electrode (cathode) to the positive one (anode). The system used was Mini Protean III (Bio-Rad, Hercules, California, US).

The samples were run in electrophoresis buffer made of 400 mM Tris acetate and 10 mM EDTA (*Ethylenediaminetetraacetic acid*).

| Component | Separating Gel | | | Stacking Gel |
|---|----------------|--------------|--------------|--------------|
| | 6% | 10% | 15% | |
| 30% Acrylamide/0,8% bis- Acrylamide (#A1672, Panreac) | 1.2 mL | 2 mL | 3 mL | 0.5 mL |
| 4X 0,5 M Tris-HCl/ 0,4 % SDS pH 6.8 | - | - | - | 1.25 mL |
| 4X 1,5 M Tris-HCl/ 0,4 % SDS pH 8.8 | 2 mL | 2 mL | 2 mL | - |
| MilliQ water | 4.6 mL | 3.8 mL | 2.8 mL | 3.2 mL |
| 10% SDS (Sodium Dodecyl Sulfate) | 80 μ L | 80 μ L | 80 μ L | 80 μ L |
| 10% APS (ammonium persulfate) | 40 μ L | 40 μ L | 40 μ L | 25 μ L |
| TEMED (#T9281, Sigma-Aldrich) | 12.5 μ L | 12.5 μ L | 12.5 μ L | 8 μ L |

Table 10 Composition of gels used in Polyacrylamide gel electrophoresis

3.4.3.1. Immunoblotting

Once separated, in order for the proteins to be accessible for antibody detection, they were transferred to a membrane either 0.45 μ m nitrocellulose (GE Healthcare, Hamersham, UK #10600002) or 0.45 μ m PVDF (GE Healthcare, Hamersham, UK #10600023) with the help of an electric field. PVDF membranes were used, instead of nitrocellulose membranes, to study high molecular weight proteins. Membranes were activated beforehand with either water (nitrocellulose) or methanol (PVDF). Transfer was performed at a constant voltage of 100 V in all cases in transfer buffer (48 mM Tris-Base, 39 mM glycine, 0.1% SDS, 20% ethanol, 10% Tween 20 was added for big proteins).

After transfer, a blocking step is required to prevent antibodies from binding to the membrane non-specifically. In our case, a solution of 5% bovine serum albumin or non-fat dry milk with 0.1% Tween (adding a small % of detergent is optional) was applied for 1 hour at room temperature.

Following blocking, the membranes were incubated with the primary antibodies that recognized the target protein (see *table 11* primary antibodies used). For most experiments, membranes were incubated overnight at 4°C and afterwards washed 3-5 times with PBS-Tween 0.1%. For actin, membranes were incubated 2 hours at room temperature.

After the complex antigen-antibody was formed, membranes were incubated with a second antibody coupled with a horseradish peroxidase (HRP) for 1 hour at room temperature (secondary antibodies *Table 12*). Membranes were washed 3-5 times with PBS-Tween (0.1% Tween) to remove excess antibody. In order to visualize the proteins, the HRP was incubated for 1-2 min with an enzyme called luminol (Immobilon® Crescendo Western HRP Substrate, #WBLUR0500, Burlington, Massachusetts, US) together they give a chemiluminescent reaction that can impress photographic films. The visualization was performed using Amersham Imager 600 (GE Healthcare, Hamersham, UK).

Western bands were quantified using ImageJ bundled with 64-bit Java 1.8.0_172 and were normalized to the indicated housekeeping protein, in most cases actin.

Table 11 Primary antibodies used for immunoblotting

| Antibody | Type | Specie | Epitope | Dilution&incubation solution | Company & Catalogue |
|-----------------------|------------|--------|-------------------------------------|--------------------------------------|--|
| HA | Monoclonal | Rat | HA peptide sequence [YPYDVPDYA] | 1:1000 in BSA 5%-PBS-T | Roche (Basel, Switzerland) # 11867423001 |
| CIC-5 | Polyclonal | Rabbit | N-terminal end | 1:500-1:1000 in BSA 5%-PBS-T | Aviva Systems Biology (San Diego, CA USA) #OAA01462 |
| LRP-2/ Megalin | Monoclonal | Mouse | LDL-receptor class A repeats 19-21. | 9. 1:1000 in non-fatty milk 5%-PBS-T | Millipore (Burlington Massachusetts,US) #MABS489 |
| Cubilin | Polyclonal | Sheep | from AA Ser36 to Gly126 | 1:1000 in non-fatty milk 5%-PBS-T | R&D Systems, (Minneapolis, MN, USA) # AF3700 |
| Actin | Monoclonal | Mouse | N-terminal end | 1:2000 in BSA 5%-PBS-T | Millipore (Burlington Massachusetts,US) #A1978 |
| Calnexin | Polyclonal | Rabbit | C-terminal end | 1:2000 in non-fatty milk 5%-PBS-T | Abcam (Cambridge, UK) #ab22595 |

Table 12 Secondary antibodies used for immunoblotting

| Secondary antibody | Company | Catalogue |
|-----------------------------------|------------|-----------|
| Donkey anti-goat IgG-HRP | Santa Cruz | sc-2020 |
| Goat anti-rat IgG-HRP | Santa Cruz | Sc-2006 |
| Donkey anti-mouse IgG-HRP | Santa Cruz | sc-2096 |
| Donkey anti-rabbit IgG-HRP | Santa Cruz | sc-2313 |
| Donkey anti-sheep IgG-HRP | Santa Cruz | sc-2473 |

3.4.4. Immunocytochemistry and confocal microscopy

Immunofluorescence (applied to cells, immunocytochemistry) is a very commonly used technique to visualize cellular macromolecules (proteins, lipids, nucleic acids, antigens, tags) using fluorophores.

The biological sample of interest is incubated with an antibody specific to the macromolecule of interest. This antibody can be directly coupled to a fluorophore (direct fluorescence) or may be detected by a secondary antibody conjugated to a fluorophore (indirect fluorescence). The sample is then visualized with a fluorescence microscope, in our case, confocal microscope, where the laser light is focused onto a defined spot at a specific depth within the sample. This leads to the emission of fluorescent light at exactly this point, in fact a pinhole inside the optical pathway cuts off signals that are out of focus. Confocal microscopy allows imaging one single optical plane and, by scanning several optical planes and stacking them, 3D reconstructions can be visualized. Several lasers and emission/excitation filters can be used so that more than one target macromolecule can be visualized at the same time. In case overlapping of the fluorophores signals is detected we would say that the two macromolecules are in the same cellular compartment or co-localize.

For immunocytochemistry experiments, cells were cultivated in 24-well plates on glass coverslips. After taking out the media and wash

them thoroughly with PBS (5 washes, 5 minutes each) cells were fixed with 4% paraformaldehyde (PFA, #P6148, Sigma Aldrich, St.Louis, Missouri, US) for 15 min at room temperature under the hood and then, washed with PBS to remove the excess PFA. In order to allow the antibodies to bind to their specific antigens, a permeabilization step, together with blocking was made, by incubating the samples with 5% BSA + Triton x100 0.2% for 10 minutes at room temperature. After, samples were incubated with the primary antibody (shown in *table 13*, diluted in the same as blocking solution,) overnight at 4°C. Incubation with secondary antibody was performed for 1 hour at room temperature. Together with the secondary antibodies, DAPI (#D3571, Invitrogen, (Carlsbad, California, US)) was added to stain the nucleus. Coverslips were then embedded with mounting media FluorSave™ Reagent (#345789, Millipore, Burlington Massachusetts) on a glass slide and visualized under the confocal microscope (Leica TCS SP5 or Leica TCS SP8 X (Leica Biosystems, Wetzlar, Germany)) using the oil inversion 63x Plan Apo NA 1.4 objective. Excitation and emission wavelengths varied according to the fluorophore used. Images were acquired and further analysed using ImageJ³⁵⁴; for Colocalization analyses of two fluorescent channels Mander's Coefficient was used by JACOP plugin (Just Another Colocalization Plugin³⁵⁵). All images analysed were taken on the same day under the same conditions and the same Z-step (0.29 µm).

Table 13 Antibodies used for Immunocytochemistry

| Antibody | Spice & Type | Dilution | Company&Catalogue |
|---|-------------------|----------|---|
| Primary antibody | | | |
| HA | Rat polyclonal | 1:100 | Roche (Basel, Switzerland) # 11867423001 |
| Rab5 | Rabbit monoclonal | 1:100 | Cell signaling (Danvers, MA, US) #3547s |
| LAMP1 | Rabbit polyclonal | 1:200 | Santa cruz (Santa Cruz, California, US) #sc-5570 |
| Phalloidin, Alexa Fluor 546 | Dye | 1:1000 | Invitrogen (Carlsbad, California, US) # A22283 |
| DNA staining solution (DAPI or 4',6-diamidino-2-phenylindole) | Dye | 1:20000 | Invitrogen (Carlsbad, California, US) #D3571 |
| Secondary antibody | | | |
| Alexa Fluor® 488 donkey anti-rabbit IgG | | 1:1000 | Invitrogen (Carlsbad, California, US) #A21206 |
| Alexa Fluor® 488 goat anti-rat IgG (H+L) | | 1:1000 | Abcam (Cambrifdge, UK) #ab150157) |
| Alexa Fluor® 555 Donkey anti-Rabbit IgG | | 1:1000 | Life Technologies A-31572 |

3.5. Functional assays

3.5.1. CIC-5 and mutant proteins half-life

The half-life of a protein is defined as the time it takes for newly synthesized protein to be reduced by 50% relative to the level at the beginning of the chase. Cycloheximide is a naturally occurring fungicide produced by the bacterium *Streptomyces griseus* that binds the site C of the ribosome blocking the elongation of all newly synthesized proteins³⁵⁶. Thus, when adding

cycloheximide to cultured cells, the protein synthesis is blocked and by measuring the desired protein level at different time-points the time for the protein to be reduced by half of the initial concentration can be determined. A weak point in this approach is that all protein synthesis is blocked, thus the turnover may not be reflected correctly as in normal growth conditions.

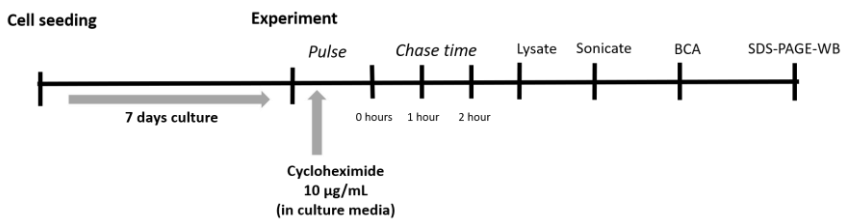


Figure 23 CIC-5 half-life. Scheme of experimental design. BCA: bicinchoninic acid assay. SDS: Sodium Dodecyl Sulphate page: Polyacrylamide gel electrophoreses. WB Western blot

For this procedure, cells were cultured in 6-well plates for seven days after confluency.

Cycloheximide (Sigma Aldrich, Sant Louis, Missouri, US #01810) was added at 10 µl/mL. Samples for t=0h were lysate with lysis buffer as described in section 3.4.1 (Materials and Methods) and lysates stored at -20 °C. The other samples were chased for the determined time course, in our case 1 hour and 2 hours, and lysates were collected at these points. Afterwards, the procedure followed was as described for SDS-PAGE and Western Blot (see section 3.4.3 and 3.4.4 in Materials and Methods).

The relative concentration of the protein at time 0 was defined as 100%. The percentage of the protein at each indicated time point

was normalized by comparing the relative concentration of the protein with that at time 0.

3.5.2. Endocytosis quantification via fluorimetry of fluorescent albumin and dextran uptake

Reabsorption of protein and other filtered macromolecules via the processes of receptor-mediated and non-specific fluid-phase endocytosis is a key function of the kidney proximal tubule as indicated previously (see section 4 in Introduction). Receptor-mediated endocytosis impairment is the main defect in DD1, so it is necessary to trace and quantify endocytosis in our cell model to discern the processes of endocytosis involved in the pathology and to test the effectiveness of potential future therapies, for example, by quantifying the recovery of endocytosis, which is impaired in PTCs in DD1.

With this aim we quantified albumin endocytosis by performing fluorimetry assays, both with a generic marker for receptor mediated endocytosis, albumin, and for fluid-phase endocytosis, dextran. *Figure 24* schematizes the assay.

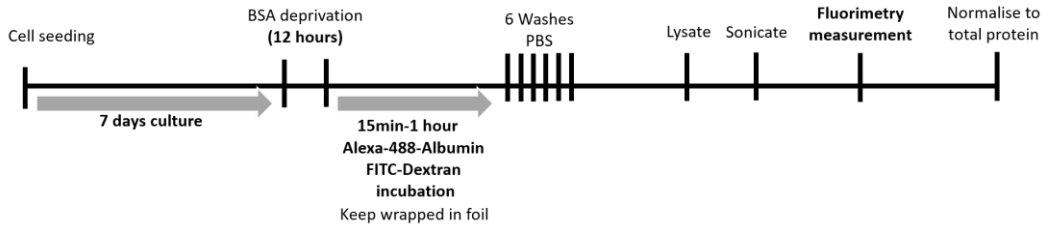


Figure 24. Endocytosis quantification via fluorimetry of fluorescent albumin and dextran uptake. Scheme of experimental design. BSA Bovine serum albumin

In a nutshell, cells were seed in 24-well plates and cultured post-confluency for 7 days. For evaluating receptor-mediated endocytosis, cells were depleted from foetal bovine serum or phenol-red 12 hours before the assays and incubated with 50 µg/mL of 488 fluorescent albumin (Thermo Fisher Scientific, Inc Waltha, MA, USA, #A13100) in isotonic solution (*see table 14* for composition) for 60 minutes at 37°C in 5% CO₂ and a relative humidity of 90% while wrapped into foil. After incubation, cells were washed 6 times with ice-cold PBS to stop endocytosis and to remove the soluble portion of fluorescence from the bound or internalized albumin (the number of washes was determined by measuring the fluorescence in the last rinsing solution (not significantly higher than background fluorescence after six washes)).

Table 14 Isotonic solution composition

| Compound | Stock Concentration |
|--|---------------------|
| NaCl | 140 mM |
| KCl | 2.5 mM |
| CaCl ₂ | 1.2 mM |
| MgCl ₂ | 0.5 mM |
| Glucose | 5 mM |
| HEPES | 10 mM HEPES |
| 305 mosmol/l, pH 7.4 adjusted with Tris | |

Cells were then lysated (in 20 mM MOPS, Triton X-100 0.1% at pH 7.4). The intracellular fluorescence was measured using a single-beam fluorimeter (Thermo Scientific Varioskan LUX Multimode Microplate Reader) at an excitation wavelength of 485 ± 10 nm and emission wavelength 530 ± 10 nm. Background fluorescence (considered that given by the lysis buffer itself) was subtracted in all the conditions. Fluorescence values were normalized to the total protein as measured by BCA (see methods). Results are expressed as fluorescence (AU)/[protein]. For competition assays, cells were incubated with 488-labelled albumin in the presence of 5 mg/mL unlabelled albumin (100 fold labelled albumin). The measures were expressed as a percentage of the baseline albumin uptake, without competition. Likewise, measurements were repeated after blocking receptor-mediated endocytosis by addition of bafilomycin A1, a specific potent inhibitor of vacuolar-type H⁺-ATPases which stops endocytosis by avoiding acidification in the endo-lysosomal pathway³⁵⁷.

As for fluid-phase endocytosis assessment, we replicated the same procedures with incubation 50 µg/mL FITC-Dextran (Thermo Fisher, Scientific, Inc Waltha, MA, USA, #D1820) and competition was implemented by using non-labelled dextran (Thermo Fisher Scientific, Inc Waltha, MA, USA #D1819).

Finally, in an attempt to isolate albumin endocytosis via receptor-mediated pathway, endocytosed albumin fluorescence was measured after high amounts of non-labelled dextran were implemented seeking to saturate fluid- phase endocytosis.

3.5.3. Confocal microscopy Endocytosis Assay

For evaluation of endocytosis pathways by laser confocal microscopy, cells were cultured in 24-well plates on glass coverslips for seven days. On the day of the experiment, cells were thoroughly washed with PBS and left in isotonic solution (composition as described before) with no phenol red or FBS for at least two hours. Cells were incubated for 60 min with either Alexa Fluor 488 albumin or FITC-dextran (50 µg/mL). Following six washes to discard extra non-endocytosed cargoes, cells were fixed and procedure for immunocytochemistry followed as described in section 3.4.5. Albumin colocalization with phalloidin, a specific dye for actin filaments used as a membrane marker, and with LAMP1, a marker for lysosomes, was calculated using JACOP plugin from FIJI software (as also indicated in section 3.5.3) .

3.5.4. Endo-lysosomal pH measurement using a fluorescence dye

Acidification of intracellular organelles is essential for many physiological functions, among others, for normal endocytic vesicle trafficking along the endo-lysosomal pathway and subsequent degradation of ligands (see section 4.2.1 in introduction). One of the causes of Dent's Disease is the failure to acidify the inner media of endosomes and so, the incapacity for a functional endocytosis to occur. It was then valuable to assess intraorganellar pH in the different cell lines to complete the characterization of the cell model.

For pH measurement, a pH-sensitive fluorescent dye, LysoSensor™ Yellow/Blue DND-160 (ThermoFisher Scientific, Inc Waltham, MA, USA) was used. This probe allows for ratiometric measurement of intraorganellar pH through use of dual-wavelength fluorescence-based analysis. LysoSensor emits yellow fluorescence in acidic environment and blue fluorescence in alkaline condition; as pH decreases, the protonation relieves the inherent fluorescence quenching of the dye (probably due to intramolecular transfer of pyridyl oxazole fluorophore induced by protonation) and the protonated groups emit yellow fluorescence. So, fluorescence intensity values recorded for emission at two different wavelengths are pH dependent³⁵⁸ and by calculating the ratios between them, differences in pH can be assessed.

The confocal laser-scanning microscope SP8 TCS (Leica Biosystems, Wetzlar, Germany) was used for image acquisition. Laser and filter settings were adjusted at excitation peak of 405 nm and emission peaks at wavelengths 440 nm and 540 nm. Images were obtained with 63X objective at a frame size of 1,024 × 1,024 pixels.

For this assay, cells were cultured 35mm diameter glass bottom dishes (Ibidi, Gräfelfing, Germany, # 81156) for seven days. On the day of the experiment, cells were incubated at 37°C in 1 mL of pre-warmed, normal cell culture medium containing LysoSensor™ Yellow/Blue DND- 160 diluted 2 µL /mL for 5 minutes and then rinsed twice with PBS1x.

For data analysis, fluorescence intensity values were recorded and quantified for emissions at both wavelengths (440 and 540 nm) for the determined regions of interest; background intensity was subtracted. Ratio of intensity of emission at shorter wavelength (440 nm): intensity of emission at longer wavelength (540 nm) for each region of interest was calculated. Ratios for intensities at shorter and longer wavelength were calculated and pH was expressed normalized to the pH in control cell lines.

3.6. Statistics

All data shown are mean \pm SEM. In all cases a D'Agostino– Pearson omnibus normality test was performed before any hypothesis contrast test. Statistical analysis was performed using Student's t test (continuous data, two groups) or one-way analysis of variance (ANOVA) followed by Bonferroni's post hoc test for the comparison of more than 2 groups (GraphPad Prism 6 (RRID:SCR_002798)). For data that did not fit a normal distribution, we used Mann–Whitney's unpaired t test and nonparametric ANOVA (Kruskal–Wallis) followed by Dunn's post hoc test. Criteria for a significant statistically significant difference were: * $p < 0.05$; **, $p < 0.01$, *** $p < 0.001$, **** $p < 0.0001$.

3.7. Images

If not indicated otherwise, figures were created with Biorender except those showing experimental results.

RESULTS

1. Chapter 1. Dent's disease type 1: picture of the current situation in Europe

1.1. Survey respondents

A total of 37 nephrologist from 36 centres in 12 European countries (*Figure 25*) participated in this survey. For reasons data protection, the societies of nephrology circulated a link to the survey. As a result, we were unable to assess the exact response rate as we do not know how many nephrologists received the questionnaire.

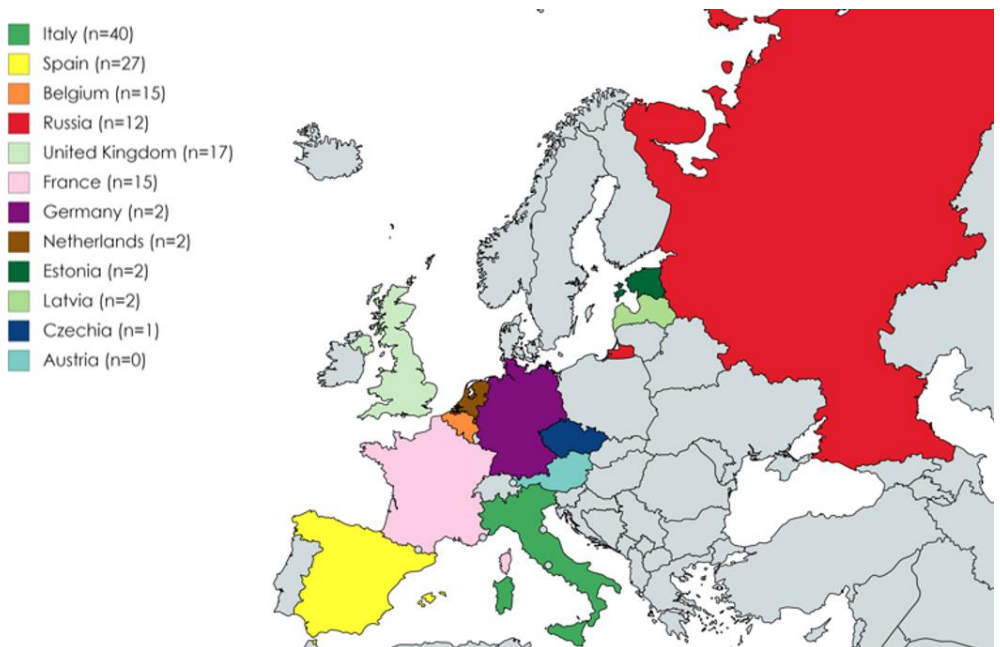


Figure 25 Map of reported Dent's Disease type 1 patients in Europe

The respondents reported 135 patients with DD1 with follow-up in these centres. We considered for further analysis those with availability of at least 50% of the data required (Figure 26). We retrospectively analysed data from 98 male patients belonging to 89 unrelated families with genetically diagnosed DD1, 59 (60.2%) children-adolescents and 39 (39.7%) adults (>18 years old). Nine pairs of siblings were enrolled.

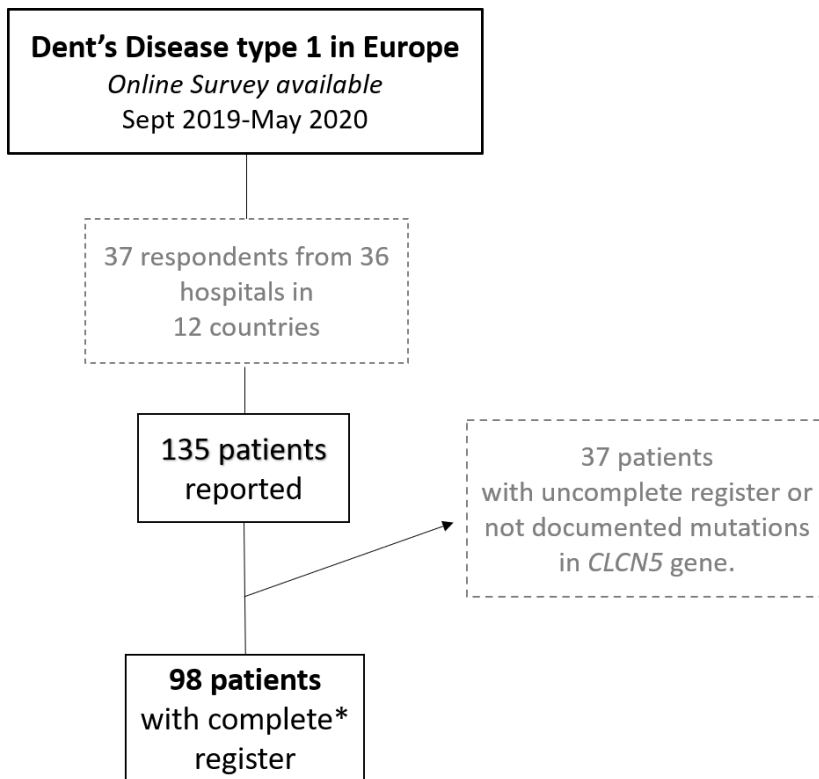


Figure 26 Flowchart of patients' inclusion. *More than 50% of answered questions in the survey

1.2. Presentation at diagnosis

Average age at the time of clinical diagnosis was 7 [3-12] years old (six patients were <1 year old).

As shown in *figure 27*, main key diagnostic signs or symptoms were proteinuria in almost half of the cases (46/98; 46.9%), nephrocalcinosis (11/98;11.2%) or detection of nephrocalcinosis (12/98;12.2%) as an incidental finding during ultrasound *examination* performed for other reasons. Only in 11.2% (11/98) cases, the diagnosis followed family screening, although 52% (51/93) of patients were found to present a positive family history of DD1 after directed questioning.

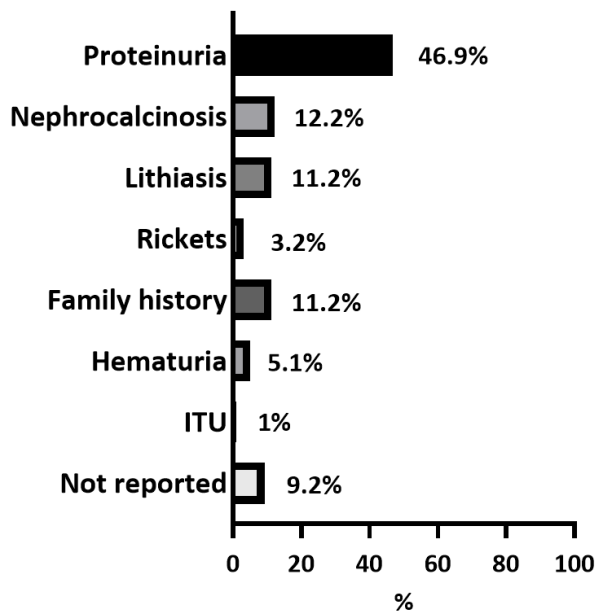


Figure 27 Key signs/symptoms leading to Dent's Disease type 1 diagnosis.

1.3. Phenotypic characteristics

As shown in *table 15*, all patients showed LMWP. Forty per cent of those with available data had hypercalciuria (21/52) and 68% (53/78) nephrocalcinosis. Twenty-five patients (25/93; 26.9%) presented with at least one episode of kidney stones with a median age of 18 [IQR 5-29] years at presentation of the first episode. Bone abnormalities (rickets) were present in 18.8% (17/90) of patients. Seven patients (7/93;7.5%) suffered at least one bone fracture with a median age of 5 [range 0-51] years. Growth was affected in 20.5% (16/58) of patients; 3 patients were receiving growth hormone at the time of last follow-up.

Calciuria was inferred according to the different normal values for age^{338,339}. All those patients with increased renal calcium loss had eGFR higher than 50 ml/min/1.73m². When considering patients with eGFR> 60ml/min, 50% (23/46) had hypercalciuria. As for other solutes physiologically reabsorbed by the proximal tubule, aminoaciduria and glycosuria were present in 55.8% (21/38) and 14% (10/71) of patients with available data, respectively (*Table 15*).

Table 15 . Phenotypic findings in patients with Dent's Disease 1

| | <i>Dent's Disease type 1</i> | <i>N</i> |
|--|------------------------------|----------|
| Age at diagnosis, years (median, [IQR]) | 7 [3-12] | 98 |
| LMWP ^a (yes) (n, %) | 98 (100%) | 98 |
| Hypercalciuria (yes) (n, %) | 26 (48.1%) | 54 |
| Nephrolithiasis (yes) (n, %) | 25 (26.9%) | 93 |
| Nephrocalcinosis (yes) (n, %) | 53 (67.9%) | 78 |
| Aminoaciduria (yes) (n, %) | 21 (55.3%) | 38 |
| Glycosuria (yes) (n, %) | 10 (14.1%) | 71 |
| Hypophosphatemia (yes) (n, %) | 27 (35.5%) | 76 |
| Hypokalemia or use of K supplementation (yes) (n, %) | 19 (25.6%) | 74 |
| Rickets (yes) (n, %) | 17 (18.9%) | 90 |
| Fractures (yes) (n, %) | 7 (7.5%) | 93 |
| Failure to thrive (yes) (n, %) | 6 (8.21%) | 73 |
| Short stature (yes) (n, %) | 16 (20.5%) | 78 |
| HTN ^b (yes) (n, %) | 7 (7.5%) | 93 |

^a LMWP. Low Molecular Weight Proteinuria ^bHTN Hypertension

Nine patients (9/77, 11.6%) were born prematurely with mean weight 1.9±0.3 kg and median height 51 [50-54] cm.

Median age at last follow-up was 9 [15-23] years. Biochemical parameters at last blood test available are shown in *table 16*. Nineteen patients (19/74;25.6%,) had plasma potassium concentration lower than normal range or needed potassium supplements. Twenty-seven patients (27/76;35.52%) showed hypophosphatemia. The presence of hypophosphatemia did not associate the presence of rickets (p=0.7).

1.4. Renal function

At last follow-up, (follow-up time was 5 [2,9.5] years) 57.1% (51/91) of patients had an impaired eGFR (<90mL/min/1.73m²), mostly presenting with CKD grade 2. As seen in *figure 28*, the grade of CKD was variable among patients according to age, although as shown in *table 16*, mean age increased as CKD progressed. Eight patients (8.1%) reached end stage renal disease at a mean age of 37.2 ± 7.6 years. Only two patients older than 30 years had eGFR >90ml/min.

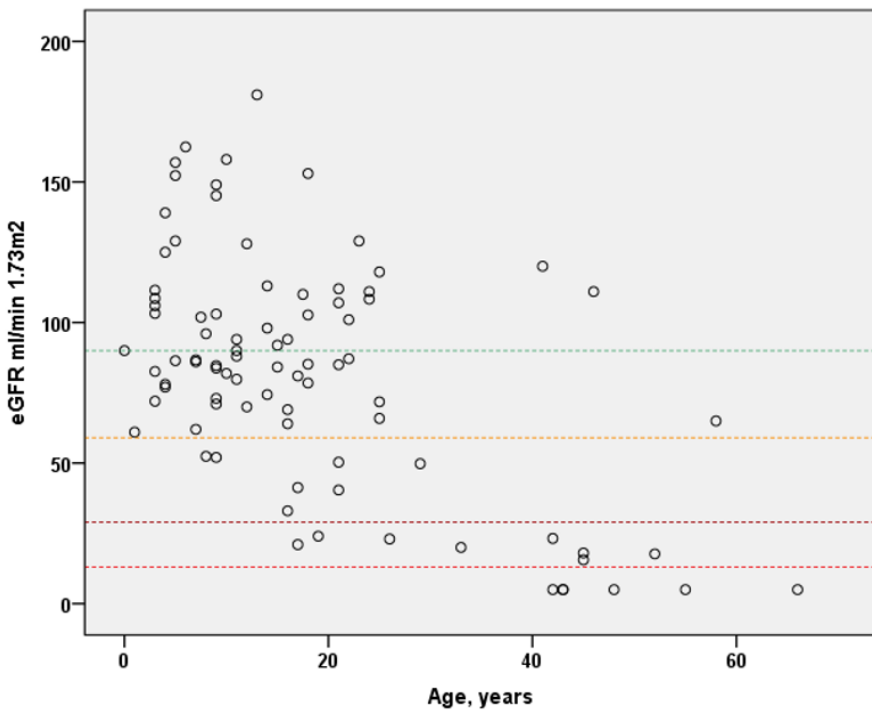


Figure 28 eGFR according to age. Dashed lines separate CKD 5 grades

Proteinuria was a consistent finding in all patients. Nonetheless, different LMW proteins were tested and different units reported

so that it was difficult to evaluate these results homogeneously and so, LMW proteinuria is shown as a qualitative variable. Median proteinuria values are shown in *table 16* as for protein/creatinine 1500 [500-2700] mg/g and albumin/creatinine ratio 270 [90-675] mg/g.

Table 16 Kidney function and electrolyte balance parameters at last follow up

| | Dent's Disease 1 patients | N |
|---|----------------------------------|----------|
| Age at last follow-up, years (median, [IQR]) | 9 [15-23] | 76 |
| Serum Creatinine, mg/dL (median, [IQR]) | 0.74 [0,52-1,17] | 62 |
| eGFR ^a , mL/min/1.73m ² (mean±SD) | 86,5 ±42,3 | 91 |
| Serum potassium, mmol/L (mean±SD) | 3,93±0,49 | 81 |
| Total serum calcium, mg/dL (mean±SD) | 9,35±1,8 | 81 |
| Serum phosphate, mg/dL (median, [IQR]) | 3,6 [2,9-4,1] | 76 |
| Protein/creatinine ratio mg/g (median, [IQR]) | 1500 [500-2700] | 55 |
| Albumin/creatinine ratio mg/g (median, | 270 [90-675] | 35 |
| LMWP ^b (yes) (n, %) | 58 (100%) | 58 |
| U _{Ca} /Cr ^c , mg/mg (median,[IQR]) | 0,25[0,15-0,49] | 50 |
| CKD^d | | |
| Stage 2 (60-89ml/min/1.73m ²) | 29 of 91 (31.9%) | 91 |
| Age stage 2 (years; mean,SD) | 13.2±10.6 | |
| Stage 3 (30-59ml/min/1.73m ²) | 7 of 91 (7.7%) | 91 |
| Age stage 3 (years; mean,SD) | 17.3±7.3 | |
| Stage 4 (15-29ml/min/1.73m ²) | 8 of 91 (8.8%) | 91 |
| Age stage 4 (years; mean,SD) | 35.1±13.6 | |
| Stage 5 (<15ml/min/1.73m ²) or RRT ^e | 8 of 91 (8.8%) | 91 |
| Age stage 5 (years; mean,SD) | 37.2±7.6 | |

^aeGFR, *estimated glomerular filtrate rate*; ^bLMWP. Low Molecular Weight Proteinuria ^cU_{Ca}/cr, Urine calcium/creatinine ratio; ^dCKD. Chronic kidney Disease ^eRRT Renal Replacement Therapy

None of the baseline signs/symptoms could statistically be considered a risk factor for CKD development.

1.5. Phenotype according to age

As mention this cohort includes patients with a wide range of age. By comparing the patients in our cohort according to their age at last follow-up (<18 years old and >18 years old) we confirmed that there are changes in phenotype over time.

As seen in table 17, those currently younger patients were diagnosed at earlier ages than those patients who are >18 years old (18 [10-41] vs. 4 [1-7]; $p < 0.001$), possibly due to a more spread awareness of the disease nowadays. Within the group >18 years, more patients had had at least one episode of kidney stones (48.6% vs. 12.5%; $p < 0.001$). Remarkably, hypercalciuria was more present in younger patients (62.5% vs. 7.14%; $p < 0.001$). In contrast, hypophosphatemia was more present within the older group (>18 years, 30.7% vs. <18 years, 45.8%; $p = 0.006$). Expectedly, more patients in the older group presented with hypertension (>18 years, 16.2% vs. <18 years, 1.7%; $p = 0.035$)

Table 17 Phenotypic findings in patients with Dent's Disease 1. Differences according to age.

| | <18 years old (n=59) | >18years old (n=39) | p |
|--|------------------------------------|-----------------------------------|------------------|
| Age at diagnosis, years (median, [IQR]) | 4 [1-7] | 18 [10-41] | <0.001 |
| Hypercalciuria (yes) (n, %) | 25/40 (62.5%) | 1/14 (7.1%) | <0.001 |
| Nephrolithiasis (yes) (n, %) | 7/56 (12.5%) | 18/37 (48.6%) | 0.001 |
| Nephrocalcinosis (yes) (n, %) | 28/46 (60.8%) | 25/32 (78.1%) | 0.24 |
| Aminoaciduria (yes) (n, %) | 15/23 (65.2%) | 6/15 (40%) | 0.31 |
| Glycosuria (yes) (n, %) | 2/43 (4.6%) | 8/28 (28.5%) | 0.02 |
| Hypophosphatemia (yes) (n, %) | 16/52 (30.7%) | 11/24 (45.8%) | 0.006 |
| Hypokalemia (yes) (n, %) | 16/57 (28%) | 3/31 (9.6%) | 0.09 |
| Rickets (yes) (n, %) | 10/52 (19.2%) | 7/38 (18.4%) | 0.47 |
| Fractures (yes) (n, %) | 4/56 (7.1%) | 3/37 (8.1%) | 0.95 |
| Lower height-for-age (yes) (n, %) | 11/51 (21.8%) | 5 /27(18.5%) | 0.11 |
| HTN (yes) (n, %) | 1/56 (1.7%) | 6/37 (16.2%) | 0.035 |

% are calculated on the available data per each feature. Abreviation. ^aHTN Hypertension.

As seen in *table 18* and as expected, renal function was worst in patients older than 18 years, with higher creatinine (1.72 ± 1.16 mg/dl vs. 0.67 ± 0.35 mg/dl; $p < 0.001$). Importantly, calcium urinary loss with urine as measured by calcium/creatinine ratio was significantly lower in >18 years patients ($0.15 [0.11-0.18]$ vs. $0.34 [0.2-0.59]$; $p = 0.003$)

Table 18 Kidney function and electrolyte balance parameters at last follow-up. Differences according to age

| | <18 years old (n=59) | >18years old (n=39) | p |
|--|-------------------------|------------------------|------------------|
| Age at last follow-up, years (median, [IQR]) | 9 [5-14] | 26 [21-40] | <0.001 |
| Creatinine, mg/dL (mean±SD) | 0.67± 0.35 | 1.72±1.16 | <0.001 |
| eGFR, mL/min/1.73m² (mean±SD) | 95.9±34.1 | 78.4±44.5 | 0.045 |
| Serum potassium, mmol/L (mean±SD) | 3.9±0.49 | 3.8±0.49 | 0.97 |
| Serum total calcium, mg/dL (mean±SD) | 9.8±1.3 | 8.6±2.2 | 0.001 |
| Serum phosphate, mg/dL (median, [IQR]) | 3.9[3.4-4.4] | 2.8[2.2-3.1] | <0.001 |
| Protein/creatinine, mg/g (median, [IQR]) | 1500 [500- 2744] | 1500 [485- 2322] | 0.46 |
| Albumin/creatinine, mg/g (median, [IQR]) | 255[62-420] | 275[144-541] | 0.73 |
| U_{Ca}/Cr^c, mg/mg (median,[IQR]) CKD ^d | 0.34 [0.2-0.59] | 0.15[0.11-0.18] | 0.003 |
| No renal failure | 27/54 (50%) | 25/37 (32.4%) | 0.21 |
| Stage 2 (60-89ml/min/1.73m ²) | 22/54 (40%) | 3/37 (18.9%) | 0.073 |
| Stage 3 (30-59ml/min/1.73m ²) | 4/54 (7.4%) | 3/37 (8.1%) | 0.82 |
| Stage 4 (15-29ml/min/1.73m ²) | 1/54 (1.8%) | 7/37 (18.9%) | 0.015 |

^aeGFR, *estimated glomerular filtrate rate*; ^b LMWP. Low Molecular Weight Proteinuria ^cU_{Ca}/Cr, Urine calcium/creatinine ratio; ^dCKD. Chronic kidney Disease

1.6. Gene mutation spectrum

At least 86% (84/98) of reported patients had genetic diagnosis confirmation. Specific information about the *CLCN5* mutation was reported in 76 cases, amongst them there were 49 different mutations. Most common mutations identified in our study were missense mutations (36.7%), nonsense mutations (32.6%), splice-site mutations (14.3%), frameshift mutations (8.1%), in-frame

mutations (6.1%) and one large exon deletion (2%) (Figure 29). In 22 cases, mutation details were not provided. We did not find any previous reference in literature of 9 of these mutations. A list of all reported mutations is provided in Annex 5.

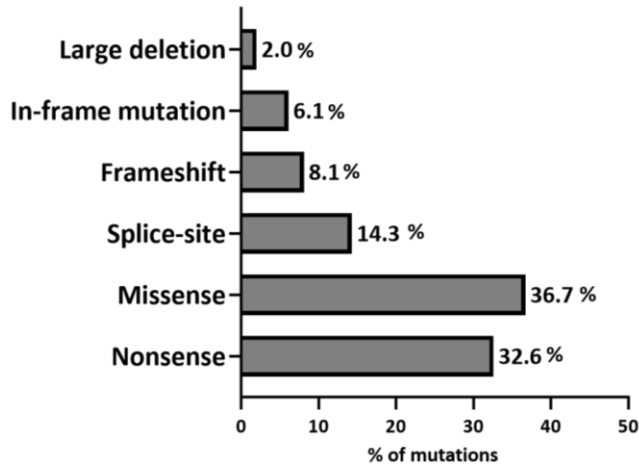


Figure 29 Type of CLCN5 mutations reported

1.7. Phenotype according to mutation severity

According to previous reports¹³⁰ and in view of the absence of in vitro data for many of the mutations, we arbitrary classified the mutations as severe (nonsense, frameshift, large deletion or splice-site mutations) and less severe (missense and in-frame mutations). No significant differences between severe and less severe mutations were found in terms of age at diagnosis (8 [3-13] vs. 6.5 [1.75-11.3] years; $p=0.33$), growth (patients with short stature, 10 (20.8%) vs. 5 (17.9%); $p=0.74$) and development or renal loss of cargos such as aminoaciduria (11 (22.9%) vs. 5 (17.9%) patients;

p=0.11), glycosuria (3 (6.2%) vs. 2 (7.1%); p=0.58) or calciuria (0.28 mg/mg [0.13-0.55] vs. 0.21mg/mg [0.11-0.43]; p= 0.548) (see *Table 19*). However, nephrocalcinosis was significantly more present in those patients with severe mutations than in those with less severe mutations (62.5% vs. 32.1%; p=0.03).

Table 19 Phenotypic findings in patients with Dent's Disease 1. Differences between severe and less severe mutations

| | Severe mutation (n=48) | Less severe mutation (n=28) | p |
|---|-------------------------------|------------------------------------|-------------|
| Age at diagnosis, years (median, [IQR]) | 8 [3-13] | 6.5 [1.75- | 0.33 |
| Premature (yes) (n, %) | 4/48 (8.3%) | 3/28 (10.7%) | 0.31 |
| Hypercalciuria (yes) (n, %) | 15/48 (31.2%) | 4/28 (14.3%) | 0.25 |
| Nephrolithiasis (yes) (n, %) | 9/48 (18.8%) | 6/27 (22.2%) | 0.93 |
| Nephrocalcinosis (yes) (n, %) | 30/48 (62.5%) | 9/28 (32.1%) | 0.03 |
| Aminoaciduria (yes) (n, %) | 11/48 (22.9%) | 5/28 (17.9%) | 0.11 |
| Glycosuria (yes) (n, %) | 3/48 (6.2%) | 2/28 (7.1%) | 0.58 |
| Hypophosphatemia (yes) (n, %) | 10/45 (22.2%) | 11/26 (42.3%) | 0.2 |
| Hypokalemia or Nomokaliemia with K supplementation (yes) (n, %) | 12/48 (25%) | 5/28 (17.9%) | 0.60 |
| Rickets (yes) (n, %) | 10/48 (20.8%) | 3/27 (11.1%) | 0.53 |
| Fractures (yes) (n, %) | 5/48 (10.4%) | 0 (0%) | 0.21 |
| Failure to thrive (yes) (n, %) | 6/48 (12.8%) | 3/26 (11.5%) | 0.96 |
| Lower height-for-age (yes) (n, %) | 10/48 (20.8%) | 5/28 (17.9%) | 0.74 |
| HTN ^a (yes) (n, %) | 5/48 (10.4%) | 1/28 (3.8%) | 0.56 |

% are calculated on the available data per each feature. Abbreviation. ^aHTN Hypertension.

Proteinuria as assessed by protein/creatinine ratio was also higher in patients with severe mutations (1802mg/g [500-2733] vs. 500mg/g [500-1500]; p=0.03). Nonetheless, albuminuria was lower in patients with more severe mutations (90mg/g [43.5-292] vs. 202mg/g [92.7-541]; p=0.03) (see *Table 20*).

Table 20 Kidney function and electrolyte balance parameters at last follow-up. Differences between severe and less severe mutations

| | Severe mutation (n=48) | Less severe mutation (n=28) | p |
|--|-----------------------------------|--|---------------|
| Age at last follow-up, years (median, Creatinine, mg/dL (mean±SD) | 15 [9-23.3] 1.01± 0.78 | 15 [7.15-21.2] 1.02±0.8 | 0.249 0.95 |
| eGFR ^a , mL/min/1.73m ² (mean±SD) | 78.8±43.5 | 86.3±42.1 | 0.47 |
| Serum potassium, mmol/L (mean±SD) | 3.8±0.52 | 3.9±0.47 | 0.36 |
| Serum total calcium, mg/dL (mean±SD) | 8.9±2.2 | 9.7±1.1 | 0.076 |
| Serum phosphate, mg/dL (median, [IQR]) | 3.8[2.9-4.1] | 3.4[2.8-4] | 0.245 |
| Protein/creatinine, mg/g (median, [IQR]) | 1802 [500- | 500 [500- | 0.03 |
| Albumin/creatinine, mg/g (median, | 90[43.5-292] | 202.10[92.7- | 0.047 |
| U _{Ca/Cr} ^c , mg/mg (median,[IQR]) | 0.28 [0.13- 0.55] | 0.21[0.11- 0.43] | 0.5 |
| CKD^d | | | |
| No renal failure | 18/48 (37.5%) | 12/28 (42.9%) | 0.44 |
| Stage 2 (60-89ml/min/1.73m²) | 16/48 (33.3%) | 9/28 (32.2%) | 0.55 |
| Age stage 2; years | 11.6±6.3 | 16.5±17.6 | 0.31 |
| Stage 3 (30-59ml/min/1.73m²) | 4/48 (8.3%) | 2/28 (7.1%) | 0.54 |
| Age stage 3; years | 15.7±4.9 | 14.5±9.1 | 0.8 |
| Stage 4 (15-29ml/min/1.73m²) | 4/48 (8.3%) | 2/28 (7.1%) | 0.54 |
| Age stage 4; years | 29.25±17.6 | 39±8.4 | 0.5 |
| Stage 5 (<15ml/min/1.73m²) or nnt^e | 5/48 (10.4%) | 1/28 (3.7%) | 0.33 |
| Age stage 5; years | 37.8±4.4 | 29 | 0.1 |

^aeGFR, estimated glomerular filtrate rate; ^b LMWP. Low Molecular Weight Proteinuria ^cU_{Ca/Cr},Urine calcium/creatinine ratio; ^dCKD. Chronic kidney Disease

Even so, eGFR was not significantly different between the groups (severe 78.8±43.5 vs. less severe 86.3±42.1; p=0.47) and the distribution of eGFR according to age was similarly variable in the two groups (*Figure 30*). When considering each grade of CKD separately, although not significantly different, patients with more severe mutations tended to be younger than those with less severe mutations in every group.

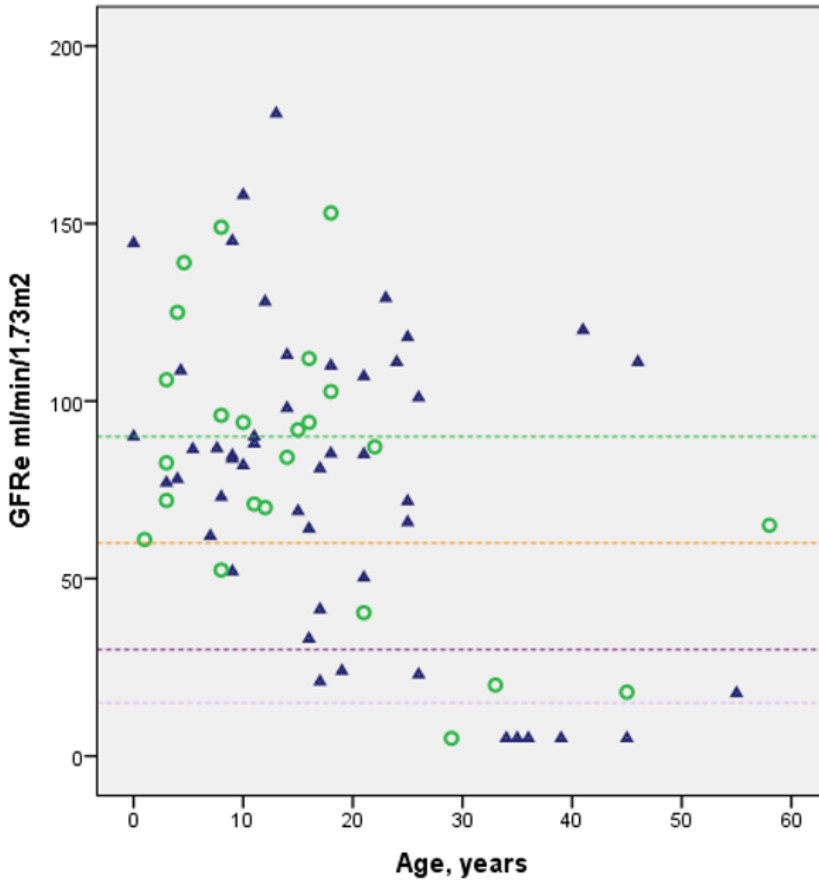


Figure 30 Evolution of eGFR according to age. Differences between severe (blue triangles) and less severe mutations (green circles). Dashed lines separate CKD 5 grades

1.8. Treatment

Thirty-two (32/98; 32.6%) patients were receiving thiazides at last follow-up. Eight (8/98; 8.1%) patients received angiotensin-converting enzyme inhibitors or angiotensin receptor blockers (ACEI/ARB). The effect of these treatments on protein excretion could not be evaluated as we did not have data on proteinuria

before their initiation. Among other treatments, seven patients (7/98; 7.1%) were receiving potassium sparing diuretics, 11 patients (11/98;11.2 %) were receiving potassium supplements and 49 patients (49/78; 62.8%) potassium citrate. Thirty patients (13/98; 13.3%) were also taking phosphate supplements.

2. Chapter 2. miRNA signature in uEVs from DD1 patients

2.1. Study population

DD1 is a rare disease with a limited number of diagnosed patients, therefore, from those Spanish nephrologist contacted before, a national call was made for patients' recruitment and samples were collected in several hospitals from different cities in Spain.

Thus, this study finally included:

- a) Twenty-five patients with genetically confirmed DD1 who had been diagnosed over 14 different hospitals in Spain (Figure 31)
- b) Ten age, sex and race matched healthy control.

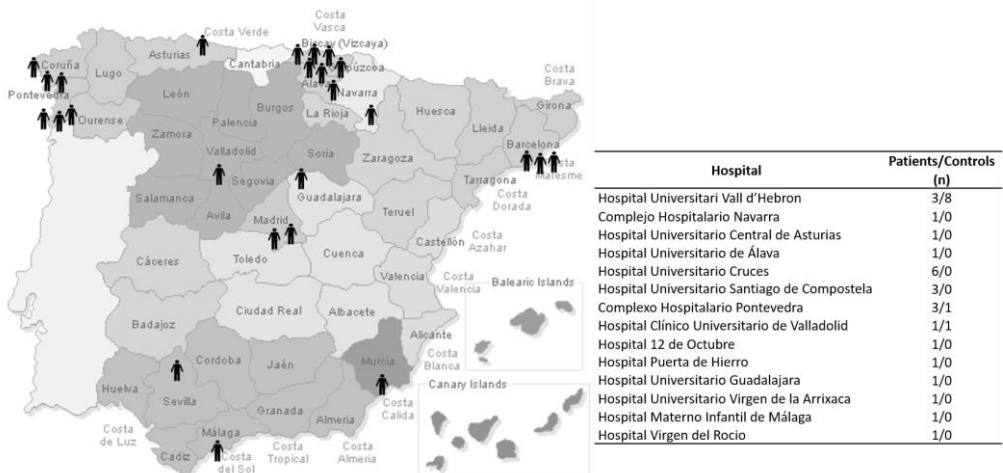


Figure 31 Origin of DD1 patients' samples

Patients and healthy subjects' demographical parameters are shown in *table 21*. There were no differences as for age, race or

sex (all the individuals studied were male). Other DD1 phenotypic traits are shown in the table.

Table 21 Basic demographics and clinical features of the discovery cohort

| | Dent's Disease Patients (n=25) | Healthy controls (n=10) | p |
|---|---|--|----------|
| Age at last follow-up, years (median,[IQR]) | 11.5 [4.75-19] | 10 [8.5-25] | 0.67 |
| Sex, male (n, %) | 25 (100%) | 10(100%) | n.a |
| CKD | | | |
| No renal failure (>90 ml/min/1.73m2) | 12 (52.2%) | 10 (100%) | 0.007 |
| Stage 2 (60-89ml/min/1.73m2) | 5 (21.7%) | 0 (0%) | 0.291 |
| Stage 3 (30-59ml/min/1.73m2) | 3 (13%) | 0 (0%) | 0.53 |
| Stage 4 (15-29ml/min/1.73m2) | 3 (13%) | 0 (0%) | 0.53 |
| Stage 5 (<15ml/min/1.73m2) or RRT | 0 (0%) | 0 (0%) | na |
| Nephrocalcinosis, yes (n,%) | 13 (52%) | 0 (0%) | na |
| Lithiasis yes (n,%) | 4 (16%) | 0 (0%) | na |
| Incomplete Fanconi Syndrome (glucosuria and/or aminoaciduria) yes (n,%) | 4 (16%) | 0 (0%) | na |
| Rickets yes (n,%) | 3 (12%) | 0 (0%) | na |

Individual written informed consent was collected from each participant or their parents or legal tutors before enrolment in compliance with the Ethics Committee of the “Hospital Vall d’Hebrón” which approved the study (approval number PR(AG)149/2020/ 314/C/2020).

2.1. Isolation and characterization of urinary exosomes

In order to validate the purity of exosomes obtained from urine, after isolation following the protocol described before (see section 2.3 in Materials and Methods), morphology, shape, and size of exosomes were analysed.

Morphological characterization of uEVs was performed by Cryo-TEM direct visualisation. Our results revealed single, double or multi-layered vesicles as well as different sized uEVs with no obvious impurities (*Figure 32A*).

Size distribution and relative concentration of microvesicles were assessed by means of nanoparticle tracking analysis (NTA) in samples randomly selected (n=12 patients, n=5 control). The relative concentration of uEVs was similar between controls and patients' groups, although presented certain variability among the examined samples (*Figure 32B*). As seen in *figure 32C*, most vesicles detected had less than 200 nm diameter as expected for exosomes. Interestingly, patients' exosomes were significantly larger than those of control subjects (average controls 100.9 ± 8.53 nm vs. patients 145 ± 8.53 nm; $p < 0.01$).

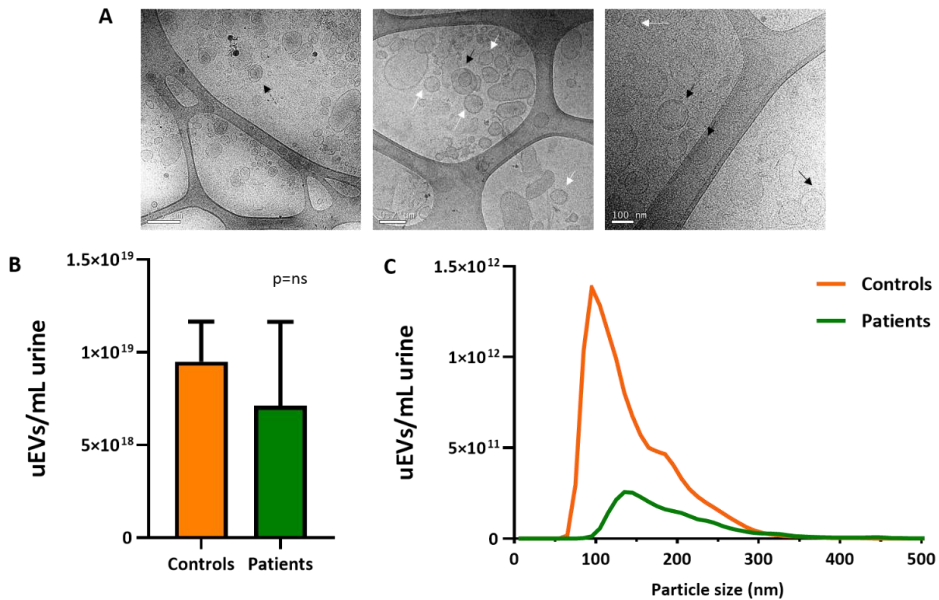


Figure 32 Characterisation of isolated uEVs. A. Micrographs with different scales (500 nm, 200 nm and 100 nm from left to right) show single (white arrow), double (black solid arrow) or multi-layered (black dashed arrow) vesicles. B. uEVs concentration. No significant (ns) differences were found between patients and controls. C. NTA size and particle distribution plot. Most vesicles were <200 nm in diameter as expected for exosomes. Abbreviations: uEVs. Urinary Exosome-liker Vesicles. Ns. Non-significative

In addition, two exosome-associated markers (namely Alix and CD81)³⁵⁹ were assessed by western blot (WB) to further confirm the presence of urinary exosomes (Figure 33). Both markers were detected in all the exosome mixtures (both in patient and control samples) and absent in the supernatant from each sample, which was used as negative control to confirm lack of contamination from cell debris or others. Moreover, we used an endoplasmic reticulum marker (Grp78) to demonstrate the absence of intracellular structures in the exosome suspensions. HepG2 cell

line lysate was used as a positive control for Grp78 detection. As shown in *figure 33* Grp78 could only be detected in HepG2 cell lysate but not in any of the exosome mixture.

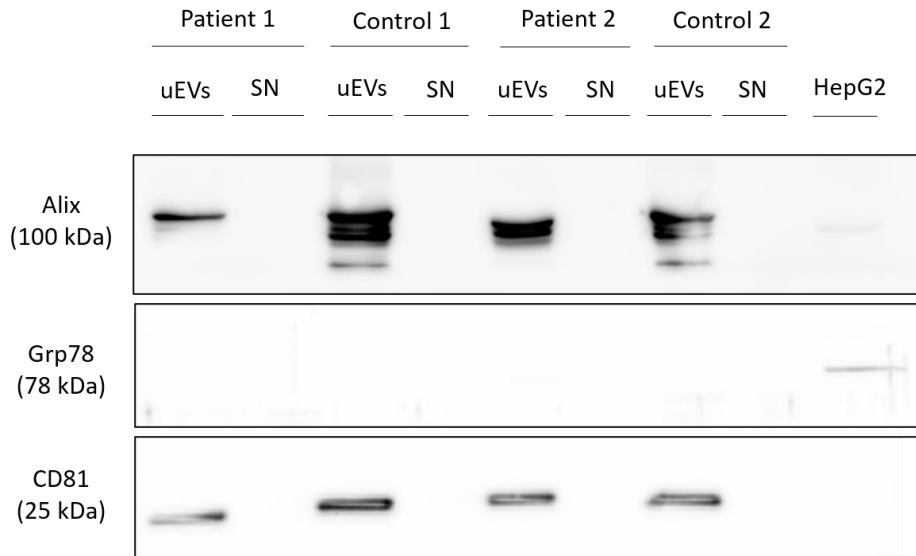


Figure 33 Immunoblotting of exosome associated markers. Urinary exosome mixture (uEVs) and supernatant (SN) lysates from both patients and controls were blotted against exosome associated markers (Alix and CD81) and endoplasmic reticulum marker (Grp78). HepG2 cell lysate was used as positive control for Grp78 and as negative control for exome associated-markers Alix and CD81. Alix and CD81 were present in uEVs of both patients and controls were absent in the supernatants of all individuals. Grp78 was absent in all the samples and positive in the HepG2 cell lysate. Abbreviations: uEVs: Urinary Exosome-like Vesicles. SN Supernatant. Grp78: Glucose regulatory protein 78; CD81: Cluster of Differentiation 81; HepG2 Hepatocellular carcinoma G2 cell line.

2.2. RNA extraction and quantification

After exosome isolation and appropriate characterization, exosome RNA was extracted with *miRNeasy Mini kit*. Quantification of RNA levels was performed using *BioAnalyzer 2100* in combination with *RNA 6000 Pico LabChip kit*. Similar

electropherograms were obtained for all the samples. Total quantification of RNA showed no differences between controls and patients (concentration ranging from 1000-5000 pg/ μ L) (figure 34A). The electropherograms showed parallel shapes and RNA integrity in all samples and, as shown in an example, in figure 34B, there was a high peak corresponding to small RNA (in this case 250 nt RNA) and two lower peaks of larger size corresponding to either 18S or 28S ribosomal RNAs (average size 1800 and 2800, respectively) as indicated.

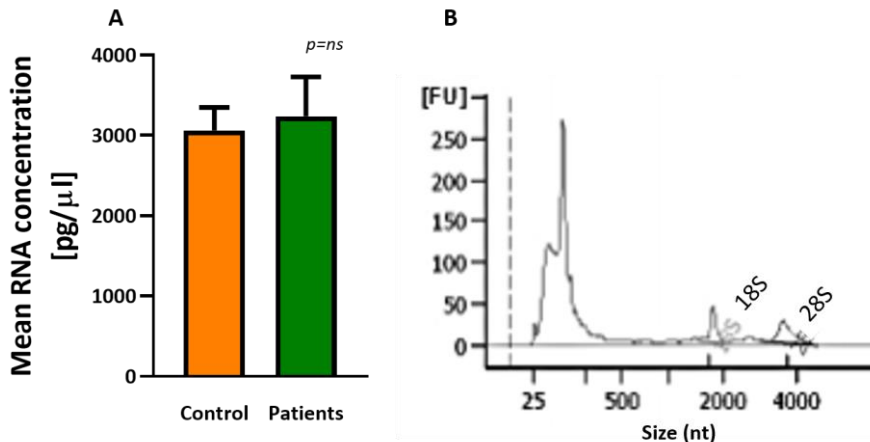


Figure 34 Exosome RNA quantification and profiling A. Total RNA extracted from uEVs was quantified by BioAnalyzer 2100. No statistically significant differences were noticed between controls and patients. B Example of an electropherogram from one of the profiled RNA samples. All graphs showed a larger amount of smaller size RNA. Two peaks of superior size corresponding to ribosomal RNA (18S and 28S) were detected in a much-reduced amount. Abbreviations: uEVs: Urinary Exosome-like Vesicles. FU. Arbitrary fluorescence units. Nt. Nucleotides. Ns. No statistically significant.

2.3. miRNA quantification by OpenArrays qPCR

Analysis of the exosomes-associated miRNA was performed using Taqman OpenArray technology. 754 human miRNA were amplified

in each sample and, so, we obtained 754 Crt values for each subject. miRNA with a Crt value >28, AmpScore <1.24 or Cqconf < 0.8 were considered unamplified for further analysis.

2.3.1. miRNA differentially expressed

2.3.1.1. DD1 patients vs. healthy controls

In a first approach, t-test analysis was applied to establish the miRNA differentially expressed between patients and controls. Results of this analysis revealed 82 miRNA significantly dysregulated between the groups (p. adjusted <0.05) (*List in Annex VII*). Of interest, almost all miRNA were significantly upregulated in patients compared to healthy controls, except for three miRNA, that were downregulated (*Figure 35*).

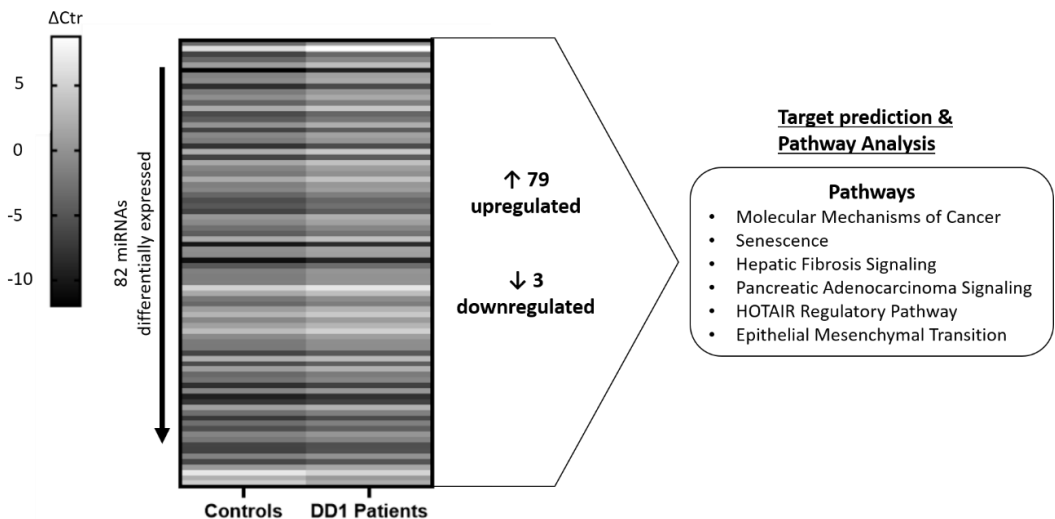


Figure 35 miRNA differentially expressed between controls and DD1. Graph represents ΔC_{tr} controls and ΔC_{tr} patients from miRNA differentially expressed (p.adj<0.05). Main

pathways in which these miRNA and their mRNA targets are involved as assessed by Ingenuity Pathway Analysis (IPA). Abbreviation:DD1. Dent's Disease type 1.

To analyse the targets of these miRNA and the functions and pathways they are involved in, the differentially expressed miRNA were uploaded to IPA (Ingenuity Pathway Analysis). IPA of differentially expressed miRNA revealed 493 significant canonical pathways and 51 significant molecular and cellular functions in various diseases. *Figures 36 and 37* show the top 25 functions and 25 pathways respectively in which the differentially expressed miRNA are involved.

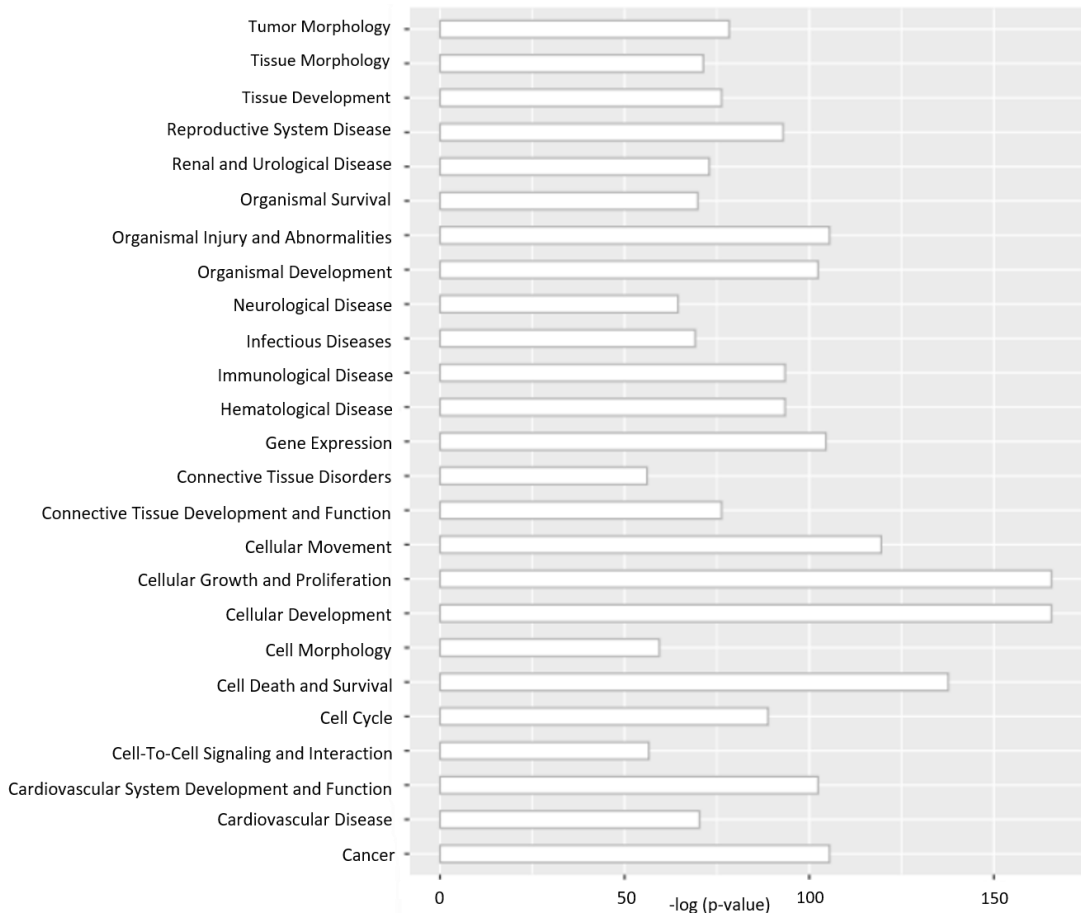


Figure 36 Top 25 functions in which the target mRNA for the differentially expressed miRNA between controls and patients are involved as assessed by Ingenuity Pathway Analysis.



Figure 37 Top 25 pathways in which the target mRNA for the differentially expressed miRNA between controls and patients are involved as assessed by Ingenuity Pathway Analysis.

The major experimentally assessed contributing genes to the top six canonical pathways are shown in (annex VIII). Likewise, the top six functions altered by the dysregulated miRNA are annex IX with their corresponding genes.

2.3.1.2. Top 6 miRNA differentially expressed between DD1 patients and controls

In a second more restrictive approach, those miRNA which were more differentially up- or downregulated (adj. p-value < 0.05; $0.15 < RQ > 2$) in patients compared to controls were chosen for more thorough analysis. The differential expression analysis yielded a list of 6 miRNA graphed in *figure 38*.

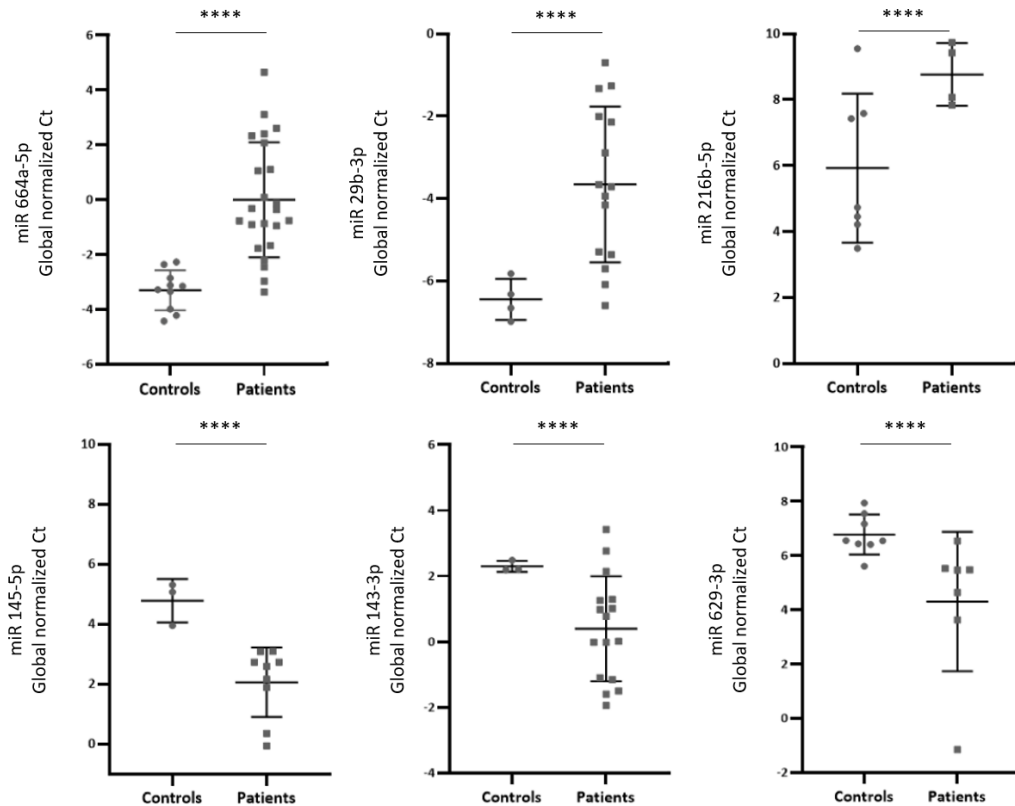
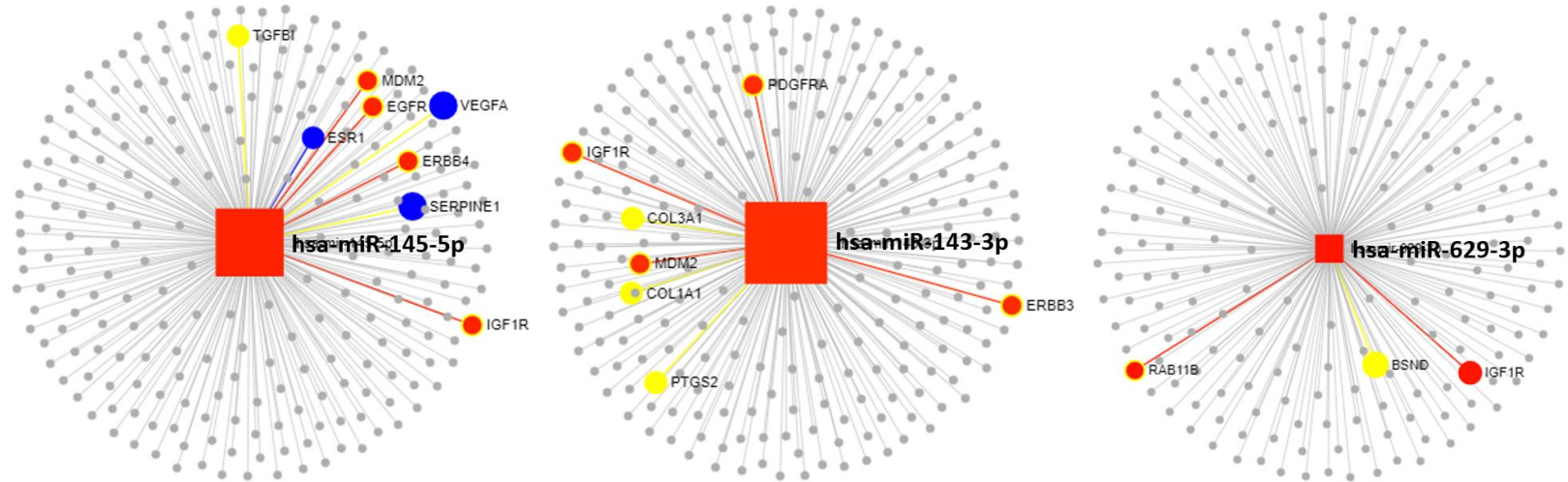


Figure 38 Top six miRNA differentially expressed between DD1 patients and healthy controls. Global normalized Ct for controls and patients are plotted as mean ± SEM, **** $p < 0.001$.

Six most dysregulated miRNA presented as targets genes involved in inflammation, senescence and fibrosis, pathways like TGF- β signaling pathway, p53 pathway, Wnt/ β -catenin signaling pathway, cell cycle regulation, MAPK signaling pathway and JAK-STAT signaling pathway. However, when considering each miRNA separately and bearing in mind those disease and pathways potentially related to DD1, most of these miRNA targeted genes involved in fibrosis, kidney pathologies and endocytosis. As depicted in figures 39 and 40, miR-143-3p targets genes related to fibrosis such as *COL3A1* and *COL1A1*; also miR-29b-3p targets fibrosis-related genes such as *TGF- β* , *STAT3* or *COL3A1* and *COL1A1*. *miR-629-3p* and *miR-29b-3p* regulate genes in the *RAB11* family, implied in endocytosis in the proximal tubule³⁶⁰ and also thought to regulate the endocytosis and recycling of the epithelial sodium channel (ENaC) in the cortical collecting duct³⁶¹. Some others target genes related to other tubulopathies; remarkably, the hsa-miR-629-3p has as a target the gene *BSND*, which encodes for Barttin, a potential regulator for several chloride channels or miR-664a-3p which regulates mRNA related to some forms of glomerulosclerosis^{88,362}.

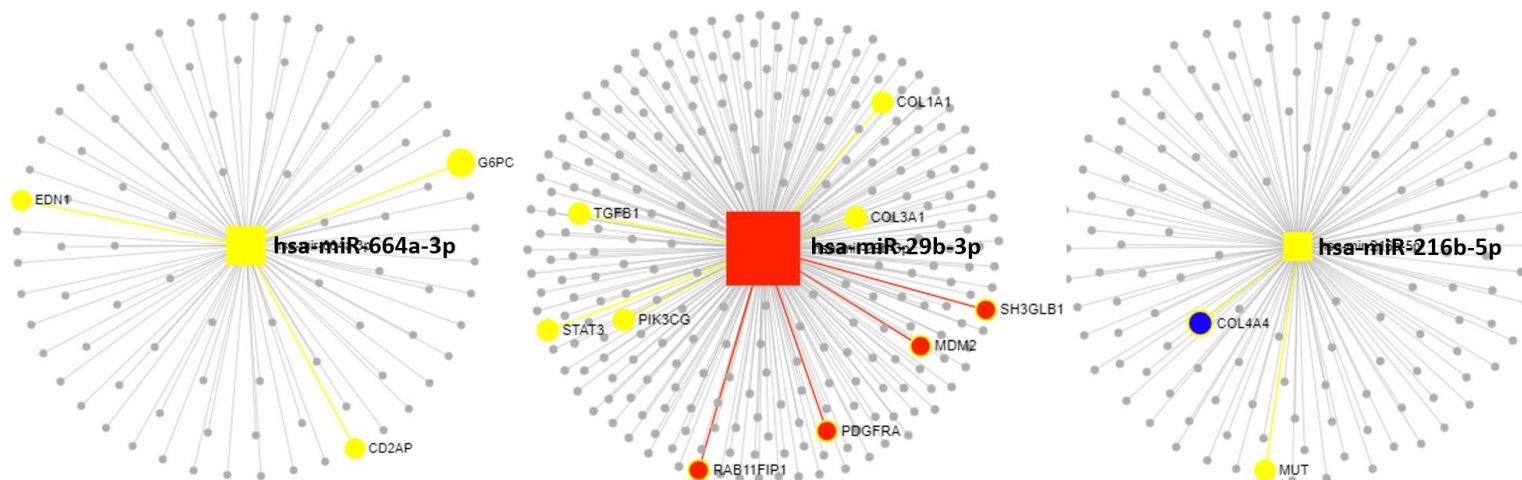


has-miR-145-5p targets genes involved both in endocytosis regulation (red dots) and atherosclerosis (blue dots). miR-145-5p has also been described in diabetic nephropathy pathophysiology (yellow dots)

has-miR-143-3p targets genes involved both in fibrosis development (yellow dots) and endocytosis regulation (red dots).

has-miR-629-3p targets genes involved in endocytosis regulation (red dots). This miRNA has as a target BSND which encodes for an essential beta subunit for CLC-k channel. Its mutation causes Bartter Syndrome.

Figure 39. Genes targeted by the top 3 downregulated miRNA differentially expressed between DD1 patient and control. Genes were either experimentally observed or highly predicted by Ingenuity Pathway Analysis and miRNet as source of information. Genes associated to some kidney disease-associated process are plotted. Note that the sizes of the nodes (square representing the miRNA) are relative to the number of target genes.



has-miR-664a-3p targets genes involved in focal glomerulosclerosis (yellow dots).

has-miR-29b-3p targets genes involved in endocytosis regulation (red dots) and in regulation of kidney fibrosis (yellow dots).

has-miR-216b-5p targets genes involved in chronic kidney disease (yellow dots) (MUT & COL4A4). COL4A4 (blue dot) is involved in the pathogenesis of Alport Syndrome.

Figure 40 Genes targeted by the top 3 upregulated miRNA differentially expressed between DD1 patient and control. Genes were either experimentally observed or highly predicted by Ingenuity Pathway Analysis and miRNet as source of information. Genes related to some kidney disease-associated process are plotted. Note that the sizes of the nodes (square representing the miRNA) are relative to the number of target genes.

2.3.1.3. DD1 patients: different phenotypes, different miRNA

Finally, we compared the miRNA of patients with different DD1 phenotypes. No differences were found in miRNA expression either between those patients who presented with nephrocalcinosis and those who did not; nor between patients who had suffered from rickets. We did find differences between miRNA expression such as miR-660-5p, miR-187-3p, miR-200a-5p, in patients with $FGe > 90$ mL/min/1.73m² and patients with some degree of CKD ($FGe < 90$ mL/min) (Figure 41). Due to the limited size of the study population, no comparison could be done between different degrees of CKD.

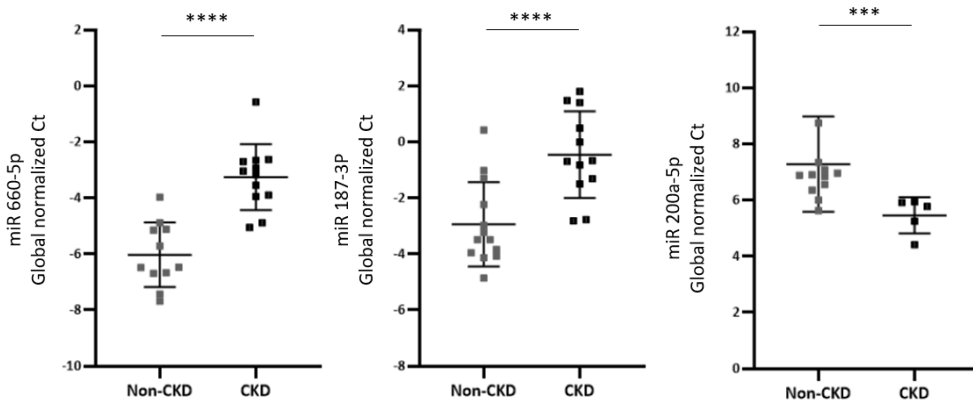


Figure 41 miRNA differentially expressed between patients with no CKD ($Fge > 90$ ml/min) and patients with CKD ($Fge < 90$ ml/min/1.73m²). Global normalized Ct for patients with no CKD (grey squares) and patients with CKD (black squares) are plotted as mean \pm SEM, *** $p < 0.001$, **** $p < 0.0001$

We also found significant differences as for miRNA in uEVs from patients with incomplete Fanconi Syndrome. miR-143-3p was downregulated in patients with urinary loss of amino acids or phosphate in comparison to those patients without this affection. Likewise, both miR-17-5p and miR-181a-5p were upregulated in patients who had presented with some lithiasis episode (*Figure 42*).

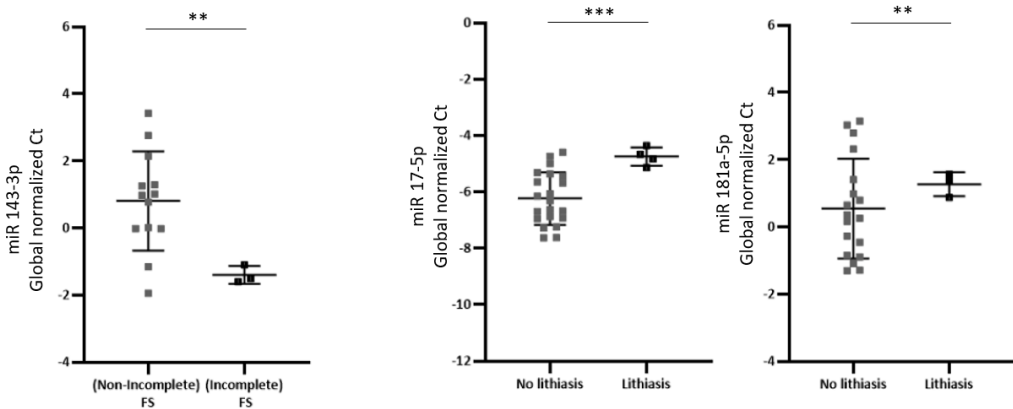


Figure 42 miRNA differentially expressed between patients with and without (incomplete) Fanconi Syndrome (FS) and miRNA differentially expressed between patients with and without lithiasis. Global normalized Ct for patients with no (incomplete) Fanconi Syndrome or lithiasis (black squares) are plotted as mean \pm SEM, ** $p < 0.01$, *** $p < 0.001$; **** $p < 0.0001$

3. Chapter 3: Validation of DD1 cellular model

3.1. mRNA and protein CLC-5 levels in RPTEC stable cell lines

This research follows from a bigger project with a holistic approach of DD1. Cell lines employed in this section were previously generated by our group (Renal Physiopathology Group, Vall d'Hebrón, Barcelona) as described before (see section 3.2 in materials and methods).

First of all, RNA was extracted from all cell lines, retrotranscribed into cDNA and then we sequenced the shRNA targeted *CLCN5* region to confirm that cell lines rClc5 WT, rClc5 E527D (in this section named as E527D), rClc5 I524K (in this section named as I524K) and rClc5 V523del (in this section named as V523del) contained the rescue sequence (as shown in *Figure 43A*). The region where the mutations had been previously introduced by site-directed mutagenesis showed E527D, I524K and V523del correct emplacement (*Figure 43B*)

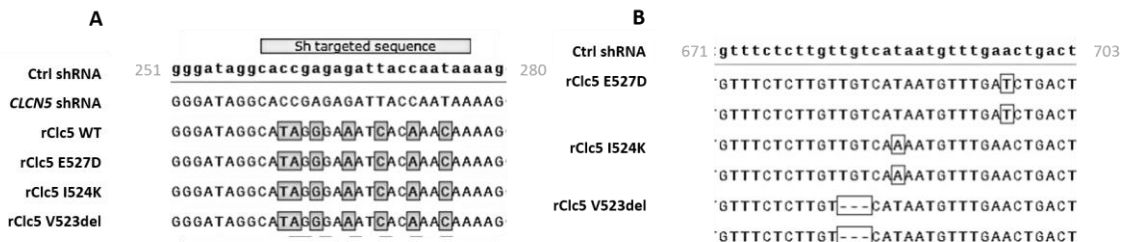


Figure 43 Sequencing of the shRNA targeted *CLCN5* region (A) and of the introduced mutations E527D, I524K and V523del (B)

Next, we checked both *CLCN5* knockdown (KD) efficiency and *CLCN5* overexpression levels for all cell lines. Endogenous *CLCN5* levels were used to test KD efficiency while HA levels were quantified for the *CLCN5* overexpression. As seen in *Figure 44A*, levels of endogenous *CLCN5* were reduced in all cell lines in comparison with the control shRNA cell line (KD efficiency as compared to Ctrl shRNA were 0.87% CLCN5 shRNA, 0.69% rClc5 WT, 0.92% rClc5 E527D, 0.97% rClc5 I524K, 0.92% V523del.) In addition, all cell lines carrying the overexpression vector (rWT, E527D, I524K and V523del) had detectable HA mRNA levels (*Figure 44B*).

This procedure was performed every time new cells were thawed and also periodically to evaluate whether the KD and overexpression levels were correct.

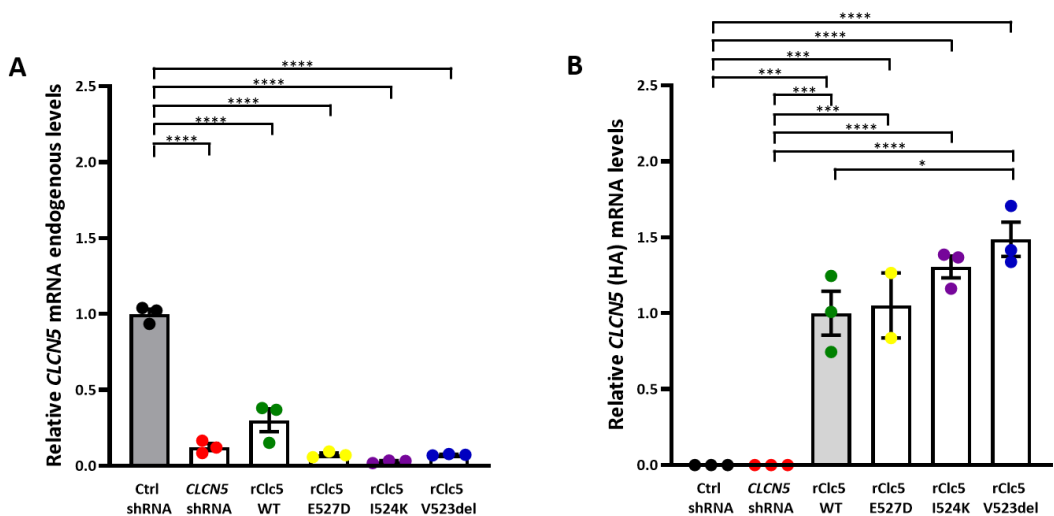


Figure 44 Endogenous and exogenous *CLCN5* mRNA levels. A. Endogenous *CLCN5* was efficiently silenced in all cell lines as compared to Ctrl shRNA. B. WT cell line and the

Mutants with the overexpression vector showed detectable HA mRNA levels. Levels normalised to rClc5. **** $p < 0.0001$, *** $p < 0.001$, ** $p < 0.01$, * $p < 0.05$

Additionally, protein expression levels were evaluated. First, we attempted to detect endogenous CIC-5. However, all antibodies against CIC-5 tested in our lab gave unspecific bands for all the cell lines (For example, antibody #OAAN01462 from Aviva Systems Biology shown in *Figure 45*) so we proceed to check the expression of the rescue cell lines taking advantage of the HA-tag.

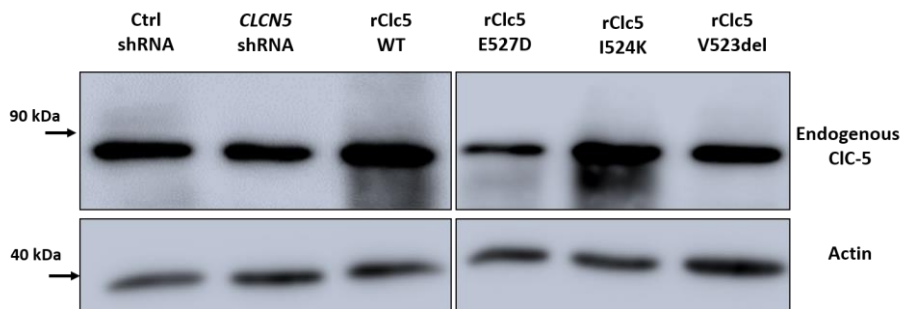


Figure 45 Immunoblotting against endogenous CIC-5. Different antibodies tested gave unspecific bands for all the cell lines

As seen in *Figure 46*, anti-HA antibody revealed reliable bands of the expected molecular weight. At the protein level, CIC-5 was detected as a lower band running at 80-90 kDa and a higher diffuse band running as a smear at about 100 kDa, which was consistent with previous reports and would account for the mature and the immature forms^{95,363}

Our results showed that CIC-5 WT together with E527D presented higher levels of CLC-5-HA protein than I524K and V523del despite the same amount of total protein was loaded. Importantly, CIC-5

detected levels were much lower in the I524K cell line, which is known to be retained in the ER, and in V523del mutant, which remains elusive whether it remains also stuck in the ER.

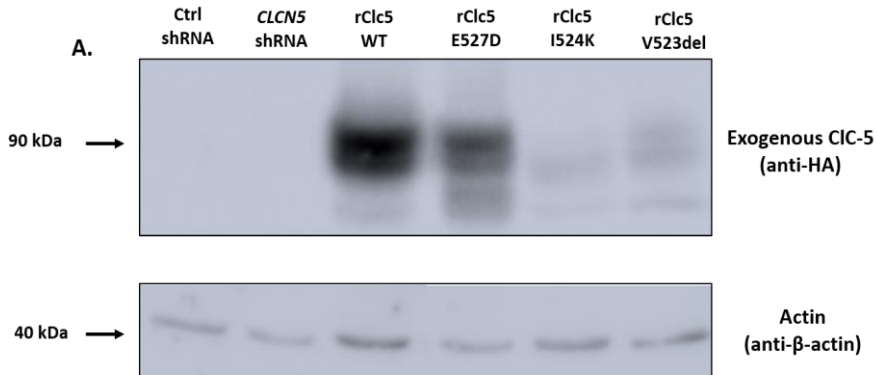


Figure 46 Exogenous-CIC5 quantification. A. Protein expression of CIC-5-HA and actin. B. Quantification of CIC5-HA normalized by actin. * $p < 0.05$

3.2. Comparison of CIC-5 half-life between WT and Mutants: V523del has a longer span.

Before moving forward with successive assays, it was necessary to evaluate if any of the Mutants had a half-life (time for 50% of the protein to be degraded) too short as to disrupt experiments. The rate of degradation of CIC-5 in the WT and Mutant cell lines was determined by a time-course experiment using cycloheximide to block the synthesis of new proteins followed by Western blotting detection.

Our data revealed that WT CIC-5 had a half-life ~ 2 hours (similar to what was described before for endogenous CIC-5^{162,364}). Surprisingly, the I524K and E527D mutated cell lines showed a CIC-

5 half-life (2 hours) similar to the WT CIC-5; I524K in fact presented a much faster reduction during the first hour, while the mutant V523del had a more elongated half-life (> 2 hours) (Figure 47).

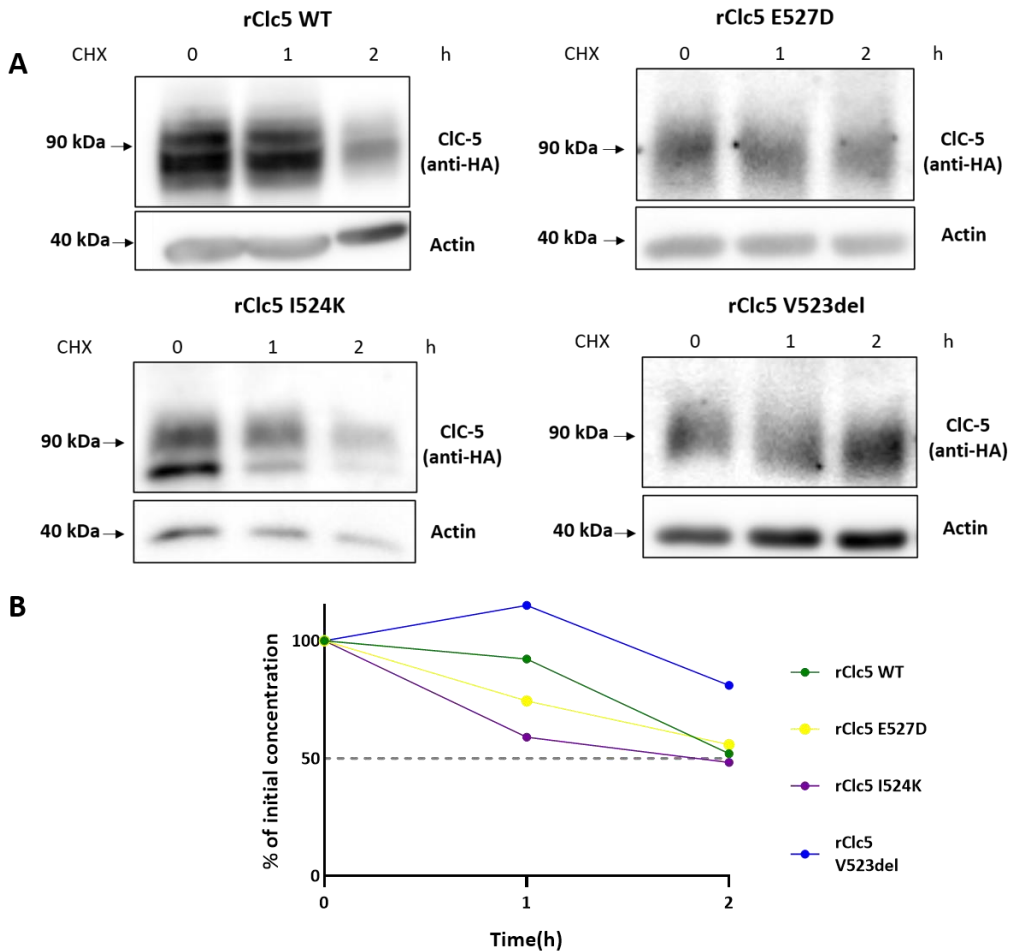


Figure 47 Cycloheximide-chase analysis of WT and mutant CIC-5 A. Cells were exposed to cycloheximide (CHX) for different chase times to assess protein half-life. B. CIC-5 concentration as % of initial concentration per time point.

3.3. CLC-5 WT and Mutants' localization in the endo-lysosomal pathway

To evaluate whether mutations affect trafficking of CLC-5 along the endo-lysosomal pathway, confocal microscopy imaging was performed to stain different compartments of this pathway. First, we tested the localization of WT and Mutant CLC-5 at the early endosomes using Rab5 as a marker of this compartment ⁴⁵. As shown in *Figure 48*, WT CLC-5 clearly colocalizes with Rab5 (Manders' Coefficient=0.3), as described before ⁹⁵. Mutant E527D showed less colocalization with Rab5 than WT CLC-5 (Manders' coefficient = 0.15) but still more than V523del (Manders' coefficient = 0.1) and I524K (Manders' coefficient = 0.08) which showed little colocalization with Rab5. A reduced localization of I524K in early endosomes is somehow expectable, as most of the CLC-5 protein would be retained in the ER.

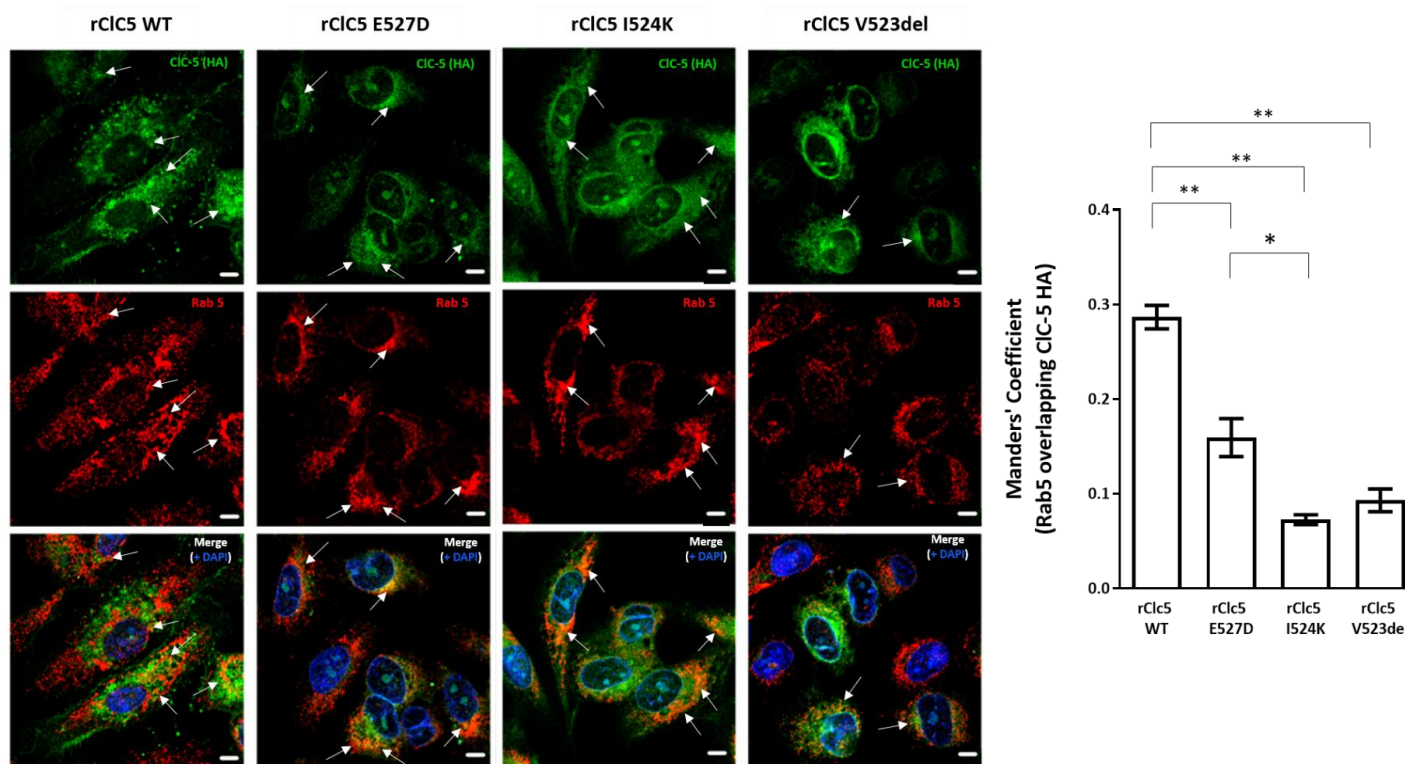


Figure 48. Establishment of CIC-5 localisation in Early endosomes. Left. Immunofluorescence of CIC-5-HA (green) and Rab5 (early endosome marker, in red) in RPTEC/hTERT1 cell. Right. Quantification of CIC-5-HA colocalization with early endosomes by Manders' Coefficient. Scale bar 5 μ m $p^* < 0.05$. $p^{**} < 0.01$

Next, to discard that Mutants were miss-targeted for degradation, colocalization of CIC-5-HA with LAMP1, a marker for lysosomes, was tested (*Figure 49*). Our results showed less colocalization in Mutants than in WT cell line, especially low for I524K mutant, which correlates with the expression data (WT is expressed at higher levels than the Mutants). This discards that the defects of CIC-5 function in the Mutants is due to a higher lysosomal localization that may lead to a higher rate of degradation.

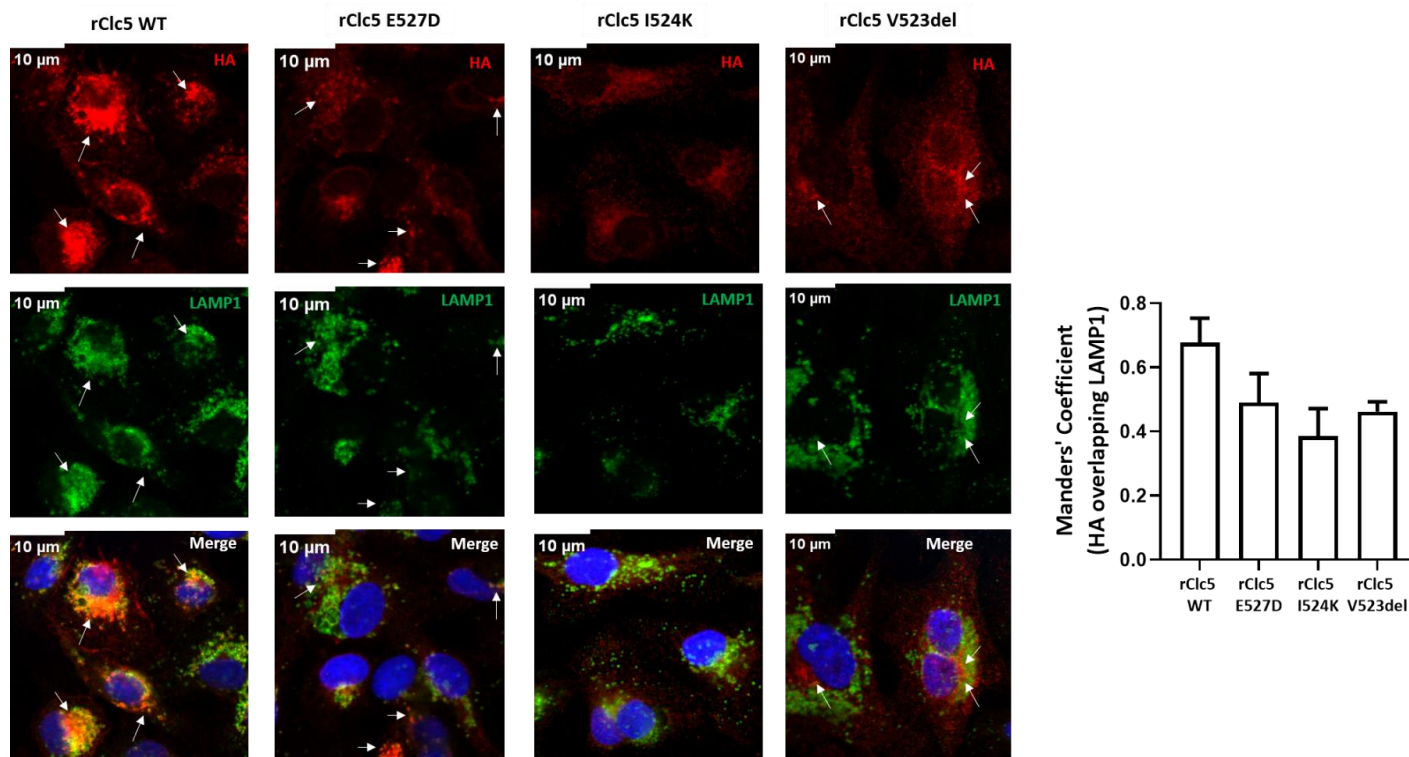


Figure 49 Establishment of CIC-5 localisation in lysosomes. Left. Immunofluorescence of CIC-5-HA (green) and LAMP1 (early endosome marker, in red) in RPTEC/TERT1 cell. Right. Quantification of CIC-5-HA colocalization with lysosomes by Manders'Coefficient. Scale bar 5 μm $p^*<0.10$. $p^{**}<0.01$

3.4. Assessment of receptor-mediated and fluid-phase endocytosis in DD1 cell model.

3.4.1. Evaluation of receptor-mediated and fluid-phase endocytosis via fluorimetry.

One of the aims of generating a cell model for DD1 is to have an in vitro system as reliable as possible to test the effectiveness of potential future therapies, for example, by quantifying the recovery of endocytosis, which is impaired in PTCs in DD1 ⁹⁸.

In order to quantify receptor-mediated endocytosis, which is essential for proteins, vitamin-binding proteins, hormones and essential cargoes uptake in PTCs (see section 4.2, Introduction) and also to assess fluid-phase endocytosis, differentiated RPTEC control cells were incubated with fluorescent albumin (a cargo mainly for receptor-mediated endocytosis) and fluorescent dextran (marker of fluid-phase endocytosis). After several washes to ensure the removal of the non-uptaken fraction of labelled cargoes, cells were lysated and Alexa fluor 488 albumin and FITC-dextran fluorescence was quantified by means of fluorimetry, using black bottom plates. As shown in *Figure 50A*, after a given time of incubation with labelled albumin, intracellular fluorescence detection started decreasing implying that (1) probably the number of receptors is limited, so that no more cargo can be endocytosed if there are no unoccupied receptors on the cell membrane and (2) the system degrades more albumin than it uptakes after 1 hour incubation.

As for fluid-phase endocytosis, fluorescence of internalised dextran increased over time suggesting it is a continuous process with no limiting factor, as already described in literature^{75,365}.

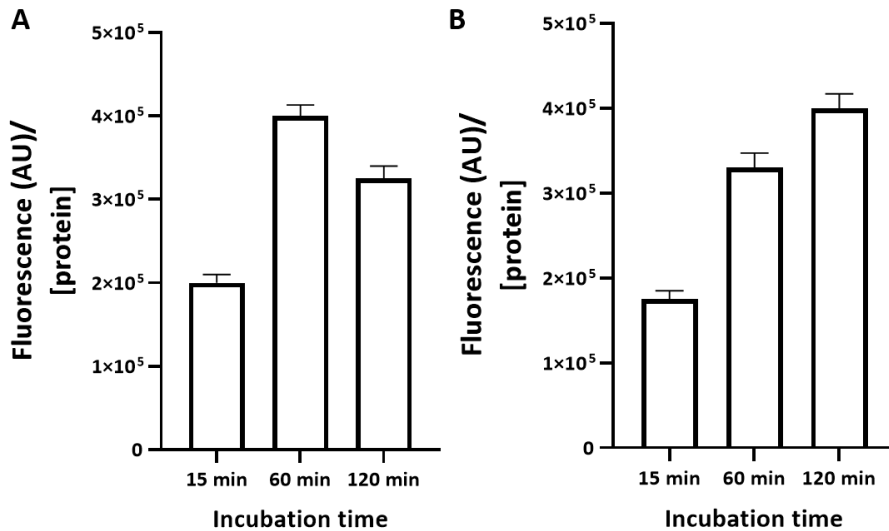


Figure 50 Quantification of receptor-mediated and fluid-phase endocytosis in RPTEC. Ctrl cells were incubated for 15 min, 60 min and 120 min with AlexaFluor 488-albumin, 50 $\mu\text{g}/\text{mL}$ (A) and (B) FITC-Dextran 50 $\mu\text{g}/\text{mL}$. After several washes, cell lysate fluorescence was measured by fluorimetry for both cargoes and normalized to the protein total concentration, to assess receptor-mediated (A) and fluid-phase (B) uptake dynamics.

In order to better assess the specificity of albumin uptake by receptor-mediated endocytosis, we performed competition assays using non-labelled albumin, seeking to see a reduction in albumin fluorescence given the competition for the receptors present on the plasma membrane. Increasing concentrations of non-labelled albumin gradually reduced the labelled albumin signal, so that competition with 200-fold excess unlabelled albumin (10mg/mL) reduced up to 40% the detection of labelled albumin (Figure 51A).

The obligatory question derived from these results was if the remaining 60% of labelled albumin detection was due to (1) invalidity of the model to quantify receptor-mediated-endocytosis as assessed by the little reduction showed with competition (2) additional endocytosis of albumin via fluid-phase endocytosis; (3) detection of albumin attached to the cell membrane despite several washes with no detection of fluorescence (not over the background) in the last rinsing solution.

To discard (1), we evaluate the proportion of albumin being retrieved exclusively by receptor-mediated endocytosis by adding bafilomycin-A1, which is a V-ATPase inhibitor that blocks receptor-mediated endocytosis by preventing endosomal acidification (see Introduction. Section 4.2.2) ³⁵⁷. As seen in *figure 51B* this blockade caused 40% reduction in albumin uptake, the same as by challenging fluorescent albumin with non-labelled albumin.

In order to see the net effect of the receptor-mediated endocytosis and to evaluate (2), the possibility that albumin was being retrieved by fluid-phase endocytosis, we attempted to saturate this fluid-phase uptake by exerting competition with dextran. We observed that competition with 200-fold non-labelled dextran reduced by a 20% the uptake of albumin. Curiously, there was a 20% increment of albumin uptake with 2mg/mL dextran competition. *Figure 51C*

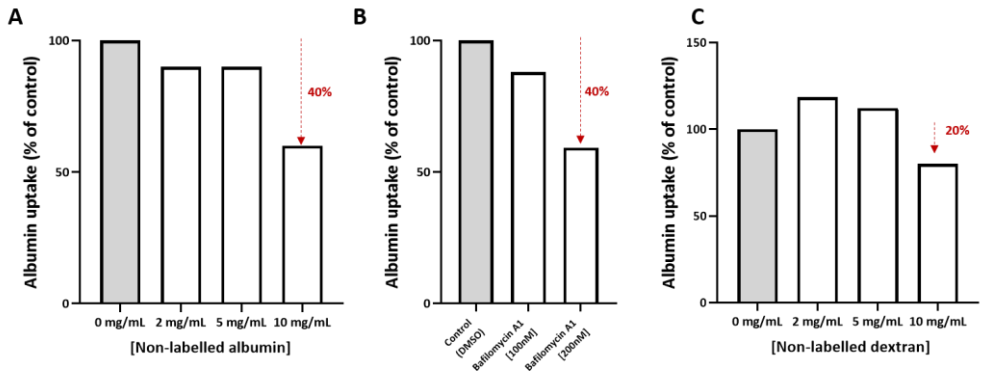


Figure 51 Quantification of receptor-mediated endocytosis of fluorescent albumin in competition with non-labelled albumin, non-labelled dextran or inhibited by Bafilomycin A1. Control cells were incubated with fluorescent albumin 50 $\mu\text{g}/\text{mL}$ and in competition with (A) different concentration of non-labelled albumin, (B) together with different concentration of bafilomycin, inhibitor of the V-ATPase, to block receptor-mediated endocytosis and (C) in competition with different concentrations of dextran. Albumin uptake was measured by fluorimetry and is plotted as % of uptake without competition of inhibition with bafilomycin (grey bar)

3.4.1.1. Evaluation of receptor-mediated endocytosis by *CIC5* Mutants

Albumin uptake was also assessed for the different cell lines both with and without competition with non-labelled albumin. In both Ctrl shRNA and rCIC-5 WT, competition with non-labelled albumin caused a reduction of 42.3% and 49.1% compared to the uptake without competition. The albumin uptake by the *CLCN5* KD presented a reduction of 38% as compared to Ctrl shRNA, which was further reduced by competition with non-labelled albumin reaching 59% reduction as to the Ctrl shRNA. Regarding the Mutants, as compared to the CIC-5 WT both I524K and V523del were found to have a significant reduction in albumin uptake (14% and 13 % respectively as compared CIC-5 WT), further reduced by

competition with non-labelled albumin. To our surprise, E527D mutant did not alter endocytosis as compared to the CLC-5 WT, despite showing significant reduction

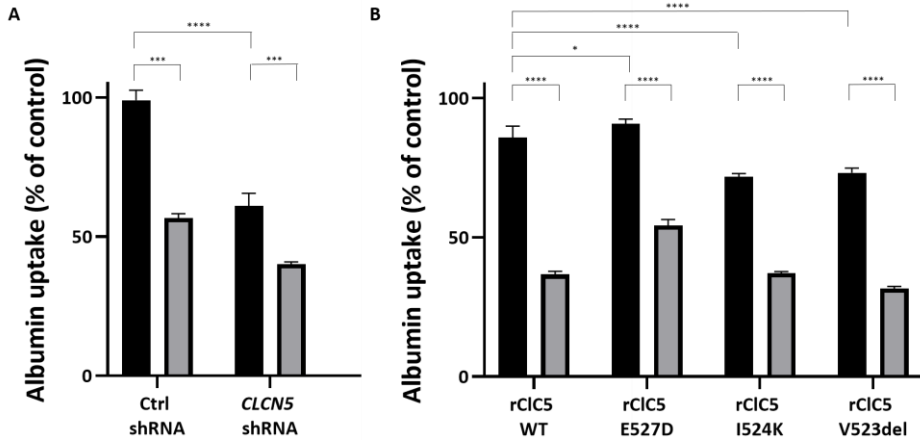


Figure 52 Albumin endocytosis by control cell lines and the Mutants. After incubation with fluorescent albumin, with no competition (black bars) and with non-labelled albumin competition (grey bars). Fluorescence was measured by fluorimetry and plotted as % of the Ctrl shRNA without competition. A. Albumin uptake by Ctrl shRNA and CLCN5 shRNA. B Albumin uptake by CLC-5 WT and the Mutants. **** $p < 0.0001$, *** $p < 0.001$, * $p < 0.05$

3.4.2. Evaluation of receptor-mediated and fluid-phase endocytosis via confocal microscopy.

As mentioned before, the results showing a remaining 60% of labelled albumin detection despite blocking and challenging by competition receptor-mediated endocytosis, led us to suggest this albumin was not intracellular but attached to the plasma membrane,

To discard this effect, we studied both receptor-mediated and fluid-phase endocytosis by immunocytochemistry, which makes it

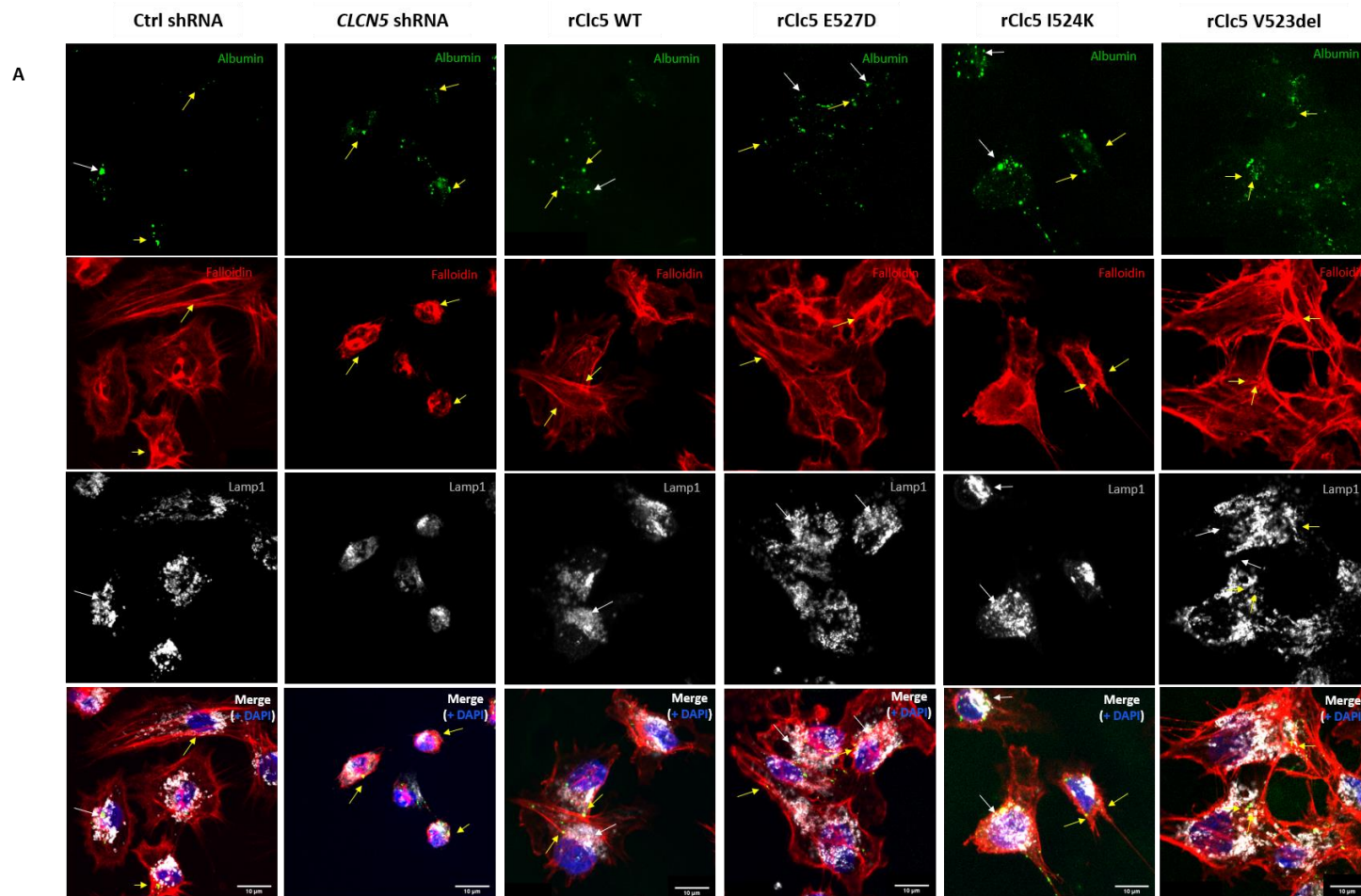
possible to visualize cargos and to assess whether they are found in given cell structures. Imaging of the cells by laser confocal microscopy was used to evaluate markers for both receptor-mediated and fluid-phase endocytosis after 60 minutes incubation with either Alexa Fluor Albumin or FICT-dextran.

Colocalization of albumin with a marker of cell membrane, phalloidin, was measured to evaluate the ratio of albumin persistently attached to the cell membrane despite washes. Likewise, we evaluated the colocalization with LAMP1 of both albumin and dextran to check whether after 1-hour incubation, the cargoes had completed the endo-lysosomal trafficking and were already colocalizing with lysosomes to be degraded.

By assessing the colocalization of albumin with phalloidin our results show that albumin partially remains attached to the cell membrane, especially in *CLCN5* shRNA and E527D (Manders' Coefficient 0.8 and 0.6 respectively) *Figure 53A*.

Albumin colocalization with LAMP1 was evaluated and no major differences were observed between WT and mutant CLC-5 regarding albumin reaching the lysosomes after one hour (*Figure 53C*).

It is worth mentioning a detail detected by confocal imaging and is the apparent *CLCN5* shRNA membrane retraction as shown by phalloidin staining, which could entail a cytoskeleton defect.



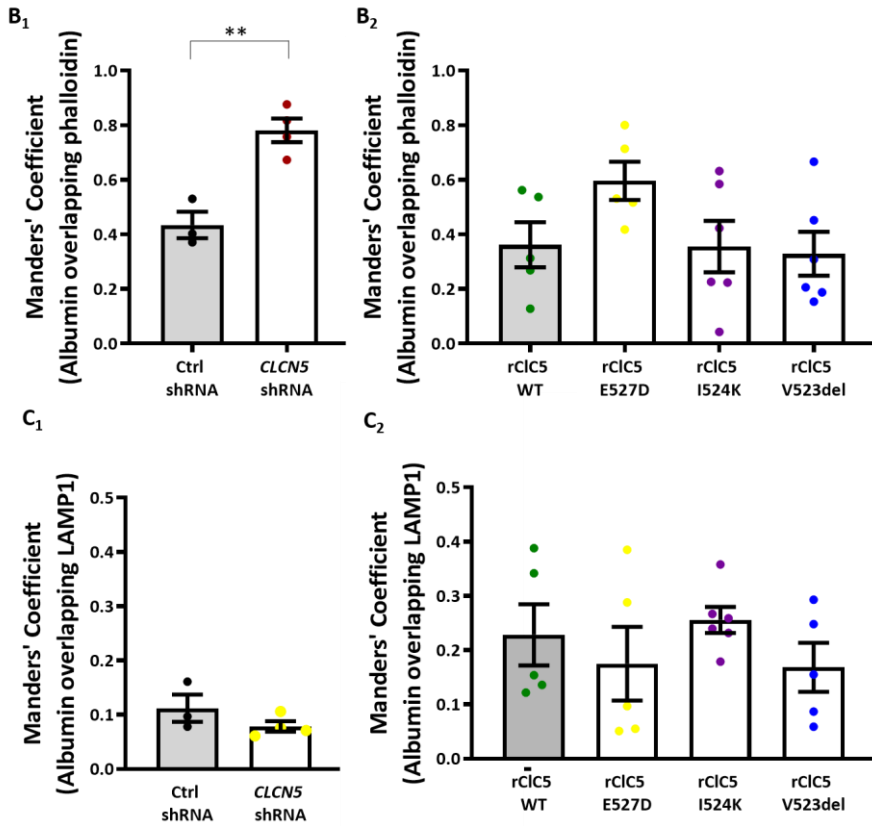
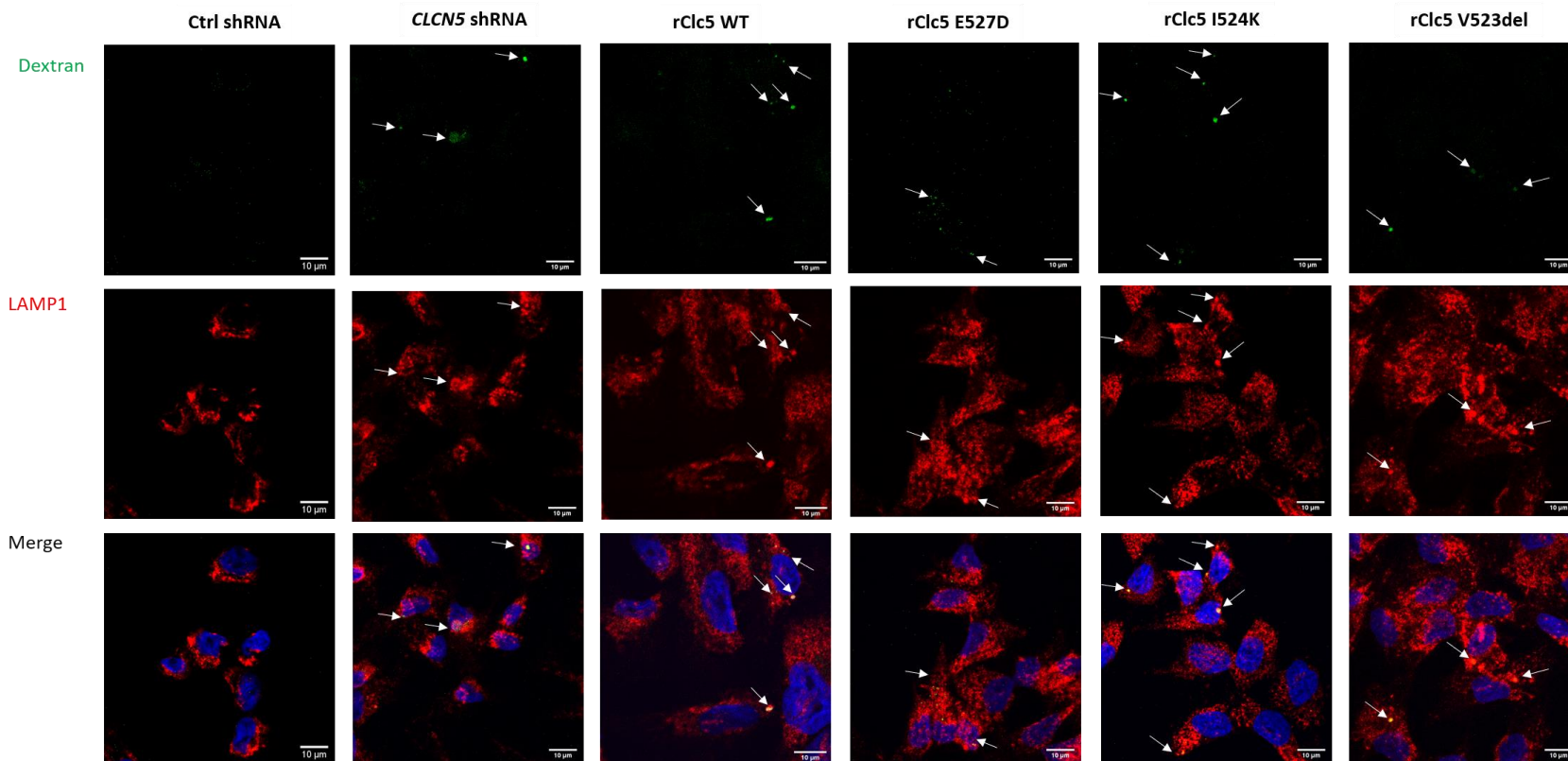


Figure 53 Albumin does not remain attached to the cell membrane and gets to the lysosomes unaffectedly in control cell lines and in the Mutants Differentiated RPTEC were treated with albumin for 1 hour . A. Immunocytochemistry and visualisation by confocal microscopy of cells stained for phalloidin (a marker of cell membrane) and for LAMP1 (a marker for lysosomes). Colocalization of both markers with albumin was analysed using imageJ. Manders' Coefficient was calculated. B. Colocalization of albumin with phalloidin assessed by Manders' Coefficient (B₁) Ctrl shRNA vs. CLCN5 shRNA and (B₂) CLC-5 WT vs. CLC-5 Mutants. C. Colocalization of albumin with LAMP1 assessed by Manders' Coefficient (C₁) Ctrl shRNA vs. CLCN5 shRNA and (C₂) CLC-5 WT vs. CLC-5 Mutants). Scale bar 10 μ m. $p^{**}<0.01$

Similarly, to assess the integrity of the fluid-phase endocytosis pathway, we tested uptake of dextran, a cargo mainly retrieved by the cells via this pathway. In preliminary experiments, we pulse-chased the control cell line with FITC-dextran for 4 hours (the first hour cells were fixed and imaged every 15 minutes). By assessing dextran colocalization with LAMP1 (a marker for lysosomes) we determined that the maximum localization of dextran in lysosomes occurred 1 hour after the initial pulse. Thus, after one-hour incubation, colocalization of the colloid with lysosomes (LAMP1) was assessed in our cell models.

As seen in *Figure 54A* and quantified in *Figure 54B*, Mutants I524K and V523del showed higher colocalization of dextran with lysosomes compared to control cell lines, which might again entail a lower trafficking or impaired degradation



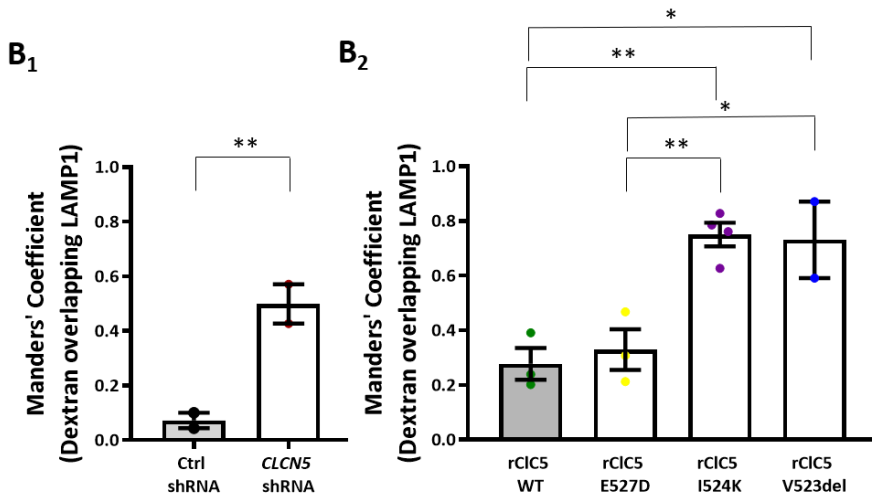


Figure 54 Fluid-phase endocytosis assessment. Dextran degradation in lysosomes was slower in Mutants I524K and V523del. Differentiated RPTEC were treated with FITC-dextran for 1 hour. A. Immunocytochemistry and visualisation by confocal microscopy of cells stained for LAMP1 (a marker for lysosomes). Colocalization of dextran with LAMP1 was analysed using imageJ. Manders' Coefficient was calculated. B. Colocalization of albumin with phalloidin assessed by Manders' Coefficient (B₁) Ctrl shRNA vs. CLCN5 shRNA and (B₂) CLCN5 WT vs. CLCN5 Mutants. Scale bar 10 μ m. $p^{**}<0.01$; $p^*<0.05$

3.4.3. Endo-lysosomal pH measurement

Lysosomal pH was assessed by using the pH-sensitive fluorescence dye LysoSensorTM Yellow/Blue DND- 160. First, this dye allows for qualitative detection of acidic vesicles by fluorescence microscopy, so that we assessed the integrity of lysosomes both in size and shape between different cell lines. Secondly, this probe allows for ratiometric measurement of intraorganellar pH. In acidic environment the probe emits yellow fluorescence so, measurement of fluorescence

intensity at 2 different excitation/emission wavelength pairs gives pH dependent ratios.

Comparison of the normalized LysoSensor ratios showed increased pH for *CLCN5* shRNA as compared to the Ctrl shRNA and Mutants I524K and E527D also showed more alkaline pH as compared to CLC-5 WT yet none of the differences reached statistically significant differences. No differences in pH were detected for the mutant V523del (Figure 55).

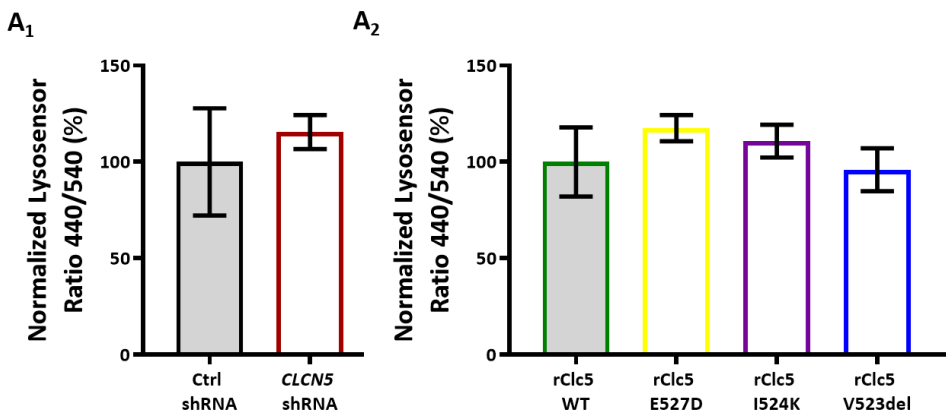


Figure 55 Measurement of intraorganellar pH in RPTEC/TERT1 using the ratiometric dye LysoSensor™ Yellow/Blue DND-160. Cells were incubated with LysoSensor for 5 minutes and imaged using confocal microscopy. Fluorescence intensity was measured at emission wavelengths 440 and 540 nm and ratios between intensities at both wavelengths were calculated. Results are plotted in % as compared to the control cell lines. the Ctrl shRNA (A₁) pH of *CLCN5* shRNA as compared to control Ctrl shRNA and (A₂) pH of CLC-5 Mutants as compared to the control cell line CLC-5 WT.

3.4.4. Endocytosis Receptor complex main components: Megalin and cubilin

Main players of the receptor-mediated endocytosis include megalin and cubilin, which form the receptor complex key for

cargo uptake in the proximal tubular cells (see introduction, section 4.2.1). Previous studies have postulated that the effect of CLC5 Mutants on endocytosis could be due to a defective recycling of these receptor³⁶⁶. Indeed, previous cell models¹⁷² and the Clcn5 KO mice presents lower levels of cubilin and megalin¹⁰⁸. Therefore, we proceed to evaluate the expression of both megalin and cubilin at mRNA level by RT-qPCR and at protein level by WB. Surprisingly, megalin expression could not be consistently detected in any of our cell lines, either at mRNA or at protein level.

As for cubilin, mRNA levels were significantly lower in *CLCN5* shRNA as compared to Ctrl shRNA and in E527D and I524K Mutants compared to CLC-5 WT. Nevertheless, no significant alterations were observed at the protein level.

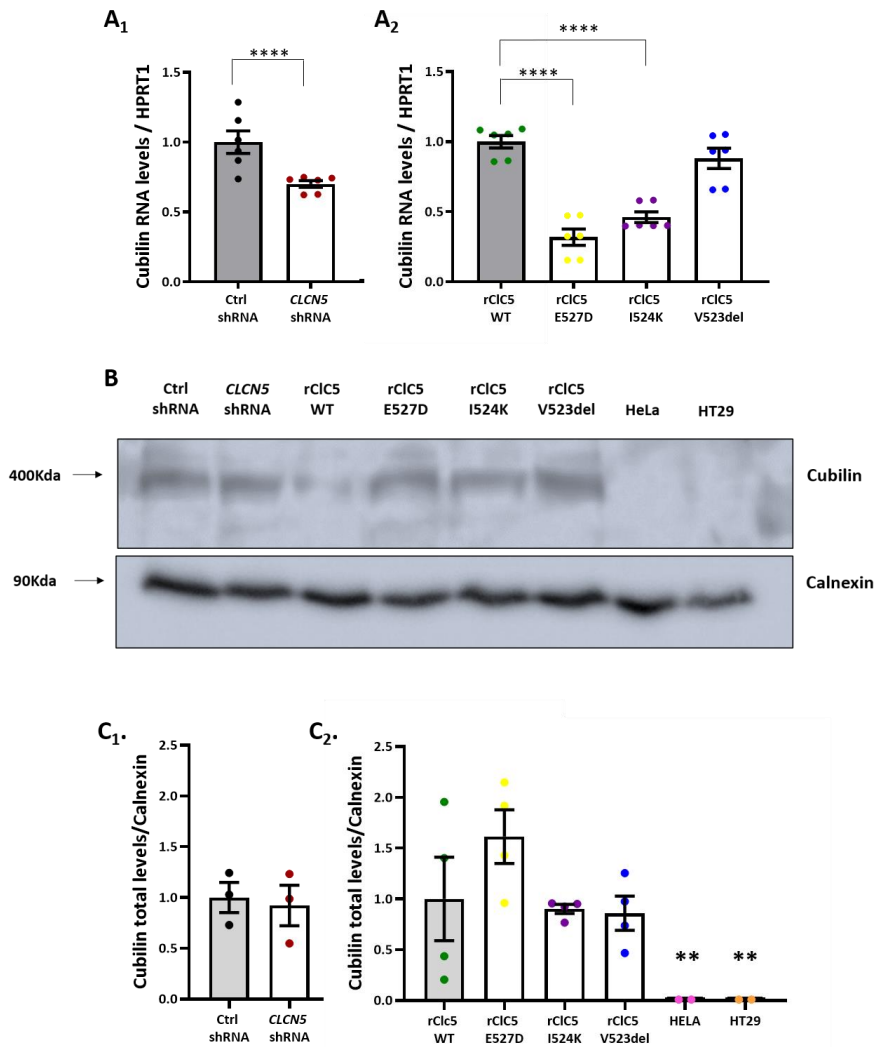


Figure 56 Assessment of cubilin expression in RPTEC/TERT1 cells. A. Cubilin mRNA levels were assessed and normalised to housekeeping gene HPRT1. (A₁) CLCN5 shRNA cubilin mRNA levels compared to control Ctrl shRNA (A₂) cubilin mRNA in CIC-5 Mutants compared to the control cell line CIC-5 WT B. Cubilin protein levels were assessed by western blot and normalised to calnexin levels. HeLa and HT29 were used as negative control. C. Quantification of cubilin protein expression (B₁) CLCN5 shRNA cubilin expression compared to control Ctrl shRNA (B₂) cubilin expression in CIC-5 Mutants compared to the control cell line CIC-5 WT. HPRT1. Hypoxanthine Phosphoribosyltransferase 1. p**<0.01; *p<0.05

DISCUSSION

1. Dent's disease type 1: picture of the current situation in Europe

We show a still image of the current situation of Dent's Disease type 1 (DD1) in Europe by describing the clinical situation and management of 98 genetically diagnosed DD1 patients. To the best of our knowledge this is the first report including cases of DD1 from twelve countries in our continent, with a wide range of ages including both children and adults.

In addition to verify some phenotypic traits already described in previous cohorts, we confirm that there are differences between European/USA and Asian cohorts specially as for the age of diagnosis; raising again the need for more spread awareness of the disease to increase diagnosis and avoid erroneous treatments. Likewise, we give evidence that there are changes in phenotype over time. We confirm as well that the therapeutic approaches are supportive and variable. Of interest is the description of 9 previously non-reported mutations and the association between the mutation severity with some phenotypic features.

1.1 A survey as a source of information

In the absence of current accessible, regularly up-dated, international registries of DD1 patients, a fair and appropriate approach was to survey the physicians in charge of these patients. We did so, and we got quite an amazing feedback from European

colleagues, specially bearing in mind that we are addressing a rare disease, and so, the cases are scarce and scattered all over the world.

Even though, the rate of responders per country was very variable, and so the survey did not manage one of its the purposes, to approximate DD1 prevalence in Europe. Furthermore, some records were not properly completed, and we could not include information about 37 patients.

Overall, we finally included 98 individuals from 89 families and considering that the estimated worldwide prevalence is of 400 affected families ¹¹⁴, the information gathered is very useful to draw some relevant conclusions about the disease in our continent.

1.2 Diagnosis

In our cohort, median age at diagnosis was 7 [3-12] years, earlier than in other European cohorts^{113,130} in which diagnosis occurs around 11 [5.4-20.7] years, but still later than in other countries as Japan, where Dent's Disease is usually detected as asymptomatic proteinuria at the age of 3 years, or in China³⁶⁷ at a median age of 4 [0.58-12] years old. This is probably because urinalysis including proteinuria is routinely performed to Japanese ³⁶⁸ and Chinese³⁶⁹ children at school, contrarily to European countries and US where such a screening is not performed³⁷⁰. This reflects that, even if nowadays detection in Europe occurs earlier in patients' life (the aforementioned cohorts include patients diagnosed many years

ago), major steps should be taken to diagnose before and possibly more this disease, maybe by implementing urine analysis as part of school medical check-ups.

As described here, a wide range of key signs led to the diagnosis of the disease in our cohort. Remarkably, only 50% of cases had a positive family history. This can be partially explained because, as in other X-linked inherited conditions, *de novo* mutations can arise. Indeed, *Tosetto et al.* estimated that around 8% of mutations can appear *de novo* in the *CLCN5* gene¹¹³, which still would not justify that half of our cohort did not have or were not aware of the disease family history.

Remarkably, despite just half of the cohort was diagnosed after finding of proteinuria, when tested, all patients presented with LMWP (Low molecular weight proteinuria). LMWP or tubular proteinuria (α 1-microglobulin, β 2-microglobulin, retinol binding protein) is the most consistent finding in our cohort and the hallmark of the disease and so, its identification is key for Dent's Disease diagnosis. Unfortunately, testing for LMWP is not routinely performed, but total proteinuria and albuminuria are more frequently assessed. Albuminuria is more frequently associated with other nephropathies such as glomerulonephritis, diabetic nephropathy or hypertensive nephropathy, which are far more common than DD1. Nonetheless, DD1 patients usually present albuminuria as well. Thus, the measurement of proteins in urine may be misleading. For example, nephrotic range (>3.5g in 24h)

total proteinuria is mostly associated with glomerular pathology, but these high rates can occasionally be detected in DD1²² and similarly, albuminuria, which is mostly deemed of glomerular origin, can also be found in DD1 and other tubulopathies, even exceed 1.5g/g³⁷¹. These patients often get kidney biopsies pursuing to diagnose a glomerulopathy and they even get to receive futile immunosuppressive medications; thus, the diagnosis of the disease is significantly delayed or not reached at all and patients get potent drugs with non-negligible side effect.

In an attempt to reduce the potential misdiagnosis of DD1, various authors have proposed algorithms based on different ratios using total proteinuria, albuminuria and tubular proteinuria^{24,372}. All of them agree that males with proteinuria, especially if total protein excretion exceeds albuminuria, should be assessed for LMWP and, if increased, should be screened for *CLCN5/OCRL* mutations, even if no other canonical signs are met¹³¹. In our cohort, all cases except one, fulfilled this rule and presented LMWP higher than albuminuria.

On the whole, the presentation of DD1 is variable and the correct diagnosis is often challenging, as it is a rare disease we do not usually think about. Even so, regular checking for proteinuria, including LMWP, should help reducing misdiagnosis.

1.3 Phenotype

It has become widely accepted that the triad of symptoms which better describes DD1 is LMWP, hypercalciuria and nephrocalcinosis and/or nephrolithiasis. Nonetheless, as this study reflects, this triad is not always present. While LMWP was found in all the patients, only 48.1% showed hypercalciuria (50% considering eGFR >60ml/min), 68% showed nephrocalcinosis and 27% had some episode of kidney stones in our cohort. These findings are similar to those previously reported in European/US series with regard to nephrocalcinosis (74% in other series¹²⁹) and nephrolithiasis (other series describe 33-49%^{113,146}). Prevalence of hypercalciuria in our cohort was lower than that described before, which accounts for up to 80-94% of patients^{114,154}. A possible reason for this less presence of hypercalciuria in our cohort is its intermittent detection¹⁵⁴ or to a larger rate of CKD in our cohort, as there is a progressive normalization of calciuria with the decrease of eGFR^{130,373}. Incomplete Fanconi syndrome in the form of glycosuria and aminoaciduria were found similar to what formerly described in as much as 14% (17% in European cohorts¹²⁹) and 55% (41-76% in previous series^{114,374}) of our patients respectively.

Rickets and failure to thrive were reported in 19% and 20.5 % of cases. The prevalence of rickets is very variable among different described cohorts and it ranges from 2% in a Japanese cohort¹³⁹ to 30% in the Spanish study by *Ramos-Trujillo et al.*³³² and to 48% in an Italian cohort¹¹³. In our cohort the presence of

hypophosphatemia did not associate to the presence of bone abnormalities as others have described³⁷⁵.

1.3.1. Different clinical spectrum Europe/US vs. Japan?

Interestingly, the clinical presentation among Japanese patients differs largely from that in European cohorts despite an almost identical genetic background¹³⁹. Thus, *Sekine et al.* in the large cohort of 61 DD1 Japanese patients described a much lower incidence for hypercalciuria (51%), nephrocalcinosis (35%) or rickets (0%). There is no accepted explanation for these differences; one can postulate that prompt diagnosis may play a crucial role in, for example, preventing bone abnormalities and that is why, in Japan, where detection occurs much earlier, the incidence of rickets is much lower than in European cohorts. Environmental factors such as nutrition may also have a contributory role to the development of hypercalciuria and nephrocalcinosis. Nonetheless, the most reasonable hypothesis is that in Japan more asymptomatic or paucisymptomatic patients are diagnosed owing to the urinary scholar screening, so increasing the denominator decreases the fraction, and the prevalence of the different clinical manifestations is lower.

1.3.2. Phenotype changes over time

In accordance with previous reviews, the phenotype evolves from a mainly proximal tubulopathy to a mixed disorder, as exemplified by the normalisation of calciuria with the decrease of eGFR¹³⁰.

We also found increased hypophosphatemia and glycosuria in older patients, which could be explained by more progressed proximal tubular cells dedifferentiation and potentially less receptors for glucose and phosphate in the membrane of proximal tubular cells^{28,130}

The increased prevalence of hypertension among older patients is expectable, as this condition increases as CKD progresses³⁷⁶.

1.3.3. Unusual clinical presentation

As for acid-base homeostasis and electrolyte balance in these patients, data on blood gas samples were not available, so we cannot assert whether these patients presented with metabolic alkalosis or acidosis, both reported in variable rates in previous cohorts^{114,374}. As for ions, 25.6% showed hypokalaemia or needed potassium supplements to maintain normal serum potassium levels (potassium citrate not included). This is in accordance with the blended phenotype including DD1 and Bartter-like symptoms described in previous cohorts^{114,130}. Bartter Syndrome (BS) is caused by gene mutations affecting proteins involved in electrolyte homeostasis in the thick ascending limb (TAL) of Henle's loop; up to now, no mutations in those genes have been found in DD1 patients showing this blended phenotype, which accounts for a quarter of our cohort. So, it would be fascinating to study the whole genome in these patients and, if further mutations are discarded, efforts should be focus on discovering new essential roles of CIC-5 in the thick ascending limb of Henle's loop. Indeed, it

was very recently reported that Barttin (an essential subunit for ClC-Ka and ClC-Kb chloride channels) the protein impaired in BS type 4, appears to regulate the subcellular localization and posttranslational modification of ClC-5 and so hypothesised that abnormal Barttin-ClC-5 interactions may be responsible for this phenotype in DD1 patients¹³⁶.

1.4 Renal function

The major complication of DD1 is the progression of CKD in 30 to 80% of patients between their thirties and their fifties¹²⁹. In our cohort 57.1% of patients showed impaired renal function and 8% of patients got to end stage renal disease at a median age of 37.2 ± 7.6 years. Unfortunately, we did not have data on renal function from different points during follow-up, so we could not estimate the decline of GFR individually and the potential factors involved in the rate of drop.

Unfortunately, we could not quantitatively evaluate LMWP for all patients as different LMW proteins were tested and different units reported, yet again, it is a remarkable finding that total proteinuria in these patients was 1500 [500-2700] mg/g and albuminuria 270 [90-675] mg/g, so there was an important gap between both measurements that should not be overlooked and make physicians think on tubular proteinuria when assessing patients' renal diagnosis.

1.5 Mutations

In the population of our study, beyond previous reports, missense mutations were the most common pathogenic mutations, accounting for 36%, followed by nonsense mutations (32%) and splice-site mutations (14%), while other mutation types were present in less than 10%. Until April 2020, 265 different mutations had been described and reviewed in various reports^{114,137,139,332}. Forty-nine different mutations were reported by the respondents of the survey and, amongst them, we could not find previous references in literature for 9 of them, which implies there are potentially many more pathogenic mutations to be discovered and reported. From this, it follows that a worldwide effort should be done in order to gather as much information as possible and build accessible international updated registries, especially when dealing with rare diseases.

1.5.1. Severity of mutations may impact on clinical phenotype

Although many mutations have been studied and several classifications established^{130,161,164}, a correlation between the type of mutation, CIC-5 domain affected or the protein function/expression with DD1 phenotype has not been identified³³³. Here we grouped the patients according to the severity of the mutations, as previously described by *Blanchard et al*¹³⁰. In their study, they found no genotype-phenotype correlation either at diagnosis nor at changes in eGFR, proteinuria, calciuria or plasma

potassium concentration with age. Differently, we found that patients with more severe mutations (nonsense, frameshift, large deletion, or splice-site mutations) presented with higher rate of nephrocalcinosis and higher proteinuria (as assessed by protein/creatinine ratio) than those patients with less severe mutations (missense and in-frame). As for kidney function, though no statistically significant differences were reached between the two groups, it is to be underscored that patients with more severe mutations reached later stages of kidney disease at a younger age. This is a new discovery as no other reports had pointed in this direction and so, confirmation is needed, if possible, with a larger cohort of patients.

1.6 Treatment

There is no specific therapy for patients with DD1, so in usual clinical practice, pharmacological intervention generally aims to reduce proteinuria, hypercalciuria or rickets, and prevent nephrolithiasis or nephrocalcinosis. As exemplified by clinical management in our cohort, clinical approaches are indeed very variable and individually tailored. Thirty-two per cent of the cohort were receiving thiazides at the time of the survey; indeed, thiazide diuretics have proved effective against hypercalciuria in DD1 patients¹⁶⁵. Nonetheless tight control of secondary effects, such as dizziness or dehydration, and dosing is essential especially in paediatric population. In fact, the first clinical trial on DD1 patients, conducted in France from 2003 to 2008 (ClinicalTrials.gov

Identifier: NCT00638482), demonstrated that high doses of thiazides could prevent nephrocalcinosis in children but also with significant adverse events, which prompted the trial to be stopped early. Likewise, a high-citrate diet showed to slow progression of CKD in *CLCN5* knockout mice¹⁶⁶ and so, 62.8% of our study cohort were receiving it as potassium citrate. The treatment with ACEI/ARB is more controversial. In theory, drugs inhibiting the renin-angiotensin-aldosterone system should not be effective for tubular proteinuria and, on top of that, they are badly tolerated by children due to its hypotensive effect. Nonetheless, they have proved effective in few cases hypothetically because glomerular damage is present in these few DD1 patients^{130,167}.

Overall, the treatment available is just supportive but there is no targeted therapy available, and no specific clinical trials are currently ongoing to try to prevent the progression of this disease to CKD or to cure it.

1.7 Summary and limitations

In conclusion, DD1 has an heterogenous presentation and so its diagnosis is challenging. As stated, it is essential to increase awareness of this rare disease, also among nephrologist, in order to diagnose it earlier and better. In fact, in the presence of LMWP in male patients, further investigations should be taken even if no other key signs/symptoms are present and even if there is no family history of tubulopathies. Would it be worthy to screen for proteinuria at school? On one hand, most of our findings match

with those previously reported on European/US cohorts and reassert the differences in phenotype as compared to Japanese DD1 patients, who have less proportion of patients with nephrocalcinosis, hypercalciuria and rickets. On the other hand, contrary to previous reports in literature, we found a genotype-phenotype correlation: patients with more severe mutations showed more proteinuria and higher rate of nephrocalcinosis with non-statistically significant impact on renal function, yet confirmation is required with a larger cohort.

It is important to underline that, as proved by comparing with the Japanese cohort, this is probably a misdiagnosed disease. Thus, aside from potentially screening children for proteinuria at school, more specific diagnostic tools would be helpful, such as urine biomarkers that facilitated a rapid and precise diagnosis. Likewise, as said, we probably need more insight about the disease to discover targeted drugs, as it is a debt to DD1 patients to find a treatment.

The main limitation of our study is its retrospective nature and the amount of missing data. Our review is based on a restricted number of results from the last clinical follow-up, gathered mostly via an online form and therefore, some reports are incomplete. One of the initial aims of the survey was to estimate the prevalence of Dent's Disease type 1 in Europe. This has not been possible as the data provided shows great inconsistency as for the

number of cases reported per country. On the other hand, we could not accurately assess quantitatively LMWP, because different LMW proteins were tested and different units reported, making it difficult to evaluate these results homogeneously. Moreover, specific information on the mutation of *CLCN5* was not available for all patients. It would have been highly informative to have data on renal function in more than one check-ups during follow-up to estimate the glomerular filtration-decrease rate.

On the contrary, and paradoxically, the main strength of this study is the significant sample size considering DD1 a rare disease and that data kindly provided by the nephrologist in charge of the patients was in most cases accurately supplied. It is also remarkable that patients from a wide range of age were included.

2. miRNA signature in uEVs from DD1 patients

Earlier studies have shown that miRNA contribute to the development of nephropathies, CKD or its progression³⁷⁷. Their discovery and interpretation may provide a basis for identifying mechanisms involved in both physiological and pathological states. Some miRNA have been postulated as non-invasive diagnostic and some as prognostic biomarkers. Moreover, there are some ongoing clinical trials using miRNA as therapies for kidney diseases³³⁰. Thus, we suggest that the investigation of

urinary exosome-derived miRNA in DD1 might help to understand some processes involved in the disease, the presence of given phenotypes and the development and progression of CKD in these patients. More difficultly, but still under the scope, study of urinary miRNA in this rare disease may provide markers for diagnosis, prognosis and possible therapies.

In this study, the first to explore the miRNA signature in Dent's Disease type 1, we took a systems biology approach to discover dysregulated miRNA in DD1. Starting with human urinary exosomes isolation, we first identified differentially expressed exosome miRNA between DD1 patients and healthy controls. By ingenuity pathway analysis, we analysed those pathways and functions in which the dysregulated miRNA are involved, revealing that many regulate processes related to proliferation, cell cycle, inflammation, immune system and fibrosis. Six miRNA were found to be particularly dysregulated in DD1 patients and, remarkably, the study of their mRNA and gene targets revealed that most of them were involved in endocytosis, inflammation and fibrosis. Interestingly, one of them, miR-629-3p, was found possibly involved in the pathogenesis of another tubulopathy, Bartter Syndrome, a disease which has been speculated to share pathogenic mechanisms with DD1.

In the following lines, we will discuss every part of the process as well as the potential implications of our results.

2.1. uEVs isolation and RNA extraction

To begin with, freshly collected urine samples from several hospitals in Spain were sent to VHIR to be processed. This step set up the first challenge, given that the very few patients with diagnosed DD1 are randomly distributed throughout the Spanish territory with no accessible open register. So, after locating the patients and contacting their nephrologists, samples were sent to be processed maximum 24 hours after collection, except for three samples, which had to be frozen preserved after one first centrifugation due to logistical problems. Although some authors³⁷⁸ have suggested direct freezing at -80°C might better preserve exosomes, others have shown that exosomes and their loads are stable in urine under different storage conditions getting comparable results with freshly processes samples or after repeated freeze–thaw cycles^{379,380}. So, in our study, despite obliged different initial processing of three samples, no differences were found as for concentration and integrity of exosome miRNA compared to the rest of the samples. In accordance with previous investigations³⁸¹, there were no discrepancies concerning miRNA global expression as measured in Cq. However, our findings are contrary to some other previous research by *Sanz-Rubio et al.* who found

higher Ct values in miRNA obtain from frozen compared to those obtained from fresh processed exosome mixture³⁸².

At this point, it is important to highlight that isolated urinary exosome-like vesicles (uEVs) mixture are enriched in exosomes but they probably contain other extracellular vesicles, so exosomes will be referred mostly by exosome-like vesicles.

For uEVs isolation, differential centrifugation method was preferred to other techniques. No previous data has been published involving uEVs in DD1 patients and so, the efficiency of exosome isolation per urine sample in DD1 patients' was unknown. In fact, we dread for the number of potential exosomes in these patients' urine, since endocytosis and the endo-lysosomal pathway are involved in exosome formation and both are impaired in DD1. Thus, unlike other methods, which can only process volumes in the range of microliters or few millilitres, large amounts of initial sample, 400 mL, could be processed by this technique³⁸³ with reduced costs. Moreover, ultracentrifugation is considered the gold-standard technique for exosome isolation accounting for over 56% users in the field ³⁸⁴, even with the development of new methods. As such, this technique has been widely used in our laboratory and has already been proved efficient in isolating exosomes to study other rare tubulopathies³⁸⁵. Nonetheless, ultracentrifugation has its drawbacks as it can suffer from clogging and vesicle trapping and can give an heterogenous sample with different origin and various sized vesicles. Importantly, ultracentrifugation is not an

appropriate technique for clinical practice, as it is arduous, time consuming and few samples can be processed at a time; it is optimal for a discovery approach as the one presented here, but other methods will need to be optimised to be used in the future, for example, in diagnostic screening. In this respect, the most promising isolation technique, yet still to be fully developed, is immunocapture, based on specific interaction between membrane-bound antigens of exosomes and immobilized antibodies. This method is highly specific, much better in purity and integrity of the isolated exosomes and requires small volume samples for analysis in an amazingly simple, timesaving but still high-costly manner²⁵⁴.

Importantly, as there are not exosome-specific markers, consensus has been reached on the three characterisation steps necessary to consider exosome isolation valid³⁸⁶. By cryo-TEM we could prove the integrity of uEVs in the studied sample in accordance with previous studies^{387,388}. By NTA the quantification of EVs showed substantial concentration of them though considerably variable between individual samples despite identical isolation method. This variation was independent of renal function or proteinuria degree, but other factors might play a role such as the amount of Tamm Horsfall (THP) protein. THP, also known as uromodulin, is the most abundant protein in urine under physiological conditions and its function is not completely understood. It is found in the urine, as a high-molecular-weight polymer assembled into filaments or matrices and can entrap

substantial quantities of urinary exosomes as shown by *Fernandez-Llama et al.*^{256,389}. While no differences as for uEVs concentration were found between patients and controls, it is interesting to note that differences were observed as for exosomes 'size, which was significantly larger in patients compared to controls. Under certain assumptions, at least three possible hypothesis could explain these results: (1) modification in the release of exosomes due to endo-lysosomal pathway impairment, disfunction of CIC-5 by some of the yet unknown protein-protein interactions may cause the release of bigger vesicles (2) a potential interaction with the high amount of LMWP which might trap smaller exosomes in patients and (3) a higher amount of Tamm–Horsfall protein (THP) in DD1 patients, which is just hypothetical because it was not measured in our cohort. As far as we know, no previous research has investigated the amount of uromodulin or THP in DD1 patients as compared to healthy individuals, yet some reports describing DD1 kidney histology have reported voluminous casts composed of THP distending the collecting ducts¹²⁸ and so, smaller exosomes would be trapped in the THP net.

Although different RNA extraction methods were previously tested in our laboratory³⁸⁵, according to our own experience and evidenced by previous literature³⁹⁰ we used the miRNeasy kit, the most efficient kit that isolated the highest percentage of miRNA³⁹¹. We got considerably abundant concentrations of mostly short RNA compatible with miRNA; slight variation in

concentration between samples was overcome by the amplification step after reverse transcription, increasing uniformly the amount of cDNA per miRNA. Thus, further analyses were performed on the basis of homogenous samples in the study cohort. As for miRNA detection, we preferred Openarray method mainly because (1) qPCR- based techniques are the gold standard given their sensitivity and specificity³⁹², (2) it is possible to work with very low amounts of initial sample³⁹³ and (3) it is a quantitative method and so it does not need a second validation step³⁹⁴.

2.2. Exosome miRNA in DD1 patients. Dysregulated pathways.

The 82 miRNA that appeared significantly dysregulated between patients and healthy individuals were subjected to target prediction and pathway analysis, based on experimental observations. This analysis demonstrated that these miRNA were associated with specific pathways involved in kidney disease states. Several of the top dysregulated pathways associated common intermediate processes and share fates: inflammation, senescence and fibrosis.

So, the dysregulated miRNA were involved in PTEN signalling pathway, p53 signalling pathway, cyclins and cell cycle regulation, cell cycle: G1/S checkpoint regulation pathway, HOTAIR regulatory pathway, regulation of the Epithelial-to-mesenchymal transition

(ETM) by growth factors, senescence pathway and hepatic fibrosis signalling pathway amongst others. We will try to theorise on the role of unbalanced miRNA in DD1 patients, though it is important to stress that the direction of miRNA-target mRNA interaction may not be as direct as just inhibitor (see Introduction, section 8.6) and thus, all interactions should be confirmed either by miRNA mimics or miRNA inhibitors in vitro or in vivo (as described in the same section. Introduction, section 8.6). With this purpose (amongst others), we created a cell model to further validate these interactions (see Chapter 3).

As shown by *Lovisa et al.*³⁹⁵ epithelial tubular cells with an initial damage start a EMT program mediated through the Transforming growth factor- β (TGF- β). TGF- β , traditionally considered the master regulator of fibrosis, is a target for many of the dysregulated miRNA in DD1 patients (e.g. hsa-miR-29b-3p, hsa-miR-143-3p, hsa-miR-30c-5p, hsa-let-7g-5p, hsa-miR-128-3p, hsa-miR-125b-5p). TGF- β regulates EMT by its downstream mediators, controlling renal fibrosis positively by Smad3 (and negatively by Smad7)^{396,397}. Hence, Smad3 activation further damages proximal tubular cells, generates a pathological secretome and induces cell cycle arrest. The increased host injury response results in an increased immune reaction with recruitment of myofibroblast, increased apoptosis and a vicious cycle of damage-host response, which leads to chronic fibrosis³⁹⁸. Our results showed that miRNA targeting TGF- β are dysregulated in patients compared to healthy individuals, some were downregulated (miR-145-5p), which

would lead to higher levels of TGF- β and subsequent Smad3 activation, boosting thus CKD. Nonetheless, some other TGF- β -regulator miRNA are upregulated (miR-29b-3p), hypothetically trying to counteract the effects of the previous.

Likewise, p53 is a well-known tumour suppressor, involved in the regulation of various cell biologic processes, including apoptosis and cell cycle arrest. p53 pathway has been described to mediate in several cases of acute kidney injury, for example secondary to well-known nephrotoxic drugs such as cisplatin or doxorubicin³⁹⁹, or in a mouse model of ischemia-reperfusion injury⁴⁰⁰. Interestingly, a siRNA targeting p53 (QPI-1002) is currently undergoing phase III clinical trials to prevent AKI following cardiac surgery⁴⁰¹. All miRNA involved in p53 signalling pathway were found upregulated in DD1, which hypothetically would entail the inactivation of this pathway in a protective approach.

In addition, cyclins regulate cell cycle progression; G1/S and G2/M checkpoints are in charge of inspection for cell size and for damaged DNA presence⁴⁰², so detection of either defective cell growth or aberrant strands cause the cell cycle to arrest, which, if prolonged, leads to cell senescence⁴⁰³ and maladaptive repair with profibrotic factors release⁴⁰⁴. These pathways were shown dysregulated in DD1 patients and, alluding to some previous reports⁴⁰⁵, one might speculate that impairment in endo-lysosomal system, specially of lysosome-dependent degradation, could play an important role in cell cycle arrest by leading to

mitotic errors which would be detected by cell cycle checkpoints⁴⁰⁶.

The LncRNA HOX transcript antisense RNA (HOTAIR), which was also found imbalanced in DD1 patients, is a long non-coding RNA (LncRNA) that secondary regulates other proteins, such as Notch or Bcl-2 signalling pathways⁴⁰⁷ involved in proliferation, and invasion specially in cancer⁴⁰⁸, but also related to other pathologies such as liver fibrosis⁴⁰⁹ or cardiomyopathies⁴¹⁰. As for kidney disease, HOTAIR has been proved to stimulate epithelial-to-mesenchymal transition (EMT)⁴¹¹, also aberrant in DD1 patients, which causes tubulointerstitial fibrosis⁴¹² and kidney injury secondary to sepsis⁴¹³.

On the contrary, PTEN (phosphatase and tensin homolog) signalling pathway is supposed to play a protective role by interfering with activation of multiple profibrotic signalling pathways, leading to tissue fibrosis inhibition^{414,415}. For example, it negatively regulates phosphoinositide 3-kinase (PI3K)/Akt signalling pathway, which leads to apoptosis and tubular cell atrophy with consequent fibrosis or nephron loss, as especially described in diabetic nephropathy⁴¹⁶. Thus, PTEN activation implies an attempt to protect kidney parenchyma from extracellular matrix (ECM) deposition. Contrarily, its downregulation enhances kidney fibrosis as indicated by a series of recent studies in which either pharmacological⁴¹⁷ or selective genetical inhibition⁴¹⁸ of PTEN in a mouse model supported this conclusion. In DD1 patients, PTEN-regulatory miRNA were both downregulated (has-miR-143-5p and

has-miR-145-3p), enhancing its protective role, and upregulated (hsa-miR-99b-5p hsa-miR-10a-5p, hsa-miR-125b-5p) increasing the profibrotic nature of PTEN decrease, so it is difficult to imagine the global direction of these interactions.

Besides, the cancer molecular pathways appeared strongly linked to the dysregulated miRNA as these pathways include many proteins that are common to the aforementioned profibrotic and inflammatory pathways. Nonetheless, this does not imply a malignancy could be more frequent in DD1 patients, but that processes like cell dedifferentiation, cell cycle arrest, immune system imbalance or enhance of proinflammatory factors are dysregulated in both diseases.

All these results support the assumption that progression to CKD in DD1 would happen after a chain of events that have already been described after tubular damage by other causes. The sustained injury in DD1, CIC-5 loss-of-function leading to impaired endocytosis¹²⁷ and impaired trafficking causing defective lysosomal degradation³⁶⁶ would lead to increased tubular proteinuria (which worsens intracellular degradation mechanisms)⁴¹⁹, loss of plasma membrane receptors¹⁴³ and urinary loss of cargoes (vitamin-binding proteins or enzymes). This could potentially enhance intracellular waste accumulation and oxidative stress⁴²⁰ which would cause loss of cell-cell contact and dedifferentiation of the polarized epithelial phenotype contributing partially to tubular dysfunction³⁹⁵ and resulting in the incomplete Fanconi Syndrome observed in some DD1 patients⁴²¹.

Simultaneously, in an attempt to protect tubular cells, pathways and regenerative mechanisms such as PTEN⁴¹⁵ would be activated. Nonetheless, in this case the insult is maintained, and regenerative mechanisms are overwhelmed. In DD1, as in other tubulopathies or tubule damage processes, the activation of pro-inflammatory factors and pathways (TGF- β), the production of reactive oxygen species (ROS) and the dysregulation of cell growth-related processes via cyclins would lead to cell cycle arrest. As maintained, injury would cause cell apoptosis and necrosis (p53 pathway, PTEN downregulation), secretion of more inflammatory mediators, RAS activation, EMT (TGF- β , HOTAIR) and induction of a senescence-related phenotype⁴²². Overall, it would generate an excess accumulation of interstitial extracellular matrix (ECM) and myofibroblasts ultimately resulting in tubulointerstitial fibrosis that would contribute to nephron loss and thus to CKD progression.

2.3. Downregulated miRNA in DD1 uEVs

Considering separately the most dysregulated miRNA, those which showed wider differences between patients and controls ($0.15 < RQ < 2$; $\text{adj.}p < 0.05$) and considering them and the direction of its dysregulation (up or downregulated) individually, we hypothesise that DD1 patients show both early signs of renal damage and of repair mechanisms trying to prevent progression to CKD.

Among all dysregulated miRNA only three were downregulated: miR-145-5p, miR-143-3p and 629-3p.

2.3.1. miR-145-5p and miR-143-3p

miR-143-3p and miR-145-5p are members of the same cluster and are found enriched in blood vessel as they regulate vascular smooth muscular cells (VSMC) contractility, endothelial cell proliferation and angiogenesis by targeting several transcription factors such as Kruppel-like factor (KLF) 5 and ETS Like-1 protein Elk-1 (ELK-1). They are inversely regulated by angiotensin converting enzyme (ACE), myocardin and KLF-4. Their expression is reduced when VSMC are activated after a vascular injury or stress^{423,424} and, on the contrary, they have been described upregulated in the plasma of patients with coronary artery disease, stable or unstable angina or acute myocardial infarction⁴²⁵. In line with these statements, our results revealed genes associated to atherosclerosis (*VEGFA*, *ESR1*, *Serpentine*) as targets for miR-145-5p. Likewise, genes involved in endocytosis and PTCs polarisation (*MDM2*, *EGFR*, *ERBB3* and *ERBB4*)^{426–428} are targets for these miRNA according to our findings, which might entail a link to DD1. Moreover the cluster has been studied more intensively than other candidates in regard to regulation and its tumorigenesis affecting function^{429,430}

MiR-145-5p has been previously found both up- and downregulated in several kidney diseases: it has been found decreased in plasma in a group of 90 Stage III–IV CKD patients

with correlation to the progressive loss of eGFR⁴³¹ independent of the cause of CKD. On the contrary, *Brigant et al.*⁴³² found both miR-145-5p and miR-143-3p upregulated in patients undergoing haemodialysis in comparison with healthy controls. In fact, miR-145-5p has been reported to regulate signalling pathways that enhance the activation of NF-kappa-B, MAPK1, MAPK3 and JNK, leading to renal fibrosis⁴³¹.

Most importantly, related to tubular damage, miR-145-5p has been hypothesised as a biomarker for interstitial fibrosis and tubular atrophy in kidney graft recipients, as it was found significantly downregulated and displayed a high diagnostic accuracy compared to stable graft function, urinary tract infection, borderline rejection, T-cell mediated rejection and antibody mediated rejection patients⁴³³.

Besides, hsa-miR-145-5p has as a target MUC1, which is expressed throughout the distal nephron and in physiological conditions provides a protective function by maintenance of a luminal epithelial mucobarrier. MUC1 also plays a role in EMT and regulates ILK signalling pathway, a pathway with anti-inflammatory properties in renal inflammation⁴³⁴. Mutation of MUC1 causes a rare form of tubulointerstitial fibrosis known as Autosomal Dominant Tubulointerstitial Kidney Disease encoding a new peptide (MUC1-fs) that accumulates inside the MUC1-expressing renal tubular epithelial cells. How this novel peptide product causes tubulointerstitial fibrosis remains unknown⁴³⁵.

In DD1 patients, miR-145-5p was downregulated, which could be a sign of early tubular atrophy (as shown in kidney graft) together with activation of inflammation and fibrosis cascades potentially facilitated by a dysregulation of the luminal epithelial mucobarrier due to a dysregulation of MUC1.

miR-143-3p has been found decreased related to inflammatory response of renal tubular epithelial cells to hyperuricemia⁴³⁶. Its upregulation has been associated to regulation of MAPK pathway and decrease of proliferation and migration, especially in the context of cancer⁴³⁷. Its dysregulation has been involved in the proliferation and fibrosis of mesangial cells in diabetic nephropathy⁴³⁸. Thus, an upregulation would seem protective and prevent inflammation and fibrosis, but its downregulation would have the contrary effect, as in DD1 patients, in whom it might indicate an enhance tubular cell damage with increased inflammatory response and possibly pro-fibrotic machinery, as indicated by miR-143-3p target genes *COL1A1*, *COL3A1* and *PTGS2*⁴³⁹.

2.3.2. miR-629-3p

miR-629-3p has been less studied and so, there are less experimentally observed mRNA targets linked to this miRNA. Nonetheless, its role has been particularly explored in cancer where it seems to enhance tumor cell proliferation and invasion via TGF β /Smad/FOXO signalling conferring worse prognosis (for

example in lung or pancreatic cancer and in clear cell renal cell carcinoma⁴⁴⁰).

As related to kidney, mir-629-3p was found up-regulated in biopsy tissue from kidney grafts with acute rejection⁴⁴¹. Interestingly, this miRNA targets *RAB11*, key for endocytosis³⁶⁰ and recycling endosomes⁴⁴ proper functioning, thus playing a putative role in the decrease of membrane receptors, megalin and cubilin, potentially due to impaired recycling, observed in DD1. Most importantly, miR-629-3p targets *BDNP*, which encodes for Barttin, whose mutations have been described as causative of Bartter Syndrome (BS) type 4a (BS4a, OMIM#602522). Along the thick ascending limbs of the Henle's loop, Barttin regulates the function and localization of ClC-K type chloride channels that belong to the same protein family as ClC-5⁴⁴³. Besides, several DD1 cases have been reported with overlapping symptomatology with BS as hypokalemic metabolic alkalosis and hyperaldosteronism^{134,135}. The shared features in some cases and the homology of Barttin and ClC-5 function, led *Wojciechowski et al*¹³⁶ to investigate in a cell model the interaction between them and concluded that Barttin controls the processing, trafficking and intracellular targeting of ClC-5 aside from its known function as ClC-K controller⁸⁸. All in all, it is tempting to speculate that miR-629-3p is downregulated in DD1 patients in an attempt to enhance Barttin regulatory function, maybe trying to make up for ClC-5 deficiency or trying to enhance the activity of the residual protein. This finding should be further corroborated in a confirmation

patient cohort, and, if verified, it would support the findings by *Wojciechowski et al.* and might set the grounds for a diagnostic biomarker.

2.4. UPREGULATED miRNA in DD1

2.4.1. miR-29 family

As for the differentially upregulated miRNA, miR-29 family has been reported to be extensively associated with kidney pathology, particularly as antifibrotic modulators. MiR-29 family up-regulation would play a protective role for renal parenchyma as they repress the expression of TGF- β 1 and the collagen genes *COL1A2*, *COL3A1* and *COL4A1* in proximal tubular cells, podocytes, as well as mesangial cells⁴⁴⁴. On the contrary, it is reduced in other kidney pathologies like urinary obstruction⁴⁴⁵ or IgA nephropathy where it was found significantly reduced in patients' urine compared to that of healthy controls, and correlated with the degree of proteinuria and renal function⁴⁴⁴. miR-29b has been found upregulated in renal medullary tissues, with a negative regulatory effect on collagen and extracellular matrix accumulation in hypertensive renal injury⁴⁴⁵ and also in diabetic nephropathy⁴⁴⁶.

Thus, the upregulation of miR29b-3p in DD1 patients would suggest that protective mechanisms to prevent the progression of CKD are activated from early stages in an attempt to reduce the deposition of extracellular matrix.

2.4.2. miR-216b-5p

The dysregulation of miR-216b-5p has been described associated with senescence. This miRNA regulates Protein kinase CKII (CK2) that catalyses the phosphorylation of a large number of cytoplasmic and nuclear proteins. miR-216b-5p upregulation has been found to induce cellular senescence via p53/p21 pathway. These modifications have been specially observed in relation with colon cancer^{447,448}.

Retrieved experimentally validated targets showed that miR-216b-5p regulates MUT, which encodes for methylmalonyl-CoA mutase. The deficiency of this enzyme causes methylmalonic acidemia (MMA), which leads to chronic tubulointerstitial nephritis and ultrastructural changes in the proximal tubule mitochondria associated with aberrant tubular function and progression to end stage renal disease⁴⁴⁹. Although focal giant mitochondria have been described in DD1 patients' biopsies¹⁰⁹ it is not a frequent finding, as far as we know from the literature, so the significance of mitochondria regulation by MUT in DD1 patients is still to be investigated. Likewise *COL4A4*, which was found as a target for miR-216b-5p, is mainly associated to Alport Syndrome⁴⁵⁰, an hereditary disorder affecting the glomerular basement membrane, but also to familial forms of glomerulosclerosis⁴⁵¹, which might also entail a link to DD1 patients with glomerulosclerosis lesions in their biopsies.

2.4.3. miR-664a-3p

Finally, downregulation of miR-664a-3p has been described associated with obstructive sleep apnea with or without increased carotid intima-media thickness and, thus, it has been hypothesized as a potential atherosclerosis mediator biomarker⁴⁵². In cervical cancer it has been shown downregulated, especially when associated to lymphatic invasion and distant metastasis⁴⁵³. In contrast, it was upregulated in gastric cancer cells where it might contribute to EMT process⁴⁵⁴ and also in chronic obstructive pulmonary disease specially affected by cigarette smoke extract, probably as hypothesised by *Zhong et al* as a result of higher inflammation factors⁴⁵⁵.

Interestingly, miR-664a-3p was described by ingenuity pathway analysis to target genes involved in glomerulosclerosis of different causes. Thus, miR-664a-3p regulates *EDN1* which encodes for Endothelin 1, involved in focal segmental glomerulosclerosis⁴⁵⁶ and other causes of glomerulosclerosis as diabetic nephropathy⁴⁵⁷. It also controls *CD2AP*, the gene for CD2-associated protein, which as well causes focal segmental glomerulosclerosis^{458,459}. Finally this miRNA is also involved in the regulation of *G6PC*, the gene for glucose-6-phosphatase, which has been reported to cause glycogen storage disease type 1a, a disease with deficient lysosomal degradation, as DD1, with known progression to CKD due to several kidney lesions, among them, glomerulosclerosis⁴⁶⁰. This finding associates with the fact that

some DD1 patients present with glomerulosclerosis in their biopsies^{131,156}, but unfortunately, we do not have kidney histological data from our cohort. Nonetheless, we can postulate that mutations in *CLCN5* could have an effect in other pathways related to glomerulosclerosis, such as Endothelin-1 pathway, which would explain partially why some patients present this type of glomerular histological lesions even when *CLC-5* is predominantly expressed in the renal tubule system, but also in the glomeruli¹³².

2.5. Different miRNA in DD1 patients with different phenotype

2.5.1. miRNA in DD1 patients with CKD

As for the miRNA differentially expressed in patients with $FG_{e} < 90$ ml/min and $FG > 90$ ml/min, miR-660-5p and miR-187-3p were found upregulated and miR-200a-5p was found downregulated. miR-200a has already been associated with renal fibrosis⁴⁶¹, particularly in the context of diabetic kidney disease. *Wang et al.*, demonstrated that expression of miR-200a downregulated Smad-3 activity and the expression of matrix proteins and prevented TGF- β -dependent EMT⁴⁶². The other way around, miR-200a inhibition in streptozotocin-induced diabetic mice significantly exacerbated cortical and glomerular fibrogenesis, tightly linking dysregulated miR-200a with the development of diabetic

nephropathy. All in all, downregulation of miR-200a, as in DD1 patients with CKD, independent of the degree, would be associated to aberrant regulation of oxidative stress, fibrogenesis and EMT in renal cells⁴⁶³.

As for miR-660-5p, found upregulated in DD1 patients with GFR < 90 ml/min has not formerly been associated with renal pathology; it has been described upregulated in heart failure⁴⁶⁴ and in association with cell migration, invasion, proliferation and apoptosis in renal cell carcinoma through p53 stimulation⁴⁶⁵. As stated before, p53 is one of the pathways that mediated kidney injury after distinct triggers, so our results support the possible contributory role of upregulated miR-660-5p to CKD progression in DD1.

Likewise, miR-187 was upregulated in DD1 patients with CKD. This miRNA has been especially associated to increased invasive potential in certain tumours like breast⁴⁶⁶ or lung⁴⁶⁷. miR-187 was also shown to be differentially expressed in mice after ischemia-reperfusion injury⁴⁶⁸ and further, it was found to improved ischemia/reperfusion induced acute renal failure⁴⁶⁹ by blocking pro-apoptotic pathways like TNF- α in kidney cells⁴⁷⁰. Thus, we could hypothesise that miR-187-3p upregulation in DD1 patients might entail an attempt to protect tubular cells from maintained injury.

2.5.2. miRNA in DD1 patients with Fanconi Syndrome

Patients showing some of the symptoms of Fanconi Syndrome (Incomplete Fanconi Syndrome) such as glucosuria, phosphaturia and/or aminoaciduria showed downregulated miR-143-5p. This finding would be in accordance with the aforesaid hypothesis (see section 2.3.1) that this downregulation reflects a major tubular injury by enhancement of pro-inflammatory pathways. Cell dedifferentiation would follow this maladaptive response to injury so that PT cells would lose their specific membrane transporters with consequent loss of the solutes they are deemed to reabsorb in physiological conditions.

2.5.3. miRNA in DD1 patients with kidney stones

Furthermore, two miRNA were found dysregulated in patients with history of nephrolithiasis compared to those without. miR-17-5p is one of the most scavenger miRNA as it regulates multiple targets and is involved in multiple functions such as autophagy, cell cycle regulation and apoptosis⁴⁷¹, yet it has also been named the first 'longevimiR' as miR-17-5p-overexpressing mouse show an extended lifespan⁴⁷². It is difficult to conjecture the role of miR-17-5p in the formation of kidney stones. Interestingly, though, miR-181a, which was found upregulated in DD1 patients prone to form nephrolithiasis, was also found upregulated in calcium-oxalate stone-forming rats compared to the controls⁴⁷³

though the pathways involved in stone formation were not clarified. All things considered, though, a larger cohort of patients with kidney stone disease would be necessary to corroborate these findings, as the group of stone-forming patients was rather small.

2.6. Summary and Limitations

In summary, DD1 patients have as many exosome-like vesicles in the urine as controls, although the isolated uEVs are bigger than those in controls.

The analyses of uEVs miRNA in DD1 patients, as compared to healthy controls, presented 82 differentially expressed uEVs miRNA, which target genes involved in kidney disease related pathways such as p53 signalling pathway, regulation of the Epithelial-to-mesenchymal transition (ETM) by growth factors and senescence pathway and senescence amongst others. Thus, some of the top dysregulated miRNA would be involved in incipient cellular damage, inflammation and progression of fibrosis (downregulation of miR-145-5p and hsa-miR-143-3p), but some other would be aimed as protective factors for the restoration/regeneration of tubule cells (miR-29b-3p upregulation). Interestingly, two of the six top dysregulated miRNA between patients and healthy controls might give some insight in the pathophysiology of two characteristic phenotypes of DD1: miR-629-3p, by regulating Barttin gen (*BDNP*) might be related to

Barttel Syndrome-like symptoms often shown in DD1 as hypokaliemia or less frequent alkalosis. Likewise, miR-664a-3p dysregulation in DD1 patients might play a role in the development of glomerulosclerosis in some patients' biopsies.

There are few limitations of our study that should be considered. First, we detected the urinary miRNA without determining their cellular source. It is, however, interesting to note that the miRNA we detected have been found in renal tubular epithelial cells and podocytes in other studies, and therefore we assume that these miRNA are representative of the kidneys and the urinary tract. Secondly, the fact that DD1 is a rare disease with very few patients diagnosed and not much biological, biomolecular data, makes it difficult to ascertain the information from existing datasets, where Dent's Disease does not appear. One of the main limitations of our study is that we cannot directly validate the function of miRNA as we do not have tissue samples to measure the expression levels of their target genes and the consequences of their dysregulation, which would be of special importance when the miRNA level is considered to be pathogenically relevant. In this respect, as addressed in the following section, we created a cell model to, among other purposes, validate the direction of these interactions. Another major limitation, aside from the reduced sample size is that we could not gather in a timely manner a second DD1 patient cohort to validate our results, although this step will be taken soon.

As a final remark, DD1 exemplifies a kidney disease with justified requirement of exosome- based biomarker discovery because: (1)there is a lack of diagnostic tools; despite nowadays gene sequencing is more widely available, 25% of patients with a clinical diagnosed Dent's Disease do not have a mutation in *CLCN5* or *OCRL*, (2) kidney biopsy which is considered the gold standard for most kidney disease (glomerular) is useless in DD1, as no specific findings are expected; (3)there are still many unanswered questions about the physiopathology of the disease and, genomics, proteomics, lipidomic might cast new lights on these processes.

3. Validation of DD1 cellular model

In this thesis we have characterized new cellular models for Dent's Disease type 1 represented by a collection of cell lines carrying: a CLC-5 WT gene, a silenced *CLCN5* gene or three different *CLCN5* gene mutations categorized according to their localisation and functional defects (E52D class 2, I524K class 1 and V523del non functionally characterised yet)^{161,164}.

3.1. RPTEC/ hTERT1 cells as a model for Dent's Disease

As reviewed from previous literature, this is the first study to use RPTEC/hTERT1 immortalized cell line, considered the most

representative cell line for healthy proximal tubule cells, to functionally characterise mutated CIC-5.

Other cell lines have been classically used in the study of proximal tubule physiological processes and deficiencies and Dent's Disease in particular. For instance, *Xenopus laevis* oocytes have been used for electrophysiological analysis of expressed CIC-5⁹⁰. These cells, though very efficient and largely used as expression systems for functional characterization of ion channels, are far from resemble the complex system of transporters, channels and receptors in human proximal tubule. Similarly, although Opossum kidney (OK) cells have been used for studying the intracellular localization of CIC-5⁴⁷⁴ and for characterising some PTCs receptors⁴⁷⁵, many other receptors are not expressed in these cells⁴⁷⁶ and, more importantly, they do not have a human origin, but they come from *Didelphis virginiana*, so they would not be further useful for our future aims (mRNA and miRNA studies, drug testing, among others). As for Human Embryonic Kidney 293 cells (HEK293), widely used in cell biology, and also in research related to the kidney proximal tubular cells and DD1¹⁷¹, they have demonstrated no evident tissue-specific gene expression signature, in fact, the markers of renal progenitor cells, neuronal cells and adrenal gland⁴⁷⁷. Moreover, they display limited number of human renal transporters, and so do not accurately reflect the situation in vivo and the complex interplay between multiple transporters. What is more, they have been described to have an aberrant karyotype

and to deregulate pathways such as pRB/p53 implied in processes we are interested to further investigate in DD1⁴⁷⁷.

The most reliable cell model previously used are the conditionally immortalized proximal tubular cells from DD1 patients¹⁷², as they come directly from patients, yet the genetic background attributable to every patient individually may have an influence in the results, when the specific impact of individual mutations want to be investigated.

Thus, a cell model was created by using RPTEC/hTERT1 which is a well-differentiated and stable proximal tubular cell line derived from a healthy human donor. These cells have conserved polarization, cilia, most membrane transporters and receptors^{348,478} and transport activities including albumin endocytosis³⁴⁹. Moreover, we took advantage of the clean genetic background provided by immortalized cell lines so that every change displayed respect the WT can be attributable to the disease. In fact, these cell lines have already been successfully used to assess drug nephrotoxicity⁴⁷⁹ and to study the pathophysiology of some nephropathies such as diabetic nephropathy³⁴⁹.

3.2. CIC-5 mutants

As discussed below, our findings prove that this is a good cell model to study the effects of CIC-5 mutants and confirm that I524k and E527D mutants, which had already been functionally analysed, do belong to class 1 and class 2 respectively⁴⁸⁰. As for V523del,

which had been only partially evaluated by previous works⁴⁸¹, our findings suggest that it may belong to class 3, but results do not allow to fully confirm it, as we will explain in detail below.

3.2.1. CIC-5 protein expression and half-life

As expected, no differences at mRNA levels for *CLCN5* were detected but, interestingly, protein levels of CIC-5 carrying I524K or V523del mutations were lower than CIC-5 WT, as detected by HA tag. As a class 1 mutation, proved to be retained in the ER¹⁶⁴, I524K is rapidly degraded and thus protein levels were reduced³⁶³. As for class 2 mutant, E527D showed protein levels comparable to those of the WT which implies this mutant stability is maintained. V523del reduced protein levels could entail less translation or reduced stability^{161,364}.

Protein turnover shows the balance between synthesis and degradation, which is required for protein proper function and metabolism. Its determination allows to establish whether the protein is too straightforwardly degraded or if, on the contrary, it is not being degraded and so new protein synthesis is blocked⁴⁸².

In the present investigation, CIC-5 half-life was determined for all cell lines. In agreement with previous reports^{95,162}, the CIC-5 WT levels were reduced at half of initial amount after ~1.5-2 h chase. In comparison with WT CIC-5 and E527D, V523del showed delayed processing which could imply a delay either in trafficking through

the endo-lysosomal pathway or in degradation once it gets to the lysosomes. On the contrary, I524K showed a degradation pace similar to that of control cell line; indeed, during the first hour a sharp decrease was shown by this mutation. On one hand, this is in accordance with previous publications, where class 1 mutations are rapidly degraded in response to ER retention so that these mutations do not reach the mature form¹⁶². On the other hand, and given this rapid degradation, even a much shorter half-life would have been expected for a class 1 mutant, yet it is to be highlighted that particularly this mutant, I524K, has been reported to preserve certain protein stability as compared to other Class 1¹⁶¹.

A reason for performing short chase (2 hours) was to ensure stability of the protein at least for the duration time of subsequent experiments like endocytosis test, with length shorter than 2 hours. It would have been optimal to extend the chase for at least until V523del had reached its half-life point, to precisely assess the difference to the wild type and so this, shall be done in future experiments.

All considered, we can conclude that, considering CIC-5 half-life, V523del is not a class 1 mutation. Our results do not allow us to discern whether it is a class 2 or 3 mutation, though.

3.2.2. CIC-5 subcellular distribution

Evaluation of CIC-5 trafficking along the endo-lysosomal pathway was assessed by colocalization of the protein with different compartment in the system.

Our findings suggest that all the mutants showed reduced localization in early endosomes, specially I524K and V523del; E527D showed slight reduction compared to WT. Thus, we confirm that class 1 mutation I524K displays the littlest colocalization with early endosomes as stated by *Smith et al.*, which is a very reasonable finding because, as said, this mutant is mainly retained in the ER. The same authors showed that E527D colocalized as WT in the early endosome; our results though show a slight reduction in E527D colocalization with early endosomes which could be due to different cell lines used (they used HK-MSR) or different constructs (they used CIC-5-YPF, with the tag at the Ct like ours)¹⁶¹. As regards V523del mutant, colocalization with early endosomes was also decreased, as speculated for this mutant's half-life, this could imply a delayed trafficking along the lysosomal pathway. Overall, the reduced presence of CIC-5 in early endosomes accounts for one of the most relevant pathophysiological mechanism of Dent's Disease: impairment of either endosomal acidification or of its electrogenic capacity by creating Cl⁻ currents. In fact, all three mutations have been described to present diminished or abolished Cl⁻ currents^{161,481}. As for acidification, we will address it below (see section3.3.3, Discussion).

Previous results by our group (manuscript in preparation) showed that all mutants displayed reduced localization in plasma membrane as compared to the WT (WT Manders' coefficient 0.32 vs. mutants Manders' coefficient less than 0.02). These findings are in line with the previous study by *Smith et al.*, which showed decreased surface expression of E527D and I524K (V523del has not been formerly studied¹⁶⁴). The role of CIC-5 in the plasma membrane is not well understood¹⁶¹, but it has been hypothesised it is essential for tethering the receptor complex together³⁶⁶ and leading to its internalisation, potentially by some of the protein-protein interactions yielded by the Ct of CIC-5, such as Nedd4.2 or NHERF which according to previous reports would shunt CIC-5 from the plasma membrane into the endocytic pathway⁴⁸³.

Likewise, results from our group showed that E527D (Manders' coefficient 0.29) and I524K (Manders' coefficient 0.39) accumulated at the ER (marked with KDEL, amino acid sequence in ER resistant protein) to a greater extent than WT (Manders' coefficient 0.1), while V523del (Manders' coefficient 0.17) did not. This (1) confirms that I524K is mostly retained at the ER as previously reported, so that this mutation belongs to class 1¹⁶¹ (2) contradicts *Smith et al.* in the subcellular distribution of E527D, as their results suggested this mutant does not localize in the ER, while ours showed E527D is partially retained in the ER; again it is difficult to find an explanation for this as both their YFP-tag and our HA-tag were placed at the Ct, and although we used different antibodies for ER staining with possible different epitopes, it is very

unlike the differences are due to this fact. It may be due to the type of construct used or to the cell line itself. Although it is to be considered other studies described a partial localisation of E527D in the ER¹⁶⁴ and, (3) importantly, demonstrates that V523del does not fit in class 1, as it does not localize with the ER.

Still referring to CIC-5 along the endo-lysosomal pathway, in physiological conditions, most of the proteins involved in endocytosis are recycled to the plasma membrane to maintain their proper function rather than being degraded^{62,108}. Additionally, there are no reports in literature about the proportion of CIC-5 that is meant to enter degradation pathway. So, we used WT CIC-5 colocalization with lysosomes as reference for normal degradation rate. Although differences did not reach statistical significance, all mutants compared to WT showed lower colocalization with lysosomes, especially the I524K. We cannot fully discard that this is not due to a lower expression of the protein in the mutants, yet as qualitatively appreciated from the immunocytochemistry it would not seem so. Conjecturing further explanations, this slightly reduced colocalization of the mutants with the lysosomes might be due to a slower trafficking of the mutant proteins along the pathway. Another possible reason is that the mutants are degraded elsewhere. In fact, our findings would support the hypothesis suggested by some authors who indicated that aberrant CIC-5 is degraded via proteasome and that it is ubiquitinated and targeted to the autophagosomes instead of following the conventional pathway, especially for those mutants

retained at the ER^{162,363}. Thus, further experiments using both inhibitors of lysosomal degradation such as leupeptine and proteasome inhibitors like MG132 (carbobenzoxy-Leu-Leu-leucinal) would be useful to know which of the degradation pathways is more involved.

3.3. A consistent model for endocytosis assessment with some drawbacks

3.3.1. Quantification by fluorimetry

We report here different methods for receptor-mediated and fluid-phase endocytosis assessment in our cell model. In a first attempt to quantify endocytosis, a protocol for fluorimetry measurement of fluorescent cargoes was optimized: Alexa 488 albumin was used as marker for receptor-mediated endocytosis and FITC-dextran as a cargo for fluid-phase endocytosis. Recovery of normally filtered albumin in physiological conditions happens mainly via receptor-mediated endocytosis, with a major affinity to cubilin⁶³. For this reason, as said, despite in our hands RPTEC/hTERT1 did not express megalin, we consider these cells endocytic capacity for albumin as conserved. On the other hand, high concentrations of albumin need recovery via fluid-phase⁶⁴.

When applying fluorimetry to measure albumin and dextran recovery, we came up against a stumbling-block: there is no feasible manner, at least by available means, that fluid-phase endocytosis of albumin can be separated from the measurement of

receptor-mediated endocytosis. On one hand, to properly visualize the process, the amount of albumin we need to incubate the cells with is probably much higher than that a sole proximal tubule cell handles in physiological conditions. Thus, with our experimental obliged settings, it is possible that fluid-phase endocytosis is required and anyway, fluid-phase uptake has been described as a continuous, non-saturable process⁷⁵.

A proof of this fact is that despite saturating receptor-mediated endocytosis by either adding competition with non-labelled albumin or by adding the specific inhibitor of vacuolar *H⁺-ATPase*, Bafilomycin (which stops vesicle acidification and so receptor-mediated endocytosis), still a 60% of initial fluorescent albumin signal is detected. We can think about different putative reasons for this finding. (1) we are detecting fluorescent albumin resistant to washes that remains attached to the cell membrane; indeed we demonstrated that there was colocalization of albumin with plasma membrane (phalloidin) specially for E527D; (2) addition of bafilomycin also impairs degradation, so this 60% may account for albumin that is not being degraded. (3) corresponds to albumin being endocytosed via fluid-phase.

There are no inhibitors for fluid-phase endocytosis and it is a known non-saturate system⁴⁷⁴; adding huge concentration of non-labelled dextran did not significantly reduce the amount of detectable albumin. Nonetheless, competition with 10 mg/mL dextran (200-fold the concentration of initial fluorescent albumin) showed reduction of 20% of labelled albumin uptake. This was

surprising; as said, dextran is not expected to exert competition due to the unspecific nature of the fluid-phase uptake with no limiting factor. Nonetheless, 10 mg/mL of dextran is a huge concentration of this colloid. In fact, classical studies by *Christensen et al.* demonstrated that in a rat model, the infusion of high concentration of dextran did not change protein absorption pathway as assessed by evaluation of the protein lysozyme. Nonetheless, they reported an increase in the number and size of lysosomes in proximal tubule cells^{484,485}. So, the 20% decrease in fluorescent-albumin detection could somehow account for an increase degradation due to an increased number of lysosomes rather than to a decrease in the uptake, yet this hypothesis should be further confirmed by visualising lysosomes during albumin uptake. Another surprising finding was the 20% increment of albumin uptake with 2mg/mL dextran competition, one theory is that by budding of endocytic vesicles for fluid phase endocytosis, some of the albumin attached to the cell membrane enters the cell, yet to proof this hypothesis a high-resolution microscopy, probably electron microscopy would be necessary.

Considering these drawbacks, overall albumin uptake was measured by fluorimetry for all cell lines with and without competition. As compared to control cell lines, I524K and V523del showed reduced quantification of endocytosed albumin, with further reduction of uptake in all of them when adding non-labelled albumin for competition. This further reduction after challenging labelled with non-labelled albumin is possibly due to a

residual endocytosis activity by receptors that is completely saturated when adding competition. The fact that we do not measure any reduction in albumin uptake by E527D is probably due to important amount of albumin attached to the cell membrane. Why does albumin remain attach to this mutant's membrane in particular remains elusive, as all cells, mutants and WT followed the same experimental procedure.

All taken together our cell model is able to reproduce one of the hallmarks of the disease, proteinuria due to reduced endocytosis¹⁷². This quantitative procedure could be used to test potential therapeutics in our cell model, as the restoration of endocytosis to the WT levels could be measured.

In a near future, fluid-phase endocytosis should be thoroughly analysed as we did not quantify this pathway by fluorimetry in the mutants.

3.3.2. Assessment of endocytosis by immunofluorescence imaging.

By confocal microscopy imaging, fluorescent albumin and dextran were separately monitored to assess receptor-mediated and fluid-phase endocytosis. By measuring albumin colocalization with the membrane marker phalloidin, evidence was drawn that part of the albumin measured was in fact stuck to the cell membrane even after performing multiple washes. Interestingly, the mutant E527D showed the higher rate of albumin colocalizing with plasma

membrane, also showed less reduction in albumin quantification via fluorimetry¹⁶¹, as said before, this could explain why no endocytosis reduction is measured via fluorimetry for this mutant.

Our results demonstrated that compared to the WT CIC-5, mutants did not show differences in albumin colocalization with lysosomes, which entails that once endocytosed and trafficked through the endosomal pathway, albumin correctly gets to lysosomes to be degraded³⁶⁶.

Similarly, fluid-phase endocytosis was evaluated; surprisingly, dextran presented higher colocalization with lysosomes after one-hour incubation particularly in the mutants I524k and V523del, which could involve a slower trafficking of this cargo along the endo-lysosomal pathway or a deficient degradation by lysosomes. In fact, defects in lysosomal degradation due to trafficking defects have already been addressed; reduced levels of lysosomal enzymes B-hexosaminidase and cathepsin B were reported in CIC-5 KO mice¹⁴³ as their transport to the lysosomes depends on acidic environment, which is impaired in the disease.

Sticking to our results and taking together fluorimetry quantification and confocal microscopy imaging to evaluate receptor-mediated and fluid-phase endocytosis, we could detect decrease in albumin endocytosis in both I524K and V523del, as measured by fluorimetry. As shown by confocal microscopy, albumin did not accumulate in the lysosomes and was not retained attached to the membrane. Moreover, both mutants seemed to present a delay in dextran degradation as shown by persistent

colocalization of this colloid in the lysosomes after 1-hour incubation. E527D did not show a reduction in albumin uptake, as measured by fluorimetry, probably because albumin persisted attached to the cell membrane as proved by confocal microscopy. As for dextran, it did not accumulate in the lysosomes in this mutant. Previous studies¹⁷² have also studied both receptor-mediated and fluid phase endocytosis in conditionally immortalized cells from DD1 patients with different mutations. As for albumin endocytosis, these studies registered different reductions as compared to the WT (mutation 30:insH had a 43% reduction, del132-241 a 76.7% reduction and R637X a 35.1% reduction) in comparison to the WT (100%). They also analysed dextran uptake and concluded that only the R637X mutant had significantly reduced dextran uptake compared with WT (24.4%). It is true that our cell lines show a poorer decrease in endocytosis (~14%), but still the reduction rates quantified in the Mutants are measurable and significantly different to the WT. Thus, recovery of the WT phenotype as for endocytosis could be considered when evaluating the efficiency of a potential drug.

3.3.3. pH measurement

Despite increasing interest and research has arisen in the last years on Dent's Disease and the effects of the mutations on CIC-5 that cause it, there are still many questions to be solved such as the precise effect on pH or Cl⁻ concentration in the early endosomes.

First it was suggested that CIC-5 acted as a Cl⁻ shunt allowing for an efficient intraluminal acidification of endosomes by V-ATPase, so endosomal defective acidification due to CIC-5 loss-of-function would impair endocytosis⁸³). However, mouse models for DD1 questioned this hypothesis. While the first two mouse knock-down models created by Jentsch's and Guggino's groups showed endosomal impaired acidification^{107,109,173,486} and phenotypic characteristics of DD1, another mouse model created later by Jentsch's group in a study led by Novarino challenged this predominant role of defective acidification in DD1. They introduced the synthetic mutation E211A by knock-in; this mutation converts the Cl⁻/H⁺ antiporter into a pure Cl⁻ channel and surprisingly, even if early endosomes acidification was normal, the animal still showed DD1 characteristics such as LMWP and an impaired presence of megalin and cubilin⁴⁸⁷. Thus, even if all models showed the main phenotypic features of the disease, it is not clear which is the immediate cause. Likewise, from cell models, the same variable results are drawn, as exemplified by the already referred elegant study by *Gorvin et al.*, in which conditionally immortalized proximal tubule cells from patients with distinct mutations involving three different domains of CIC-5 showed differing effects on endosomal acidification: in two of them (one deletion of helices C to G, del132-241 and another located in the CBS domain, R637X) endosomal pH was more alkaline and in the third one, located in the A helix (30:insH) endosomal pH was comparable to the CIC-5 WT¹⁷². A very recent study, on the effects

of new mutations in the gating glutamate showed, as Novarino's mouse model, a normal endosomal acidification⁴⁸⁸. Hence, we deemed it relevant to assess the pH and Cl⁻ concentration in endo-lysosomal vesicles in our cell model.

As a first approach to measure endo-lysosomal pH in mutant cells, we used the LysoSensorTM Yellow/Blue DND- 160. LysoSensor is a ratiometric dye which is endocytosed reaching first the endosomes and finally arrives to the lysosomes. Depending on the lapse between incubation and imaging, we will measure a mix between early-late endosomes and lysosomes or directly lysosomes. The transition through the early endosomes takes very few minutes, while that from late endosomes to lysosomes lasts between 10 and 40 minutes³⁷, so measuring the pH in these last organelles is much approachable. Hence, in this thesis, we first set up the system to measure lysosomal pH and our plan is to continue and check the endosomal pH with a similar system, but which allows a more specific measure for early endosomes.

CIC-5 main role is modulating endosomal pH with almost no effect on the lysosomal pH⁴⁸⁹. Indeed, another member of the CIC family manages the acidification of the lysosome, namely CIC-7. Although altered lysosomal pH has been reported in other renal diseases (for example, cystinosis etc), it has not been detected in DD1 patients. Accordingly, our results from measuring lysosomal pH revealed no differences between cell lines (control vs KD or WT vs Mutants), confirming that CIC-5 does not have a major role in the acidification of the lysosome.

Considering previous information on endosomal pH affecting our Mutants, class 2 E527D is one of the few mutations that have formerly been studied; using a fluorescent ratiometric probe (pHLuorin⁴⁹⁰) to measure intravesicular pH in HEK-MSR cells expressing mutant E527D¹⁶¹, *Smith et cols.* found that the pH of the mutant was approximately 18% more basic than that of the WT. Endosomal pH has not been studied for any of the Class 1 mutants so far. Finally, class 3 mutants were found able to support normal endosomal acidification¹⁶¹. Upon assessing endosomal pH in our cell model, we will be able to conjecture more about the class V523del belongs to.

Leaving aside the particular mutations we studied, it would be priceless to functionally assess (pH, Cl⁻ currents) more pathogenic variants of CIC-5, because as deduced from these lines and as summarised by *Lourdel et al.*, from the known 265 pathogenic variants causing DD1¹⁵⁴, approximately only 30^{162,164} have been just partially studied.

3.3.4. Multi-ligand receptors in DD1 cell model

Many studies have investigated the presence of the receptors megalin and cubilin together with amnionless (CUBAM) in the context of CIC-5 mutations and several have concluded that CIC-5 plays a key role in their proper localization and function. Indeed, both proteins have been demonstrated downregulated in murine CIC-5 knock-down models^{143,491} and in human kidney biopsies of

affected males as assessed by immunohistochemistry^{137,145,480}. The few quantitative data existing on the reduction of megalin and cubilin was provided by kidney biopsies immunoblotting in CIC-5-KO mice as compared to WT mice, showing 28% and 73% reduction, respectively¹⁴³. *Gorvin et al.* imaged megalin in the ciPTEC from DD1 patients, showing an impaired recycling in some of the mutants, but did not quantify the expression¹⁷². Although the exact mechanism causing this loss of megalin and cubilin remains elusive, the main hypothesis would support that there is a defective recycling of both receptors, so that they would reach the lysosomes and be degraded compared to non-defective PTECs where all the receptors would be recycled to the cell membrane. This assumption is supported by the fact that no changes at mRNA levels were found³⁶⁶.

Considering our cell prototype, unfortunately, megalin could not be detected in our RPTEC/hTERT1 model either at mRNA nor at protein level. As mentioned, this receptor has been previously detected by immunocytochemistry⁴⁹² in this immortalized cell line but, assessment of megalin at mRNA or measurable protein levels in RPTEC/hTERT remains briefly addressed in literature. Actually, despite this cell line is supposed to have intact receptor-complex, according to www.proteinatlas.org⁴⁹³ RPTEC/hTERT cells do not express megalin, contrary to cubilin, which is present in these cells. Recovery of normally filtered albumin in physiological conditions happens mainly via receptor-mediated endocytosis, with a major affinity to cubilin⁶³; megalin would come into play when non-

physiologic amounts of albumin get to the proximal tubule; this happens with glomerulopathy, which is out of scope in this project¹⁵. For this reason, despite we could not demonstrate that RPTEC/HTERT1 express megalin, we consider these cells endocytic capacity for albumin as conserved and we considered our model reliable.

In contrast, we were able to assess cubilin in our cell model and, despite mRNA levels were found significantly lower in *CLCN5* shRNA and in mutants E527D and I524K, no differences were seen at protein level by WB. In parallel with our findings, *Norden and cols* demonstrated that cubilin was normally present in the urine of DD1 patients as compared to healthy controls and concluded that, contrary to megalin, the results for cubilin were consistent with a normal recycling of the receptor to the apical cell surface of the proximal tubule cells⁶¹. On the other hand, contrary to our results and as stated before, the two aforementioned mice models^{107,143} presented a drop of both cubilin and megalin expression in kidney tissue with no changes at mRNA levels. To our knowledge, no prior studies have examined the levels of megalin or cubilin in a DD1 cell model by RT-qPCR or immunoblotting so we can just refer to studies evaluating immunohistochemistry. An explanation for cubilin comparable levels acquired among all the cell lines in our model would be that alterations of *CIC-5* impact many downstream pathways such as those implied in differentiation, cell-cycle arrest or proliferation enhanced by cell-to-cell interaction. These interactions are only possible in more complex systems, as tissue,

but probably they cannot take place in a monolayer cell culture system. In this respect, it would be remarkably interesting to reproduce this model in a more complex system.

All in all, there is a considerable body of literature on megalin and cubilin reduction due to *CLCN5* mutations yet it remains to be clarified how alterations in endosomal pH or chloride concentration translate mechanistically to decrease these multi-ligand receptors. In any case, this reduction of endocytic receptors would contribute to the phenotype observed in DD1 patients, such as proteinuria, the main function here evaluated. In our cell model, although we could not detect this reduction in the presence of receptors, as said, it is probably because our cell system does not entirely reproduce what occurs in a most complex model like a tissue, thus a future plan is to replicate this cellular system in organoids.

3.4. Summary and limitations

Altogether, the RPTEC/hTERT1 cell lines carrying WT or mutant forms of *CLC-5* are a reliable model for Dent's Disease type 1. First, we have demonstrated that it reproduces the already studied features of Class 1 I524k and Class 2 E527D mutations. As for V523del, we do not have enough data yet to determine whether it belongs to class 2 or 3, but it does not belong to class 1, as it is not retained in the ER.

When first created in our lab, these mutations were chosen because they are clustering in a restrained region, discarding location-related factors influencing the findings, and because two of them had already been characterised, providing a reference to which the uncharacterized mutation could be directly compared. From our findings, summarized in *table 22* together to other groups finding, one more question arises: why a change in one amino acid can induce such different effects on the whole functioning of the protein? One possible reason is that for example, the replacement of small and hydrophobic isoleucine in I524K mutant by a larger side chain positively charged (lysine) probably alters the helical structure of the α -helix more than in E527D in which a negatively charged short chain amino acid (glutamic acid) is replaced by an equally negatively charged short chain amino acid (aspartic acid) thus, while the folding of I524K is impaired and so it is retained in the ER and rapidly degraded, in E527D the protein probably has some residual function allowing for less impaired endocytosis.

Secondly, this is a good model for receptor-mediated and fluid-phase endocytosis, despite megalin not being detected, because the cargo used, albumin, is mainly specific for cubilin, particularly in physiological conditions^{63,64,366}, so the absence of megalin would not modify the reliability of the effects seen on receptor-mediated endocytosis. The fact that we cannot detect megalin entails a limitation, as of course it would be better to reproduce the model as in human PTEC. It is also a limitation of our cell model not being

able to separately quantify receptor-mediated endocytosis from fluid phase endocytosis and probably the most important drawback is the reduced decrease in albumin uptake shown by the Mutants as, even it is significantly different to WT, a larger reduction would be expected.

Table 22 Summary of CIC-5 half-life, subcellular localisation and endocytic capacity in our cell model

| | I524K (class 1) | E527D (class 2) | V523del (class ?) |
|---|--|---|---|
| Half-life | Rapid decrease first 1h. Half-life \approx WT <i>*Other studies showed decrease half-life for rapid degradation</i> ³⁶³ | \approx WT <i>*One study found it decreased</i> ¹⁶¹ | \uparrow <i>*Not assessed by other studies</i> |
| Subcellular localisation | | | |
| Early endosomes | $\downarrow\downarrow\downarrow$ <i>In concordance to other studies</i> ¹⁶¹ | \downarrow <i>One study found it = WT</i> ¹⁶¹ | $\downarrow\downarrow$ <i>*Not assessed by other studies</i> |
| Plasma membrane | \downarrow ¹⁶⁴ | \downarrow ¹⁶⁴ | \downarrow <i>*Not assessed by other studies</i> |
| ER | $\uparrow\uparrow\uparrow$ <i>In accordance with previous studies</i> ¹⁶¹ | \uparrow <i>In accordance to</i> ¹⁶⁴ <i>but different from</i> ¹⁶¹ | \approx WT <i>*Not assessed by other studies</i> |
| Lysosomes | \approx WT | \approx WT | \approx WT |
| Acidification | | | |
| Endosomes <i>(Not assessed in this project but according to previous studies; ^{161,172})</i> | N.T | \downarrow | N.T |
| Lysosome pH <i>*Not assessed by other studies</i> | \approx WT | \approx WT | \approx WT |
| Cl⁻ currents <i>Not assessed in this project but according to previous studies; (⁴⁸¹; Smith et al., 2008)</i> | $\downarrow\downarrow\downarrow$ | \downarrow | $\downarrow\downarrow$ |

| | | | |
|--|--|---|--|
| Receptor-mediated endocytosis (considering albumin endocytosis together) | ↓↓ | ≈ WT (but albumin importantly attached to cell membrane) | ↓↓ |
| Fluid-Phase endocytosis (considering dextran endocytosis) | Slower trafficking of dextran along the endo-lysosomal pathway | ≈ WT | Slower trafficking of dextran along the endo-lysosomal pathway |

To sum up, this cellular model based on RPTEC/hTERT1 cells provides a valuable resource for the investigation of the receptor-mediated endocytic pathway and the mechanisms and roles of CLC-5 in physiology and pathology. It entails a reliable model for further test findings obtained in other models (for example, to prove differentially expressed uEVs miRNA detected in DD1 patients and check the direction of the interaction with their target genes and the pathways affected (proliferation, cell cycle arrest, inflammation, fibrosis). Furthermore, this model can be used in the assessment of compounds that may be of potential benefit in treating DD1 and other human renal proximal tubular disorders due to defects in receptor-mediated endocytosis and endosomal acidification.

CONCLUSIONS



Dent's disease type 1: picture of the current situation in Europe

- Our survey revealed that Dent's Disease type 1 (DD1) has a variable and evolving clinical presentation; all patients showed LMWP but inconsistent rates of hypercalciuria, nephrocalcinosis and kidney stones or other less common signs like hypokalaemia. In our cohort, the phenotypic presentation changed with age, together with the decrease in eGFR, so that older patients presented with more glycosuria and less hypercalciuria.
- Proteinuria was the key sign leading to DD1 diagnosis in 50% of our study cohort, but all the patients showed proteinuria when tested, as it is the hallmark of the disease. Universal school screening for proteinuria among children could help towards a more effective diagnosis.
- Our findings reasserted the phenotypic differences between European/US patients and Japanese DD1 patients, who have less prevalence of nephrocalcinosis, hypercalciuria and rickets.
- For the first time, we report that there is an enhanced proportion of nephrocalcinosis among patients carrying more severe mutations (nonsense, frameshift, large deletion or splice-site mutations), yet no other genotype-

phenotype relationship was observed and no baseline factors could predict progression to CKD.

- Our survey revealed that, as there is no curative treatment, supportive management was tailored according to each patients manifestations.

miRNA signature in uEVs from DD1 patients

- DD1 patients showed as many exosomes in urine as controls, although the isolated uEVs were bigger than those in controls.
- DD1 patients, as compared to healthy controls, presented 82 differentially expressed uEVs miRNA, which target genes involved in kidney disease related pathways such as p53 signalling pathway, regulation of the Epithelial-to-mesenchymal transition by growth factors and senescence pathway amongst others. These miRNA might entail putative therapeutic targets.
- Among the six top differentially expressed miRNA in DD1 patients uEVs some were aimed as protective factors for the restoration/regeneration of tubule cells (miR-29b-3p upregulation), but other miRNA were probably involved in incipient cellular damage, inflammation and progression of

fibrosis (downregulation of hsa-miR-145-5p and hsa-miR-143-3p).

- Two of the six top dysregulated miRNA between patients and healthy controls might give some insight in the pathophysiology of DD1: (1) miR- 629-3p, by regulating Barttin gen (*BDNP*) might be related to Barttel Syndrome-like symptoms (hipokaliemia or less frequent alkalosis) observed in some DD1 patients (2) miR-664a-3p might play a role in the development of glomerulosclerosis observed in some patients' biopsies.
- As already reported in literature, our results revealed that miR-181a is upregulated in those patients with nephrolithiasis episodes.

Validation of DD1 cellular model

- In the DD1 cell model previously created by our group, subcellular localisation of ClC-5 was consistent to that previously reported in literature for class I I524k and class II E527D mutations. V523del, not previously characterised, did not localize in the endoplasmic reticulum.
- Our cell model reproduces defective endocytosis which is responsible for proteinuria observed in DD1 patients. Cells

carrying I524k and V523del mutants showed impaired albumin endocytosis and slow trafficking of dextran along the endo-lysosomal pathway.

- According to our findings, mutants E527D, I524K and V523del cells showed stable cubilin levels and non-affected lysosomal pH. Our results showed that RPTEC/hTERT1 cells do not express Megalin.
- Our RPTEC/hTERT1 DD1 cell model with different *CLCN5* mutations provides a valuable prototype for additional investigations of impaired pathways in this rare tubulopathy.

REFERENCES

1. Skorecki, K., Chertow, G. M., Marsden, P. A., Brenner, B. M. & Rector, F. C. *Brenner & Rector's the kidney*. (Elsevier, 2016).
2. Hernando Avedaño, L., Aljans García, P., Arias Rodríguez, M. & Caramelo Díaz, C. Ejido de los Ríos J, Lamas Pérez S. *Nefrol. clínica [CD-ROM]*. Madrid Editor. Médica Panam. (1998).
3. Macgregor, G. A., Markandu, N. D., Roulston, J. E., Jones, J. C. & Morton, J. J. Maintenance of blood pressure by the renin-angiotensin system in normal man. *Nature* **291**, 329–331 (1981).
4. Rose, B. D. Clinical physiology of acid-base and electrolyte disorders. (1977).
5. Christensen, E. I. & Nielsen, S. Structural and functional features of protein handling in the kidney proximal tubule. in *Seminars in nephrology* **11**, 414–439 (Elsevier, 1991).
6. Maack, T., Johnson, V., Kau, S. T., Figueiredo, J. & Sigulem, D. Renal filtration, transport, and metabolism of low-molecular-weight proteins: a review. *Kidney Int.* **16**, 251–270 (1979).
7. Sands, J. M. & Verlander, J. W. Functional Anatomy of the Kidney. *Compr. Toxicol. Second Ed.* **7**, 1–22 (2010).
8. Hummel, C. S. *et al.* Glucose transport by human renal Na⁺/D-glucose cotransporters SGLT1 and SGLT2. *Am. J. Physiol. Physiol.* **300**, C14–C21 (2011).
9. Fairweather, S. J., Bröer, A., O'Mara, M. L. & Bröer, S. Intestinal peptidases form functional complexes with the neutral amino acid transporter BOAT1. *Biochem. J.* **446**, 135–148 (2012).
10. Collazo, R. *et al.* Acute regulation of Na⁺/H⁺ exchanger NHE3 by parathyroid hormone via NHE3 phosphorylation and dynamin-dependent endocytosis. *J. Biol. Chem.* **275**, 31601–31608 (2000).
11. Pan, W. *et al.* The epithelial sodium/proton exchanger, NHE3, is necessary for renal and intestinal calcium (re) absorption. *Am. J. Physiol. Physiol.* **302**, F943–F956 (2012).
12. Mehrotra, S. *et al.* Pre transplant PRA (penal reactive antibody) and DSA (donor specific antibody) screening status and outcome after renal transplantation. *Indian J. Transplant.* **9**, 7–12 (2015).
13. Tojo, A. & Kinugasa, S. Mechanisms of glomerular albumin filtration and tubular reabsorption. *Int. J. Nephrol.* **2012**, (2012).
14. Bökenkamp, A. Proteinuria—take a closer look! (2020).
15. Dickson, L. E., Wagner, M. C., Sandoval, R. M. & Molitoris, B. A. The proximal tubule and albuminuria: Really! *J. Am. Soc. Nephrol.* **25**, 443–453 (2014).
16. Lencer, W. I., Weyer, P., Verkman, A. S., Ausiello, D. A. & Brown, D. FITC-Dextran as a probe for endosome function and localization in kidney. *Am. J. Physiol. - Cell Physiol.* **258**, 309–317 (1990).

17. van Deurs, B., Petersen, O. W., Olsnes, S. & Sandvig, K. The ways of endocytosis. in *International review of cytology* **117**, 131–177 (Elsevier, 1989).
18. Iseki, K., Ikemiya, Y., Iseki, C. & Takishita, S. Proteinuria and the risk of developing end-stage renal disease. *Kidney Int.* **63**, 1468–1474 (2003).
19. Zhang, C. *et al.* Proteinuria is an independent risk factor for first incident stroke in adults under treatment for hypertension in China. *J. Am. Heart Assoc.* **4**, 1–12 (2015).
20. Kwon, Y. *et al.* Dipstick proteinuria predicts all-cause mortality in general population: A study of 17 million Korean adults. *PLoS One* **13**, 1–12 (2018).
21. Remuzzi, A., Sangalli, F., Fassi, A. & Remuzzi, G. Albumin concentration in the Bowman's capsule: multiphoton microscopy vs micropuncture technique. *Kidney Int.* **72**, 1410–1411 (2007).
22. van Berkel, Y., Ludwig, M., van Wijk, J. A. E. & Bökenkamp, A. Proteinuria in Dent disease: a review of the literature. *Pediatr. Nephrol.* **32**, 1851–1859 (2017).
23. Peterson, P. A., Evrin, P. E. & Berggård, I. Differentiation of glomerular, tubular, and normal proteinuria: determinations of urinary excretion of beta-2-macroglobulin, albumin, and total protein. *J. Clin. Invest.* **48**, 1189–1198 (1969).
24. Beara-Lasic, L. *et al.* Prevalence of low molecular weight proteinuria and Dent disease 1 CLCN5 mutations in proteinuric cohorts. *Pediatr. Nephrol.* **35**, 633–640 (2020).
25. Yamazaki, S., Watanabe, T., Sato, S. & Yoshikawa, H. Outcome of renal proximal tubular dysfunction with Fanconi syndrome caused by sodium valproate. *Pediatr. Int.* **58**, 1023–1026 (2016).
26. Mount, D. B. Thick ascending limb of the loop of henle. *Clin. J. Am. Soc. Nephrol.* **9**, 1974–1986 (2014).
27. Blaine, J., Chonchol, M. & Levi, M. Renal control of calcium, phosphate, and magnesium homeostasis. *Clin. J. Am. Soc. Nephrol.* **10**, 1257–1272 (2015).
28. Bachmann, S. *et al.* Kidney-Specific Inactivation of the Megalin Gene Impairs Trafficking of Renal Inorganic Sodium Phosphate Cotransporter (NaPi-IIa). *J. Am. Soc. Nephrol.* **15**, 892–900 (2004).
29. Anglani, F., Giancesello, L., Beara-Lasic, L. & Lieske, J. Dent disease: A window into calcium and phosphate transport. *J. Cell. Mol. Med.* **23**, 7132–7142 (2019).
30. Moor, M. B. & Bonny, O. Ways of calcium reabsorption in the kidney. *Am. J. Physiol. - Ren. Physiol.* **310**, F1337–F1350 (2016).
31. Alexander, R. T., Cordat, E., Chambrey, R., Dimke, H. & Eladari, D.

- Acidosis and Urinary Calcium Excretion: Insights from Genetic Disorders. *J. Am. Soc. Nephrol.* **27**, 3511–3520 (2016).
32. Subramanya, A. R. & Ellison, D. H. Distal convoluted tubule. *Clin. J. Am. Soc. Nephrol.* **9**, 2147–2163 (2014).
 33. Brunette, M. G., Chan, M., Ferriere, C. & Roberts, K. D. Site of 1,25(OH)₂ vitamin D₃ synthesis in the kidney [27]. *Nature* **276**, 287–289 (1978).
 34. Guo, W. *et al.* HHS Public Access. *Cell Rep.* **11**, 1651–1666 (2015).
 35. Bienaimé, F., Prié, D., Friedlander, G. & Souberbielle, J. C. Vitamin D metabolism and activity in the parathyroid gland. *Mol. Cell. Endocrinol.* **347**, 30–41 (2011).
 36. Schuh, C. D. *et al.* Combined structural and functional imaging of the kidney reveals major axial differences in proximal tubule endocytosis. *J. Am. Soc. Nephrol.* **29**, 2696–2712 (2018).
 37. Huotari, J. & Helenius, A. Endosome maturation. *EMBO J.* **30**, 3481–3500 (2011).
 38. Jovic, M., Sharma, M., Rahajeng, J. & Caplan, S. The early endosome: A busy sorting station for proteins at the crossroads. *Histol. Histopathol.* **25**, 99–112 (2010).
 39. Goldenring, J. R. Recycling endosomes. *Curr. Opin. Cell Biol.* **35**, 117–122 (2015).
 40. Van Niel, G., d’Angelo, G. & Raposo, G. Shedding light on the cell biology of extracellular vesicles. *Nat. Rev. Mol. cell Biol.* **19**, 213 (2018).
 41. Futter, C. E., Pearse, A., Hewlett, L. J. & Hopkins, C. R. Multivesicular endosomes containing internalized EGF-EGF receptor complexes mature and then fuse directly with lysosomes. *J. Cell Biol.* **132**, 1011–1023 (1996).
 42. Luzio, J. P., Pryor, P. R. & Bright, N. A. Lysosomes: fusion and function. *Nat. Rev. Mol. cell Biol.* **8**, 622–632 (2007).
 43. Hao, M. & Maxfield, F. R. Characterization of rapid membrane internalization and recycling. *J. Biol. Chem.* **275**, 15279–15286 (2000).
 44. Jullié, D., Choquet, D. & Perraïs, D. Recycling endosomes undergo rapid closure of a fusion pore on exocytosis in neuronal dendrites. *J. Neurosci.* **34**, 11106–11118 (2014).
 45. Schnatwinkel, C. *et al.* The Rab5 effector Rabankyrin-5 regulates and coordinates different endocytic mechanisms. *PLoS Biol.* **2**, (2004).
 46. Vanlandingham, P. A. & Ceresa, B. P. Rab7 regulates late endocytic trafficking downstream of multivesicular body biogenesis and cargo sequestration. *J. Biol. Chem.* **284**, 12110–

- 12124 (2009).
47. Redpath, G. M. I., Betzler, V. M., Rossatti, P. & Rossy, J. Membrane Heterogeneity Controls Cellular Endocytic Trafficking. *Front. Cell Dev. Biol.* **8**, 1–19 (2020).
 48. Christensen, E. I., Birn, H., Verroust, P. & Moestrup, S. K. Membrane receptors for endocytosis in the renal proximal tubule. *Int. Rev. Cytol.* **180**, 237–284 (1998).
 49. Anzenberger, U. *et al.* Elucidation of megalin/LRP2-dependent endocytic transport processes in the larval zebrafish pronephros. *J. Cell Sci.* **119**, 2127–2137 (2006).
 50. Christensen, E. I., Birn, H., Storm, T., Weyer, K. & Nielsen, R. Endocytic receptors in the renal proximal tubule. *Physiology* **27**, 223–236 (2012).
 51. De, S., Kuwahara, S. & Saito, A. The endocytic receptor megalin and its associated proteins in proximal tubule epithelial cells. *Membranes (Basel)*. **4**, 333–335 (2014).
 52. Christensen, E. I. & Birn, H. Megalin and cubilin: Multifunctional endocytic receptors. *Nat. Rev. Mol. Cell Biol.* **3**, 258–268 (2002).
 53. Yamazaki, H. *et al.* Differentiation-induced cultured podocytes express endocytically active megalin, a heyman nephritis antigen. *Nephron - Exp. Nephrol.* **96**, 52–59 (2004).
 54. Yammani, R. R., Seetharam, S. & Seetharam, B. Cubilin and megalin expression and their interaction in the rat intestine: Effect of thyroidectomy. *Am. J. Physiol. - Endocrinol. Metab.* **281**, 900–907 (2001).
 55. Fyfe, J. C. *et al.* The functional cobalamin (vitamin B12)-intrinsic factor receptor is a novel complex of cubilin and amnionless. *Blood* **103**, 1573–1579 (2004).
 56. Coudroy, G. *et al.* Contribution of cubilin and amnionless to processing and membrane targeting of cubilin-amnionless complex. *J. Am. Soc. Nephrol.* **16**, 2330–2337 (2005).
 57. Strope, S., Rivi, R., Metzger, T. & Lacy, E. Mouse amnionless, which is required for primitive streak assembly, mediates cell-surface localization and endocytic function of cubilin on visceral endoderm and kidney proximal tubules. *Development* **131**, 4787–4795 (2004).
 58. Amsellem, S. *et al.* Cubilin is essential for albumin reabsorption in the renal proximal tubule. *J. Am. Soc. Nephrol.* **21**, 1859–1867 (2010).
 59. Eshbach, M. L. & Weisz, O. A. Receptor-Mediated Endocytosis in the Proximal Tubule. *Annu. Rev. Physiol.* **79**, 425–448 (2017).
 60. Gekle, M. Renal tubule albumin transport. *Annu. Rev. Physiol.* **67**,

- 573–594 (2005).
61. Norden, A. G. W. *et al.* Urinary megalin deficiency implicates abnormal tubular endocytic function in Fanconi syndrome. *J. Am. Soc. Nephrol.* **13**, 125–133 (2002).
 62. Weyer, K. *et al.* Mouse model of proximal tubule endocytic dysfunction. *Nephrol. Dial. Transplant.* **26**, 3446–3451 (2011).
 63. Birn, H. *et al.* Cubilin is an albumin binding protein important for renal tubular albumin reabsorption. *J. Clin. Invest.* **105**, 1353–1361 (2000).
 64. Ren, Q. *et al.* Distinct functions of megalin and cubilin receptors in recovery of normal and nephrotic levels of filtered albumin. *Am. J. Physiol. Physiol.* **318**, F1284–F1294 (2020).
 65. Nielsen, R. *et al.* Endocytosis provides a major alternative pathway for lysosomal biogenesis in kidney proximal tubular cells. *Proc. Natl. Acad. Sci. U. S. A.* **104**, 5407–5412 (2007).
 66. Hryciw, D. H. *et al.* The interaction between megalin and CIC-5 is scaffolded by the Na⁺-H⁺ exchanger regulatory factor 2 (NHERF2) in proximal tubule cells. *Int. J. Biochem. Cell Biol.* **44**, 815–823 (2012).
 67. Gluck, S. L. *et al.* Physiology and biochemistry of the kidney vacuolar H⁺-ATPase. *Annu. Rev. Physiol.* **58**, 427–445 (1996).
 68. Gekle, M. *et al.* Inhibition of Na⁺-H⁺ exchange impairs receptor-mediated albumin endocytosis in renal proximal tubule-derived epithelial cells from opossum. *J. Physiol.* **520**, 709–721 (1999).
 69. Carraro-Lacroix, L. R., Lessa, L. M. A., Fernandez, R. & Manic, G. Physiological implications of the regulation of vacuolar H⁺-ATPase by chloride ions. *Brazilian J. Med. Biol. Res.* **42**, 155–163 (2009).
 70. Stauber, T. & Jentsch, T. J. Chloride in vesicular trafficking and function. *Annu. Rev. Physiol.* **75**, 453–477 (2013).
 71. Scheel, O., Zdebik, A. A., Lourdel, S. & Jentsch, T. J. Voltage-dependent electrogenic chloride/proton exchange by endosomal CLC proteins. *Nature* **436**, 424–427 (2005).
 72. Graves, A. R., Curran, P. K., Smith, C. L. & Mindell, J. A. The Cl⁻/H⁺ antiporter CIC-7 is the primary chloride permeation pathway in lysosomes. *Nature* **453**, 788–792 (2008).
 73. Tenten, V. *et al.* Albumin is recycled from the primary urine by tubular transcytosis. *J. Am. Soc. Nephrol.* **24**, 1966–1980 (2013).
 74. Mayor, S., Parton, R. G. & Donaldson, J. G. Clathrin-independent pathways of endocytosis. *Cold Spring Harb. Perspect. Biol.* **6**, a016758 (2014).
 75. Alberts, B. *et al.* Molecular biology of the cell. (2018).
 76. Jentsch, T. J., Friedrich, T., Schriever, A. & Yamada, H. The CLC

- chloride channel family. *Pflugers Arch.* **437**, 783–795 (1999).
77. Poroca, D. R., Pelis, R. M. & Chappe, V. M. ClC channels and transporters: Structure, physiological functions, and implications in human chloride channelopathies. *Front. Pharmacol.* **8**, 1–25 (2017).
 78. Konrad, M. *et al.* Mutations in the chloride channel gene CLCNKB as a cause of classic Bartter syndrome. *J. Am. Soc. Nephrol.* **11**, 1449–1459 (2000).
 79. Saint-Martin, C. *et al.* Two novel CLCN2 mutations accelerating chloride channel deactivation are associated with idiopathic generalized epilepsy. *Hum. Mutat.* **30**, 397–405 (2009).
 80. Pusch, M. Myotonia caused by mutations in the muscle chloride channel gene CLCN1. *Hum. Mutat.* **19**, 423–434 (2002).
 81. Wellhauser, L. A. *Structural and Functional Regulation of the Human Chloride/Proton Antiporter ClC-5 by ATP and Scaffold NHERF2 Interactions Structural and Functional Regulation of the Human Chloride/Proton Transporter ClC-5 by ATP and Scaffold NHERF2 Interactions.* (2010).
 82. Devuyt, O., Christie, P. T., Courtoy, P. J., Beauwens, R. & Thakker, R. V. Intra-renal and subcellular distribution of the human chloride channel, CLC-5, reveals a pathophysiological basis for Dent’s disease. *Hum. Mol. Genet.* **8**, 247–257 (1999).
 83. Günther, W., Lüchow, A., Cluzeaud, F., Vandewalle, A. & Jentsch, T. J. CLC-5, the chloride channel mutated in Dent’s disease, colocalizes with the proton pump in endocytotically active kidney cells. *Proc. Natl. Acad. Sci. U. S. A.* **95**, 8075–8080 (1998).
 84. Pham, P. C. *et al.* Hypertonicity increases CLC-5 expression in mouse medullary thick ascending limb cells. *Am. J. Physiol. - Ren. Physiol.* **287**, 747–752 (2004).
 85. Sayer, J. A., Carr, G., Pearce, S. H. S., Goodship, T. H. J. & Simmons, N. L. Disordered calcium crystal handling in antisense CLC-5-treated collecting duct cells. *Biochem. Biophys. Res. Commun.* **300**, 305–310 (2003).
 86. Ceol, M. *et al.* Involvement of the Tubular ClC-Type Exchanger CLC-5 in Glomeruli of Human Proteinuric Nephropathies. *PLoS One* **7**, 3–9 (2012).
 87. Solanki, A. K. *et al.* A Novel CLCN5 Mutation Associated With Focal Segmental Glomerulosclerosis and Podocyte Injury. *Kidney Int. Reports* **3**, 1443–1453 (2018).
 88. Estévez, R. *et al.* Barttin is a Cl⁻ channel β -subunit crucial for renal Cl⁻ reabsorption and inner ear K⁺ secretion. *Nature* **414**, 558–561 (2001).

89. Piwon, N., Günther, W., Schwake, M., Bösl, M. R. & Jentsch, T. J. CLC-5 Cl⁻-channel disruption impairs endocytosis in a mouse model for Dent's disease. *Nature* **408**, 369–373 (2000).
90. Steinmeyer, K., Schwappach, B., Bens, M., Vandewalle, A. & Jentsch, T. J. Cloning and functional expression of rat CLC-5, a chloride channel related to kidney disease. *J. Biol. Chem.* **270**, 31172–31177 (1995).
91. Vandewalle, A. *et al.* Tissue distribution and subcellular localization of the CLC-5 chloride channel in rat intestinal cells. *Am. J. Physiol. Physiol.* **280**, C373–C381 (2001).
92. Fisher, S. E. *et al.* Cloning and characterization of CLCN5, the human kidney chloride channel gene implicated in Dent disease (an X-linked hereditary nephrolithiasis). *Genomics* **29**, 598–606 (1995).
93. Dutzler, R., Campbell, E. B., Cadene, M., Chait, B. T. & MacKinnon, R. X-ray structure of a CLC chloride channel at 3.0 Å reveals the molecular basis of anion selectivity. *Nature* **415**, 287–294 (2002).
94. Picollo, A. & Pusch, M. Chloride/proton antiporter activity of mammalian CLC proteins CLC-4 and CLC-5. *Nature* **436**, 420–423 (2005).
95. Grand, T. *et al.* Novel CLCN5 mutations in patients with dents disease result in altered ion currents or impaired exchanger processing. *Kidney Int.* **76**, 999–1005 (2009).
96. Wu, F. *et al.* Modeling study of human renal chloride channel (hCLC-5) mutations suggests a structural-functional relationship. *Kidney Int.* **63**, 1426–1432 (2003).
97. Grieschat, M. & Alekov, A. K. Glutamate 268 regulates transport probability of the anion/proton exchanger CLC-5. *J. Biol. Chem.* **287**, 8101–8109 (2012).
98. Novarino, G., Weinert, S., Rickheit, G. & Jentsch, T. J. Endosomal chloride-proton exchange rather than chloride conductance is crucial for renal endocytosis. *Science (80-)*. **328**, 1398–1401 (2010).
99. Carr, G., Simmons, N. & Sayer, J. A role for CBS domain 2 in trafficking of chloride channel CLC-5. *Biochem. Biophys. Res. Commun.* **310**, 600–605 (2003).
100. Schwake, M., Friedrich, T. & Jentsch, T. J. An Internalization Signal in CLC-5, an Endosomal Cl⁻ Channel Mutated in Dent's Disease. *J. Biol. Chem.* **276**, 12049–12054 (2001).
101. Hryciw, D. H. *et al.* Regulation of albumin endocytosis by PSD95/Dlg/ZO-1 (PDZ) scaffolds: Interaction of Na⁺-H⁺ exchange regulatory factor-2 with CLC-5. *J. Biol. Chem.* **281**, 16068–16077

- (2006).
102. Hryciw, D. H. *et al.* Nedd4-2 functionally interacts with CLC-5: Involvement in constitutive albumin endocytosis in proximal tubule cells. *J. Biol. Chem.* **279**, 54996–55007 (2004).
 103. Rickheit, G. *et al.* Role of CLC-5 in renal endocytosis is unique among CLC exchangers and does not require PY-motif-dependent ubiquitylation. *J. Biol. Chem.* **285**, 17595–17603 (2010).
 104. Hryciw, D. H. *et al.* Cofilin interacts with CLC-5 and regulates albumin uptake in proximal tubule cell lines. *J. Biol. Chem.* **278**, 40169–40176 (2003).
 105. Reed, A. A. C. *et al.* CLC-5 and KIF3B interact to facilitate CLC-5 plasma membrane expression, endocytosis, and microtubular transport: relevance to pathophysiology of Dent’s disease. *Am. J. Physiol. Physiol.* **298**, F365–F380 (2010).
 106. Zhou, L., Ouyang, L., Chen, K. & Wang, X. Research progress on KIF3B and related diseases. *Ann. Transl. Med.* **7**, (2019).
 107. Piwon, N., Gunther, W., Schwake, M., Bosl, M. R. & Jentsch, T. J. CLC-5 Cl⁻-channel disruption impairs endocytosis in a mouse model for Dent’s disease. *Nature* **408**, 369–373 (2000).
 108. Nielsen, R. *et al.* Loss of chloride channel CLC-5 impairs endocytosis by defective trafficking of megalin and cubilin in kidney proximal tubules. **100**, (2003).
 109. Wang, S. S. *et al.* Mice lacking renal chloride channel, CLC-5, are a model for Dent’s disease, a nephrolithiasis disorder associated with defective receptor-mediated endocytosis. *Hum. Mol. Genet.* **9**, 2937–2945 (2000).
 110. Sayer, J. A., Carr, G. & Simmons, N. L. Calcium phosphate and calcium oxalate crystal handling is dependent upon CLC-5 expression in mouse collecting duct cells. *Biochim. Biophys. Acta - Mol. Basis Dis.* **1689**, 83–90 (2004).
 111. Unit, C. & Louvain, D. Altered polarity and expression of H⁺-ATPase without ultrastructural changes in kidneys of Dent’s disease patients P IERRE V ERROUST , R AJESH V . T HAKKER , S TEVEN J . S CHEINMAN , P IERRE J . C OURTOY , **63**, 1285–1295 (2003).
 112. Wu, F. *et al.* Modeling study of human renal chloride channel (hCLC-5) mutations suggests a structural-functional relationship. *Kidney Int.* (2003). doi:10.1046/j.1523-1755.2003.00859.x
 113. Tosetto, E. *et al.* Phenotypic and genetic heterogeneity in Dent’s disease - The results of an Italian collaborative study. *Nephrol. Dial. Transplant.* **21**, 2452–2463 (2006).
 114. Mansour-Hendili, L. *et al.* Mutation Update of the CLCN5 Gene

- Responsible for Dent Disease 1. *Hum. Mutat.* (2015). doi:10.1002/humu.22804
115. Eurordis, M. EURORDIS. Rare Diseases Europe. <http://www.eurordis.org/>. (2000).
 116. Eurordis. The Voice of Rare Disease Patients in Europe. 7–9 (2011).
 117. Dent, C. E. & Friedman, M. Hypercalcuric rickets associated with renal tubular damage. *Arch. Dis. Child.* (1964). doi:10.1136/adc.39.205.240
 118. Salti, I. S. & Hemady, K. Hypercalciuric rickets: A rare cause of nephrolithiasis. *Nephron* **25**, 222–226 (1980).
 119. Murakami, T. *et al.* Asymptomatic low molecular weight proteinuria: studies in five patients. *Clin. Nephrol.* **28**, 93 (1987).
 120. Suzuki, Y., Okada, T., Higuchi, A., Mase, D. & Kobayashi, O. Asymptomatic low molecular weight proteinuria: a report on 5 cases. *Clin. Nephrol.* **23**, 249–254 (1985).
 121. Wrong, O. M. Dent's disease: a familial renal tubular syndrome with hypercalciuria, tubular proteinuria, rickets, nephrocalcinosis and eventual renal failure. *QJ Med* **77**, 1086–1087 (1990).
 122. Wrong, O. M., Norden, A. G. W. & Feest, T. G. Dent's disease; a familial proximal renal tubular syndrome with low-molecular-weight proteinuria, hypercalciuria, nephrocalcinosis, metabolic bone disease, progressive renal failure and a marked male predominance. *Qjm* **87**, 473–493 (1994).
 123. Reinhart, S. C. *et al.* Characterization of carrier females and affected males with X-linked recessive nephrolithiasis. *J. Am. Soc. Nephrol.* **5**, 1451–1461 (1995).
 124. Enia, G., Zoccali, C., Bolino, A. & Romeo, G. A NEW X-LINKED HYPOPHOSPHATEMIC RICKETS WITH HYPERCALCIURIA LEADING TO PROGRESSIVE RENAL-FAILURE. in *KIDNEY INTERNATIONAL* **43**, 758 (BLACKWELL SCIENCE INC 238 MAIN ST, CAMBRIDGE, MA 02142, 1993).
 125. Frymoyer, P. A. *et al.* X-Linked Recessive Nephrolithiasis with Renal Failure. *N. Engl. J. Med.* **325**, 681–686 (1991).
 126. Lloyd, S. E. *et al.* Idiopathic low molecular weight proteinuria associated with hypercalciuric nephrocalcinosis in Japanese children is due to mutations of the renal chloride channel (CLCN5). *J. Clin. Invest.* **99**, 967–974 (1997).
 127. Devuyt, O. & Thakker, R. V. Dent's disease. *Orphanet J. Rare Dis.* **5**, 28 (2010).
 128. Hodgin, J. B., Corey, H. E., Kaplan, B. S. & D'Agati, V. D. Dent disease presenting as partial Fanconi syndrome and

- hypercalciuria. *Kidney Int.* **73**, 1320–1323 (2008).
129. Claverie-Martín, F., Ramos-Trujillo, E. & García-Nieto, V. Dent's disease: Clinical features and molecular basis. *Pediatr. Nephrol.* (2011). doi:10.1007/s00467-010-1657-0
 130. Blanchard, A. *et al.* Observations of a large Dent disease cohort. *Kidney Int.* **90**, 430–439 (2016).
 131. Wang, X. *et al.* Glomerular pathology in dent disease and its association with kidney function. *Clin. J. Am. Soc. Nephrol.* **11**, 2168–2176 (2016).
 132. Frishberg, Y. *et al.* Dent's disease manifesting as focal glomerulosclerosis: Is it the tip of the iceberg? *Pediatr. Nephrol.* **24**, 2369–2373 (2009).
 133. Besbas, N., Ozaltin, F., Jeck, N., Seyberth, H. & Ludwig, M. CLCN5 mutation (R347X) associated with hypokalaemic metabolic alkalosis in a Turkish child: An unusual presentation of Dent's disease. *Nephrol. Dial. Transplant.* **20**, 1476–1479 (2005).
 134. Bogdanović, R. *et al.* A novel CLCN5 mutation in a boy with Bartter-like syndrome and partial growth hormone deficiency. *Pediatr. Nephrol.* **25**, 2363–2368 (2010).
 135. Okamoto, T., Tajima, T., Hirayama, T. & Sasaki, S. A patient with Dent disease and features of Bartter syndrome caused by a novel mutation of CLCN5. *Eur. J. Pediatr.* **171**, 401–404 (2012).
 136. Wojciechowski, D. *et al.* Barttin regulates the subcellular localization and posttranslational modification of human Cl⁻/H⁺Antiporter CIC-5. *Front. Physiol.* **9**, 1–9 (2018).
 137. Giancesello, L. *et al.* Genetic analyses in dent disease and characterization of CLCN5 mutations in kidney biopsies. *Int. J. Mol. Sci.* **21**, 1–20 (2020).
 138. Gambaro, G. *et al.* Living Kidney Donation in a Type 1 Dent's Disease Patient from His Mother. *Kidney Blood Press. Res.* **44**, 1306–1312 (2019).
 139. Sekine, T. *et al.* Japanese Dent disease has a wider clinical spectrum than Dent disease in Europe/USA: Genetic and clinical studies of 86 unrelated patients with low-molecular-weight proteinuria. *Nephrol. Dial. Transplant.* **29**, 376–384 (2014).
 140. Wang, Y. *et al.* CIC-5: role in endocytosis in the proximal tubule. *Am. J. Physiol. Physiol.* **289**, F850–F862 (2005).
 141. Lieske, J. C. & Toback, F. G. Regulation of renal epithelial cell endocytosis of calcium oxalate monohydrate crystals. *Am. J. Physiol.* **264**, F800-7 (1993).
 142. Kawakami, H., Murakami, T. & Kajii, T. Normal values for 24-h urinary protein excretion: total and low molecular weight

- proteins with a sex-related difference. *Clin. Nephrol.* **33**, 232–236 (1990).
143. Christensen, E. I. *et al.* Loss of chloride channel CLC-5 impairs endocytosis by defective trafficking of megalin and cubilin in kidney proximal tubules. *Proc. Natl. Acad. Sci.* **100**, 8472–8477 (2003).
 144. Norden, A. G. W. *et al.* Urinary Megalin Deficiency Implicates Abnormal Tubular Endocytic Function in Fanconi Syndrome. 125–133 (2002).
 145. Santo, Y. *et al.* Examination of megalin in renal tubular epithelium from patients with Dent disease. *Pediatr. Nephrol.* **19**, 612–615 (2004).
 146. Dinour, D. *et al.* Truncating mutations in the chloride/proton clc-5 antiporter gene in seven jewish israeli families with dent's 1 disease. *Nephron - Clin. Pract.* **112**, (2009).
 147. Ishimura, E. *et al.* Serum levels of 1,25-dihydroxyvitamin D, 24,25-dihydroxyvitamin D, and 25-hydroxyvitamin D in nondialyzed patients with chronic renal failure. *Kidney Int.* **55**, 1019–1027 (1999).
 148. Thakker, R. V. Chloride channels cough up. *Nat. Genet.* **17**, 125–127 (1997).
 149. Yamamoto, K. *et al.* Characterization of renal chloride channel (CLCN5) mutations in Dent's disease. *J. Am. Soc. Nephrol.* **11**, 1460–1468 (2000).
 150. Anglani, F. *et al.* Nephrolithiasis, kidney failure and bone disorders in Dent disease patients with and without CLCN5 mutations. *Springerplus* **4**, (2015).
 151. Devuyt, O. & Luciani, A. Chloride transporters and receptor-mediated endocytosis in the renal proximal tubule. *Journal of Physiology* (2015). doi:10.1113/JP270087
 152. Blanchard, A. *et al.* Effect of Hydrochlorothiazide on Urinary Calcium Excretion in Dent Disease: An Uncontrolled Trial. *Am. J. Kidney Dis.* **52**, 1084–1095 (2008).
 153. Souza-Menezes, J., Morales, M. M., Tukaye, D. N., Guggino, S. E. & Guggino, W. B. Absence of CLC5 in knockout mice leads to glycosuria, impaired renal glucose handling and low proximal tubule GLUT2 protein expression. *Cell. Physiol. Biochem.* **20**, 455–464 (2007).
 154. Gianesello, L. *et al.* From protein uptake to Dent disease : an overview of the CLCN5 gene. *Gene* 144662 (2020). doi:10.1016/j.gene.2020.144662
 155. Grgic, I. *et al.* Targeted proximal tubule injury triggers interstitial

- fibrosis and glomerulosclerosis. *Kidney Int.* **82**, 172–183 (2012).
156. Copelovitch, L., Nash, M. A. & Kaplan, B. S. Hypothesis: Dent disease is an underrecognized cause of focal glomerulosclerosis. *Clin. J. Am. Soc. Nephrol.* (2007). doi:10.2215/CJN.00900207
 157. Cramer, M. T. *et al.* Expanding the phenotype of proteinuria in Dent disease. A case series. *Pediatr. Nephrol.* **29**, 2051–2054 (2014).
 158. Tran, P. V. Dysfunction of Intraflagellar Transport Proteins beyond the Primary Cilium. *J. Am. Soc. Nephrol.* **25**, 2385 LP – 2386 (2014).
 159. Bullich, G. *et al.* Contribution of the TTC21B gene to glomerular and cystic kidney diseases. *Nephrol. Dial. Transplant.* **32**, 151–156 (2016).
 160. Yamazaki, H. *et al.* Atypical phenotype of type I Bartter syndrome accompanied by focal segmental glomerulosclerosis. *Pediatr. Nephrol.* **24**, 415–418 (2009).
 161. Smith, A. J., Reed, A. A. C., Loh, N. Y., Thakker, R. V. & Lippiat, J. D. Characterization of Dent’s disease mutations of CLC-5 reveals a correlation between functional and cell biological consequences and protein structure. *AJP Ren. Physiol.* (2008). doi:10.1152/ajprenal.90526.2008
 162. ne Sakhi, I. *et al.* Diversity of functional alterations of the {CLC}-5 exchanger in the region of the proton glutamate in patients with Dent disease 1. (2020). doi:10.22541/au.160133521.16801247
 163. Ramos-Trujillo, E. *et al.* Dent’s disease: Identification of seven new pathogenic mutations in the CLCN5 gene. *J. Pediatr. Genet.* (2013). doi:10.3233/PGE-13061
 164. Lourdel, S. *et al.* CLC-5 mutations associated with Dent’s disease: A major role of the dimer interface. *Pflugers Arch. Eur. J. Physiol.* **463**, 247–256 (2012).
 165. Raja, K. A. *et al.* Responsiveness of hypercalciuria to thiazide in Dent’s disease. *J. Am. Soc. Nephrol.* **13**, 2938–2944 (2002).
 166. Cebotaru, V. *et al.* High citrate diet delays progression of renal insufficiency in the CLC-5 knockout mouse model of Dent’s disease. *Kidney Int.* **68**, 642–652 (2005).
 167. Zaniew, M. *et al.* Dent disease in Poland: what we have learned so far? *Int. Urol. Nephrol.* **49**, 2005–2017 (2017).
 168. Lloyd, S. E. *et al.* Characterisation of Renal Chloride Channel, CLCN5, Mutations in Hypercalciuric Nephrolithiasis (Kidney Stones) Disorders. *Hum. Mol. Genet.* **6**, 1233–1239 (1997).
 169. Lloyd, S. E. *et al.* A common molecular basis for three inherited kidney stone diseases. *Nature* **379**, 445–449 (1996).

170. Chang, M. H. *et al.* Cl⁻ and H⁺ coupling properties and subcellular localizations of wildtype and disease-associated variants of the voltage-gated Cl⁻/H⁺ exchanger CLC-5. *J. Biol. Chem.* **295**, 1464–1473 (2020).
171. Grand, T. *et al.* Heterogeneity in the processing of CLCN5 mutants related to Dent disease. *Hum. Mutat.* **32**, 476–483 (2011).
172. Gorvin, C. M. *et al.* Receptor-mediated endocytosis and endosomal acidification is impaired in proximal tubule epithelial cells of Dent disease patients. *Proc. Natl. Acad. Sci. U. S. A.* **110**, 7014–7019 (2013).
173. Günther, W., Piwon, N. & Jentsch, T. J. The CLC-5 chloride channel knock-out mouse - An animal model for Dent's disease. *Pflugers Arch. Eur. J. Physiol.* **445**, 456–462 (2003).
174. Kalluri, R. & LeBleu, V. S. The biology, function, and biomedical applications of exosomes. *Science (80-.)*. **367**, (2020).
175. Gould, S. J. & Raposo, G. As we wait: coping with an imperfect nomenclature for extracellular vesicles. *J. Extracell. vesicles* **2**, 20389 (2013).
176. Théry, C. *et al.* Minimal information for studies of extracellular vesicles 2018 (MISEV2018): a position statement of the International Society for Extracellular Vesicles and update of the MISEV2014 guidelines. *J. Extracell. vesicles* **7**, 1535750 (2018).
177. Caruso, S. & Poon, I. K. H. Apoptotic cell-derived extracellular vesicles: more than just debris. *Front. Immunol.* **9**, 1486 (2018).
178. Cocucci, E. & Meldolesi, J. Ectosomes and exosomes: Shedding the confusion between extracellular vesicles. *Trends Cell Biol.* **25**, 364–372 (2015).
179. Chargaff, E. & West, R. The biological significance of the thromboplastic protein of blood. *J Biol Chem* **166**, 189–197 (1946).
180. Anderson, H. C. Vesicles associated with calcification in the matrix of epiphyseal cartilage. *J. Cell Biol.* **41**, 59–72 (1969).
181. Dvorak, H. F. *et al.* Tumor shedding and coagulation. *Science (80-.)*. **212**, 923–924 (1981).
182. Stegmayr, B. & Ronquist, G. Promotive effect on human sperm progressive motility by prostasomes. *Urol. Res.* **10**, 253–257 (1982).
183. Harding, C., Heuser, J. & Stahl, P. Endocytosis and intracellular processing of transferrin and colloidal gold-transferrin in rat reticulocytes: demonstration of a pathway for receptor shedding. *Eur. J. Cell Biol.* **35**, 256–263 (1984).
184. Pan, B.-T. & Johnstone, R. M. Fate of the transferrin receptor during maturation of sheep reticulocytes in vitro: selective

- externalization of the receptor. *Cell* **33**, 967–978 (1983).
185. Möbius, W. *et al.* Recycling compartments and the internal vesicles of multivesicular bodies harbor most of the cholesterol found in the endocytic pathway. *Traffic* **4**, 222–231 (2003).
 186. Wubbolts, R. *et al.* Proteomic and biochemical analyses of human B cell-derived exosomes Potential implications for their function and multivesicular body formation. *J. Biol. Chem.* **278**, 10963–10972 (2003).
 187. Wenzel, E. M. *et al.* Concerted ESCRT and clathrin recruitment waves define the timing and morphology of intraluminal vesicle formation. *Nat. Commun.* **9**, (2018).
 188. Hurley, J. H. & Hanson, P. I. Membrane budding and scission by the ESCRT machinery: it's all in the neck. *Nat. Rev. Mol. cell Biol.* **11**, 556–566 (2010).
 189. Wollert, T., Wunder, C., Lippincott-Schwartz, J. & Hurley, J. H. Membrane scission by the ESCRT-III complex. *Nature* **458**, 172–177 (2009).
 190. Stuffers, S., Sem Wegner, C., Stenmark, H. & Brech, A. Multivesicular endosome biogenesis in the absence of ESCRTs. *Traffic* **10**, 925–937 (2009).
 191. Trajkovic, K. *et al.* Ceramide triggers budding of exosome vesicles into multivesicular endosomes. *Science (80-)*. **319**, 1244–1247 (2008).
 192. Ghossoub, R. *et al.* Syntenin-ALIX exosome biogenesis and budding into multivesicular bodies are controlled by ARF6 and PLD2. *Nat. Commun.* **5**, 1–12 (2014).
 193. Hanson, P. I. & Cashikar, A. Multivesicular body morphogenesis. *Annu. Rev. Cell Dev. Biol.* **28**, 337–362 (2012).
 194. Colombo, M. *et al.* Analysis of ESCRT functions in exosome biogenesis, composition and secretion highlights the heterogeneity of extracellular vesicles. *J. Cell Sci.* **126**, 5553–5565 (2013).
 195. Perez-Hernandez, D. *et al.* The intracellular interactome of tetraspanin-enriched microdomains reveals their function as sorting machineries toward exosomes. *J. Biol. Chem.* **288**, 11649–11661 (2013).
 196. Escrevente, C., Keller, S., Altevogt, P. & Costa, J. Interaction and uptake of exosomes by ovarian cancer cells. *BMC Cancer* **11**, 108 (2011).
 197. Gonzales, P. A. *et al.* Large-scale proteomics and phosphoproteomics of urinary exosomes. *J. Am. Soc. Nephrol.* **20**, 363–379 (2009).

198. Østergaard, O. *et al.* Quantitative proteome profiling of normal human circulating microparticles. *J. Proteome Res.* **11**, 2154–2163 (2012).
199. Jeppesen, D. K. *et al.* Quantitative proteomics of fractionated membrane and lumen exosome proteins from isogenic metastatic and nonmetastatic bladder cancer cells reveal differential expression of EMT factors. *Proteomics* **14**, 699–712 (2014).
200. Villarroya-Beltri, C. *et al.* ISGylation controls exosome secretion by promoting lysosomal degradation of MVB proteins. *Nat. Commun.* **7**, (2016).
201. Keerthikumar, S. *et al.* ExoCarta: a web-based compendium of exosomal cargo. *J. Mol. Biol.* **428**, 688–692 (2016).
202. Zhang, H. *et al.* Identification of distinct nanoparticles and subsets of extracellular vesicles by asymmetric flow field-flow fractionation. *Nat. Cell Biol.* **20**, 332–343 (2018).
203. Kleijmeer, M. J., Stoorvogel, W., Griffith, J. M., Yoshie, O. & Geuze, H. J. Selective enrichment of tetraspan proteins on the internal vesicles of multivesicular endosomes and on exosomes secreted by human B-lymphocytes. *J. Biol. Chem.* **273**, 20121–20127 (1998).
204. Laulagnier, K. *et al.* Mast cell-and dendritic cell-derived exosomes display a specific lipid composition and an unusual membrane organization. *Biochem. J.* **380**, 161–171 (2004).
205. Colombo, M., Raposo, G. & Théry, C. Biogenesis, secretion, and intercellular interactions of exosomes and other extracellular vesicles. *Annu. Rev. Cell Dev. Biol.* **30**, 255–289 (2014).
206. Kalra, H. *et al.* Vesiclepedia: a compendium for extracellular vesicles with continuous community annotation. *PLoS Biol* **10**, e1001450 (2012).
207. Pathan, M. *et al.* Vesiclepedia 2019: a compendium of RNA, proteins, lipids and metabolites in extracellular vesicles. *Nucleic Acids Res.* **47**, D516–D519 (2019).
208. Van Balkom, B. W. M., Pisitkun, T., Verhaar, M. C. & Knepper, M. A. Exosomes and the kidney: Prospects for diagnosis and therapy of renal diseases. *Kidney International* (2011). doi:10.1038/ki.2011.292
209. Lasda, E. & Parker, R. Circular RNAs co-precipitate with extracellular vesicles: a possible mechanism for circRNA clearance. *PLoS One* **11**, e0148407 (2016).
210. Chevillet, J. R. *et al.* Quantitative and stoichiometric analysis of the microRNA content of exosomes. *Proc. Natl. Acad. Sci.* **111**, 14888–14893 (2014).

211. Dayanand, K. 乳鼠心肌提取 HHS Public Access. *Physiol. Behav.* **176**, 139–148 (2018).
212. Crescitelli, R. *et al.* Distinct RNA profiles in subpopulations of extracellular vesicles: apoptotic bodies, microvesicles and exosomes. *J. Extracell. vesicles* **2**, 20677 (2013).
213. Ratajczak, J. *et al.* Embryonic stem cell-derived microvesicles reprogram hematopoietic progenitors: evidence for horizontal transfer of mRNA and protein delivery. *Leukemia* **20**, 847–856 (2006).
214. Valadi, H. *et al.* Exosome-mediated transfer of mRNAs and microRNAs is a novel mechanism of genetic exchange between cells. *Nat. Cell Biol.* **9**, 654–659 (2007).
215. Ikonen, E. Roles of lipid rafts in membrane transport. *Curr. Opin. Cell Biol.* **13**, 470–477 (2001).
216. Stenmark, H. Rab GTPases as coordinators of vesicle traffic. *Nat. Rev. Mol. cell Biol.* **10**, 513–525 (2009).
217. Zylbersztejn, K. & Galli, T. Vesicular traffic in cell navigation. *FEBS J.* **278**, 4497–4505 (2011).
218. Caby, M. P., Lankar, D., Vincendeau-Scherrer, C., Raposo, G. & Bonnerot, C. Exosomal-like vesicles are present in human blood plasma. *Int. Immunol.* **17**, 879–887 (2005).
219. Pisitkun, T., Shen, R.-F. & Knepper, M. A. Identification and proteomic profiling of exosomes in human urine. *Proc. Natl. Acad. Sci.* **101**, 13368–13373 (2004).
220. Street, J. M. *et al.* Identification and proteomic profiling of exosomes in human cerebrospinal fluid. *J. Transl. Med.* **10**, 5 (2012).
221. Palanisamy, V. *et al.* Nanostructural and Transcriptomic Analyses of Human Saliva Derived Exosomes. *PLoS One* **5**, e8577 (2010).
222. Bard, M. P. *et al.* Proteomic analysis of exosomes isolated from human malignant pleural effusions. *Am. J. Respir. Cell Mol. Biol.* **31**, 114–121 (2004).
223. Runz, S. *et al.* Malignant ascites-derived exosomes of ovarian carcinoma patients contain CD24 and EpCAM. *Gynecol. Oncol.* **107**, 563–571 (2007).
224. Admyre, C. *et al.* Exosomes with Immune Modulatory Features Are Present in Human Breast Milk. *J. Immunol.* **179**, 1969–1978 (2007).
225. Kulshreshtha, A., Ahmad, T., Agrawal, A. & Ghosh, B. Proinflammatory role of epithelial cell-derived exosomes in allergic airway inflammation. *J. Allergy Clin. Immunol.* **131**, 1194–1203.e14 (2013).

226. Yáñez-Mó, M. *et al.* Biological properties of extracellular vesicles and their physiological functions. *J. Extracell. Vesicles* **4**, 1–60 (2015).
227. Montecalvo, A. *et al.* Mechanism of transfer of functional microRNAs between mouse dendritic cells via exosomes. *Blood* **119**, 756–766 (2012).
228. Fitzner, D. *et al.* Selective transfer of exosomes from oligodendrocytes to microglia by macropinocytosis. *J. Cell Sci.* **124**, 447–458 (2011).
229. Morelli, A. E. *et al.* Endocytosis, intracellular sorting, and processing of exosomes by dendritic cells. *Blood* **104**, 3257–3266 (2004).
230. Rana, S., Yue, S., Stadel, D. & Zöller, M. Toward tailored exosomes: The exosomal tetraspanin web contributes to target cell selection. *Int. J. Biochem. Cell Biol.* **44**, 1574–1584 (2012).
231. Frühbeis, C. *et al.* Neurotransmitter-Triggered Transfer of Exosomes Mediates Oligodendrocyte–Neuron Communication. *PLOS Biol.* **11**, e1001604 (2013).
232. Svensson, K. J. *et al.* Exosome uptake depends on ERK1/2-heat shock protein 27 signaling and lipid Raft-mediated endocytosis negatively regulated by caveolin-1. *J. Biol. Chem.* **288**, 17713–17724 (2013).
233. Nanbo, A., Kawanishi, E., Yoshida, R. & Yoshiyama, H. Exosomes Derived from Epstein-Barr Virus-Infected Cells Are Internalized via Caveola-Dependent Endocytosis and Promote Phenotypic Modulation in Target Cells. *J. Virol.* **87**, 10334–10347 (2013).
234. Tian, T., Wang, Y., Wang, H., Zhu, Z. & Xiao, Z. Visualizing of the cellular uptake and intracellular trafficking of exosomes by live-cell microscopy. *J. Cell. Biochem.* **111**, 488–496 (2010).
235. Hong, C. S., Funk, S., Muller, L., Boyiadzis, M. & Whiteside, T. L. Isolation of biologically active and morphologically intact exosomes from plasma of patients with cancer. *J. Extracell. Vesicles* **5**, (2016).
236. Simons, M. & Raposo, G. Exosomes - vesicular carriers for intercellular communication. *Curr. Opin. Cell Biol.* **21**, 575–581 (2009).
237. Foster, B. P. *et al.* Extracellular vesicles in blood, milk and body fluids of the female and male urogenital tract and with special regard to reproduction. *Crit. Rev. Clin. Lab. Sci.* **53**, 379–395 (2016).
238. Utsugi-Kobukai, S., Fujimaki, H., Hotta, C., Nakazawa, M. & Minami, M. MHC class I-mediated exogenous antigen

- presentation by exosomes secreted from immature and mature bone marrow derived dendritic cells. *Immunol. Lett.* **89**, 125–131 (2003).
239. Hayes, J., Peruzzi, P. P. & Lawler, S. MicroRNAs in cancer: Biomarkers, functions and therapy. *Trends Mol. Med.* **20**, 460–469 (2014).
240. Zhou, S. *et al.* miRNAs in cardiovascular diseases: potential biomarkers, therapeutic targets and challenges. *Acta Pharmacol. Sin.* **39**, 1073–1084 (2018).
241. Kalani, A., Tyagi, A. & Tyagi, N. Exosomes: Mediators of Neurodegeneration, Neuroprotection and Therapeutics. *Mol. Neurobiol.* **49**, 590–600 (2014).
242. Gildea, J. J. *et al.* Exosomal transfer from human renal proximal tubule cells to distal tubule and collecting duct cells. *Clin. Biochem.* **47**, 89–94 (2014).
243. Hiemstra, T. F. *et al.* Human urinary exosomes as innate immune effectors. *J. Am. Soc. Nephrol.* **25**, 2017–2027 (2014).
244. Hogan, M. C. *et al.* Characterization of PKD protein-positive exosome-like vesicles. *J. Am. Soc. Nephrol.* **20**, 278–288 (2009).
245. Bruschi, M. *et al.* Proteomic analysis of urinary microvesicles and exosomes in medullary sponge kidney disease and autosomal dominant polycystic kidney disease. *Clin. J. Am. Soc. Nephrol.* **14**, 834–843 (2019).
246. Witwer, K. W. *et al.* Standardization of sample collection, isolation and analysis methods in extracellular vesicle research. *J. Extracell. Vesicles* **2**, (2013).
247. Willms, E. *et al.* Cells release subpopulations of exosomes with distinct molecular and biological properties. *Sci. Rep.* **6**, 1–12 (2016).
248. Taylor, D. D. & Shah, S. Methods of isolating extracellular vesicles impact down-stream analyses of their cargoes. *Methods* **87**, 3–10 (2015).
249. A.W., C. F. *et al.* Methodological Guidelines to Study Extracellular Vesicles. *Circ. Res.* **120**, 1632–1648 (2017).
250. Helwa, I. *et al.* A comparative study of serum exosome isolation using differential ultracentrifugation and three commercial reagents. *PLoS One* **12**, 1–22 (2017).
251. Greening, D. W., Xu, R., Ji, H., Tauro, B. J. & Simpson, R. J. A protocol for exosome isolation and characterization: evaluation of ultracentrifugation, density-gradient separation, and immunoaffinity capture methods. in *Proteomic Profiling* 179–209 (Springer, 2015).

252. Böing, A. N. *et al.* Single-step isolation of extracellular vesicles by size-exclusion chromatography. *J. Extracell. Vesicles* **3**, (2014).
253. Nordin, J. Z. *et al.* Ultrafiltration with size-exclusion liquid chromatography for high yield isolation of extracellular vesicles preserving intact biophysical and functional properties. *Nanomedicine Nanotechnology, Biol. Med.* **11**, 879–883 (2015).
254. Fang, S. *et al.* Clinical application of a microfluidic chip for immunocapture and quantification of circulating exosomes to assist breast cancer diagnosis and molecular classification. *PLoS One* **12**, 7–9 (2017).
255. Rood, I. M. *et al.* Comparison of three methods for isolation of urinary microvesicles to identify biomarkers of nephrotic syndrome. *Kidney Int.* **78**, 810–816 (2010).
256. Fernández-Llama, P. *et al.* Tamm-Horsfall protein and urinary exosome isolation. *Kidney Int.* **77**, 736–742 (2010).
257. Coresh, J. *et al.* Calibration and random variation of the serum creatinine assay as critical elements of using equations to estimate glomerular filtration rate. *Am. J. Kidney Dis.* **39**, 920–929 (2002).
258. Koritzinsky, E. H., Street, J. M., Star, R. A. & Yuen, P. S. T. Quantification of Exosomes. *J. Cell. Physiol.* **232**, 1587–1590 (2017).
259. Conde-Vancells, J. *et al.* Characterization and Comprehensive Proteome Profiling of Exosomes Secreted by Hepatocytes. *J. Proteome Res.* **7**, 5157–5166 (2008).
260. Raposo, G. & Stoorvogel, W. Extracellular vesicles: Exosomes, microvesicles, and friends. *J. Cell Biol.* **200**, 373–383 (2013).
261. Dragovic, R. A. *et al.* Sizing and phenotyping of cellular vesicles using Nanoparticle Tracking Analysis. *Nanomedicine Nanotechnology, Biol. Med.* **7**, 780–788 (2011).
262. Yoshioka, Y. *et al.* Comparative marker analysis of extracellular vesicles in different human cancer types. *J. Extracell. Vesicles* **2**, (2013).
263. Lee, S. *et al.* Lee *et al.* Reply: *Phys. Rev. Lett.* **99**, 843–854 (2007).
264. Wightman, B., Ha, I. & Ruvkun, G. Posttranscriptional regulation of the heterochronic gene *lin-14* by *lin-4* mediates temporal pattern formation in *C. elegans*. *Cell* **75**, 855–862 (1993).
265. Parrish, S., Fleenor, J., Xu, S. Q., Mello, C. & Fire, A. Functional anatomy of a dsRNA trigger: Differential requirement for the two trigger strands in RNA interference. *Mol. Cell* **6**, 1077–1087 (2000).
266. Calin, G. A. *et al.* Frequent deletions and down-regulation of

- micro-RNA genes miR15 and miR16 at 13q14 in chronic lymphocytic leukemia. *Proc. Natl. Acad. Sci. U. S. A.* **99**, 15524–15529 (2002).
267. Eulalio, A., Huntzinger, E. & Izaurralde, E. Getting to the Root of miRNA-Mediated Gene Silencing. *Cell* **132**, 9–14 (2008).
268. Xie, W., Ted Brown, W. & Denman, R. B. Translational regulation by non-protein-coding RNAs: Different targets, common themes. *Biochem. Biophys. Res. Commun.* **373**, 462–466 (2008).
269. Filipowicz, W., Bhattacharyya, S. N. & Sonenberg, N. Mechanisms of post-transcriptional regulation by microRNAs: Are the answers in sight? *Nat. Rev. Genet.* **9**, 102–114 (2008).
270. Krol, J., Loedige, I. & Filipowicz, W. The widespread regulation of microRNA biogenesis, function and decay. *Nat. Rev. Genet.* **11**, 597–610 (2010).
271. Ceman, S. & Saugstad, J. MicroRNAs: Meta-controllers of gene expression in synaptic activity emerge as genetic and diagnostic markers of human disease. *Pharmacol. Ther.* **130**, 26–37 (2011).
272. Szabo, G. & Bala, S. MicroRNAs in liver disease. *Nat. Rev. Gastroenterol. Hepatol.* **10**, 542–552 (2013).
273. Wiemer, E. A. C. The role of microRNAs in cancer: No small matter. *Eur. J. Cancer* **43**, 1529–1544 (2007).
274. Arroyo, J. D. *et al.* Argonaute2 complexes carry a population of circulating microRNAs independent of vesicles in human plasma. *Proc. Natl. Acad. Sci. U. S. A.* **108**, 5003–5008 (2011).
275. Cheng, L., Sun, X., Scicluna, B. J., Coleman, B. M. & Hill, A. F. Characterization and deep sequencing analysis of exosomal and non-exosomal miRNA in human urine. *Kidney Int.* **86**, 433–444 (2014).
276. Weber, J. A. *et al.* The MicroRNA Spectrum in 12 Body Fluids. *Clin. Chem.* **56**, 1733–1741 (2010).
277. Naskalski, J. W. & Celiński, A. Determining of actual activities of acid and alkaline ribonuclease in human serum and urine. *Mater. Med. Pol.* **23**, 107–110 (1991).
278. McDonald, J. S., Milosevic, D., Reddi, H. V., Grebe, S. K. & Algeciras-Schimmich, A. Analysis of circulating microRNA: Preanalytical and analytical challenges. *Clin. Chem.* **57**, 833–840 (2011).
279. Bartel, D. P. MicroRNAs: Target Recognition and Regulatory Functions. *Cell* **136**, 215–233 (2009).
280. Djuranovic, S., Nahvi, A. & Green, R. A parsimonious model for gene regulation by miRNAs. *Science (80-.)*. **331**, 550–553 (2011).
281. Ambros, V. The functions of animal microRNAs. *Nature* **431**, 350–

- 355 (2004).
282. Kloosterman, W. P. & Plasterk, R. H. A. The Diverse Functions of MicroRNAs in Animal Development and Disease. *Dev. Cell* **11**, 441–450 (2006).
 283. Xiao, C. & Rajewsky, K. MicroRNA Control in the Immune System: Basic Principles. *Cell* **136**, 26–36 (2009).
 284. Zhao, Z. *et al.* Mechanisms of lncRNA/microRNA interactions in angiogenesis. *Life Sci.* **254**, 116900 (2020).
 285. Stefanski, A. L. *et al.* Murine trophoblast-derived and pregnancy-associated exosome-enriched extracellular vesicle microRNAs: Implications for placenta driven effects on maternal physiology. *PLoS One* **14**, e0210675 (2019).
 286. Suh, N. MicroRNA controls of cellular senescence. *BMB Rep.* **51**, 493–499 (2018).
 287. Cava, C., Bertoli, G. & Castiglioni, I. Portrait of Tissue-Specific Coexpression Networks of Noncoding RNAs (miRNA and lncRNA) and mRNAs in Normal Tissues. *Comput. Math. Methods Med.* **2019**, (2019).
 288. Mendell, J. T. & Olson, E. N. MicroRNAs in stress signaling and human disease. *Cell* **148**, 1172–1187 (2012).
 289. Wang, G. *et al.* Expression of microRNAs in the urinary sediment of patients with IgA nephropathy. *Dis. Markers* **28**, 79–86 (2010).
 290. Van Rooij, E. *et al.* A signature pattern of stress-responsive microRNAs that can evoke cardiac hypertrophy and heart failure. *Proc. Natl. Acad. Sci. U. S. A.* **103**, 18255–18260 (2006).
 291. Thum, T. *et al.* MicroRNAs in the human heart: A clue to fetal gene reprogramming in heart failure. *Circulation* **116**, 258–267 (2007).
 292. van de Bunt, M. *et al.* The miRNA Profile of Human Pancreatic Islets and Beta-Cells and Relationship to Type 2 Diabetes Pathogenesis. *PLoS One* **8**, e55272 (2013).
 293. Shimono, Y. *et al.* Downregulation of miRNA-200c Links Breast Cancer Stem Cells with Normal Stem Cells. *Cell* **138**, 592–603 (2009).
 294. Baumgart, S. *et al.* Exosomes of invasive urothelial carcinoma cells are characterized by a specific miRNA expression signature. *Oncotarget* **8**, 58278–58291 (2017).
 295. Cojocneanu, R. *et al.* Plasma and tissue specific miRNA expression pattern and functional analysis associated to colorectal cancer patients. *Cancers (Basel)*. **12**, (2020).
 296. Lampignano, R., Klotten, V., Krahn, T. & Schlange, T. Integrating circulating miRNA analysis in the clinical management of lung

- cancer: Present or future? *Mol. Aspects Med.* **72**, 100844 (2020).
297. Bonneau, E., Neveu, B., Kostantin, E., Tsongalis, G. J. & De Guire, V. How close are miRNAs from clinical practice? A perspective on the diagnostic and therapeutic market. *Electron. J. Int. Fed. Clin. Chem. Lab. Med.* **30**, 114–127 (2019).
298. Saliminejad, K., Khorram Khorshid, H. R., Soleymani Fard, S. & Ghaffari, S. H. An overview of microRNAs: Biology, functions, therapeutics, and analysis methods. *J. Cell. Physiol.* **234**, 5451–5465 (2019).
299. Fareh, M. *et al.* TRBP ensures efficient Dicer processing of precursor microRNA in RNA-crowded environments. *Nat. Commun.* **7**, 1–11 (2016).
300. Lewkowicz, P. *et al.* Dysregulated RNA-induced silencing complex (RISC) assembly within CNS corresponds with abnormal miRNA expression during autoimmune demyelination. *J. Neurosci.* **35**, 7521–7537 (2015).
301. Desvignes, T. *et al.* MiRNA Nomenclature: A View Incorporating Genetic Origins, Biosynthetic Pathways, and Sequence Variants. *Trends Genet.* **31**, 613–626 (2015).
302. Hunt, E. A., Broyles, D., Head, T. & Deo, S. K. MicroRNA Detection: Current Technology and Research Strategies. *Annu. Rev. Anal. Chem.* **8**, 217–237 (2015).
303. Johnson, B. N. & Mutharasan, R. Biosensor-based microRNA detection: Techniques, design, performance, and challenges. *Analyst* **139**, 1576–1588 (2014).
304. Pichler, M. & Calin, G. A. MicroRNAs in cancer: from developmental genes in worms to their clinical application in patients. *Br. J. Cancer* **113**, 569–573 (2015).
305. Chu, Y.-W. *et al.* miRgo: integrating various off-the-shelf tools for identification of microRNA–target interactions by heterogeneous features and a novel evaluation indicator. *Sci. Rep.* **10**, 1466 (2020).
306. Riffo-Campos, Á. L., Riquelme, I. & Brebi-Mieville, P. Tools for sequence-based miRNA target prediction: What to choose? *Int. J. Mol. Sci.* **17**, (2016).
307. Peterson, S. M. *et al.* Common features of microRNA target prediction tools. *Front. Genet.* **5**, 1–10 (2014).
308. Huang, H.-Y. *et al.* miRTarBase 2020: updates to the experimentally validated microRNA–target interaction database. *Nucleic Acids Res.* **48**, D148–D154 (2020).
309. Dweep, H., Sticht, C., Pandey, P. & Gretz, N. MiRWalk - Database: Prediction of possible miRNA binding sites by ‘walking’ the genes

- of three genomes. *J. Biomed. Inform.* **44**, 839–847 (2011).
310. Chang, L., Zhou, G., Soufan, O. & Xia, J. miRNet 2.0: network-based visual analytics for miRNA functional analysis and systems biology. *Nucleic Acids Res.* **48**, W244–W251 (2020).
 311. Søkilde, R., Newie, I., Persson, H., Borg, Å. & Rovira, C. Passenger strand loading in overexpression experiments using microRNA mimics. *RNA Biol.* **12**, 787–791 (2015).
 312. Scherr, M. *et al.* Lentivirus-mediated antagomir expression for specific inhibition of miRNA function. *Nucleic Acids Res.* **35**, e149–e149 (2007).
 313. Mendell, J. T. & Olson, E. N. MicroRNAs in Stress Signaling and Human Disease. *Cell* **148**, 1172–1187 (2012).
 314. Chandrasekaran, K. *et al.* Role of microRNAs in kidney homeostasis and disease. *Kidney Int.* **81**, 617–627 (2012).
 315. Sun, Y. *et al.* Development of a micro-array to detect human and mouse microRNAs and characterization of expression in human organs. *Nucleic Acids Res.* **32**, e188–e188 (2004).
 316. Baskerville, S. & Bartel, D. P. Microarray profiling of microRNAs reveals frequent coexpression with neighboring miRNAs and host genes. *Rna* **11**, 241–247 (2005).
 317. Landgraf, P. *et al.* A Mammalian microRNA Expression Atlas Based on Small RNA Library Sequencing. *Cell* **129**, 1401–1414 (2007).
 318. Nagalakshmi, V. K. *et al.* Dicer regulates the development of nephrogenic and ureteric compartments in the mammalian kidney. *Kidney Int.* **79**, 317–330 (2011).
 319. Mladinov, D., Liu, Y., Mattson, D. L. & Liang, M. MicroRNAs contribute to the maintenance of cell-type-specific physiological characteristics: MiR-192 targets Na⁺/K⁺-ATPase β 1. *Nucleic Acids Res.* **41**, 1273–1283 (2013).
 320. King, L. S. & Agre, P. Pathophysiology of the Aquaporin Water Channels. *Annu. Rev. Physiol.* **58**, 619–648 (1996).
 321. Sepramaniam, S. *et al.* MicroRNA 320a functions as a novel endogenous modulator of aquaporins 1 and 4 as well as a potential therapeutic target in cerebral ischemia. *J. Biol. Chem.* **285**, 29223–29230 (2010).
 322. Gomes, A., da Silva, I. V., Rodrigues, C. M. P., Castro, R. E. & Soveral, G. The Emerging Role of microRNAs in Aquaporin Regulation. *Frontiers in Chemistry* **6**, 238 (2018).
 323. Huang, W. *et al.* Tonicity-responsive microRNAs contribute to the maximal induction of osmoregulatory transcription factor OREBP in response to high-NaCl hypertonicity. *Nucleic Acids Res.* **39**, 475–485 (2011).

324. Sequeira-Lopez, M. L. S. *et al.* The microRNA-processing enzyme dicer maintains juxtaglomerular cells. *J. Am. Soc. Nephrol.* **21**, 460–467 (2010).
325. Szeto, C.-C. *et al.* Micro-RNA expression in the urinary sediment of patients with chronic kidney diseases. *Dis. Markers* **33**, 137–144 (2012).
326. Zununi Vahed, S. *et al.* Differential expression of circulating miR-21, miR-142-3p and miR-155 in renal transplant recipients with impaired graft function. *Int. Urol. Nephrol.* **49**, 1681–1689 (2017).
327. Peiró-Chova, L. *et al.* High stability of microRNAs in tissue samples of compromised quality. *Virchows Arch.* **463**, 765–774 (2013).
328. Lorenzen, J. M. & Thum, T. Circulating and Urinary microRNAs in Kidney Disease. *Clin. J. Am. Soc. Nephrol.* **7**, 1528 LP – 1533 (2012).
329. Saikumar, J., Ramachandran, K. & Vaidya, V. S. Noninvasive Micromarkers. *Clin. Chem.* **60**, 1158–1173 (2014).
330. Torra, R. & Furlano, M. New therapeutic options for Alport syndrome. *Nephrol. Dial. Transplant.* **34**, 1272–1279 (2019).
331. Mejía, N. *et al.* RenalTube: A network tool for clinical and genetic diagnosis of primary tubulopathies. *Eur. J. Pediatr.* **172**, 775–780 (2013).
332. Ramos-Trujillo, E. *et al.* Dent's disease: Identification of seven new pathogenic mutations in the CLCN5 gene. *J. Pediatr. Genet.* **2**, 133–140 (2013).
333. Giancesello, L., Del, D., Franca, P. & Lorenzo, A. Genetics and phenotypic heterogeneity of Dent disease : the dark side of the moon. *Hum. Genet.* (2020). doi:10.1007/s00439-020-02219-2
334. Bonthuis, M. *et al.* Use of national and international growth charts for studying height in european children: Development of up-to-date european height-for-age charts. *PLoS One* **7**, 1–11 (2012).
335. Fraga Rodriguez, G. & Huertes Diaz, B. Evaluación Básica De La Función Renal En Pediatría. *Asoc. Esp. Pediatr.* **1**, 21–35 (2014).
336. Levey, A. S. & Stevens, L. A. Estimating GFR Using the CKD Epidemiology Collaboration (CKD-EPI) Creatinine Equation: More Accurate GFR Estimates, Lower CKD Prevalence Estimates, and Better Risk Predictions. *Am. J. Kidney Dis.* **55**, 622–627 (2010).
337. So, N. P., Osorio, A. V., Simon, S. D. & Alon, U. S. Normal urinary calcium/creatinine ratios in African-American and Caucasian children. *Pediatr. Nephrol.* **16**, 133–139 (2001).
338. Abeling, N. G. G. M. Pediatric Reference Values for Calcium, Magnesium and Inorganic Phosphorus in Serum Obtained from Bhattacharya Plots for Data from Unselected Patients. *Clin. Chem.*

- Lab. Med.* **24**, 233–242 (1986).
339. Rath, B. *et al.* Urinary calcium creatinine ratio and hypercalciuria. *Indian Pediatr.* **31**, 311–316 (1994).
340. Coresh, J. *et al.* Calibration and random variation of the serum creatinine assay as critical elements of using equations to estimate glomerular filtration rate. *Am. J. Kidney Dis.* **39**, 920–929 (2002).
341. Kastelowitz, N. & Yin, H. Exosomes and microvesicles: Identification and targeting by particle size and lipid chemical probes. *ChemBioChem* **15**, 923–928 (2014).
342. Vestad, B. *et al.* Size and concentration analyses of extracellular vesicles by nanoparticle tracking analysis: a variation study. *J. Extracell. Vesicles* **6**, (2017).
343. Livak, K. J. & Schmittgen, T. D. Analysis of relative gene expression data using real-time quantitative PCR and the 2- $\Delta\Delta$ CT method. *methods* **25**, 402–408 (2001).
344. Mestdagh, P. *et al.* A novel and universal method for microRNA RT-qPCR data normalization. *Genome Biol.* **10**, (2009).
345. Klipper-Aurbach, Y. *et al.* Mathematical formulae for the prediction of the residual beta cell function during the first two years of disease in children and adolescents with insulin-dependent diabetes mellitus. *Med. Hypotheses* **45**, 486–490 (1995).
346. Karagkouni, D. *et al.* DIANA-TarBase v8: A decade-long collection of experimentally supported miRNA-gene interactions. *Nucleic Acids Res.* **46**, D239–D245 (2018).
347. Secker, P. F., Luks, L., Schlichenmaier, N. & Dietrich, D. R. RPTEC/TERT1 cells form highly differentiated tubules when cultured in a 3D matrix. *ALTEX* **35**, 223–234 (2018).
348. Wieser, M. *et al.* hTERT alone immortalizes epithelial cells of renal proximal tubules without changing their functional characteristics. *Am. J. Physiol. - Ren. Physiol.* **295**, (2008).
349. Slyne, J., Slattery, C., McMorrow, T. & Ryan, M. P. New developments concerning the proximal tubule in diabetic nephropathy: In vitro models and mechanisms. *Nephrol. Dial. Transplant.* **30**, iv60–iv67 (2015).
350. Montgomery, M. K., Xu, S. & Fire, A. RNA as a target of double-stranded RNA-mediated genetic interference in *Caenorhabditis elegans*. *Proc. Natl. Acad. Sci.* **95**, 15502–15507 (1998).
351. Taxman, D. J. *et al.* Criteria for effective design, construction, and gene knockdown by shRNA vectors. *BMC Biotechnol.* **6**, 1–16 (2006).

352. Hyochol Ahn, et al, 2017. 乳鼠心肌提取 HHS Public Access. *Physiol. Behav.* **176**, 139–148 (2017).
353. Ho, S. N., Hunt, H. D., Horton, R. M., Pullen, J. K. & Pease, L. R. Site-directed mutagenesis by overlap extension using the polymerase chain reaction. *Gene* **77**, 51–59 (1989).
354. Schindelin, J. *et al.* Fiji: an open-source platform for biological-image analysis. *Nat. Methods* **9**, 676–682 (2012).
355. Bolte, S. & Cordelières, F. P. A guided tour into subcellular colocalization analysis in light microscopy. *J. Microsc.* **224**, 213–232 (2006).
356. Oksvold, M. P., Pedersen, N. M., Forfang, L. & Smeland, E. B. Effect of cycloheximide on epidermal growth factor receptor trafficking and signaling. *FEBS Lett.* **586**, 3575–3581 (2012).
357. Smith, A. J. & Lippiat, J. D. Direct endosomal acidification by the outwardly rectifying CLC-5 Cl⁻/H⁺ exchanger. *J. Physiol.* **588**, 2033–2045 (2010).
358. Diwu, Z., Chen, C.-S., Zhang, C., Klaubert, D. H. & Haugland, R. P. A novel acidotropic pH indicator and its potential application in labeling acidic organelles of live cells. *Chem. Biol.* **6**, 411–418 (1999).
359. Willms, E., Cabañas, C., Mäger, I., Wood, M. J. A. & Vader, P. Extracellular Vesicle Heterogeneity: Subpopulations, Isolation Techniques, and Diverse Functions in Cancer Progression . *Frontiers in Immunology* **9**, 738 (2018).
360. Mattila, P. E., Raghavan, V., Rbaibi, Y., Baty, C. J. & Weisz, O. A. Rab11a-positive compartments in proximal tubule cells sort fluid-phase and membrane cargo. *Am. J. Physiol. Physiol.* **306**, C441–C449 (2014).
361. Butterworth, M. B. *et al.* Rab11b regulates the trafficking and recycling of the epithelial sodium channel (ENaC). *Am. J. Physiol. Physiol.* **302**, F581–F590 (2012).
362. Scholl, U. *et al.* Barttin modulates trafficking and function of CLC-K channels. *Proc. Natl. Acad. Sci. U. S. A.* **103**, 11411–11416 (2006).
363. D’Antonio, C. *et al.* Conformational defects underlie proteasomal degradation of Dent’s disease-causing mutants of CLC-5. *Biochem. J.* **452**, 391–400 (2013).
364. Grand, T. *et al.* Heterogeneity in the processing of CLCN5 mutants related to Dent disease. *Hum. Mutat.* (2011). doi:10.1002/humu.21467
365. Schwegler, J. S., Heppelmann, B., Mildenerger, S. & Silbernagl, S. Receptor-mediated endocytosis of albumin in cultured opossum kidney cells: a model for proximal tubular protein reabsorption.

- Pflügers Arch. Eur. J. Physiol.* **418**, 383–392 (1991).
366. Shipman, K. E. & Weisz, O. A. Making a Dent in Dent Disease. *Function* **1**, 1–9 (2020).
367. Ye, Q. *et al.* Multicenter study of the clinical features and mutation gene spectrum of Chinese children with Dent disease. *Clin. Genet.* **97**, 407–417 (2020).
368. Murakami, M., Hayakawa, M., Yanagihara, T. & Hukunaga, Y. Proteinuria screening for children. *Kidney Int. Suppl.* **67**, 23–27 (2005).
369. Lin, C. Y., Sheng, C. C., Chen, C. H., Lin, C. C. & Chou, P. The prevalence of heavy proteinuria and progression risk factors in children undergoing urinary screening. *Pediatr. Nephrol.* **14**, 953–959 (2000).
370. Hajar, F., Taleb, M., Aoun, B. & Shatila, A. Dipstick urine analysis screening among asymptomatic school children. *N. Am. J. Med. Sci.* **3**, 179–184 (2011).
371. Bao, Y. *et al.* Clinical and genetic analysis of Dent disease with nephrotic range albuminuria in Shaanxi, China. *Sci. China Life Sci.* **62**, 1590–1593 (2019).
372. Norden, A. G. W. *et al.* Tubular proteinuria defined by a study of Dent's (CLCN5 mutation) and other tubular diseases. *Kidney Int.* **57**, 240–249 (2000).
373. Yamada, H. *et al.* Association between Urinary Calcium Excretion and Estimated Glomerular Filtration Rate Decline in Patients with Type 2 Diabetes Mellitus: A Retrospective Single-center Observational Study. *J. Clin. Med.* **7**, 171 (2018).
374. Bo, A. & Bo, D. Dent-2 Disease: A Mild Variant of Lowe Syndrome. 94–99 (2009). doi:10.1016/j.jpeds.2009.01.049
375. Hoopes, R. R. *et al.* Evidence for genetic heterogeneity in Dent's disease. *Kidney Int.* **65**, 1615–1620 (2004).
376. Babaei, H. *Antihypertensive drugs / monograph.* (2012).
377. Trionfini, P., Benigni, A. & Remuzzi, G. MicroRNAs in kidney physiology and disease. *Nat. Rev. Nephrol.* **11**, 23–33 (2015).
378. Zhou, H. *et al.* Collection, storage, preservation, and normalization of human urinary exosomes for biomarker discovery. *Kidney Int.* **69**, 1471–1476 (2006).
379. Yun, S. J. *et al.* Cell-free microRNAs in urine as diagnostic and prognostic biomarkers of bladder cancer. *Int. J. Oncol.* **41**, 1871–1878 (2012).
380. Mall, C., Rocke, D. M., Durbin-Johnson, B. & Weiss, R. H. Stability of miRNA in human urine supports its biomarker potential. *Biomark. Med.* **7**, 623–631 (2013).

381. Lv, L. L. *et al.* Isolation and quantification of MicroRNAs from urinary exosomes/microvesicles for biomarker discovery. *Int. J. Biol. Sci.* **9**, 1021–1031 (2013).
382. Sanz-Rubio, D. *et al.* Stability of Circulating Exosomal miRNAs in Healthy Subjects article. *Sci. Rep.* **8**, 1–10 (2018).
383. Zhang, Z., Wang, C., Li, T., Liu, Z. & Li, L. Comparison of ultracentrifugation and density gradient separation methods for isolating Tca8113 human tongue cancer cell line-derived exosomes. *Oncol. Lett.* **8**, 1701–1706 (2014).
384. Zarovni, N. *et al.* Integrated isolation and quantitative analysis of exosome shuttled proteins and nucleic acids using immunocapture approaches. *Methods* **87**, 46–58 (2015).
385. Palomar, M. V., Arévalo, J., Ariceta, G. & Meseguer, A. Establishment of urinary exosome - like vesicles isolation protocol for FHHNC patients and evaluation of different exosomal RNA extraction methods. *J. Transl. Med.* 1–9 (2018). doi:10.1186/s12967-018-1651-z
386. Szataneck, R. *et al.* The methods of choice for extracellular vesicles (EVs) characterization. *Int. J. Mol. Sci.* **18**, (2017).
387. Coleman, B. M., Hanssen, E., Lawson, V. A. & Hill, A. F. Prion-infected cells regulate the release of exosomes with distinct ultrastructural features. *FASEB J.* **26**, 4160–4173 (2012).
388. Théry, C., Zitvogel, L. & Amigorena, S. Exosomes: composition, biogenesis and function. *Nat. Rev. Immunol.* **2**, 569–579 (2002).
389. Kosanović, M. & Janković, M. Isolation of urinary extracellular vesicles from Tamm-Horsfall protein–depleted urine and their application in the development of a lectin-exosome-binding assay. *Biotechniques* **57**, 143–149 (2014).
390. Magayr, T. A. *et al.* Global microRNA profiling in human urinary exosomes reveals novel disease biomarkers and cellular pathways for autosomal dominant polycystic kidney disease. *Kidney Int.* (2020). doi:10.1016/j.kint.2020.02.008
391. Cheng, L., Sun, X., Scicluna, B. J., Coleman, B. M. & Hill, A. F. Characterization and deep sequencing analysis of exosomal and non-exosomal miRNA in human urine. *Kidney Int.* **86**, 433–444 (2014).
392. Matching, T. & Test, R. Chapter 8 Chapter 8. *Test* **1937**, 162–173 (2001).
393. Mestdagh, P. *et al.* Evaluation of quantitative mirnA expression platforms in the micrornA quality control (mirQC) study. *Nat. Methods* **11**, 809–815 (2014).
394. Tan, S. J., Lao, I. K. & Ji, H. M. A New form of Microfluidic Sample

- Delivery for High Throughput Biosensor Analysis. in *Journal of Physics: Conference Series* **307**, 12002 (2011).
395. Lovisa, S. *et al.* Epithelial-to-mesenchymal transition induces cell cycle arrest and parenchymal damage in renal fibrosis. *Nat. Med.* **21**, 998–1009 (2015).
 396. Lan, H. Y. Diverse roles of TGF- β /Smads in renal fibrosis and inflammation. *Int. J. Biol. Sci.* **7**, 1056 (2011).
 397. Chang, L. *et al.* The human RNA surveillance factor UPF1 regulates tumorigenesis by targeting Smad7 in hepatocellular carcinoma. *J. Exp. Clin. Cancer Res.* **35**, 1–12 (2016).
 398. Ruiz-Ortega, M., Rayego-Mateos, S., Lamas, S., Ortiz, A. & Rodrigues-Diez, R. R. Targeting the progression of chronic kidney disease. *Nat. Rev. Nephrol.* **16**, 269–288 (2020).
 399. Lee, C. G. *et al.* Discovery of an integrative network of microRNAs and transcriptomics changes for acute kidney injury. *Kidney Int.* **86**, 943–953 (2014).
 400. Zhang, W. *et al.* Extracellular vesicles carrying miRNAs in kidney diseases: a systemic review. *Clin. Exp. Nephrol.* (2020). doi:10.1007/s10157-020-01947-z
 401. Demirjian, S. *et al.* Safety and Tolerability Study of an Intravenously Administered Small Interfering Ribonucleic Acid (siRNA) Post On-Pump Cardiothoracic Surgery in Patients at Risk of Acute Kidney Injury. *Kidney Int. Reports* **2**, 836–843 (2017).
 402. Johnson, P. F. Molecular stop signs: regulation of cell-cycle arrest by C/EBP transcription factors. *J. Cell Sci.* **118**, 2545–2555 (2005).
 403. Mombach, J. C. M., Bugs, C. A. & Chaouiya, C. Modelling the onset of senescence at the G1/S cell cycle checkpoint. *BMC Genomics* **15**, 1–11 (2014).
 404. Yang, L., Besschetnova, T. Y., Brooks, C. R., Shah, J. V. & Bonventre, J. V. Epithelial cell cycle arrest in G2/M mediates kidney fibrosis after injury. *Nat. Med.* **16**, 535–543 (2010).
 405. Samarani, M. *et al.* A lysosome–plasma membrane–sphingolipid axis linking lysosomal storage to cell growth arrest. *FASEB J.* **32**, 5685–5702 (2018).
 406. Almacellas, E. *et al.* Lysosomal degradation ensures accurate chromosomal segregation to prevent chromosomal instability. *Autophagy* **00**, 1–18 (2020).
 407. Lee, M. *et al.* The long non-coding RNA HOTAIR increases tumour growth and invasion in cervical cancer by targeting the Notch pathway. *Oncotarget* **7**, 44558–44571 (2016).
 408. Tang, Q. & Hann, S. S. HOTAIR: An oncogenic long non-coding RNA in human cancer. *Cell. Physiol. Biochem.* **47**, 893–913 (2018).

409. Yu, F., Chen, B., Dong, P. & Zheng, J. HOTAIR Epigenetically Modulates PTEN Expression via MicroRNA-29b: A Novel Mechanism in Regulation of Liver Fibrosis. *Mol. Ther.* **25**, 205–217 (2017).
410. Gao, L. *et al.* Circulating Long Noncoding RNA HOTAIR is an Essential Mediator of Acute Myocardial Infarction. *Cell. Physiol. Biochem.* **44**, 1497–1508 (2017).
411. Zhou, H. *et al.* LncRNA HOTAIR promotes renal interstitial fibrosis by regulating Notch1 pathway via the modulation of miR-124. *Nephrology* **24**, 472–480 (2019).
412. Xiong, M. *et al.* The miR-200 family regulates TGF- β 1-induced renal tubular epithelial to mesenchymal transition through Smad pathway by targeting ZEB1 and ZEB2 expression. *Am. J. Physiol. Physiol.* **302**, F369–F379 (2012).
413. Jiang, Z. J., Zhang, M. Y., Fan, Z. W., Sun, W. L. & Tang, Y. Influence of lncRNA HOTAIR on acute kidney injury in sepsis rats through regulating miR-34a/Bcl-2 pathway. *Eur. Rev. Med. Pharmacol. Sci.* **23**, 3512–3519 (2019).
414. Wang, H. *et al.* Podocyte-specific knockin of PTEN protects kidney from hyperglycemia. *Am. J. Physiol. - Ren. Physiol.* **314**, F1096–F1107 (2018).
415. Lan, R. *et al.* PTEN loss defines a TGF- β -induced tubule phenotype of failed differentiation and JNK signaling during renal fibrosis. *Am. J. Physiol. - Ren. Physiol.* **302**, (2012).
416. Lin, J. S. *et al.* Loss of PTEN promotes podocyte cytoskeletal rearrangement, aggravating diabetic nephropathy. *J. Pathol.* **236**, 30–40 (2015).
417. Zhou, J. *et al.* Inhibition of PTEN Activity Aggravates Post Renal Fibrosis in Mice with Ischemia Reperfusion-Induced Acute Kidney Injury. *Cell. Physiol. Biochem.* **43**, 1841–1854 (2018).
418. Lin, J. S. *et al.* Loss of PTEN promotes podocyte cytoskeletal rearrangement, aggravating diabetic nephropathy. *J. Pathol.* **236**, 30–40 (2015).
419. Nolin, A. C. *et al.* Proteinuria causes dysfunctional autophagy in the proximal tubule. *Am. J. Physiol. - Ren. Physiol.* **311**, F1271–F1279 (2016).
420. Gailly, P. *et al.* A novel renal carbonic anhydrase type III plays a role in proximal tubule dysfunction. *Kidney Int.* **74**, 52–61 (2008).
421. Pook, M. A. *et al.* Dent's disease, a renal Fanconi syndrome with nephrocalcinosis and kidney stones, is associated with a microdeletion involving DXS255 and maps to Xp11. 22. *Hum. Mol. Genet.* **2**, 2129–2134 (1993).

422. Docherty, M. H., O'Sullivan, E. D., Bonventre, J. V. & Ferenbach, D. A. Cellular senescence in the kidney. *J. Am. Soc. Nephrol.* **30**, 726–736 (2019).
423. Gareri, C., De Rosa, S. & Indolfi, C. MicroRNAs for restenosis and thrombosis after vascular injury. *Circ. Res.* **118**, 1170–1184 (2016).
424. Rangrez, A. Y., Massy, Z. A., Metzinger-Le Meuth, V. & Metzinger, L. miR-143 and miR-145: molecular keys to switch the phenotype of vascular smooth muscle cells. *Circ. Cardiovasc. Genet.* **4**, 197–205 (2011).
425. Vacante, F., Denby, L., Sluimer, J. C. & Baker, A. H. The function of miR-143, miR-145 and the MiR-143 host gene in cardiovascular development and disease. *Vascul. Pharmacol.* **112**, 24–30 (2019).
426. Min, X., Zhang, X., Sun, N., Acharya, S. & Kim, K.-M. Mdm2-mediated ubiquitination of PKC β II in the nucleus mediates clathrin-mediated endocytic activity. *Biochem. Pharmacol.* **170**, 113675 (2019).
427. Roepstorff, K., Grøvdal, L., Grandal, M., Lerdrup, M. & van Deurs, B. Endocytic downregulation of ErbB receptors: mechanisms and relevance in cancer. *Histochem. Cell Biol.* **129**, 563–578 (2008).
428. Veikkolainen, V. *et al.* ErbB4 modulates tubular cell polarity and lumen diameter during kidney development. *J. Am. Soc. Nephrol.* **23**, 112–122 (2012).
429. Chivukula, R. R. *et al.* An essential mesenchymal function for miR-143/145 in intestinal epithelial regeneration. *Cell* **157**, 1104–1116 (2014).
430. Zhai, W. *et al.* LncRNA-SARCC suppresses renal cell carcinoma (RCC) progression via altering the androgen receptor (AR)/miRNA-143-3p signals. *Cell Death Differ.* **24**, 1502–1517 (2017).
431. Chen, H. Y. *et al.* The protective role of Smad7 in diabetic kidney disease: mechanism and therapeutic potential. *Diabetes* **60**, 590–601 (2011).
432. Brigant, B. *et al.* Serum microRNAs are altered in various stages of chronic kidney disease: A preliminary study. *Clin. Kidney J.* **10**, 30–37 (2017).
433. Matz, M. *et al.* MicroRNA regulation in blood cells of renal transplanted patients with interstitial fibrosis/ tubular atrophy and antibody-mediated rejection. *PLoS One* **13**, 1–15 (2018).
434. Faruq, O. & Vecchione, A. microRNA: diagnostic perspective. *Front. Med.* **2**, 51 (2015).
435. LaFavers, K. A. & El-Achkar, T. M. Autosomal dominant tubulointerstitial kidney disease: a new tool to guide genetic testing. *Kidney Int.* **98**, 549–552 (2020).

436. Zhou, Z., Dong, Y., Zhou, H., Liu, J. & Zhao, W. MiR-143-3p directly targets GLUT9 to reduce uric acid reabsorption and inflammatory response of renal tubular epithelial cells. *Biochem. Biophys. Res. Commun.* **517**, 413–420 (2019).
437. Xia, C., Yang, Y., Kong, F., Kong, Q. & Shan, C. MiR-143-3p inhibits the proliferation, cell migration and invasion of human breast cancer cells by modulating the expression of MAPK7. *Biochimie* **147**, 98–104 (2018).
438. Ge, X. *et al.* Circular RNA Circ_0000064 promotes the proliferation and fibrosis of mesangial cells via miR-143 in diabetic nephropathy. *Gene* **758**, 144952 (2020).
439. Kim, J. H. *et al.* Gene expression profiling of anti-GBM glomerulonephritis model: the role of NF- κ B in immune complex kidney disease. *Kidney Int.* **66**, 1826–1837 (2004).
440. Jingushi, K. *et al.* MiR-629 targets TRIM33 to promote TGF β /smad signaling and metastatic phenotypes in ccRCC. *Mol. Cancer Res.* **13**, 565–574 (2015).
441. Sui, W. *et al.* Microarray analysis of MicroRNA expression in acute rejection after renal transplantation. *Transpl. Immunol.* **19**, 81–85 (2008).
442. Nicoli, E.-R. *et al.* Lysosomal Storage and Albinism Due to Effects of a De Novo CLCN7 Variant on Lysosomal Acidification. *Am. J. Hum. Genet.* 1–12 (2019). doi:10.1016/j.ajhg.2019.04.008
443. Birkenhäger, R. *et al.* Mutation of BSND causes Bartter syndrome with sensorineural deafness and kidney failure. *Nat. Genet.* **29**, 310–314 (2001).
444. Wang, G. *et al.* Urinary miR-21, miR-29, and miR-93: Novel biomarkers of fibrosis. *Am. J. Nephrol.* **36**, 412–418 (2012).
445. Liu, X. *et al.* Tubule-derived exosomes play a central role in fibroblast activation and kidney fibrosis. *Kidney Int.* **97**, 1181–1195 (2020).
446. Chen, H. Y. *et al.* MicroRNA-29b inhibits diabetic nephropathy in db/db mice. *Mol. Ther.* **22**, 842–853 (2014).
447. Kim, S. Y., Lee, Y. H. & Bae, Y. S. MiR-186, miR-216b, miR-337-3p, and miR-760 cooperatively induce cellular senescence by targeting α subunit of protein kinase CKII in human colorectal cancer cells. *Biochem. Biophys. Res. Commun.* **429**, 173–179 (2012).
448. Kang, J. Y., Kim, J. J., Jang, S. Y. & Bae, Y. S. The p53-p21Cip1/WAF1 pathway is necessary for cellular senescence induced by the inhibition of protein kinase CKII in human colon cancer cells. *Mol. Cells* **28**, 489–494 (2009).

449. Manoli, I. *et al.* Targeting proximal tubule mitochondrial dysfunction attenuates the renal disease of methylmalonic acidemia. *Proc. Natl. Acad. Sci. U. S. A.* **110**, 13552–13557 (2013).
450. Pescucci, C. *et al.* Autosomal-dominant Alport syndrome: natural history of a disease due to COL4A3 or COL4A4 gene. *Kidney Int.* **65**, 1598–1603 (2004).
451. Voskarides, K. *et al.* COL4A3/COL4A4 mutations producing focal segmental glomerulosclerosis and renal failure in thin basement membrane nephropathy. *J. Am. Soc. Nephrol.* **18**, 3004–3016 (2007).
452. Li, K., Chen, Z., Qin, Y. & Wei, Y. MiR-664a-3p expression in patients with obstructive sleep apnea. *Medicine (Baltimore).* **97**, e9813 (2018).
453. Zhang, Y. X., Qin, L. L. & Yang, S. Y. Down-regulation of miR-664 in cervical cancer is associated with lower overall survival. *Eur. Rev. Med. Pharmacol. Sci.* **20**, 1740–1744 (2016).
454. Wang, L. *et al.* miR-664a-3p functions as an oncogene by targeting Hippo pathway in the development of gastric cancer. *Cell Prolif.* **52**, 1–14 (2019).
455. Zhong, S. *et al.* Overexpression of hsa-miR-664a-3p is associated with cigarette smoke-induced chronic obstructive pulmonary disease via targeting FHL1. *Int. J. COPD* **14**, 2319–2329 (2019).
456. Otalora, L. *et al.* Identification of glomerular and podocyte-specific genes and pathways activated by sera of patients with focal segmental glomerulosclerosis. *PLoS One* **14**, 1–19 (2019).
457. Lenoir, O. *et al.* Direct action of endothelin-1 on podocytes promotes diabetic glomerulosclerosis. *J. Am. Soc. Nephrol.* **25**, 1050–1062 (2014).
458. Takano, T. *et al.* Recessive mutation in CD2AP causes focal segmental glomerulosclerosis in humans and mice. *Kidney Int.* **95**, 57–61 (2019).
459. Löwik, M. M. *et al.* Focal segmental glomerulosclerosis in a patient homozygous for a CD2AP mutation. *Kidney Int.* **72**, 1198–1203 (2007).
460. Clar, J. *et al.* Targeted deletion of kidney glucose-6 phosphatase leads to nephropathy. *Kidney Int.* **86**, 747–756 (2014).
461. Meng, X.-M., Tang, P. M.-K., Li, J. & Lan, H. Y. TGF- β /Smad signaling in renal fibrosis. *Front. Physiol.* **6**, 82 (2015).
462. Wang, B. *et al.* MiR-200a prevents renal fibrogenesis through repression of TGF- β 2 expression. *Diabetes* **60**, 280–287 (2011).
463. Yamazaki, H. *et al.* Atypical phenotype of type I Bartter syndrome accompanied by focal segmental glomerulosclerosis. *Pediatr.*

- Nephrol.* **24**, 415–418 (2009).
464. Li, H. *et al.* Identification of cardiac-related circulating microRNA profile in human chronic heart failure. *Oncotarget* **7**, 33 (2016).
 465. Borzi, C. *et al.* mir-660-p53-mir-486 network: A new key regulatory pathway in lung tumorigenesis. *Int. J. Mol. Sci.* **18**, (2017).
 466. Mulrane, L. *et al.* miR-187 is an independent prognostic factor in breast cancer and confers increased invasive potential in vitro. *Clin. cancer Res.* **18**, 6702–6713 (2012).
 467. Azad, F. M. *et al.* Two lung development-related microRNAs, miR-134 and miR-187, are differentially expressed in lung tumors. *Gene* **577**, 221–226 (2016).
 468. Godwin, J. G. *et al.* Identification of a microRNA signature of renal ischemia reperfusion injury. *Proc. Natl. Acad. Sci.* **107**, 14339–14344 (2010).
 469. Yue, J. *et al.* MicroRNA-187 reduces acute ischemic renal podocyte injury via targeting acetylcholinesterase. *J. Surg. Res.* **244**, 302–311 (2019).
 470. Rossato, M. *et al.* IL-10-induced microRNA-187 negatively regulates TNF- α , IL-6, and IL-12p40 production in TLR4-stimulated monocytes. *Proc. Natl. Acad. Sci. U. S. A.* **109**, (2012).
 471. Wang, Z. *et al.* Prognostic value of miR-17-5 p in gastrointestinal cancers: A systematic review and meta-analysis. *Onco. Targets. Ther.* **11**, 5991–5999 (2018).
 472. Dellago, H., Bobbili, M. R. & Grillari, J. MicroRNA-17-5p: At the Crossroads of Cancer and Aging - A Mini-Review. *Gerontology* **63**, 20–28 (2016).
 473. Lan, C. *et al.* Integrative Analysis of miRNA and mRNA Expression Profiles in Calcium Oxalate Nephrolithiasis Rat Model. *Biomed Res. Int.* **2017**, (2017).
 474. Schwegler, J. S., Heppelmann, B., Mildenerger, S. & Silbernagl, S. Receptor-mediated endocytosis of albumin in cultured opossum kidney cells: a model for proximal tubular protein reabsorption. *Pflügers Arch.* **418**, 383–392 (1991).
 475. Biology, C. & Biochemistry, M. Cubilin- and megalin-mediated uptake of albumin in cultured.pdf. **58**, 1523–1533 (2000).
 476. Guillén, N., Caldas, Y. A., Levi, M. & Sorribas, V. Identification and expression analysis of type II and type III Pi transporters in the opossum kidney cell line. *Exp. Physiol.* **104**, 149–161 (2019).
 477. Stepanenko, A. A. & Dmitrenko, V. V. HEK293 in cell biology and cancer research: Phenotype, karyotype, tumorigenicity, and stress-induced genome-phenotype evolution. *Gene* **569**, 182–190

- (2015).
478. Aschauer, L., Carta, G., Vogelsang, N., Schlatter, E. & Jennings, P. Expression of xenobiotic transporters in the human renal proximal tubule cell line RPTEC/TERT1. *Toxicol. Vitro*. **30**, 95–105 (2015).
 479. Simon, B. R., Wilson, M. J. & Wickliffe, J. K. The RPTEC/TERT1 cell line models key renal cell responses to the environmental toxicants, benzo[a]pyrene and cadmium. *Toxicol. Reports* **1**, 231–242 (2014).
 480. Tanuma, A. *et al.* Functional characterization of a novel missense CLCN5 mutation causing alterations in proximal tubular endocytic machinery in Dent's disease. *Nephron - Physiol*. **107**, (2008).
 481. Wu, F. *et al.* Mutational analysis of CLC-5, cofilin and CLC-4 in patients with dent's disease. *Nephron - Physiol*. (2009). doi:10.1159/000225944
 482. Kao, S.-H. *et al.* Analysis of Protein Stability by the Cycloheximide Chase Assay. *Bio-protocol* **5**, e1374 (2015).
 483. Hryciw, D. H. *et al.* Nedd4-2 functionally interacts with CLC-5: Involvement in constitutive albumin endocytosis in proximal tubule cells. *J. Biol. Chem.* (2004). doi:10.1074/jbc.M411491200
 484. Christensen, E. I. & Maunsbach, A. B. Effects of dextran on lysosomal ultrastructure and protein digestion in renal proximal tubule. *Kidney Int.* **16**, 301–311 (1979).
 485. Christensen, E. I. & Maunsbach, A. B. Dextran is resistant to lysosomal digestion in kidney tubules. *Virchows Arch. B Cell Pathol. Incl. Mol. Pathol.* **37**, 49–59 (1981).
 486. Hara-Chikuma, M., Wang, Y., Guggino, S. E., Guggino, W. B. & Verkman, A. S. Impaired acidification in early endosomes of CLC-5 deficient proximal tubule. *Biochem. Biophys. Res. Commun.* **329**, 941–946 (2005).
 487. Novarino, G., Weinert, S., Rickheit, G. & Jentsch, T. J. Endosomal chloride-proton exchange rather than chloride conductance is crucial for renal endocytosis. *Science* **328**, 1398–1401 (2010).
 488. Bignon, Y. *et al.* A novel CLCN5 pathogenic mutation supports Dent disease with normal endosomal acidification. *Hum. Mutat.* (2018). doi:10.1002/humu.23556
 489. Jentsch, T. J. Chloride and the endosomal-lysosomal pathway: Emerging roles of CLC chloride transporters. *J. Physiol.* **578**, 633–640 (2007).
 490. Mahon, M. J. pHluorin2: an enhanced, ratiometric, pH-sensitive green fluorescent protein. *Adv. Biosci. Biotechnol.* **02**, 132–137 (2011).
 491. Gabriel, S. S. *et al.* Bone marrow transplantation improves

- proximal tubule dysfunction in a mouse model of Dent disease. *Kidney Int.* **91**, 842–855 (2017).
492. Wieser, M. *et al.* hTERT alone immortalizes epithelial cells of renal proximal tubules without changing their functional characteristics. *Am. J. Physiol. - Ren. Physiol.* **295**, 1365–1375 (2008).
493. Thul, P. J. & Lindskog, C. The human protein atlas: A spatial map of the human proteome. *Protein Sci.* **27**, 233–244 (2018).
494. Lloyd, S. E. *et al.* Characterisation of renal chloride channel, CLCN5, mutations in hypercalciuric nephrolithiasis (kidney stones) disorders. *Hum. Mol. Genet.* **6**, 1233–1239 (1997).
495. Akuta, N. *et al.* Mutations of CLCN5 in Japanese children with idiopathic low molecular weight proteinuria, hypercalciuria and nephrocalcinosis. *Kidney Int.* **52**, 911–916 (1997).
496. Hoopes, R. R. *et al.* Evidence for genetic heterogeneity in Dent's disease. in *Kidney International* (2004). doi:10.1111/j.1523-1755.2004.00571.x
497. Gene, G. *et al.* Identification of Two Novel Mutations in the CFTR. **226**, 138–143 (1994).
498. Li, F. *et al.* Dent Disease in Chinese Children and Findings from Heterozygous Mothers: Phenotypic Heterogeneity, Fetal Growth, and 10 Novel Mutations. *J. Pediatr.* **174**, 204-210.e1 (2016).
499. Matsumoto, A. *et al.* Severe osteomalacia with dent disease caused by a novel intronic mutation of the CLCN5 gene. *Intern. Med.* **57**, 3603–3610 (2018).
500. Bitsori, M., Vergadi, E. & Galanakis, E. A Novel CLCN5 Splice Site Mutation in a Boy with Incomplete Phenotype of Dent Disease. *J. Pediatr. Genet.* **5**, 1–5 (2019).
501. Wong, W. *et al.* Phenotypic variability of Dent disease in a large New Zealand kindred. *Pediatr. Nephrol.* **32**, 365–369 (2017).

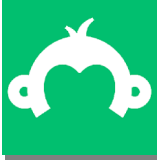
ANNEXES

1. Annex I

Table 23. Ligands for megalin and cubilin

| Ligands for Megalin | Ligans for Cubilin |
|--|------------------------------|
| Vitamin carrier proteins | |
| Transcobalamin-vitamin B12 | Intrinsic-factor vitamin B12 |
| Vitamin D-binding protein | Vitamin D binding protein |
| Retinol-binding protein | |
| Folate-binding protein | |
| Other carrier proteins | |
| Albumin | Albumin |
| Myoglobin | Myoglobin |
| Hemoglobin | Hemoglobin |
| Lactoferrin | Transferrin |
| Selenoprotein P | |
| Metallothionein | |
| Neutrophil-gelatinase-associated lipocalin | |
| Odorant binding protein | |
| Transthyretin | |
| Liver type fatty acid binding protein | |
| Sex hormone binding globulin | |
| Lipoproteins | |
| Apolipoprotein B | Apolipoprotein AI |
| Apolipoprotein E | High density lipoprotein |
| Apolipoprotein J/clusterin | |
| Apolipoprotein H | |
| Apolipoprotein M | |
| Hormones and signaling proteins | |
| Parathyroid hormone | |
| Insulin | |
| Epidermal growth factor | |
| Prolactin | |
| Thyroglobulin | |
| Sonic hedgehog protein | |
| Angiotensin II | |
| Leptin | |
| Bone morphogenic protein 4 | |
| Connective tissue growth factor | |
| Insulin like growth factor | |
| Enzymes and enzyme inhibitors | |
| Plasminogen activator inhibitor-type I | |
| Plasminogen activator inhibitor-type I-urokinase | |

| | |
|---|-----------------------------------|
| Plasminogen activator inhibitor-type I-tissue plasminogen activator | |
| Pro-urokinase | |
| Lipoprotein lipase | |
| Plasminogen | |
| α - amylase | |
| Lysozyme | |
| Cathepsin b | |
| α -galactosidase A | |
| Cystatin C | |
| Immune- and stress-related proteins | |
| Immunoglobulin light chains | Immunoglobulin light chains |
| Pancreatis associated protein 1 | Clara cell secretory protein |
| α 1-microglobulin | α 1-microglobulin |
| Drugs and toxins | |
| Aminoglycosides | Aminoglycosides |
| Polymyxin B | |
| Aprotinin | |
| Trichosantin | |
| Receptors | |
| Transcobalamin II-B12 receptor | |
| Others | |
| Ca ²⁺ | |
| Cytochrome C | |
| Seminal vesicle secretory protein II | |
| Recombinant activated factor VIIa | Recombinant activated factor VIIa |
| Coagulation factor VIII | |



2. Annex II

Dent's Disease Type 1 in Europe

Welcome to this Survey on Dent's Disease type 1 in Europe. The survey will take approximately 12 minutes.

We are launching this survey aimed at gathering information about Dent's Disease type 1 in Europe. By these few questions we mean to investigate the prevalence, the clinical phenotype and evolution as well as genetics variability and practice patterns of centers involved in the management and study of Dent patients around Europe.

In case you are interested, please complete the survey by selecting "Agree".

Results of the survey will be published and those participating with complete data will be considered as contributors.

Thank you for your consideration and best regards

Agree

Please do not forward this email as its survey link is unique to you.
[Privacy](#) | [Unsubscribe](#)

Powered by  SurveyMonkey



Dent's Disease Type 1 in Europe

Treating physician

What is your **country of practice**?

Please enter your **center** (name, city)

Please enter your **email address**

Do you follow **Dent type 1 patients**?

- Yes
- No

If yes, **how many**?

Is it the first time you fill in this survey?

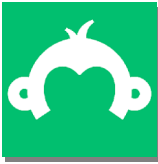
If you have already completed the survey for other patients,
please tell us how many times.

Patient's basic information

Patient's **gender**

- Male
- Female

Please write down the month and year the patient **was born**



Was the patient a **premature baby**?

- Yes
- No

How much did the patient **weight** (g) at birth? (if available)

How **long** was the patient (cm) at birth? (if available)

Diagnosis

Is there any **family history** of Dent's Disease or kidney disease?

Please list the affected members of the family below and the medical signs they presented with.

When was the patient **clinically diagnosed**?

Date

Did genetic test find a **mutated gene**? (If mutated gene is other than CLCN5, please go to the end page and finish the survey)

- CLCN5
- OCRL
- Unknown
- Genetic test could not be performed
- Other (please specify)



Which are the details of the **mutation found**? (exon, nucleotide change. for example V523del, Y272C...)

Which was the main **symptom/sign** which determined the **diagnosis**?

Patient's current situation

Which is the **patient's current age**?

Which is the patient **current weight** (kg)?

Which is the patient's **current height** (cm)?

Does the patient have **aminoaciduria** currently?

- Yes
- No
- Unknown

Does the patient have **glycosuria** currently?

- Yes
- No
- Unknown

Does the patient have **nephrocalcinosis**?

- Yes
- No
- Unknown

Has the patient had any **renal lithiasis/renal colic episode**?

- Yes



- No
- Unknown

At what **age** (if known) was the **first renal lithiasis/renal colic** episode?

Has the patient developed **rickets**?

- Yes
- No
- Unknown

Has the patient suffered any **fracture**?

- Yes
- No
- Unknown
- If yes, location and type of fracture

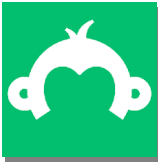
At what **age** did the patient suffer the **first fracture**?

Does the patient have **hypertension**?

- Yes
- No
- Unknown

At what **age** was the patient diagnosed with **hypertension**?

Has the patient needed **renal replacement therapy**?
(Current situation)



- No
- Dialysis
- Kidney trasnplant

At what **age** did the patient **start renal replacement therapy**?

Patient's current blood/urine tests

If you don't have these data available, please leave the field blank

Date

Current serum creatinine (mg/dl)

(umol/L = mg/dl*88.4)

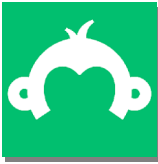
Current serum potassium (mmol/L)

Current serum calcium (mg/dl)

Current serum phosphate (mg/dl)

Current urine Ca/Cr (mg/mg)

Current urine protein/creatinine ratio (mg/g)



Current urine albumin/creatinine ratio (mg/g)

Which low molecular weight protein do you

- A1-microalbuminuria
- 2-microalbuminuria
- Retinol- binding protein

Current low molecular weight Protein (mg/mol creat)

Management

Does the patient currently receive any **treatment**?

- Potassium-sparing diuretics
- Angiotensin-converting enzyme or angiotensin receptor blockers
- Thiazides
- Potassium citrate
- Growth hormone
- None
- Does the patient get any other treatment?



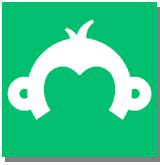
End of the Survey

Thank you very much to fill up the survey!!

If you have any doubt, please do not hesitate to contact us to carla.burballa@vhir.org.

If you have more than one followed-up patient it would be great if you could please fill-up the survey for each of them. If you do not, you can leave the page.

Thank you very much!



3. Annex III



ESTUDIO GENÉTICO-MOLECULAR DE LA ENFERMEDAD DE DENT. SOLICITUD DE COLABORACIÓN.

Apreciado compañero,

El grupo de Fisiopatología Renal del Instituto de Investigación de nuestro hospital (Vall d'Hebrón Institut de Recerca –VHIR-) estamos muy interesados en la Enfermedad de Dent. La enfermedad de Dent es de causa genética ligada al cromosoma X (principalmente por mutaciones en el gen *CLCN5*), aparece en varones, y cursa con proteinuria de bajo peso molecular, hipercalciuria, y evolución a fallo renal, sin que exista un tratamiento específico. En la actualidad estamos trabajando en un proyecto titulado *"Descubrimiento de biomarcadores, dianas y soluciones terapéuticas para la enfermedad de Dent. Implicaciones para el tratamiento del Síndrome de Fanconi Renal"* liderado por la Dra. Gema Ariceta y la Dra. Anna Meseguer, y que está englobado dentro del proyecto Renaltube (www.renaltube.com), dirigido al estudio de las tubulopatías primarias.

Se trata de un proyecto de investigación financiado íntegramente

por ASDENT (www.asdent.es) la asociación de pacientes con enfermedad de Dent, que fomenta la difusión de la enfermedad y apoya activamente la investigación en su enfermedad.

Este proyecto tiene como objetivo la identificación de nuevos genes y redes moleculares secundarias a los efectos de las mutaciones en el gen *CLCN5*, proporcionando nuevos biomarcadores de diagnóstico y pronóstico, así como dianas terapéuticas de utilidad. Para ello analizaremos distintos factores genéticos y marcadores en muestras de sangre, en suero y orina, de modo transversal. Así mismo nos gustaría estudiar algunos pacientes controles sanos (**exclusivamente varones**), sin la enfermedad, pero con una dotación genética similar, por lo que estamos interesados en estudiar a los hermanos (**varones**) no afectados de los pacientes, en el caso que fuera posible. Además, se realizará un estudio genético en los controles para descartar que puedan ser afectados.

Dado que se trata de una enfermedad rara o minoritaria, se precisa del mayor número posible de pacientes, y también de controles, para obtener unos resultados robustos. Por ello, solicitamos su colaboración en reclutar pacientes y para la obtención de muestras, que esperamos puedas combinar con las extracciones que necesitan estos pacientes en su control clínico.

Intentaremos facilitar en medida de lo posible este proceso encargándonos de la logística de la recogida de muestras en tu propio centro y de su transporte, que será libre de coste.

Asimismo y para facilitar el envío hemos comprobado la eficacia de estudiar las muestras procesadas a temperatura ambiente, si bien es deseable que se envíen lo antes posible.

Una diferencia importante en el caso de los pacientes trasplantados es que no vamos a recoger orina, sino únicamente muestras de sangre y suero. En el resto de los pacientes y también en los controles sanos, si procesaremos

orina (puede corresponder a orina que se recoja el mismo día en la consulta o en el domicilio el día previo), aunque el volumen necesario es elevado (la razón es que la cantidad de exosomas que se pueden obtener en orinas tan diluidas como las que presentan estos pacientes es muy baja).

¿QUIÉN PUEDE FORMAR PARTE DEL ESTUDIO Y QUÉ MATERIAL BIOLÓGICO ES NECESARIO?

La **inclusión** del paciente al ESTUDIO GENÉTICO-MOLECULAR DE LA ENFERMEDAD DE DENT requiere del diagnóstico genético confirmado de LA ENFERMEDAD DE DENT y los **siguientes documentos**:

- 1) Documento de **Consentimiento Informado** del paciente o de sus tutores, y del documento de **Asentimiento** para los pacientes entre los 12-18 años.
- 2) Copia del documento con el **diagnóstico genético** del paciente.
- 3) Una ficha sencilla de **información clínica del paciente**, que se detalla en el Anexo 2.
- 4) En lo posible, una copia impresa de los datos del paciente en la plataforma RenalTube (si tiene más de un control, una copia de cada uno de ellos).
- 5) Una copia del **último control analítico** con el tratamiento actual del paciente. Si además nos pudieras facilitar un breve informe sobre el estado clínico del paciente, te estaríamos muy agradecidos, aunque no es indispensable.

En caso de que fuera UN CONTROL SANO, únicamente solicitamos que nos envíes los documentos de consentimiento informado/ asentimiento, así como una copia de su analítica.

Es preferible que nos informes con 7 días de antelación antes de la obtención de las muestras para poder gestionar el envío de las

muestras por mensajería y enviarte nuevamente una copia de los documentos de *Consentimiento Informado y Asentimiento*, y la *Ficha de Información clínica* por correo electrónico. No obstante si no hubieras podido contactar antes, llámanos por favor cuando tengas las muestras y agilizaremos la recogida de las mismas

El protocolo de recogida de las muestras será el siguiente:

1. Avisar preferiblemente 7 días antes de la extracción de muestras a las personas de contacto en el VHIR. La persona a contactar es Mónica Durán Tel. 93 489 40 70, e-mail: monica.duran@vhir.org. No obstante, ante cualquier duda, contactar siempre con alguna de las otras dos investigadoras.
2. Facilitar nombre, teléfono y localización de la persona que entregará las muestras al mensajero.
3. Extracción y procesamiento de las muestras de sangre y recogida de la orina según el protocolo indicado en el Anexo 1.
4. Guardar las muestras a 4°C (EN NEVERA NO CONGELADOR) hasta la llegada del mensajero.
5. Recogida de los datos clínicos y cumplimentación de la Ficha de información clínica (Anexo 2). Impresión de los datos del paciente desde la plataforma RenalTube.
6. El mismo día de la obtención de las muestras, el centro proveedor recibirá un mensajero con el contenedor adecuado para el transporte de las mismas a 4°C.
7. A la llegada del mensajero, introducir las muestras de sangre, suero y orina en el contenedor para que el envío de vuelta al VHIR se realice de forma inmediata.

- Qué deberá incluir el paquete de envío:

- ✓ **Consentimiento informado debidamente rellenado y firmado.**
- ✓ **1 tubo de sangre con EDTA** (especificaciones detalladas en el anexo 1).
- ✓ **1 tubo de suero** (especificaciones detalladas en el anexo 1).
- ✓ **5 botes de 100mL de orina (mínimo 3)** (especificaciones detalladas en el anexo 3.1).
- ✓ **Ficha de información clínica completa** (Anexo 3.2).

- ✓ Impresión de la **ficha** del paciente de la plataforma **RenalTube** (diagnóstico y seguimiento) (no en los controles).
- ✓ **Último control analítico y el tratamiento actual del paciente.**

Las muestras se recibirán en el laboratorio de Fisiopatología Renal del Vall d'Hebrón Institut de Recerca, cuya dirección ya figurará en la caja que les haremos llegar

Contacto a:

Mónica Durán Fernández

Carla Burballa Tàrrega

Vall d'Hebrón Institut de Recerca Edifici Mediterrània
Planta 1, Laboratorio 116 – 117 Paseo Vall d'Hebrón, 119-129
08035 BARCELONA

Estamos a su disposición para cualquier consulta o aclaración.

Muchas gracias por su colaboración.

Un cordial saludo,

Dra. Gema Ariceta

Jefa de Servicio de Nefrología Pediátrica Hospital Vall d'Hebrón

Passeig Vall d'Hebrón, 119-129 08035 Barcelona

Tel. 93 489 30 82

E-mail: gariceta@vHebrón.net

Dra. Anna Meseguer

Jefa de grupo de Fisiopatología Renal CIBBIM Nanomedicina

Vall d'Hebrón Institut de Recerca Passeig Vall d'Hebrón, 119-129

08035 Barcelona

Tel. 93 489 40 61

E-mail: ana.meseguer@vhir.org

4. Annex IV

Consentimiento para el estudio con muestras biológicas codificadas de controles sanos menores de 18 años

Título del estudio: Descubrimiento de biomarcadores, nuevas dianas y soluciones terapéuticas para la enfermedad de Dent. Implicaciones para el tratamiento del Síndrome de Fanconi Renal.

Yo (*nombre y apellidos del padre, madre o tutor legal*),
 _____ como
 padre, madre o

tutor de (*nombre y apellidos del participante*) _____

con *fecha de nacimiento*

He leído la hoja de información que se me ha entregado.
 He podido hacer preguntas sobre el estudio.
 He hablado con: (nombre del investigador).

Comprendo que la participación es voluntaria.

Comprendo que puedo retirarme del estudio:

1. Cuando quiera
2. Sin tener que dar explicaciones
3. Sin que esto repercuta en mis cuidados médicos

Punto 1: DOY NO DOY mi consentimiento voluntariamente para que pueda realizarse el estudio sobre posibles factores genéticos relacionados con la enfermedad de Dent familiar en mi muestra de orina.

Punto 2: DOY NO DOY mi consentimiento voluntariamente para que mi muestra de ADN se almacene para utilizarla en otros estudios sobre factores genéticos relacionados con la enfermedad de Dent. Mi muestra de orina se identificarán con un número codificado, y mi identidad se mantendrá en secreto.


Punto 3: INDIVIDUO AFECTADO INDIVIDUO NO AFECTADO . Indicar con una X si pertenezco al grupo de individuos afectados (manifiesto Dent de tipo 1) o si pertenezco al grupo de individuos no afectados (control).

Firma y DNI
del padre, madre o tutor

Firma y DNI
del investigador

En _____, a _____ de _____ de 2019

5. Annex V

| | |
|--|---|
|  <p>Vall d'Hebron Hospital</p> | <p>Hoja de Información para Pacientes</p> <p>“Descubrimiento de biomarcadores, nuevas dianas y soluciones terapéuticas para la enfermedad de Dent. Implicaciones para el tratamiento del Síndrome de Fanconi Renal.”</p> |
| | <p>Área de aplicación: Servicio de Nefrología Pediátrica del Hospital Vall d'Hebrón</p> |

Objetivos y posibles beneficios:

Le solicitamos su participación en este proyecto de investigación cuyo objetivo principal es identificar nuevos genes y redes moleculares secundarias a los efectos de las mutaciones del gen *CLCN5* que revelarán mecanismos que subyacen a la disfunción tubular, la fibrosis y la enfermedad renal terminal, proporcionando nuevos biomarcadores diagnóstico y pronóstico, así como dianas terapéuticas de utilidad, no solo para los enfermos de Dent sino también para pacientes que sufren, por distintas causas genéticas o adquiridas, el síndrome de Fanconi.

Se trata de un estudio transversal. Los criterios de inclusión en el estudios son: diagnóstico de la Enfermedad de Dent tipo 1 con diagnóstico genético confirmativo y la existencia de un consentimiento informado firmado. También se incluirán pacientes control sin dicha enfermedad, preferentemente hermanos/as del paciente.

Es posible que de su participación en este estudio no se obtenga un beneficio directo. Sin embargo, la identificación de posibles factores relacionados con la Enfermedad de Dent podría beneficiar en un futuro a otros pacientes que la sufren y contribuir a un mejor conocimiento y tratamiento de esta enfermedad.

Descripción de los procedimientos del estudio:

Si decide participar, se le realizará una historia clínica y una exploración física detallada, se le extraerá un tubo adicional de sangre (volumen en función del peso del paciente, sin exceder los 3mL de sangre por kg de peso del paciente: Menos de 10Kg: 4mL de sangre; entre 10 y 20Kg: 6mL de sangre; más de 20Kg: 8mL de sangre. El volumen total de sangre extraída se repartirá de la siguiente forma: un mínimo de 2mL, y un máximo de 3mL, de sangre en tubo con EDTA y un mínimo de 2mL de sangre en un tubo sin anticoagulante, siendo este último en el que se recogerá un mayor volumen siempre que sea posible). En caso que se requiera más cantidad de sangre, se recogerá en diferentes tiempos, coincidiendo siempre con otra analítica de control periódica y sin sobrepasar en cada una de ellas los límites de volumen mencionados. También se le recogerá una muestra de orina (300mL).

Usted será informado de los objetivos del estudio así como de las molestias que puede suponer para usted el hecho de participar. Y se le responderán las dudas que usted pueda tener en relación al estudio.

Si decide participar, se recogerán los datos referentes a su historia clínica necesarios para el objetivo del proyecto de investigación.

No recibirá ninguna compensación económica ni de cualquier otro tipo por participar en el estudio. Los datos que proporcione su participación no tendrán ningún uso comercial.

Las muestras biológicas sobrantes, que no sean utilizadas para este estudio, pasarán a formar parte de una colección. Dicha se almacenará en el Institut de Recerca Vall d'Hebrón (ver apartado Uso futuro de las muestras).

Los datos que se obtengan para este estudio serán codificados y los datos personales que se recojan serán siempre confidenciales. La información será almacenada en soporte informático. Los datos recogidos se tratarán de forma codificada garantizando su anonimato.

Su participación en el estudio es totalmente voluntaria, y si decide no participar recibirá todos los cuidados médicos que necesite y la relación con el equipo médico que le atiende no se verá afectada.

Molestias y posibles riesgos:

La toma de la muestra de sangre puede provocar una sensación de ardor en el punto donde se introduce la aguja en la piel y ocasionar un pequeño hematoma o una leve infección que desaparecerá a los pocos días. Más raramente puede aparecer mareo en el momento de la extracción de sangre.

Lugar de realización del análisis:

La investigación biomédica con sus muestras biológicas se realizará en las instalaciones del laboratorio de *Fisiopatología renal - CIBBIM*, del Vall d'Hebrón Institut de Recerca.

Protección de datos personales:

De acuerdo con la Ley 15/1999 de Protección de Datos de Carácter Personal, los datos personales que se obtengan serán los necesarios para cubrir los fines del estudio. En ninguno de los informes del estudio aparecerá su nombre, y su identidad no será revelada a persona alguna salvo para cumplir con los fines del estudio, y en el caso de urgencia médica o requerimiento legal. Cualquier información de carácter personal que pueda ser identificable será conservada por métodos informáticos en condiciones de seguridad por la Dra. M^a Gema Ariceta Iraola y la Dra. Anna Meseguer Navarro. El acceso a dicha información quedará restringido al personal del servicio de pediatría, designado

al efecto o a otro personal autorizado que estará obligado a mantener la confidencialidad de la información.

De acuerdo con la ley vigente, tiene usted derecho al acceso de sus datos personales; asimismo, y si está justificado, tiene derecho a su rectificación y cancelación. Si así lo desea, deberá solicitarlo al médico que le atiende en este estudio.

Implicaciones de la información obtenida con el estudio:

Si decide participar en el estudio, es posible que del análisis de sus muestras biológicas se obtenga información relevante para su salud o la de su familia. De acuerdo con la legislación vigente, tiene derecho a ser informado de los datos que se obtengan en el curso del estudio. En el caso de que usted lo solicite, se le podrá facilitar información acerca de los estudios de investigación en los que hayan utilizado las muestras. En caso de ser menor de edad y que su tutor o representante legal haya firmado este consentimiento informado, se le garantizará el acceso a dicha información cuando cumpla la mayoría de edad.

Si quiere conocer los resultados de investigación relevantes para su salud que se obtengan, infórmese a través de su médico sobre las implicaciones que esta información puede tener para su persona y su familia. Esta información se le comunicará si lo desea; en el caso de que prefiera no ser informado, su decisión se respetará. No obstante, cuando esta información, según criterio del médico responsable, sea necesaria para evitar un grave perjuicio para su salud o la de sus familiares biológicos, se informará a un familiar próximo o a un representante.

Si necesita más información sobre este estudio puede contactar con el investigador responsable, la Dra. *M^a Gema Ariceta Iraola* del Servicio de *Nefrología pediátrica*. Tel. 934893082 y la Dra. *Anna Meseguer Navarro* del laboratorio de *Fisiopatología renal - CIBBIM*, del *Vall d'Hebrón Institut de Recerca*. Tel. 934894061.

Uso futuro de las muestras:

Le pedimos su consentimiento para que autorice almacenar las muestras, el régimen de conservación será en forma de colección,

en el Hospital Universitario Vall d'Hebrón para que puedan ser utilizadas en otros proyectos de investigación biomédica, nacionales o internacionales. Cualquier estudio de investigación para el que se solicite la utilización de estas muestras deberá disponer de la aprobación del Comité de Ética de Investigación Clínica (CEIC) del Hospital Universitario Vall d'Hebrón u otros comités que se establezcan según la legislación vigente. Este comité vela para que los investigadores desarrollen sus estudios siguiendo siempre las más estrictas normas éticas y legales. Las muestras obtenidas se almacenarán, en régimen de colección, en el *Institut de Recerca Vall d'Hebrón* y el responsable de las mismas será la Dra. *M^a Gema Ariceta Iraola* del Servicio de *Nefrología pediátrica*. Tel. 934893082 y la Dra. *Anna Meseguer Navarro* del laboratorio de *Fisiopatología renal - CIBBIM*, del *Vall d'Hebrón Institut de Recerca*. Tel. 934894061.

La cesión de muestras y datos asociados se realizará de manera que el investigador receptor no pueda conocer su identidad.

Si necesita más información puede contactar con las responsables del proyecto de investigación en el Hospital Universitario Vall d'Hebrón (gariceta@vHebrón.net) e Institut de Recerca Vall d'Hebrón (VHIR) (ana.meseguer@vhir.org).

Derecho de revocación del consentimiento:

Su participación en el estudio es completamente voluntaria y, si decide no participar recibirá toda la atención médica que necesite y en ningún caso afectará la relación con el equipo médico que le atiende.

Si cambia de opinión después de dar las muestras biológicas para investigación biomédica, puede pedir que se destruyan las muestras; para ello puede contactar con con la Dra. *M^a Gema Ariceta Iraola* del Servicio de *Nefrología pediátrica*, Dra. *Anna Meseguer Navarro*.

| Type of mutation | Nucleotide | Protein | Exon/Intron | Reference |
|-------------------------|-------------------|----------------|--------------------|---|
| Nonsense | c.706G>T | p.Glu236* | Exon 6 | Not reference found |
| Nonsense | c.706G>T | p.Glu236* | Exon 6 | Not reference found |
| Nonsense | c.1851C>G | p.Tyr617* | Exon 10 | 149,167 |
| Nonsense | c.1851C>G | p.Tyr617* | Exon 10 | 149,167 |
| Nonsense | c.1851C>G | p.Tyr617* | Exon 10 | 149,167 |
| Nonsense | c.1798C>T | p.Gln600* | Exon 10 | 113,114 |
| Nonsense | c.2110C>T | p.Arg704* | Exon 11 | 114,139,494 |
| Nonsense | c.2110C>T | p.Arg704* | Exon 11 | 114,139,494 |
| Nonsense | c.364delA | Trp122* | Exon 4 | 114,132 |
| Nonsense | c.1039C>T | p.Arg347* | Exon 8 | 113,114,481,495,496 |
| Nonsense | c.100C>T | p.Arg34* | Exon 2 | 139,332 |
| Nonsense | c.1399C>T | p.Arg467* | Exon 9 | 113 |
| Nonsense | c.1909C>T | p.Arg637* | Exon 10 | 114,497 |
| Nonsense | c.2110C>T | p.Arg704* | Exon 11 | 114,332 |
| Nonsense | c.1399C>T | p.Arg467* | Exon 9 | 113 |
| Nonsense | c.1909C>T | p.Arg637* | Exon 10 | 114,497 |
| Nonsense | c.1909C>T | p.Arg637* | Exon 10 | 114,497 |
| Nonsense | c.2320C>T | p.Arg774* | Exon 12 | https://www.malacards.org/card/dent_disease_1?limit%5BClinVarVariations%5D=200&showAll=True |
| Nonsense | c.364delA | Trp122* | Exon 5 | 114,132 |
| Nonsense | c.1039C>T | p.Arg347* | Exon 8 | 113,114,481,495,496 |
| Nonsense | c.1039C>T | p.Arg347* | Exon 8 | 113,114,481,495,496 |
| Nonsense | c.1942C>T | p.Arg648* | Exon 11 | 113,114,130 |
| Nonsense | c.1399C>T | p.Arg467* | Exon 9 | 113 |
| Nonsense | c.1942C>T | p.Arg648* | Exon 11 | 113,114,130 |
| Nonsense | c.100C>T | p.Arg34* | Exon 2 | 139,332 |
| Nonsense | c.2152C>T | p.Arg718* | Exon 12 | 95,114,375 |
| Nonsense | c.2320 C>T | p.Arg774* | Exon 12 | https://www.malacards.org/card/dent_disease_1?limit%5BClinVarVariations%5D=200&showAll=True |
| Nonsense | c.1467G>A | p.Trp489* | Exon 9 | 114,139 |
| Nonsense | c.492T >G | p.Tyr164* | Exon 5 | 114,332 |
| Nonsense | c.1942C>T | p.Arg648* | Exon 11 | 113,114,130 |

| | | | | |
|-----------------------|----------------------------|--|-----------------|---|
| <i>Nonesense</i> | <i>c.243G>T</i> | <i>p.Trp81*</i> | <i>Exon 4</i> | 498 |
| <i>Nonesense</i> | <i>c.1399C>T</i> | <i>p.Arg467*</i> | <i>Exon 9</i> | 113 |
| <i>Nonesense</i> | <i>c.1942C>T</i> | <i>p.Arg648*</i> | <i>Exon 11</i> | 113,114,130 |
| <i>Nonesense</i> | <i>c.1942C>T</i> | <i>p.Arg648*</i> | <i>Exon 11</i> | 113,114,130 |
| <i>Frameshift</i> | <i>c.468del</i> | <i>p.Glu157Lysfs*51</i> | <i>Exon 5</i> | <i>No reference found</i> |
| <i>Frameshift</i> | <i>c.100_101insG</i> | <i>p.Glu35fs</i> | <i>Exon 2</i> | 137 |
| <i>Frameshift</i> | <i>c.510delC</i> | <i>p.Ile70fs</i> | <i>Exon 2</i> | <i>No reference found</i> |
| <i>Frameshift</i> | <i>c.597_598dup</i> | <i>p.Leu200Argfs*8</i> | <i>Exon 6</i> | 114 |
| <i>Deletion</i> | <i>c.1951delA</i> | <i>p.?</i> | <i>Exon 11</i> | <i>No reference found</i> |
| <i>Splice-site</i> | <i>IVS7+1 G>T</i> | <i>p.?</i> | <i>Intron 7</i> | <i>No reference found</i> |
| <i>Splice-site</i> | <i>IVS3 +2 G>C</i> | <i>p.?</i> | <i>Intron 3</i> | 113 |
| <i>Splice-site</i> | <i>IVS5+5 G>T</i> | <i>p.?</i> | <i>Intron 5</i> | 113 |
| <i>Splice-site</i> | <i>IVS5+5 G>T</i> | <i>p.?</i> | <i>Intron 5</i> | 113 |
| <i>Splice-site</i> | <i>c.1348-1G>T</i> | <i>skipping 26 bases exon 9, truncated CBS domains</i> | <i>Intron 9</i> | 137,499 |
| <i>Splice-site</i> | <i>c.206-2 A>G</i> | <i>p.?</i> | <i>Intron 3</i> | 500 |
| <i>Splice-site</i> | <i>IVS3 -1</i> | <i>p.?</i> | <i>Intron 3</i> | 113 |
| <i>Splice-site</i> | <i>IVS8+1G>T</i> | <i>p.?</i> | <i>Intron 8</i> | <i>No reference found</i> |
| <i>Large deletion</i> | <i>c.(?-30)(*220_?)del</i> | <i>p.?</i> | <i>2_12</i> | 114,495 |
| <i>Missense</i> | <i>c.1546C>T</i> | <i>p.Arg516Trp</i> | <i>Exon 10</i> | 114,161 |
| <i>Missense</i> | <i>c.1639T>G</i> | <i>p.Trp547Gly</i> | <i>Exon 10</i> | 114,332 |
| <i>Missense</i> | <i>c.1619C>T</i> | <i>p.Ala540Val</i> | <i>Exon 10</i> | 114,501 |
| <i>Missense</i> | <i>c.1862C>T</i> | <i>p.Pro621Leu</i> | <i>Exon 10</i> | 113,114 |
| <i>Missense</i> | <i>c.1213 G>A</i> | <i>Not reported</i> | <i>Exon 8</i> | <i>No reference found</i> |
| <i>Missense</i> | <i>c.842C>T</i> | <i>P.Ser281Leu</i> | <i>Exon 8</i> | <i>POSTER. FP763. WHETHER WOMEN ASYMPTOMATIC OR SYMPTOMATIC CARRIERS OF DENT DISEASE?</i> |
| <i>Missense</i> | <i>c.842C>T</i> | <i>P.Ser281Leu</i> | <i>Exon 8</i> | <i>POSTER. FP763. WHETHER WOMEN ASYMPTOMATIC OR SYMPTOMATIC CARRIERS OF DENT DISEASE?</i> |
| <i>Missense</i> | <i>c.801A>C</i> | <i>p.Glu267Asp</i> | <i>Exon 7</i> | 114 |

| | | | | |
|----------|---------------------|---------------|---------|---|
| Missense | c.2119C>T | p.Arg707Ter | Exon 12 | https://www.malacards.org/card/dent_disease_1?limit%5BClinVarVariations%5D=200&showAll=True |
| Missense | c.731C>T | p.Ser244Leu | Exon 7 | 114,494 |
| Missense | c.731C>T | p.Ser244Leu | Exon 7 | 114,494 |
| Missense | c.941C>T | p.Ser314Leu | Exon 7 | https://www.gepedia.com/gene_disease/461556/ |
| Missense | c.1070 G>T | p.Gly260Val | Exon 7 | 113,114 |
| Missense | c.1384G >A | p.Gly462Ser | Exon 9 | 114,332,364 |
| Missense | c.903A>T | p.Lys301Asn | Exon 8 | Not reference found |
| Missense | c.1397G >A | p.Gly466Asp | Exon 9 | 114,332 |
| Missense | c.674T>C | p.Leu225Pro a | Exon 6 | 114,332,364 |
| Missense | c.1546C>T | p.Arg516Trp | Exon 10 | 114,161,495 |
| Missense | c.941C>T | p.Ser314Leu | Exon 7 | https://www.gepedia.com/gene_disease/461556/ |
| Missense | c.941C>T | p.Ser314Leu | Exon 7 | https://www.gepedia.com/gene_disease/461556/ |
| Missense | c.815A>G | p.Tyr272Cys | Exon 8 | 113,114 |
| Missense | c.815A>G | p.Tyr272Cys | Exon 8 | 113,114 |
| Missense | c.1791A>T | p.Glu597Asp | Exon 10 | Not reference found |
| Missense | c.1025A>G | p.Tyr342Cys | Exon 8 | https://www.malacards.org/card/dent_disease_1 |
| Missense | c.1397G >A | p.Gly466Asp | Exon 9 | 114,332 |
| Inframe | c.801_803del | p.Glu267del | Exon 7 | 139 |
| Inframe | c.782_784 | p.Gly261del | Exon 7 | 113,114 |
| Inframe | c.1566_c.1568delTGT | p.Val523del | Exon 10 | 332,481 |

7. Annex VII

Table 1. 82 miRNA differentially expressed between patients and controls

| miRNA | DDCt | RQ | pval | p.adi | miRNA | DDCt | RQ | pval | p.adi |
|-----------------------------|------|------|---------|---------|----------------------------|------|------|---------|---------|
| Upregulated miRNA | | | | | | | | | |
| hsa-miR-664a-3p 478193 mir | 3,30 | 0,10 | 2,1E-07 | 4,7E-05 | hsa-miR-181a-3p 479405 mir | 1,75 | 0,30 | 5,4E-04 | 2,9E-03 |
| hsa-miR-429 477849 mir | 2,05 | 0,24 | 6,9E-07 | 7,7E-05 | hsa-miR-499a-5p 478139 mir | 1,66 | 0,32 | 5,4E-04 | 2,9E-03 |
| hsa-miR-365a-3p 478065 mir | 2,17 | 0,22 | 1,5E-06 | 1,1E-04 | hsa-miR-132-3p 477900 mir | 1,63 | 0,32 | 6,1E-04 | 3,2E-03 |
| hsa-miR-425-5p 478094 mir | 1,50 | 0,35 | 2,8E-06 | 1,6E-04 | hsa-let-7i-3p 477862 mir | 1,46 | 0,36 | 7,6E-04 | 3,8E-03 |
| hsa-miR-200b-3p 477963 mir | 2,56 | 0,17 | 3,6E-06 | 1,6E-04 | hsa-miR-342-3p 478043 mir | 1,68 | 0,31 | 8,1E-04 | 4,0E-03 |
| hsa-miR-224-5p 477986 mir | 2,57 | 0,17 | 4,5E-06 | 1,7E-04 | hsa-miR-598-3p 478172 mir | 1,46 | 0,36 | 9,9E-04 | 4,8E-03 |
| hsa-miR-191-5p 477952 mir | 1,72 | 0,30 | 5,2E-06 | 1,7E-04 | hsa-miR-455-3p 478112 mir | 1,60 | 0,33 | 1,1E-03 | 5,4E-03 |
| hsa-miR-128-3p 477892 mir | 2,43 | 0,18 | 7,6E-06 | 2,1E-04 | hsa-miR-22-5p 477987 mir | 1,39 | 0,38 | 1,2E-03 | 5,4E-03 |
| hsa-miR-28-5p 478000 mir | 1,70 | 0,31 | 1,0E-05 | 2,5E-04 | hsa-miR-450a-5p 478106 mir | 1,70 | 0,31 | 1,3E-03 | 5,8E-03 |
| hsa-miR-186-5p 477940 mir | 1,93 | 0,26 | 1,2E-05 | 2,7E-04 | hsa-miR-181a-5p 477857 mir | 1,53 | 0,35 | 1,4E-03 | 6,2E-03 |
| hsa-miR-30c-5p 478008 mir | 1,74 | 0,30 | 2,3E-05 | 4,5E-04 | hsa-miR-99b-5p 478343 mir | 2,17 | 0,22 | 1,6E-03 | 6,6E-03 |
| hsa-miR-10a-5p 479241 mir | 2,32 | 0,20 | 3,0E-05 | 5,3E-04 | hsa-miR-196b-5p 478585 mir | 1,51 | 0,35 | 1,5E-03 | 6,6E-03 |
| hsa-miR-29b-2-5p 478003 mir | 1,95 | 0,26 | 3,1E-05 | 5,3E-04 | hsa-miR-148a-3p 477814 mir | 1,40 | 0,38 | 1,6E-03 | 6,8E-03 |
| hsa-miR-26a-5p 477995 mir | 1,77 | 0,29 | 3,4E-05 | 5,3E-04 | hsa-miR-185-5p 477939 mir | 1,61 | 0,33 | 1,7E-03 | 7,0E-03 |
| hsa-miR-324-5p 478024 mir | 1,94 | 0,26 | 3,6E-05 | 5,4E-04 | hsa-miR-181c-5p 477934 mir | 1,65 | 0,32 | 2,2E-03 | 8,9E-03 |
| hsa-miR-361-5p 478056 mir | 2,17 | 0,22 | 4,5E-05 | 5,6E-04 | hsa-miR-30b-5p 478007 mir | 1,46 | 0,36 | 2,3E-03 | 9,1E-03 |
| hsa-miR-660-5p 478192 mir | 2,14 | 0,23 | 4,5E-05 | 5,6E-04 | hsa-miR-34a-3p 478047 mir | 1,70 | 0,31 | 2,4E-03 | 9,3E-03 |
| hsa-miR-25-3p 477994 mir | 1,79 | 0,29 | 4,1E-05 | 5,6E-04 | hsa-miR-500a-3p 478951 mir | 1,46 | 0,36 | 2,5E-03 | 9,7E-03 |
| hsa-miR-1180-3p 477869 mir | 2,16 | 0,22 | 5,2E-05 | 6,1E-04 | hsa-miR-744-5p 478200 mir | 0,88 | 0,54 | 2,6E-03 | 9,7E-03 |
| hsa-miR-29b-3p 478369 mir | 2,79 | 0,14 | 9,3E-05 | 9,4E-04 | hsa-miR-1296-5p 479451 mir | 2,14 | 0,23 | 2,8E-03 | 1,0E-02 |
| hsa-miR-29c-5p 478005 mir | 2,20 | 0,22 | 8,9E-05 | 9,4E-04 | hsa-let-7e-3p 479281 mir | 1,76 | 0,29 | 2,9E-03 | 1,0E-02 |
| hsa-miR-652-3p 478189 mir | 1,58 | 0,33 | 9,3E-05 | 9,4E-04 | hsa-miR-221-5p 478778 mir | 1,61 | 0,33 | 2,9E-03 | 1,0E-02 |
| hsa-miR-9-3p 478211 mir | 1,65 | 0,32 | 9,8E-05 | 9,5E-04 | hsa-miR-200a-5p 478752 mir | 1,70 | 0,31 | 3,3E-03 | 1,2E-02 |
| hsa-miR-339-5p 478040 mir | 1,87 | 0,27 | 1,1E-04 | 9,7E-04 | hsa-miR-888-5p 479192 mir | 2,10 | 0,23 | 3,6E-03 | 1,2E-02 |
| hsa-miR-148b-3p 477824 mir | 1,71 | 0,30 | 1,6E-04 | 1,3E-03 | hsa-miR-125b-5p 477885 mir | 1,47 | 0,36 | 3,9E-03 | 1,3E-02 |
| hsa-miR-93-5p 478210 mir | 1,48 | 0,36 | 1,6E-04 | 1,3E-03 | hsa-let-7g-5p 478580 mir | 0,96 | 0,52 | 4,6E-03 | 1,5E-02 |
| hsa-miR-17-5p 478447 mir | 1,43 | 0,37 | 1,6E-04 | 1,3E-03 | hsa-miR-125a-5p 477884 mir | 1,35 | 0,39 | 5,2E-03 | 1,7E-02 |
| hsa-miR-769-5p 478203 mir | 2,44 | 0,18 | 1,7E-04 | 1,3E-03 | hsa-miR-29c-3p 479229 mir | 2,11 | 0,23 | 5,4E-03 | 1,7E-02 |

| | | | | | | | | | |
|----------------------------|------|------|---------|---------|----------------------------|------|------|---------|---------|
| hsa-miR-28-3p 477999 mir | 1,99 | 0,25 | 1,8E-04 | 1,4E-03 | hsa-miR-101-3p 477863 mir | 1,96 | 0,26 | 7,2E-03 | 2,3E-02 |
| hsa-miR-362-5p 478059 mir | 1,92 | 0,26 | 2,0E-04 | 1,5E-03 | hsa-miR-19a-3p 479228 mir | 1,60 | 0,33 | 7,1E-03 | 2,3E-02 |
| hsa-miR-187-3p 477941 mir | 1,93 | 0,26 | 2,8E-04 | 1,9E-03 | hsa-miR-140-5p 477909 mir | 1,88 | 0,27 | 7,4E-03 | 2,3E-02 |
| hsa-miR-152-3p 477921 mir | 2,20 | 0,22 | 3,1E-04 | 2,1E-03 | hsa-miR-501-5p 478142 mir | 1,43 | 0,37 | 9,2E-03 | 2,8E-02 |
| hsa-miR-28-3p 477999 mir | 1,99 | 0,25 | 1,8E-04 | 1,4E-03 | hsa-miR-101-3p 477863 mir | 1,96 | 0,26 | 7,2E-03 | 2,3E-02 |
| hsa-miR-362-5p 478059 mir | 1,92 | 0,26 | 2,0E-04 | 1,5E-03 | hsa-miR-19a-3p 479228 mir | 1,60 | 0,33 | 7,1E-03 | 2,3E-02 |
| hsa-miR-187-3p 477941 mir | 1,93 | 0,26 | 2,8E-04 | 1,9E-03 | hsa-miR-140-5p 477909 mir | 1,88 | 0,27 | 7,4E-03 | 2,3E-02 |
| hsa-miR-152-3p 477921 mir | 2,20 | 0,22 | 3,1E-04 | 2,1E-03 | hsa-miR-501-5p 478142 mir | 1,43 | 0,37 | 9,2E-03 | 2,8E-02 |
| hsa-miR-500a-5p 478309 mir | 1,93 | 0,26 | 3,3E-04 | 2,2E-03 | hsa-miR-31-5p 478015 mir | 0,91 | 0,53 | 9,4E-03 | 2,8E-02 |
| hsa-miR-326 478027 mir | 2,17 | 0,22 | 3,6E-04 | 2,2E-03 | hsa-miR-24-3p 477992 mir | 0,92 | 0,53 | 9,8E-03 | 2,9E-02 |
| hsa-miR-361-3p 478055 mir | 1,94 | 0,26 | 3,6E-04 | 2,2E-03 | hsa-miR-193a-5p 477954 mir | 1,71 | 0,31 | 1,0E-02 | 3,0E-02 |
| hsa-miR-328-3p 478028 mir | 1,23 | 0,43 | 4,5E-04 | 2,7E-03 | hsa-miR-31-3p 478012 mir | 1,11 | 0,46 | 1,1E-02 | 3,2E-02 |
| hsa-miR-151a-3p 477919 mir | 2,57 | 0,17 | 4,8E-04 | 2,8E-03 | hsa-miR-505-5p 478957 mir | 2,00 | 0,25 | 1,2E-02 | 3,3E-02 |
| hsa-let-7f-2-3p 477843 mir | 1,77 | 0,29 | 4,8E-04 | 2,8E-03 | hsa-miR-140-3p 477908 mir | 2,14 | 0,23 | 1,7E-02 | 4,7E-02 |
| hsa-miR-20a-5p 478586 mir | 1,12 | 0,46 | 5,0E-04 | 2,8E-03 | hsa-miR-216b-5p 479456 mir | 2,84 | 0,14 | 1,8E-02 | 4,9E-02 |
| hsa-miR-455-5p 478113 mir | 1,81 | 0,29 | 1,8E-02 | 4,9E-02 | | | | | |
| Downregulated miRNA | | | | | | | | | |
| hsa-miR-143-3p 477912 mir | -1,9 | 3,7 | 2,6E-04 | 1,9E-03 | | | | | |
| hsa-miR-629-3p 478182 mir | -1,6 | 3,0 | 9,8E-03 | 2,9E-02 | | | | | |
| hsa-miR-145-5p 477916 mir | -2,7 | 6,6 | 3,4E-03 | 1,2E-02 | | | | | |

8. Annex VIII

TABLE . Target genes for the differentially expressed miRNA classified within the 25 top functions involved

| Function | Genes involved |
|------------------------------------|--|
| Tissue Morphology | ABCG2,ADORA2B,AKT1,AR,BAK1,BAX,BCL2,BCL2L1,BECN1,BMF,BRCA1,BSG,CASP3,CCND1,CCNE1,CCR5,CD276,CD44,CDC25A,CDK4,CDK6,CDKN1A,CDKN1B,CDKN2A,CDX2,CREB1,CXCL12,CXCL8,DHFR,DSP,E2F1,ERBB2,ESR1,EZH2,FOXP3,GLI1,GMFB,HIF1A,HMGA2,HMOX1,ICOS,IGF1R,IGFBP3,IGFBP5,IL10,IL2RG,IL6,JUN,KLF4,LATS2,MAP2K4,MAPK14,MMP9,MYBL2,MYC,MYCN,NOTCH1,NRAS,PDGFA,PIK3R1,PLK1,PMAIP1,PPARG,PRC1,PTGS2,RB1,RHOA,RHOB,RUNX1,STAT3,THBS1,TIMP3,TNF,TP53,TP63,TYMS,UHRF1,VCAN,VEGFA,ZBTB7A |
| Tissue Development | ACP1,ACVR1,ACVR2A,ADAMTS1,ADAMTS5,AGO1,AGO4,AKT1,ANPEP,ANXA1,APLN,APP,AR,AURKB,BCL2,BCL2L1,BCL6,BMI1,BMPR1B,BMPR2,BRCA1,BSG,CASR,CBFB,CCN2,CCND1,CCNE1,CD276,CD44,CD69,CDC42,CDH5,CDK1,CDK4,CDK6,CDKN1A,CDKN1B,CDKN1C,CDKN2A,CEP72,CES1,COL1A1,COL1A2,COL3A1,COL4A1,COL4A2,COL4A5,COL5A1,COL5A2,COL5A3,COL8A1,CREB1,CXCL12,CXCL8,DCX,DDR1,DICER1,DSP,E2F1,ELAVL1,EPHA2,ERBB2,EZH2,F11R,F2,FBN1,FBXW7,FGFR3,FHOD1,FLI1,FOXO1,FOXP3,FURIN,GAS7,GATA6,GLI1,GNAI2,H3-3A/H3-3B,H4C1,HDAC4,HIF1A,HMGA1,HMGA2,HMOX1,HOXA7,ICOS,ID1,ID2,ID3,IGF1R,IGFBP3,IGFBP5,IKZF1,IKZF4,IL10,IL1RN,IL2RG,IL6,IRS1,ITGA2,ITGA5,ITGB3,JUN,KLF4,KLHL20,KMT2A,KRAS,KRT19,LAMC1,LIN28A,LIN28B,LOXL2,MAP2,MAPK14,MAPRE1,MDM2,MET,MLLT11,MMP1,MMP14,MMP3,MMP9,MTOR,MYBL2,MYC,NAV3,NCOA3,NF1,NF2,NID1,NID2,NOTCH1,NOTCH4,NR4A2,NRAS,OSBPL8,PDGFA,PDGFB,PLCG1,PLK1,PNP,PPARG,PPM1F,PRDM1,PTEN,PTGS2,PTPRK,PXDN,RAS,RASA1,RFFL,RHOA,RHOB,RPS6KA5,RUNX1,RUNX2,S100A9,S1PR1,SATB2,SLC9A3R2,SMAD1,SMAD3,SMAD4,SMARCA5,SMO,SOX6,SOX9,SP1,SPARC,SRF,STAT3,TAGLN,TBX21,TGFB3,TGFB3R1,TGFB3R2,TGFB3R3,TGFB3R4,TGFB3R5,TGFB3R6,TGFB3R7,TGFB3R8,TGFB3R9,TGFB3R10,TGFB3R11,TGFB3R12,TGFB3R13,TGFB3R14,TGFB3R15,TGFB3R16,TGFB3R17,TGFB3R18,TGFB3R19,TGFB3R20,TGFB3R21,TGFB3R22,TGFB3R23,TGFB3R24,TGFB3R25,TGFB3R26,TGFB3R27,TGFB3R28,TGFB3R29,TGFB3R30,TGFB3R31,TGFB3R32,TGFB3R33,TGFB3R34,TGFB3R35,TGFB3R36,TGFB3R37,TGFB3R38,TGFB3R39,TGFB3R40,TGFB3R41,TGFB3R42,TGFB3R43,TGFB3R44,TGFB3R45,TGFB3R46,TGFB3R47,TGFB3R48,TGFB3R49,TGFB3R50,TGFB3R51,TGFB3R52,TGFB3R53,TGFB3R54,TGFB3R55,TGFB3R56,TGFB3R57,TGFB3R58,TGFB3R59,TGFB3R60,TGFB3R61,TGFB3R62,TGFB3R63,TGFB3R64,TGFB3R65,TGFB3R66,TGFB3R67,TGFB3R68,TGFB3R69,TGFB3R70,TGFB3R71,TGFB3R72,TGFB3R73,TGFB3R74,TGFB3R75,TGFB3R76,TGFB3R77,TGFB3R78,TGFB3R79,TGFB3R80,TGFB3R81,TGFB3R82,TGFB3R83,TGFB3R84,TGFB3R85,TGFB3R86,TGFB3R87,TGFB3R88,TGFB3R89,TGFB3R90,TGFB3R91,TGFB3R92,TGFB3R93,TGFB3R94,TGFB3R95,TGFB3R96,TGFB3R97,TGFB3R98,TGFB3R99,TGFB3R100 |
| Reproductive System Disease | AARSD1,ABCG2,ABTB1,ACBD3,ACE2,ACSS1,ACVR1,ACVR1B,ACVR2A,ADAMTS1,ADAMTS14,ADAMTS15,ADAMTS2,ADAMTS5,ADGRG1,ADORA2B,AFF1,AGO1,AGO4,AHNAK,AICDA,AJUBA,AKAP8,AKT1,ALOX5,ANAPC1,ANPEP,ANXA1,AP2A1,APAF1,API5,APP,AR,ARHGAP32,ARID3A,ARID3B,ARID4B,ATAD3B,ATP6V0A1,ATRX,AURKB,BACE1,BAK1,BAMBI,BAP1,BAX,BCL2,BCL2L1,BCL2L11,BCL6,BECN1,BMI1,BMP2K, |

| | |
|-------------------------------------|--|
| | <p>BMPR1B,BMPR2,BNIP2,BRCA1,BSG,CALCOCO2,CAMTA1,CAPG,CAPN8,CARHSP1,CASP3,CASP6,CASP7,CASR,CAV2,CBFB,CBX7,CCKBR,CCN2,CCNA2,CCND1,CCNE1,CCNE2,CCR5,CD276,CD44,CD69,CDC25A,CDC42,CDCP1,CDH5,CDIPT,CDK1,CDK4,CDK6,CDKN1A,CDKN1B,CDKN2A,CDX2,CEBPG,CEMIP2,CEP72,CES1,CHD1,CHMP2A,CLINT1,CNOT8,CNOT9,COIL,COL15A1,COL1A1,COL1A2,COL3A1,COL4A1,COL4A2,COL4A5,COL5A1,COL5A2,COL5A3,COL8A1,CORO2B,CPNE8,CREB1,CRIM1,CRP,CRTAP,CSDE1,CXCL12,CXCL8,CYP1A1,DCX,DDIT3,DDR1,DDX19B,DDX43,DHFR,DHX57,DICER1,DIO3,DNMT1,DNMT3A,DNMT3B,DOCK5,DOCK7,DRD3,DSP,DUSP1,DUSP2,E2F1,E2F2,E2F3,EGR2,EIF4E,EIF4G2,ELAVL1,ELMO2,ELMOD2,EOMES,EPHA2,ERBB2,ERBB3,ERBB4,ERBIN,ERRF1,ESR1,EZH2,F11R,F2,FADS2,FANCD2,FBN1,FBXW7,FEN1,FGF16,FGFR3,FLI1,FNDC3A,FNDC3B,FOXO1,FOXP3,FRG1,FSCN1,GAK,GALNT1,GALNT7,GATA6,GLI1,GNAI2,GPD2,GPR160,GPR37,GRIA2,GRM3,GSE1,GTPBP3,H3-3A/H3-3B,HBP1,HDAC4,HIF1A,HIPK3,HMGA1,HMGA2,HMOX1,HNRNPK,HNRNPM,HOTAIR,HOXA1,HOXA11,HOXC8,HOXD10,HTR1A,HYOU1,ICOS,ID1,ID2,IDH1,IFIT5,IFRD1,IGF1R,IGF2BP1,IGF2BP2,IGF2BP3,IGFBP3,IGFBP5,IKBKB,IKZF1,IL10,IL1RN,IL2RG,IL6,IPO4,IRS1,ITCH,ITGA2,ITGA5,ITGB3,JAK1,JARI</p> <p>D2,JPH2,JUN,KLF4,KLF5,KLHL20,KLK10,KMT2A,KRAS,KRT19,KRT5,KRT7,KRT85,LAMC1,LATS2,LDLR,LIN28A,LIN28B,LINC00472,LIPA,LMNB2,LOXL2,LRRC8C,LTN1,MAN1A1,MAP2,MAP2K4,MAP2K7,MAP4K4,MAPK7,MAPRE1,MARCKS,MARS2,MAZ,MBNL1,MCL1,MDM2,MECP2,MET,MICA,MITF,MLF1,MLLT1,MLLT11,MMP1,MMP14,MMP3,MMP9,MTDH,MTOR,MTRR,MUC1,MYBL2,MYC,MYCN,MYD88,MYLIP,MYO10,MYO5A,NAPG,NASP,NAV3,NCL,NCOA3,NDUFA4,NEDD4,NEUROD1,NF1,NF2,NID1,NID2,NOTCH1,NOTCH4,NR1H2,NR4A2,NRAS,NT5C3A,NT5E,NTRK3,NUCB1,NXN,OSBPL2,OSBPL8,OSBPL9,OTULINL,P4HA2,PADI1,PAFAH1B2,PAK5,PARP8,PCDHB10,PCGF1,PDGFA,PDGFB,PGC,PGM1,PHF6,PIGR,PIK3R1,PIK3R3,PKD2,PLCG1,PLEC,PLK1,PMAIP1,PNP,POM121/POM121C,PPARG,PPM1D,PPM1F,PPP2R2A,PPP3CA,PPP3R1,PPT2,PRC1,PRDM1,PRIM1,PRRC2A,PTEN,PTGFRN,PTGS2,PTPN12,PTPN13,PTPRD,PTPRK,PURA,PXDN,RABGAP1L,RABL6,RAS,RAS A1,RB1,RBL2,RBM19,RBMS1,RDH10,RELN,RERE,RHOA,RHOB,ROBO4,RPS6KA5,RPTOR,RTKN,RUNX1,RUNX2,S100A9,S1PR1,SATB2,SCD,S CYL1,SEC62,SGPL1,SH3BP4,SHROOM2,SIGMAR1,SLC12A4,SLC1A4,SLC25A13,SLC25A32,SLC38A1,SLC38A2,SLC4A10,SLC7A1,SLC7A11,SMAD3,SMAD4,SMAD5,SMARCA5,SMC1A,SMO,SMOX,SNAP25,SOX4,SOX9,SP1,SPARC,SPRYD4,SPTB,SRF,SRSF10,ST18,STAT3,STK40,STRN,S WAP70,SYT4,TAF9B,TAGLN,TCL1A,TENM2,TET1,TGFB3,TGFB1,TGFB2,THBS1,THEM4,TIMP3,TJP1,TLR4,TLR7,TMCO1,TMEM59,TMEM87A,TNF,TNFAIP2,TNFRSF10B,TNRC6A,TP53,TP63,TPM2,TPM3,TRIM9,TRMT1,TRPS1,TSPAN8,TTCC9C,TUBB2A,TWIST1,TXNIP,TYMS, TYR,TYRP1,UAP1,UGT2B17,UGT2B28,UGT8,UHRF1,USF2,USP46,UVRAG,VCAN,VEGFA,VIM,VPS39,WASF3,WDR37,WEE1,WNT1,WNT5A,Y Y1,ZBTB7A,ZEB1,ZEB2,ZFPM2,ZNF385A</p> |
| Renal and Urological Disease | <p>ABCG2,ACVR1B,ACVR2A,ADORA2B,AGO1,AHNAK,AICDA,AJUBA,AKAP8,AKT1,ANPEP,APAF1,API5,APP,AR,ATAD3B,ATRX,AURKB,BAK1,BAP1,BAX,BCL2,BCL2L1,BCL2L11,BCL6,BECN1,BRCA1,BSG,CALCOCO2,CASP3,CASP7,CASR,CBFB,CBX7,CCN2,CCND1,CCNE2,CD276,CD44,CD C42,CDCP1,CDK4,CDKN1A,CDKN1B,CDKN2A,CEMIP2,CHD1,CNOT9,COL1A2,COMMD9,CRP,CXCL12,CXCL8,CYP1A1,DAD1,DDX19B,DHFR, DICER1,DNMT3A,DOCK5,DSP,E2F1,E2F3,EIF4G2,ENTPD4,EPHA2,ERBB2,ERBB3,ERBB4,ESR1,EZH2,F2,FANCD2,FBN1,FBXW7,FGFR3,FLI1,F</p> |

| | |
|--|--|
| Organismal Survival | <p>OXO1,FRG1,FURIN,GAS7,GEMIN2,GLI1,GPR37,HBP1,HDAC4,HIF1A,HK2,HMGA1,HMOX1,HNRNPK,HNRNPM,HOXA1,HYOU1,IDH1,IGF1R,I GF2BP3,IGFBP3,IGFBP5,IKKBK,IKZF1,IL10,IL1RN,IL2RG,IL6,INSIG1,IRS1,ITCH,ITGA5,ITGB3,JAK1,JARID2,JPH2,JUN,KLF4,KLF5,KLHL20,KLK1, KMT2A,KRAS,KRT19,KRT7,LAMC1,LATS2,LIN28A,LIN28B,LOXL4,MAP2K4,MAP2K7,MAPK14,MAPK7,MAZ,MCL1,MDM2,MET,MITF,MLLT1, MLLT11,MMP9,MTOR,MUC1,MYC,MYCN,MYO5A,NASP,NAV3,NCOA3,NEDD4,NEUROD1,NF1,NF2,NOTCH1,NRAS,NT5C3A,NTRK3,NUCB1 ,PAK5,PHF6,PIK3R1,PKD2,PLAG1,PLCG1,PLEC,PLOD2,PMAIP1,PNP,PPARG,PPM1F,PPP3R1,PRC1,PRDM1,PRRC2A,PTEN,PTGS2,PTPRD,PU RA,RAB27A,RAS,RASA1,RB1,RBM8A,RERE,RHOA,RHOB,RHOG,RPTOR,RUNX1,RUNX2,S1PR1,SCD,SGPL1,SLC1A4,SLC25A24,SLC7A11,SMA D4,SMC1A,SMOX,SOX4,SOX9,SPARC,SPTB,SRF,ST18,STAT3,TDG,TET1,TGFBR1,TGFBR2,THBS1,TIMP3,TJP1,TLR4,TNF,TNFRSF10B,TP53,TP63,TPM2,TPM3,TRPS1,TUBB2A,TWIST1,TXNIP,TYMS,UGT2B17,VASN,VEGFA,VIM,WASF3,YY1,ZEB1,ZEB2,ZFP36L1</p> <p>ADGRG1,AKT1,AR,AURKB,BAP1,BAX,BBC3,BCL2,BCL2L1,BCL6,BMI1,BRCA1,BSG,CAMTA1,CCN2,CCND1,CCNE1,CD276,CD44,CDC25A,CDC P1,CDK4,CDK6,CDKN1A,CDKN1B,CDKN2A,CHMP2A,COL5A1,CRP,CXCL12,CXCL8,DICER1,DNMT3A,DNMT3B,EPHA2,ERBB2,ERBB3,ERBB4, ESR1,EZH2,FBXW7,FEN1,FOXO1,FSCN1,GATA6,GLI1,GSE1,HIF1A,HK2,HMGA2,HMOX1,HNRNPK,HOTAIR,HOXA11,HOXA7,ID1,IDH1,IGF1R ,IGF2BP1,IGF2BP3,IGFBP3,IL10,IL6,ITGA5,ITGB3,JUN,KLF4,KLF5,KMT2A,KRAS,LIN28B,LINC00472,MCL1,MET,MMP9,MTDH,MTOR,MUC1, MYBL2,MYC,MYCN,MYD88,MYLIP,NCL,NCOA3,NOTCH1,NRAS,NT5E,NTRK3,P4HA2,PHF6,PIK3R1,PPARG,PRDM1,PTEN,PTGS2,RAS,RB1,R BL2,RUNX1,SCD,SIGMAR1,SLC7A11,SOX4,SP1,STAT3,THEM4,TIMP3,TNF,TNFAIP3,TP53,TP63,TYMS,VCAN,VEGFA,VIM,ZBTB7A,ZE B1</p> |
| Organismal Injury and Abnormalities | <p>AARSD1,ABCG2,ABTB1,ACBD3,ACE2,ACP1,ACSS1,ACVR1,ACVR1B,ACVR2A,ADAMTS1,ADAMTS14,ADAMTS15,ADAMTS2,ADAMTS5,ADGR G1,ADORA2B,ADPGK,AFF1,AGO1,AGO4,AHNAK,AICDA,AJUBA,AKAP8,AKT1,ALOX5,ANAPC1,ANAPC16,ANPEP,ANXA1,AP2A1,AP2M1,APA F1,API5,APLN,APP,AR,ARHGAP32,ARID3A,ARID3B,ARID4B,ATAD3B,ATP2A2,ATP6AP1L,ATP6V0A1,ATP6V1F,ATRX,AURKB,B3GALT4,BACE 1,BAK1,BAMBI,BAP1,BAX,BBC3,BCL2,BCL2L1,BCL2L11,BCL6,BCL7A,BECN1,BMF,BMI1,BMP2K,BMPR1B,BMPR2,BNIP2,BRCA1,BSG,C11orf 58,CALCOCO2,CAMTA1,CAPG,CAPN8,CARHSP1,CASP3,CASP6,CASP7,CASR,CAV2,CBFB,CBLN2,CBX7,CCDC25,CCKBR,CCN2,CCNA2,CCND1, CCNE1,CCNE2,CCR5,CD276,CD44,CD69,CDC25A,CDC42,CDCP1,CDH5,CDIPT,CDK1,CDK4,CDK6,CDKAL1,CDKN1A,CDKN1B,CDKN1C,CDKN2 A,CDX2,CEBPG,CEMIP2,CEP72,CES1,CHD1,CHMP2A,CHORDC1,CIAO2A,CLINT1,CNOT8,CNOT9,COIL,COL15A1,COL1A1,COL1A2,COL3A1,C OL4A1,COL4A2,COL4A5,COL5A1,COL5A2,COL5A3,COL8A1,COMMD9,CORO2B,CPNE8,CREB1,CRIM1,CRP,CRTAP,CSDE1,CSNK1D,CXCL12, CXCL8,CYP1A1,DAD1,DBI,DCP2,DCX,DDIT3,DDR1,DDX19B,DDX43,DFFA,DHFR,DHX57,DICER1,DIO3,DNMT1,DNMT3A,DNMT3B,DNPEP,D OCK5,DOCK7,DRD3,DSP,DTD1,DUS1L,DUSP1,DUSP12,DUSP2,DUSP23,E2F1,E2F2,E2F3,EGR2,EIF3J,EIF4E,EIF4EBP2,EIF4G2,ELAVL1,ELMO 2,ELMOD2,ENPP6,ENTPD4,EOMES,EPHA2,ERBB2,ERBB3,ERBB4,ERBIN,ERRF1,ESR1,EZH2,F11R,F2,FADS2,FAM3C,FANCD2,FBN1,FBXO28, FBXW7,FEN1,FGF16,FGFR3,FHOD1,FLI1,FNDC3A,FNDC3B,FOXF2,FOXO1,FOXP3,FRAT2,FRG1,FSCN1,FURIN,FXR2,GAK,GALNT1,GALNT7,G AS7,GATA6,GEMIN2,GEMIN7,GLI1,GNAI2,GPD2,GPR160,GPR37,GRIA2,GRM3,GRPEL2,GSE1,GSS,GTPBP3,GYS1,H3-3A/H3- 3B,H4C1,HBP1,HDAC4,HIF1A,HIPK3,HK2,HMGA1,HMGA2,HMGN3,HMOX1,HNRNPK,HNRNPM,HOTAIR,HOXA1,HOXA11,HOXA7,HOXB8,H</p> |

| | |
|------------------------|---|
| Organismal Development | <p>OXC8,HOXD10,HOXD8,HPGD,HTR1A,HYOU1,ICOS,ID1,ID2,ID3,IDH1,IFIT5,IFRD1,IGF1R,IGF2BP1,IGF2BP2,IGF2BP3,IGFBP3,IGFBP5,IKKBK,IKZF1,IKZF4,IL10,IL1RN,IL2RG,IL6,INSIG1,IPO4,IRS1,ITCH,ITGA2,ITGA5,ITGB3,JAK1,JARID2,JPH2,JUN,KCNJ16,KCTD3,KLF13,KLF4,KLF5,KLHL20,KLK1,KLK10,KMT2A,KRAS,KRT19,KRT5,KRT7,KRT85,LAMC1,LAMP2,LATS2,LDLR,LIN28A,LIN28B,LINC00472,LIPA,LMNB2,LOXL2,LOXL4,LRRC8C,LTN1,MAD2L1,MAN1A1,MAP2,MAP2K4,MAP2K7,MAP3K12,MAP4K4,MAPK12,MAPK14,MAPK7,MAPRE1,MAPRE2,MARCKS,MARS2,MAT2A,MAZ,MBNL1,MCL1,MDFI,MDM2,MECP2,MED28,MEF2D,MET,MICA,MITF,MLF1,MLLT1,MLLT11,MMP1,MMP14,MMP3,MP9,MPDU1,MRPS24,MRPS33,MTDH,MTOR,MTPN,MTRR,MUC1,MYBL2,MYC,MYCN,MYD88,MYLIP,MYO10,MYO5A,NAPG,NASP,NAV3,NCEH1,NCL,NCOA3,NDUFA4,NEDD4,NEUROD1,NF1,NF2,NID1,NID2,NLK,NOTCH1,NOTCH4,NPR3,NR1I2,NR4A2,NRAS,NT5C3A,NT5E,NTRK3,NUCB1,NUFIP2,NXN,OSBPL2,OSBPL8,OSBPL9,OTULINL,P3H1,P4HA2,PADI1,PAFAH1B2,PAK5,PARP8,PCDHB10,PCGF1,PCTP,PDGFA,PDGFB,PERP,PEX11B,PGC,PGM1,PGRMC1,PHF6,PIGR,PIK3R1,PIK3R3,PKD2,PLAG1,PLCG1,PLEC,PLK1,PLOD2,PMAIP1,PNP,POLD2,POLR2C,POM121/POM121C,PPARG,PPIC,PPM1D,PPM1F,PPP1R7,PPP2R2A,PPP3CA,PPP3R1,PPT2,PRC1,PRDM1,PRIM1,PRPF40A,PRRC2A,PTEN,PTGFRN,PTGS2,PTPA,PTPN12,PTPN13,PTPRD,PTPRK,PTRH1,PURA,PXDN,RAB27A,RAB27B,RABGAP1L,RABL6,RAD23B,RAS,RASA1,RB1,RBL2,RBM19,RBM8A,RBMS1,RCOR1,RDH10,RELN,RERE,RFFL,RHEBL1,RHOA,RHOB,RHOG,ROBO4,RPP38,RPS6KA5,RPTOR,RRP8,RTCA,RTKN,RUNX1,RUNX2,S100A9,S1PR1,SATB2,SCD,SCYL1,SEC23A,SEC62,SGPL1,SH3BP4,SHROOM2,SIGMAR1,SLC12A4,SLC1A4,SLC25A1,SLC25A13,SLC25A24,SLC25A32,SLC38A1,SLC38A2,SLC4A10,SLC4A7,SLC7A1,SLC7A11,SLC9A3R2,SMAD1,SMAD3,SMAD4,SMAD5,SMARCA5,SMC1A,SMO,SMOX,SNAP23,SNAP25,SOX4,SOX6,SOX9,SP1,SPARC,SPCS3,SPRYD4,SPTB,SRF,SRSF10,ST18,STAT3,STK40,STRN,STX1A,STX7,SWAP70,SYPL1,SYT4,TAF9B,TAFA1,TAGLN,TBX21,TCL1A,TDG,TENM2,TET1,TGFB3,TGFBR1,TGFBR2,THBS1,THEM4,TIMP3,TJP1,TLR3,TLR4,TLR7,TMCO1,TMED10,TMED2,TMED3,TMED7,TMEM41B,TMEM59,TMEM87A, TNF, TNFAIP2, TNFAIP3, TNFRSF10B, TNRC6A, TOP2A, TOR2A, TP53, TP63, TPM2, TPM3, TRA, TRIM71, TRIM9, TRMT1, TRPS1, TSPAN8, TTC9C, TUBB2A, TUSC2, TWIST1, TXNIP, TYMS, TYR, TYRP1, UAP1, UBE2I, UGT2B15, UGT2B17, UGT2B28, UGT8, UHRF1, UNG, USF2, USP46, UVRAG, VASN, VCAN, VEGFA, VIM, VPS39, VSIR, VSNL1, WASF3, WDR37, WEE1, WNT1, WNT5A, YY1, ZBTB7A, ZEB1, ZEB2, ZFP36L1, ZFPM2, ZNF385A</p> |
| Organismal Development | <p>ACP1,ADAMTS1,ADGRG1,AGO1,AKT1,ANPEP,ANXA1,APLN,APP,ARID4B,BACE1,BCL2,BMPR2,BCRA1,BSG,CASP3,CCND1,CD276,CD44,CD42,CDH5,CDK4,CDK6,CDKN1A,CDKN1B,CDKN2A,COL1A1,COL1A2,COL4A1,COL4A2,CREB1,CXCL12,CXCL8,DICER1,E2F1,ELAVL1,EPHA2,ERBB2,F11R,F2,FGFR3,FLI1,FOXO1,GATA6,GLI1,HIF1A,HK2,HMOX1,HOXA1,HOXD10,ID1,ID3,IGFBP3,IL10,IL1RN,IL6,IRS1,ITGA2,ITGA5,ITGB3,JAK1,KLF4,KLHL20,KLK1,KMT2A,LOXL2,MAPK14,MECP2,MET,MMP14,MMP9,MTDH,MTOR,NCL,NF1,NOTCH1,NOTCH4,NR4A2,NRAS,PDGFB,PLCG1,PPARG,PTGS2,RAS,RASA1,RB1,RHOA,RHOB,RHOG,ROBO4,RUNX1,RUNX2,S1PR1,SLC9A3R2,SMAD1,SMAD4,SP1,SPARC,SRF,STX7,TGFBR1,TGFBR2,THBS1,TIMP3,TJP1,TLR4, TNF, TP53, VEGFA, VIM, WNT5A, YY1</p> |
| Neurological Disease | <p>ABCG2,ABTB1,ACE2,ACSS1,ACVR1,ACVR1B,ACVR2A,ADAMTS1,ADAMTS14,ADAMTS15,ADAMTS2,ADAMTS5,ADGRG1,ADORA2B,ADPGK,AFF1,AGO1,AGO4,AHNAK,AICDA,AJUBA,AKT1,ALOX5,ANAPC1,ANPEP,ANXA1,AP2A1,AP2M1,APAF1,APP,AR,ARHGAP32,ARID3A,ARID3B,ARID4B,ATP2A2,ATP6V0A1,ATRX,B3GALT4,BACE1,BAP1,BAX,BBC3,BCL2,BCL2L1,BCL2L11,BCL6,BCL7A,BECN1,BMF,BMI1,BMP2K,BMPR2,</p> |

BRCA1,BSG,CALCOCO2,CAMTA1,CAPN8,CASP3,CASP6,CASP7,CASR,CBFB,CCKBR,CCN2,CCNA2,CCND1,CCNE2,CCR5,CD276,CD44,CD69,CD25A,CDC42,CDCP1,CDH5,CDK1,CDK4,CDK6,CDKAL1,CDKN1A,CDKN1B,CDKN1C,CDKN2A,CEMIP2,CES1,CHD1,CHMP2A,CLINT1,COIL,COL15A1,COL1A1,COL1A2,COL3A1,COL4A1,COL4A2,COL4A5,COL5A1,COL5A2,COL5A3,CORO2B,CPNE8,CRIM1,CRP,CRTAP,CSDE1,CSNK1D,CXCL12,CXCL8,CYP1A1,DAD1,DBI,DCX,DDIT3,DDR1,DDX19B,DDX43,DHFR,DHX57,DICER1,DIO3,DNMT1,DNMT3A,DNMT3B,DNPEP,DOCK5,DOCK7,DRD3,DSP,DTD1,DUS1L,DUSP12,E2F1,E2F2,EGR2,EIF4G2,ELAVL1,ENPP6,ENTPD4,EPHA2,ERBB2,ERBB3,ERBB4,ERBIN,ERRFI1,ESR1,EZH2,F11R,F2,FADS2,FAM3C,FANCD2,FBN1,FBXW7,FEN1,FGFR3,FHOD1,FLI1,FNDC3A,FNDC3B,FOXF2,FOXO1,FOXP3,FRG1,FURIN,FXR2,GAK,GALNT1,GAS7,GEMIN2,GEMIN7,GLI1,GNAI2,GPD2,GPR37,GRIA2,GRM3,GRPEL2,GSE1,GTPBP3,H3-3A/H3-3B,H4C1,HBP1,HDAC4,HIF1A,HIPK3,HK2,HMGA1,HMOX1,HNRNPK,HNRNPM,HOXA1,HOXB8,HOXD8,HPGD,HTR1A,HYOU1,ID2,ID3,IDH1,IFRD1,IGF1R,IGF2BP2,IGF2BP3,IGFBP3,IGFBP5,IKBKB,IKZF1,IL10,IL2RG,IL6,INSIG1,IRS1,ITCH,ITGA2,ITGA5,ITGB3,JAK1,JARID2,JPH2,JUN,KCNJ16,KLF13,KLF4,KLHL20,KLK1,KMT2A,KRAS,KRT5,KRT85,LAMC1,LATS2,LDLR,LIN28A,LIN28B,LIPA,LMNB2,LOXL2,LOXL4,LTN1,MAD2L1,MAN1A1,MAP2,MAP2K4,MAP2K7,MAP3K12,MAP4K4,MAPK12,MAPK14,MAPRE1,MAPRE2,MARCKS,MARS2,MAZ,MBNL1,MCL1,MDFI,MDM2,MECP2,MEF2D,MET,MICA,MITF,MLF1,MLLT1,MLLT11,MMP1,MMP3,MMP9,MPDU1,MTDH,MTOR,MTRR,MUC1,MYBL2,MYC,MYCN,MYD88,MYO10,MYO5A,NAV3,NCEH1,NCL,NCOA3,NEDD4,NEUROD1,NF1,NF2,NID1,NID2,NLK,NOTCH1,NOTCH4,NPR3,NR1I2,NR4A2,NRAS,NT5E,NTRK3,NUCB1,NUFIP2,NXN,OSBPL2,OSBPL8,OSBPL9,P3H1,P4HA2,PADI1,PAFAH1B2,PAK5,PARP8,PCDHB10,PDGFA,PDGFB,PEPR,PGC,PGRMC1,PHF6,PIGR,PIK3R1,PKD2,PLCG1,PLEC,PLOD2,POLD2,POLR2C,POM121/POM121C,PPARG,PPM1D,PPM1F,PPP1R7,PPP2R2A,PPP3CA,PRC1,PRDM1,PRIM1,PRRC2A,PTEN,PTGFRN,PTGS2,PTPN12,PTPN13,PTPRD,PTPRK,PTRH1,PURA,PXDN,RAB27A,RABGAP1L,RABL6,RAD23B,RAS,RASA1,RB1,RBL2,RBM19,RBM8A,RCOR1,RDH10,RELN,RERE,RHOA,RHOB,ROBO4,RPS6KA5,RPTOR,RRP8,RTKN,RUNX1,RUNX2,S100A9,S1PR1,SATB2,SCD,SCYL1,SGPL1,SH3BP4,SHROOM2,SIGMAR1,SLC12A4,SLC1A4,SLC25A13,SLC38A1,SLC38A2,SLC4A10,SLC4A7,SMAD3,SMAD4,SMC1A,SMO,SNAP25,SOX4,SOX6,SOX9,SP1,SPARC,SPCS3,SPRYD4,SPTB,SRF,ST18,STAT3,STRN,SWAP70,SYPL1,TAF9B,TAGLN,TBX21,TCL1A,TDG,TENM2,TET1,TGFB3,TGFB1,TGFB2,THBS1,THEM4,TIMP3,TJP1,TLR3,TLR4,TMCO1,TMED10,TMEM59,TMEM87A,TNF,TNFAIP2,TNFAIP3,TNFRSF10B,TNRC6A,TOP2A,TOR2A,TP53,TP63,TPM3,TRIM71,TRIM9,TRMT1,TRPS1,TSPAN8,TUBB2A,TYMS,TYR,TYRP1,UGT2B28,UGT8,UHRF1,UNG,USF2,VCAN,VEGFA,VIM,VPS39,VSIR,VSNL1,WASF3,WDR37,WEE1,WNT5A,ZBTB7A,ZEB1,ZEB2,ZFP36L1,ZFPM2

**Infectious
Diseases**

ABTB1,ACE2,ACVR2A,ADAMTS5,ADORA2B,AGO1,AGO4,AHNAK,AKT1,ALOX5,ANPEP,ANXA1,AP2A1,AP2M1,APLN,AR,ARHGAP32,ARPC3,ATAD3B,ATP2A2,ATP6V0A1,BAK1,BAX,BBC3,BCL2,BCL2L1,BCL2L11,BECN1,BMP2K,BNIP2,BRCA1,BSG,CAV2,CBX7,CCR5,CD44,CD69,CDC42,CDK4,CDKN1B,CDKN2A,CES1,CHD1,CHMP2A,CHORDC1,COL3A1,COL5A1,CORO2B,CREB1,CRIM1,CRP,CXCL12,CXCL8,CYP1A1,DCP2,DDIT3,DDR1,DHFR,DICER1,DUSP1,DUSP12,E2F2,ELAVL1,EOMES,EPHA2,ESR1,EZH2,F11R,F2,FBN1,FLI1,FOXF2,FOXP3,FSCN1,FURIN,GAK,GE MIN2,GPD2,H3-3A/H3-3B,HBP1,HDAC4,HIPK3,HMGA1,HNRNPK,HNRNPM,HPGD,HTR1A,IDH1,IGF1R,IGF2BP1,IKZF1,IL10,IL1RN,IL2RG,IL6,INSIG1,ITCH,ITGB3,JA

| | |
|------------------------------|--|
| | <p>K1,JUN,KRAS,LDLR,MAN1A1,MAP3K12,MAP4K4,MAPRE1,MARCKS,MAT2A,MCL1,MDM2,MED28,MMP9,MTOR,MYC,MYD88,NCL,NCOA3,NEDD4,NF2,PCGF1,PCTP,PGM1,PGRMC1,PLCG1,PLK1,PLOD2,PMAIP1,POLR2C,POM121/POM121C,PPARG,PPP2R2A,PPP3CA,PPP3R1,PTGS2,PURA,RBM19,RFFL,RHOB,RUNX1,S100A9,SCD,SGPL1,SH3BP4,SIGMAR1,SLC4A7,SMAD3,SNAP23,SOX4,SPARC,SPCS3,STAT3,TBX21,TGFB3,TGFBR1,TLR3,TLR4,TLR7,TMED2,TMEM41B,TNF,TNFAIP2,TNFAIP3,TNFRSF10B,TOP2A,TOR2A,TP53,TPM3,TUBB2A,TXNIP,TYMS,UA P1,UBE2I,UNG,VCAN,VEGFA,VPS39,WNT1,ZEB1,ZEB2</p> |
| Immunological Disease | <p>ABCG2,ABTB1,ADAMTS2,ADAMTS5,AHNAK,AICDA,AKAP8,AKT1,ALOX5,ANAPC1,ANPEP,ANXA1,APAF1,APP,AR,ARHGAP32,ARID3A,ATRX,AURKB,B3GALT4,BAK1,BAP1,BAX,BBC3,BCL2,BCL2L1,BCL2L11,BCL6,BCL7A,BCRA1,CAMTA1,CASP3,CASP6,CASP7,CASR,CAV2,CBFB,CBX7,CCKBR,CCNA2,CCND1,CCNE2,CCR5,CD276,CD44,CD69,CDCP1,CDK1,CDK4,CDK6,CDKN1A,CDKN1B,CDKN1C,CDKN2A,CEBPG,CES1,CHD1,COL15A1,COL1A1,COL1A2,COL3A1,COL4A1,COL4A2,COL4A5,COL5A1,COL5A2,COL8A1,CPNE8,CREB1,CRP,CSDE1,CXCL12,CXCL8,CYP1A1,DAD1,DDIT3,DDR1,DHFR,DICER1,DNMT1,DNMT3A,DSP,DUSP1,DUSP2,E2F1,E2F2,E2F3,EGR2,EIF4E,ELAVL1,EOMES,EPHA2,ERBB2,ERBB3,ERBB4,ESR1,EZH2,F11R,F2,FANCD2,FBN1,FBXO28,FBXW7,FEN1,FGFR3,FHOD1,FNDC3B,FOXO1,FOXP3,GALNT1,GEMIN2,GLI1,GNAI2,GRM3,GSE1,GYS1,H3-3A/H3-3B,H4C1,HDAC4,HIF1A,HMOX1,HNRNPM,HOXA11,HOXA7,HOXD8,ICOS,ID2,ID3,IDH1,IFIT5,IFRD1,IGF1R,IGF2BP3,IGFBP3,IGFBP5,IKKBK,IKZF1,IL10,IL1RN,IL2RG,IL6,IRS1,ITGA5,ITGB3,JAK1,JARID2,JPH2,JUN,KCNJ16,KLF13,KLF4,KLK1,KMT2A,KRAS,KRT5,KRT85,LATS2,LDLR,LIPA,LOXL2,LTN1,MAP2K4,MAP4K4,MAPK14,MAPRE1,MAZ,MCL1,MDM2,MECP2,MEF2D,MET,MICA,MITF,MLF1,MMP1,MMP14,MMP3,MM P9,MRPS24,MTOR,MUC1,MYC,MYCN,MYD88,MYLIP,NASP,NAV3,NCOA3,NEDD4,NF1,NF2,NID1,NLK,NOTCH1,NOTCH4,NR4A2,NRAS,NT5C3A,NTRK3,NXN,PAK5,PCDHB10,PDGFB,PGM1,PHF6,PIGR,PIK3R1,PIK3R3,PKD2,PLAG1,PLCG1,PLK1,PMAIP1,PNP,PPARG,PPM1D,PPP1R7,PPP2R2A,PPP3CA,PPP3R1,PPT2,PRDM1,PRIM1,PRRC2A,PTEN,PTGFRN,PTGS2,PTPN13,PTPRD,PTPRK,PXDN,RAB27A,RABGAP1L,RAS,RAS A1,RB1,RBL2,RBM19,RDH10,RELN,RERE,RHOA,RHOB,RPTOR,RUNX1,RUNX2,S100A9,S1PR1,SATB2,SEC62,SHROOM2,SIGMAR1,SLC25A24,SLC25A32,SLC4A10,SLC7A1,SLC7A11,SMAD3,SMAD4,SMAD5,SMC1A,SMO,SP1,SPARC,ST18,STAT3,STK40,STRN,SWAP70,TAGLN,TBX21,TCL1A,TENM2,TET1,TGFB3,TGFB2,THBS1,THEM4,TIMP3,TJP1,TLR3,TLR4,TLR7,TNF,TNFAIP3,TNFRSF10B,TNRC6A,TOP2A,TP53,TP63,TP M2,TRA,TRIM71,TSPAN8,TUBB2A,TWIST1,TYMS,TYR,UBE2I,VCAN,VEGFA,VIM,WEE1,WNT1,WNT5A,ZEB1,ZEB2,ZFP36L1</p> |
| Hematological Disease | <p>ABCG2,ABTB1,ADAMTS5,AHNAK,AICDA,AKAP8,AKT1,ALOX5,ANAPC1,ANPEP,ANXA1,APAF1,APP,AR,ARID3A,ATRX,AURKB,B3GALT4,BAK1,BAP1,BAX,BBC3,BCL2,BCL2L1,BCL2L11,BCL6,BCL7A,BMPR2,BCRA1,CAMTA1,CASP3,CASP7,CASR,CAV2,CBFB,CBX7,CCNA2,CCND1,CCNE2,CCR5,CD44,CD69,CDC25A,CDC42,CDCP1,CDK1,CDK4,CDK6,CDKN1A,CDKN1B,CDKN1C,CDKN2A,CHD1,COL15A1,COL1A1,COL1A2,COL3A1,COL4A1,COL4A2,COL4A5,COL5A2,CPNE8,CRP,CSDE1,CXCL12,CXCL8,CYP1A1,DAD1,DDR1,DHFR,DICER1,DNMT1,DNMT3A,DSP,DUSP2,E2F1,E2F2,E2F3,EGR2,EIF4E,ELAVL1,EOMES,EPHA2,ERBB2,ERBB3,ERBB4,ESR1,EZH2,F11R,F2,FANCD2,FBN1,FBXO28,FBXW7,FEN1,FGFR3,FHOD1,FNDC3B,FOXO1,FOXP3,GEMIN2,GLI1,GNAI2,GRM3,GSE1,GSS,GYS1,HDAC4,HIF1A,HMGA2,HMOX1,HNRNPM,HOXA11,HOXA7,HOXD8,ID2,ID3,IDH1,IFIT5,IGF1R,IGF2BP3,IGFBP3,IGFBP5,IKKBK,IKZF1,IL10,IL1RN,IL2RG,IL6,IRS1,ITGA5,ITGB3,JAK1,JARID2,JPH2,JUN,KCN</p> |

| | |
|------------------------------------|--|
| | J16,KLF4,KLK1,KMT2A,KRAS,KRT5,KRT85,LATS2,LDLR,LIPA,LOXL2,LTN1,MAP2K4,MAP4K4,MAPK14,MCL1,MDM2,MET,MICA,MITF,MMP1,MMP14,MMP9,MRPS24,MTOR,MTRR,MUC1,MYBL2,MYC,MYCN,MYD88,MYLIP,NASP,NAV3,NCOA3,NF1,NID1,NLK,NOTCH1,NOTCH4,NR4A2,NRAS,NT5C3A,NTRK3,NXN,PAK5,PARP8,PCDHB10,PDGFB,PGM1,PHF6,PIGR,PIK3R1,PIK3R3,PKD2,PLAG1,PLCG1,PLK1,PLOD2,PMAIP1,PNP,PPARG,PPM1D,PPP1R7,PPP2R2A,PPP3CA,PPP3R1,PRDM1,PRIM1,PTEN,PTGFRN,PTGS2,PTPN13,PTPRD,PTPRK,PXDN,RAS,RASA1,RB1,RBL2,RBM19,RBM8A,RDH10,RELN,RHOA,RHOB,RPTOR,RUNX1,RUNX2,S100A9,S1PR1,SATB2,SGPL1,SHROOM2,SIGMAR1,SLC12A4,SLC25A24,SLC25A32,SLC4A10,SLC7A11,SMAD3,SMAD4,SMAD5,SMC1A,SMO,SOX6,SP1,SPARC,SPTB,ST18,STAT3,STK40,STRN,SWAP70,TBX21,TCL1A,TENM2,TET1,TGFB3,TGFBR1,TGFBR2,THBS1,THEM4,TIMP3,TJP1,TLR4,TLR7,TNF,TNFAIP3,TNFRSF10B,TNRC6A,TP2A,TP53,TP63,TPM2,TRA,TRIM71,TSPAN8,TUBB2A,TWIST1,TYMS,UBE2I,VCAN,VEGFA,VIM,WEE1,WNT5A,ZBTB7A,ZEB1,ZEB2,ZFP36L1 |
| Gene Expression | ABTB1,ACVR1,ACVR1B,ACVR2A,ADAMTS5,AGO1,AGO4,AKT1,ALOX5,API5,APLN,APP,AR,ARID4B,ATRX,AURKB,BAMBI,BAP1,BAX,BCL2,BCL2L1,BCL6,BMI1,BMPR1B,BMPR2,BRCA1,CASR,CBFB,CBX7,CCKBR,CCN2,CCND1,CCR5,CD44,CDC42,CDH5,CDK1,CDK4,CDK6,CDKN1A,CDKN1B,CDKN1C,CDKN2A,CDX2,CEBPG,CHD1,COL1A1,CREB1,CRIM1,CRP,CXCL12,CXCL8,CYP1A1,DDIT3,DHFR,DICER1,DNMT1,DNMT3A,DNMT3B,DUSP1,E2F1,E2F2,E2F3,EGR2,EIF4E,EIF4EBP2,EIF4G2,EOMES,ERBB2,ERBB4,ESR1,EZH2,F2,FBXW7,FHOD1,FLI1,FOXF2,FOXO1,FOXO3,GATA6,GLI1,HBP1,HDAC4,HIF1A,HIPK3,HMGA1,HMGA2,HNRNP,KHOXA1,HOXA7,HOXD8,ID1,ID2,ID3,IGF2BP1,IGF2BP2,IGF2BP3,IGFBP3,IGFBP5,IKKBK,IKZF4,IL10,IL6,ITGA5,JAK1,JUN,KLF13,KLF4,KLF5,KMT2A,KRAS,LOXL2,MAP2K4,MAP2K7,MAP3K12,MAPK12,MAPK14,MAPK7,MAZ,MDM2,MECP2,MED28,MEF2D,MET,MITF,MLLT1,MLLT11,MMP9,MTDH,MTOR,MUC1,MYBL2,MYC,MYCN,MYD88,NCOA3,NEUROD1,NOTCH1,NOTCH4,NR1I2,NR4A2,NTRK3,PCGF1,PCTP,PDGFA,PDGFB,PHF6,PIK3R1,PIK3R3,PKD2,PLAG1,PLCG1,PLK1,POLR2C,PPARG,PPM1D,PPM1F,PPP3CA,PPP3R1,PRDM1,PTEN,PTGS2,PTPRK,PURA,RAB27A,RAS,RB1,RBL2,RCOR1,RHOA,RHOB,RHOG,RPS6KA5,RRP8,RUNX1,RUNX2,SATB2,SLC38A2,SMAD1,SMAD3,SMAD4,SMARCA5,SMO,SOX4,SOX9,SP1,SRF,ST18,STAT3,TAF9B,TAGLN,TBX21,TGFB3,TGFBR1,TGFBR2,TLR3,TLR4,TNF,TNFAIP3,TNFRSF10B,TNRC6A,TP53,TP63,TRIM71,TRPS1,TWIST1,TYMS,UAP1,UBE2I,UHRF1,USF2,VEGFA,VP39,VSIR,WNT1,WNT5A,YY1,ZBTB7A,ZEB1,ZEB2,ZFP36L1,ZFPM2 |
| Connective Tissue Disorders | ABCG2,ACVR1,ADAMTS1,ADAMTS14,ADAMTS15,ADAMTS2,ADAMTS5,AKT1,ALOX5,ANXA1,APAF1,APP,AR,ARHGAP32,ATRX,B3GALT4,BAP1,BAX,BCL2,BCL2L1,BCL6,BMI1,BMPR1B,CASP3,CASP6,CCKBR,CCN2,CCR5,CD276,CD44,CD69,CDC42,CDK4,CDK6,CDKN1B,CDKN2A,CEBPG,CES1,CHD1,COL1A1,COL1A2,COL3A1,COL4A1,COL4A5,COL5A1,COL5A2,COL8A1,CREB1,CRP,CRTAP,CXCL12,CXCL8,DAD1,DDIT3,DDR1,DHFR,DNMT1,DNMT3A,DRD3,DSP,DUSP1,DUSP2,E2F2,EIF4G2,EOMES,EPHA2,ERBB2,ERBB3,ERBB4,ESR1,F11R,F2,FBN1,FGF16,FGFR3,FLI1,FOXO1,FOXP3,GALNT1,GLI1,GNAI2,GSS,H3-3A/H3-3B,H4C1,HDAC4,HIF1A,HMOX1,HNRNP,KHOXA11,HOXA7,HPGD,ICOS,ID2,IDH1,IFRD1,IGF1R,IGFBP3,IGFBP5,IKKBK,IKZF1,IL10,IL1RN,IL6,IRS1,ITGA5,ITGB3,JAK1,JUN,KLF13,KRAS,KRT5,LMNB2,MAP4K4,MAPRE1,MAZ,MCL1,MDM2,MECP2,MET,MICA,MITF,MLF1,MMP1,MMP14,MMP3,MMP9,MTOR,MUC1,MYC,MYCN,NEDD4,NF1,NF2,NOTCH1,NOTCH4,NR4A2,NRAS,NT5E,P3H1,PIK3R1,PLEC,PLOD2,PPARG,PPP1R7,PPP3CA,PPP3R1,PPT2,PRDM1,PRIM1,PRRC2A,PTEN,PTGS2,PURA,PXDN,RAB27A,RABGAP1L,RAS,RB1,RBM8A,RDH10,RHOA,RUNX1,R |

| | |
|---|---|
| | UNX2,S100A9,S1PR1,SATB2,SEC62,SGPL1,SIGMAR1,SLC1A4,SLC7A1,SLC7A11,SMAD3,SMO,SNAP25,SOX4,SOX6,SOX9,SP1,SPARC,STAT3, TAGLN,TGFB3,TGFB3,TGFB3,THBS1,TIMP3,TJP1,TLR3,TLR4,TLR7,TMCO1,TNF,TNFAIP3,TNFRSF10B,TP53,TP63,TPM2,TRA,TRPS 1,TUBB2A,TWIST1,TYMS,TYR,VCAN,VEGFA,VIM,WDR37,WNT1,WNT5A,ZBTB7A |
| Connective Tissue Development and Function | ACVR1,ACVR2A,AKT1,ANPEP,AR,AURKB,BCL2,BCL2L1,BMI1,BMPR1B,BMPR2,CASR,CCN2,CCND1,CCNE1,CD44,CDK1,CDK4,CDK6,CDKN1A ,CDKN1B,CDKN2A,COL1A1,CXCL12,CXCL8,DICER1,DNMT1,DUSP1,E2F1,E2F2,E2F3,EZH2,F2,FBN1,FBXW7,FGFR3,FLI1,FOXO1,GAS7,GLI1,H MGA1,HMGA2,ID1,ID2,ID3,IGF1R,IGFBP3,IGFBP5,IKZF4,IL10,IL6,ITGA5,KLF4,KRAS,MAPK12,MAPK14,MDM2,MET,MMP9,MTOR,MYBL2, MYC,NID2,NOTCH1,NRAS,OSBPL8,PDGFA,PDGFB,PLOD2,PPARG,PPM1D,PTEN,PTGS2,PTPRK,RAS,RB1,RBL2,RHOA,RUNX1,RUNX2,SMAD3 ,SMO,SOX6,SOX9,STAT3,TGFB2,TLR4,TNF,TNFRSF10B,TNRC6A,TP53,TP63,TWIST1,UHRF1,UNG,VCAN,VEGFA,WNT1,WNT5A,ZBTB7A,ZF P36L1,ZFPM2 |
| Cellular Movement | ACP1,ACVR1,ADAMTS1,ADAMTS15,ADAMTS5,AHNAK,AKT1,ANPEP,ANXA1,AP2M1,APLN,APP,AR,ATP2A2,ATP6V0A1,BCL2,BCL2L1,BMI1, BMPR2,BRCA1,BSG,CASP3,CASR,CCKBR,CCN2,CCNA2,CCND1,CCR5,CD44,CDC42,CDCP1,CDH5,CDK1,CDK4,CDK6,CDKN1A,CDKN1B,CDKN 2A,CDX2,CEMIP2,CES1,CHD1,COL1A1,COL1A2,COL4A2,CRP,CXCL12,CXCL8,DCX,DDR1,DICER1,DNMT1,DNMT3B,DOCK5,DSP,DUSP1,EIF4E ,ELAVL1,ELMO2,EPHA2,ERBB2,ERBB3,ERBB4,ESR1,EZH2,F11R,F2,FBN1,FBXW7,FGF16,FGFR3,FHOD1,FOXF2,FOXO1,FOXP3,FSCN1,FURIN, GATA6,GLI1,GNAI2,GRM3,GSE1,HBP1,HIF1A,HMGA1,HMGA2,HMOX1,HNRNP,K,HOTAIR,HOXA1,HOXA11,HOXA7,HOXD10,ICOS,ID1,ID2,I D3,IGF1R,IGF2BP1,IGF2BP3,IGFBP3,IGFBP5,IKZF1,IL10,IL6,IRS1,ITCH,ITGA2,ITGA5,ITGB3,JAK1,JUN,KLF4,KLF5,KLHL20,KMT2A,KRAS,KRT1 9,LIN28B,LINC00472,LOXL2,MAP2K7,MAP4K4,MAPK12,MAPK14,MAPK7,MAPRE1,MAPRE2,MARCKS,MAZ,MCL1,MDM2,MECP2,MEF2D, MET,MITF,MLLT11,MMP1,MMP14,MMP3,MMP9,MTDH,MTOR,MUC1,MYC,MYCN,MYD88,MYO10,NAV3,NCL,NCOA3,NEDD4,NEUROD1, NF1,NF2,NOTCH1,NOTCH4,NR1I2,NR4A2,NRAS,NTRK3,NUCB1,PDGFA,PDGFB,PIGR,PIK3R1,PLCG1,PLK1,PPARG,PPM1F,PPP2R2A,PPP3CA ,PTEN,PTGS2,PTPN12,PTPRK,RAS,RASA1,RB1,RELN,RFFL,RHOA,RHOB,RHOG,RPTOR,RUNX1,RUNX2,S100A9,S1PR1,SATB2,SH3BP4,SIGMA R1,SLC12A4,SLC7A11,SLC9A3R2,SMAD1,SMAD3,SMAD4,SMO,SNAP23,SOX4,SOX9,SP1,SPARC,SRF,STAT3,STRN,TAGLN,TGFB3,TGFB3,TGFB3,THBS1,TIMP3,TJP1,TLR3,TLR4,TNF,TNFRSF10B,TP53,TP63,TPM2,TPM3,TRPS1,TWIST1,UBE2I,VCAN,VEGFA,VIM,VSIR,WASF3,WNT 1,WNT5A,YY1,ZBTB7A,ZEB1,ZEB2 |
| Cellular Growth and Proliferation | ABCG2,ABTB1,ACP1,ACVR1,ACVR2A,ADAMTS1,ADAMTS15,ADORA2B,AGO1,AGO4,AHNAK,AJUBA,AKT1,ANPEP,ANXA1,APAF1,APLN,APP ,AR,ARID4B,ATP2A2,ATP6V0A1,AURKB,BAK1,BAMBI,BAP1,BAX,BBC3,BCL2,BCL2L1,BCL2L11,BCL6,BECN1,BMF,BMI1,BMPR1B,BMPR2,BR CA1,BSG,CASP3,CASP7,CASR,CBFB,CBX7,CCKBR,CCN2,CCNA2,CCND1,CCNE1,CCNE2,CCR5,CD276,CD44,CD69,CDC25A,CDC42,CDCP1,CD H5,CDK1,CDK4,CDK6,CDKN1A,CDKN1B,CDKN1C,CDKN2A,CDX2,CEMIP2,CES1,CHD1,COL1A1,COL4A2,CREB1,CSNK1D,CXCL12,CXCL8,CYP1 A1,CDX,DDIT3,DDR1,DDX43,DICER1,DNMT1,DNMT3B,DUSP1,E2F1,E2F3,EGR2,EIF4E,EIF4EBP2,ELAVL1,EPHA2,ERBB2,ERBB3,ERBB4,ERBI N,ERRFI1,ESR1,EZH2,F11R,F2,FADS2,FBXW7,FEN1,FGF16,FGFR3,FLI1,FOXF2,FOXO1,FOXP3,FSCN1,GATA6,GLI1,GRM3,GSE1,H3-3A/H3- 3B,H4C1,HBP1,HDAC4,HIF1A,HK2,HMGA1,HMGA2,HMOX1,HNRNP,K,HOTAIR,HOXA1,HOXA11,HOXA7,HPGD,ICOS,ID1,ID2,ID3,IDH1,IGF1 |

| | |
|-----------------------------|---|
| | R,IGF2BP1,IGF2BP3,IGFBP3,IGFBP5,IKKBK,IKZF1,IL10,IL1RN,IL2RG,IL6,IRS1,ITCH,ITGA2,ITGA5,ITGB3,JAK1,JARID2,JUN,KLF4,KLF5,KLHL20,KMT2A,KRAS,KRT19,LAMC1,LATS2,LIN28A,LIN28B,LINC00472,LOXL2,LOXL4,MAD2L1,MAP2K4,MAP2K7,MAP4K4,MAPK12,MAPK14,MAPK7,MAPRE1,MAZ,MCL1,MDM2,MED28,MET,MICA,MITF,MLLT11,MMP1,MMP14,MMP9,MTDH,MTOR,MUC1,MYBL2,MYC,MYCN,MYD88,NASP,NCL,NCOA3,NEDD4,NF1,NF2,NOTCH1,NOTCH4,NR112,NR4A2,NRAS,NT5C3A,NTRK3,P4HA2,PCGF1,PDGFA,PDGFB,PGRMC1,PHF6,PIK3R1,PIK3R3,PLAG1,PLCG1,PLK1,PLOD2,PNP,PPARG,PRDM1,PTEN,PTGS2,PTPN12,PTPN13,PTPRK,PURA,RABL6,RAS,RB1,RBL2,RFFL,RHOA,RHOB,RPS6KA5,RPTOR,RTKN,RUNX1,RUNX2,S100A9,S1PR1,SATB2,SCD,SEC62,SH3BP4,SLC25A13,SLC7A1,SLC7A11,SLC9A3R2,SMAD1,SMAD3,SMAD4,SMAD5,SMARCA5,SMC1A,SMO,SMOX,SOX4,SOX6,SOX9,SP1,SPARC,SRF,STAT3,TAF9B,TBX21,TCL1A,TDG,TGFB3,TGFBR1,TGFBR2,THBS1,THEM4,TIMP3,TLR3,TLR4,TLR7,TNF,TNFAIP3,TNFRSF10B,TNRC6A,TP53,TP63,TRPS1,TUBB2A,TUSC2,TWIST1,TXNIP,TYMS,TYR,TYRP1,UAP1,UBE2I,UGT2B15,UGT2B17,UHRF1,UNG,USF2,UVRAG,VCAN,VEGFA,VIM,WNT1,WNT5A,YY1,ZBTB7A,ZEB1,ZEB2,ZFP36L1 |
| Cellular Development | ABTB1,ACP1,ACVR1,ACVR2A,ADAMTS1,ADAMTS15,ADORA2B,AGO1,AGO4,AHNAK,AJUBA,AKT1,ANPEP,ANXA1,APAF1,APLN,APP,AR,ARID4B,ATP2A2,ATP6V0A1,AURKB,BAK1,BAMBI,BAP1,BAX,BBC3,BCL2,BCL2L1,BCL2L11,BCL6,BECN1,BMF,BMI1,BMPR1B,BMPR2,BCRA1,BSG,CASP3,CASP7,CASR,CBFB,CBX7,CCKBR,CCN2,CCNA2,CCND1,CCNE1,CCNE2,CCR5,CD276,CD44,CD69,CDC42,CDCP1,CDH5,CDK1,CDK4,CDK6,CDKN1A,CDKN1B,CDKN1C,CDKN2A,CDX2,CEMIP2,CES1,CHD1,COL1A1,COL4A1,COL4A2,CREB1,CSNK1D,CXCL12,CXCL8,CYP1A1,DCX,DDIT3,DDR1,DDX43,DICER1,DNMT1,DNMT3B,DSP,DUSP1,E2F1,E2F2,E2F3,EGR2,EIF4E,EIF4EBP2,ELAVL1,EPHA2,ERBB2,ERBB3,ERBB4,ERBIN,ERRFI1,ESR1,EZH2,F11R,F2,FADS2,FBN1,FBXW7,FEN1,FGF16,FGFR3,FLI1,FOXF2,FOXO1,FOXP3,FSCN1,GAS7,GATA6,GLI1,GRM3,GSE1,H3-3A/H3-3B,H4C1,HBP1,HDAC4,HIF1A,HK2,HMGA1,HMGA2,HMOX1,HNRNPK,HNRNPM,HOTAIR,HOXA1,HOXA11,HOXA7,HPGD,ICOS,ID1,ID2,ID3,IGH1,IGF1R,IGF2BP1,IGF2BP3,IGFBP3,IGFBP5,IKKBK,IKZF1,IKZF4,IL10,IL1RN,IL2RG,IL6,IRS1,ITCH,ITGA2,ITGA5,ITGB3,JAK1,JARID2,JUN,KLF4,KLF5,KLHL20,KMT2A,KRAS,KRT19,LATS2,LIN28A,LIN28B,LINC00472,LOXL2,LOXL4,MAD2L1,MAP2K4,MAP2K7,MAP3K12,MAP4K4,MAPK12,MAPK14,MAPK7,MAPRE1,MAZ,MCL1,MDM2,MED28,MET,MICA,MITF,MLLT11,MMP1,MMP14,MMP9,MTDH,MTOR,MUC1,MYBL2,MYC,MYCN,MYD88,NASP,NCL,NCOA3,NEDD4,NF1,NF2,NID2,NOTCH1,NOTCH4,NR4A2,NRAS,NT5C3A,NTRK3,OSBPL8,P4HA2,PCGF1,PDGFA,PDGFB,PGRMC1,PHF6,PIK3R1,PIK3R3,PLAG1,PLCG1,PLK1,PLOD2,PNP,PPARG,PPM1D,PRDM1,PTEN,PTGS2,PTPN12,PTPN13,PTPRK,PURA,RABL6,RAS,RB1,RBL2,RELN,RFFL,RHOA,RHOB,RPS6KA5,RPTOR,RTKN,RUNX1,RUNX2,S100A9,S1PR1,SATB2,SCD,SEC62,SH3BP4,SLC25A13,SLC7A1,SLC7A11,SLC9A3R2,SMAD1,SMAD3,SMAD4,SMAD5,SMARCA5,SMC1A,SMO,SMOX,SOX4,SOX6,SOX9,SP1,SPARC,SRF,STAT3,TAF9B,TAGLN,TBX21,TCL1A,TDG,TGFB3,TGFBR1,TGFBR2,THBS1,THEM4,TIMP3,TLR3,TLR4,TLR7,TNF,TNFAIP3,TNFRSF10B,TNRC6A,TP53,TP63,TRPS1,TUBB2A,TUSC2,TWIST1,TXNIP,TYMS,TYR,TYRP1,UAP1,UBE2I,UGT2B15,UGT2B17,UHRF1,UNG,USF2,UVRAG,VCAN,VEGFA,VIM,WNT1,WNT5A,YY1,ZBTB7A,ZEB1,ZEB2,ZFP36L1,ZFPM2 |
| Cell | BAK1,BCL2,BCL2L1,CASP3,CCND1,CCNE1,CD44,CDC42,CDCP1,CDKN1A,CDKN1C,CDKN2A,CXCL12,DDIT3,DICER1,ERBB2,ESR1,F11R,FBXW |

| | |
|-----------------------------------|--|
| Morphology | 7,FGFR3,GALNT1,ID1,IGF1R,IL6,KLF4,KRAS,KRT5,LOXL2,MAPK14,MDM2,MEF2D,MITF,MMP14,MTOR,MYC,NF1,NR1I2,PPM1F,PTEN,RB1,RBL2,RHOA,RHOB,SMAD4,STAT3,STRN,TIMP3,TNF,TP53,TP63,TPM3,TWIST1,VIM |
| Cell Death and Survival | ABCG2,ACP1,ACVR1B,ACVR2A,ADORA2B,AKAP8,AKT1,ALOX5,ANAPC1,ANPEP,ANXA1,AP2M1,APAF1,API5,APP,AR,ARID3B,ATP2A2,ATRX,AURKB,BACE1,BAK1,BAP1,BAX,BBC3,BCL2,BCL2L1,BCL2L11,BCL6,BECN1,BMF,BMI1,BMPR1B,BMPR2,BNIP2,BRCA1,BSG,CASP3,CASP6,CASP7,CASR,CCN2,CCNA2,CCND1,CCNE1,CCR5,CD44,CD69,CDC25A,CDC42,CDCP1,CDK1,CDK6,CDKN1A,CDKN1B,CDKN1C,CDKN2A,CDX2,CEES1,COL1A1,COL4A2,CREB1,CRP,CXCL12,CXCL8,DDIT3,DDR1,DDX43,DDFA,DHFR,DICER1,DNMT1,DNMT3B,DSP,DUSP1,DUSP12,DUSP2,E2F1,E2F3,EIF4E,EIF4G2,ELAVL1,EPHA2,ERBB2,ERBB3,ERBB4,ERRF1,ESR1,EZH2,F2,FANCD2,FEN1,FGFR3,FLI1,FOXO1,FOXP3,FURIN,GAK,GAS7,GATA6,GLI1,GPR37,GRIA2,GRM3,HBP1,HDAC4,HIF1A,HIPK3,HK2,HMGA1,HMGA2,HMOX1,HNRNPK,HOTAIR,HOXA1,HOXA11,HYOU1,ICOS,ID1,ID2,ID3,IDH1,IFRD1,IGF1R,IGF2BP1,IGF2BP2,IGF2BP3,IGFBP3,IGFBP5,IKBKB,IKZF1,IL10,IL1RN,IL6,INSIG1,IRS1,ITCH,ITGA2,ITGA5,ITGB3,JAK1,JUN,KLF4,KLF5,KLHL20,KMT2A,KRAS,KRT19,LAMP2,LATS2,LIN28A,LINC00472,MAD2L1,MAP2K4,MAP2K7,MAP3K12,MAP4K4,MAPK12,MAPK14,MAPK7,MAT2A,MCL1,MDM2,MED28,MET,MITF,MLL1,MMP14,MPMP9,MRM1,MTDH,MTOR,MUC1,MYBL2,MYC,MYCN,MYD88,NASP,NCL,NCOA3,NEDD4,NEUROD1,NF1,NF2,NLK,NOTCH1,NOTCH4,NR1I2,NR4A2,NRAS,NT5C3A,NT5E,NTRK3,OSBPL8,PAK5,PDGFA,PDGFB,PERP,PGRMC1,PIGR,PIK3R1,PLCG1,PLK1,PMAIP1,PPARG,PPM1D,PPM1F,PPP2R2A,PPP3R1,PRDM1,PTEN,PTGS2,PTPA,PTPN13,PTPRK,RABL6,RAD23B,RAS,RASA1,RB1,RBM8A,RHOA,RHOB,RHOG,RPTOR,RTKN,RUNX1,RUNX2,S100A9,S1PR1,SATB2,SCD,SGPL1,SHROOM2,SIGMAR1,SLC7A1,SLC7A11,SLC9A3R2,SMAD1,SMAD3,SMAD4,SMC1A,SMO,SMOX,SOX4,SOX6,SOX9,SP1,SPARC,SRF,STAT3,TAF9B,TCL1A,TDG,TGFB3,TGFBR1,TGFBR2,THBS1,TIMP3,TLR3,TLR4,TLR7,TMED10,TNF,TNFAIP3,TNFRSF10B,TP53,TP63,TRA,TRPS1,TUSC2,TWIST1,TYMS,TYR,UBE2I,UHRF1,UNG,VCAN,VEGFA,VSNL1,WEE1,WNT1,WNT5A,YY1,ZBTB7A,ZEB1 |
| Cell Cycle | ABCG2,ABTB1,ACVR1,ACVR1B,AJUBA,AKAP8,AKT1,ALOX5,AR,AURKB,BAP1,BAX,BCL2,BCL2L1,BCL6,BMI1,BMPR1B,BMPR2,BRCA1,CCKBR,CCNA2,CCND1,CCNE1,CCNE2,CD44,CDC25A,CDC42,CDK1,CDK4,CDK6,CDKN1A,CDKN1B,CDKN1C,CDKN2A,CEP72,CES1,CHMP2A,COL1A1,CREB1,CSNK1D,CXCL12,CXCL8,CYP1A1,DCX,DDIT3,DICER1,DNMT1,DNMT3B,DRD3,DTD1,DUSP1,E2F1,E2F2,E2F3,EIF4E,EIF4G2,ELAVL1,ERBB2,ERBB3,ESR1,EZH2,F2,FANCD2,FEN1,FOX2,FOXO1,FOXP3,GAK,GAS7,GATA6,GLI1,HBP1,HDAC4,HIF1A,HMGA1,HMGA2,HMOX1,HOTAIR,HPGD,ID1,ID2,ID3,IDH1,IGF1R,IGF2BP1,IGFBP3,IGFBP5,IKBKB,IL10,IL6,ITGA2,ITGA5,ITGB3,JUN,KLF13,KLF4,KMT2A,KRAS,KRT19,LATS2,LIN28A,MAD2L1,MAP2K7,MAP3K12,MAPK12,MAPK14,MAPK7,MAPRE1,MCL1,MDM2,MECP2,MET,MITF,MLF1,MMP9,MTDH,MTOR,MUC1,MYBL2,MYC,MYCN,NASP,NCOA3,NF1,NF2,NID2,NOTCH1,NR1I2,NR4A2,NRAS,PDGFB,PHF6,PKD2,PLCG1,PLK1,PLOD2,POM121/POM121C,PPARG,PPM1D,PPP2R2A,PRDM1,PRIM1,PTEN,PTPRK,RABL6,RAS,RB1,RBL2,RFFL,RHOA,RHOB,RPS6KA5,RPTOR,RUNX1,RUNX2,SATB2,SHROOM2,SMAD3,SMAD4,SMC1A,SMO,SOX6,SOX9,SP1,SPARC,SRF,STAT3,TAGLN,TET1,TGFBR1,THBS1,TLR4,TNF,TNFAIP3,TNFRSF10B,TNRC6A,TP53,TP63,TUSC2,TWIST1,TXNIP,TYMS,UBE2I,UHRF1,UNG,USF2,VEGFA,WEE1,WNT1,WNT5A,ZBTB7A,ZEB1,ZEB2 |
| Cell-To-Cell Signaling and | ABCG2,ACP1,AKT1,ALOX5,ANXA1,APP,AR,BCL2,BCL2L1,BCL6,BMI1,BMPR1B,BMPR2,BSG,CASP3,CASP7,CCND1,CCR5,CD44,CDC42,CDCP1,CDK6,CDKN1A,CDKN2A,COL1A2,CXCL12,CXCL8,DDR1,DNMT3B,DSP,E2F1,EPHA2,ERBB2,ERBB3,ESR1,F11R,F2,FOXO1,FSCN1,GLI1,HIF1A, |

| | |
|---|--|
| Interaction | HMOX1,ICOS,IGF1R,IGFBP3,IL10,IL1RN,IL2RG,IL6,IRS1,ITGA2,ITGA5,ITGB3,JAK1,JUN,LATS2,MAD2L1,MAPK14,MAPK7,MARCKS,MCL1,ME T,MMP1,MMP14,MMP3,MMP9,MTOR,MUC1,MYC,NCL,NF2,NID1,NOTCH1,NR1I2,PIK3R1,PLCG1,PPARG,PTEN,PTGS2,RASA1,RHOA,RPT OR,S1PR1,SIGMAR1,SMAD3,SMAD4,SMO,STAT3,STX1A,TGFBR1,THBS1,TIMP3,TJP1,TLR4,TNF,TNFRSF10B,TP53,TP63,TWIST1,UB E2I,VCAN,VEGFA,VIM,WNT5A,ZEB1,ZEB2 |
| Cardiovascular System Development and Function | ACP1,ADAMTS1,ADGRG1,AGO1,AKT1,ANPEP,ANXA1,APLN,APP,ARID4B,BACE1,BCL2,BMPR2,BRCA1,BSG,CASP3,CCND1,CD276,CD44,CD C42,CDH5,CDK4,CDK6,CDKN1A,CDKN1B,CDKN2A,COL1A1,COL1A2,COL4A1,COL4A2,CREB1,CXCL12,CXCL8,DICER1,DOCK5,E2F1,ELAVL1,E PHA2,ERBB2,F11R,F2,FBXW7,FGFR3,FLI1,FOXO1,GATA6,GLI1,HIF1A,HK2,HMOX1,HOXA1,HOXD10,ID1,ID3,IGFBP3,IL10,IL1RN,IL6,IRS1,IT GA2,ITGA5,ITGB3,JAK1,KLF4,KLHL20,KLK1,KMT2A,LOXL2,MAPK12,MAPK14,MDM2,MECP2,MET,MMP14,MMP9,MTDH,MTOR,NCL,NF1, NOTCH1,NOTCH4,NR4A2,NRAS,PDGFB,PLCG1,PPARG,PTGS2,RAS,RASA1,RB1,RHOA,RHOB,RHOG,ROBO4,RUNX1,RUNX2,S1PR1,SLC9A3R 2,SMAD1,SMAD3,SMAD4,SP1,SPARC,SFR,STAT3,STX7,TGFBR3,TGFBR1,TGFBR2,THBS1,TIMP3,TJP1,TLR4,TNF,TP53,VEGFA,VIM,WNT5A,YY 1 |
| Cardiovascular Disease | ANXA1,APP,AR,BCL2,BCL2L1,BCL6,BMPR1B,BMPR2,BRCA1,CASR,CCN2,CCND1,CCNE1,CCR5,CD69,CDK1,CDKN1A,CDKN1B,CDKN2A,CEBP G,COL1A1,COL1A2,COL3A1,COL4A1,COL5A1,COL5A2,CRP,CXCL12,DAD1,DDR1,DHFR,DICER1,DNMT1,DNMT3A,DRD3,DSP,ELMO2,ERBB2 ,ERBB3,ESR1,EZH2,F2,FANCD2,FBN1,FBXW7,FGFR3,FURIN,GATA6,GNAI2,GPR37,GSS,HIF1A,HMOX1,HTR1A,IDH1,IGF1R,IGFBP3,IGFBP5,I L10,IL1RN,IL2RG,IL6,IRS1,ITGA5,ITGB3,JAK1,JPH2,JUN,KLF4,KLF5,KLK1,KMT2A,KRAS,LAMC1,LAMP2,LDLR,MAP4K4,MAT2A,MDM2,MET, MMP3,MMP9,MTOR,MTRR,MYC,NF1,NOTCH1,NOTCH4,NR4A2,NRAS,NT5C3A,NT5E,PAK5,PDGFB,PIK3R1,PLCG1,PLEC,PLK1,PPARG,PPP3 CA,PPP3R1,PRDM1,PRIM1,PTEN,PTGS2,PTPN13,PTPRD,RASA1,RB1,RPTOR,RUNX1,S100A9,SIGMAR1,SLC12A4,SLC7A11,SMAD1,SMAD3, SMAD4,SMO,SPTB,STAT3,TET1,TGFBR3,TGFBR1,TGFBR2,THBS1,TIMP3,TJP1,TNF,TNFAIP3,TNRC6A,TP53,TUBB2A,TYMS,VCAN,VEG FA,VIM,VSNL1,ZEB2,ZFPM2 |
| Cancer | AARSD1,ABCG2,ABTB1,ACBD3,ACE2,ACP1,ACSS1,ACVR1,ACVR1B,ACVR2A,ADAMTS1,ADAMTS14,ADAMTS15,ADAMTS2,ADAMTS5,ADGR G1,ADORA2B,ADPGK,AFF1,AGO1,AGO4,AHNAK,AICDA,AJUBA,AKAP8,AKT1,ALOX5,ANAPC1,ANAPC16,ANPEP,ANXA1,AP2A1,AP2M1,APA F1,APIS,APLN,APP,AR,ARHGAP32,ARID3A,ARID3B,ARID4B,ATAD3B,ATP2A2,ATP6AP1L,ATP6V0A1,ATP6V1F,ATRX,AURKB,B3GALT4,BACE 1,BAK1,BAMBI,BAP1,BAX,BBC3,BCL2,BCL2L1,BCL2L11,BCL6,BCL7A,BECN1,BMF,BMI1,BMP2K,BMPR1B,BMPR2,BNIP2,BRCA1,BSG,C11orf 58,CALCOCO2,CAMTA1,CAPG,CAPN8,CARHSP1,CASP3,CASP6,CASP7,CASR,CAV2,CBFB,CBLN2,CBX7,CCDC25,CCKBR,CCN2,CCNA2,CCND1, CCNE1,CCNE2,CCR5,CD276,CD44,CD69,CDC25A,CDC42,CDCP1,CDH5,CDIPT,CDK1,CDK4,CDK6,CDKAL1,CDKN1A,CDKN1B,CDKN1C,CDKN2 A,CDX2,CEBPG,CEMIP2,CEP72,CES1,CHD1,CHMP2A,CHORDC1,CIAO2A,CLINT1,CNOT8,CNOT9,COIL,COL15A1,COL1A1,COL1A2,COL3A1,C OL4A1,COL4A2,COL4A5,COL5A1,COL5A2,COL5A3,COL8A1,COMMD9,CORO2B,CPNE8,CREB1,CRIM1,CRP,CRTP,CSDE1,CSNK1D,CXCL12, CXCL8,CYP1A1,DAD1,DBI,DCP2,DCX,DDIT3,DDR1,DDX19B,DDX43,DDFA,DHFR,DHX57,DICER1,DIO3,DNMT1,DNMT3A,DNMT3B,DNPEP,D OCK5,DOCK7,DRD3,DSP,DTD1,DUS1L,DUSP1,DUSP12,DUSP2,DUSP23,E2F1,E2F2,E2F3,EGR2,EIF3J,EIF4E,EIF4EBP2,EIF4G2,ELAVL1,ELMO |

2,ELMOD2,ENPP6,ENTPD4,EOMES,EPHA2,ERBB2,ERBB3,ERBB4,ERBIN,ERRFI1,ESR1,EZH2,F11R,F2,FADS2,FAM3C,FANCD2,FBN1,FBXO28,FBXW7,FEN1,FGF16,FGFR3,FHOD1,FLI1,FNDC3A,FNDC3B,FOXF2,FOXO1,FOXP3,FRAT2,FRG1,FSCN1,FURIN,FXR2,GAK,GALNT1,GALNT7,GAS7,GATA6,GEMIN2,GEMIN7,GLI1,GNAI2,GPD2,GPR160,GPR37,GRIA2,GRM3,GRPEL2,GSE1,GSS,GTPBP3,GYS1,H3-3A/H3-3B,H4C1,HBP1,HDAC4,HIF1A,HIPK3,HK2,HMGA1,HMGA2,HMGN3,HMOX1,HNRNPK,HNRNPM,HOTAIR,HOXA1,HOXA11,HOXA7,HOXB8,HOXC8,HOXD10,HOXD8,HPGD,HTR1A,HYOU1,ICOS,ID1,ID2,ID3,IDH1,IFIT5,IFRD1,IGF1R,IGF2BP1,IGF2BP2,IGF2BP3,IGFBP3,IGFBP5,IKBKB,IKZF1,IKZF4,IL10,IL1RN,IL2RG,IL6,INSIG1,IPO4,IRS1,ITCH,ITGA2,ITGA5,ITGB3,JAK1,JARID2,JPH2,JUN,KCNJ16,KCTD3,KLF13,KLF4,KLF5,KLHL20,KLK1,KLK10,KMT2A,KRAS,KRT19,KRT5,KRT7,KRT85,LAMC1,LAMP2,LATS2,LDLR,LIN28A,LIN28B,LINC00472,LIPA,LMNB2,LOXL2,LOXL4,LRRC8C,LTN1,MAD2L1,MAN1A1,MAP2,MAP2K4,MAP2K7,MAP3K12,MAP4K4,MAPK12,MAPK14,MAPK7,MAPRE1,MAPRE2,MARCKS,MARS2,MAT2A,MAZ,MBNL1,MCL1,MDFI,MDM2,MECP2,MED28,MEF2D,MET,MICA,MITF,MLF1,MLLT1,MLLT11,MMP1,MMP14,MMP3,MPDU1,MRPS24,MRPS33,MTDH,MTOR,MTPN,MTRR,MUC1,MYBL2,MYC,MYCN,MYD88,MYLIP,MYO10,MYO5A,NAPG,NASP,NAV3,NC EH1,NCL,NCOA3,NDUFA4,NEDD4,NEUROD1,NF1,NF2,NID1,NID2,NLK,NOTCH1,NOTCH4,NPR3,NR1I2,NR4A2,NRAS,NT5C3A,NT5E,NTRK3,NUCB1,NUFIP2,NXN,OSBPL2,OSBPL8,OSBPL9,OTULINL,P3H1,P4HA2,PADI1,PAFAH1B2,PAK5,PARP8,PCDHB10,PCGF1,PCTP,PDGFA,PDGFB,PERP,PEX11B,PGC,PGM1,PGRMC1,PHF6,PIGR,PIK3R1,PIK3R3,PKD2,PLAG1,PLCG1,PLEC,PLK1,PLOD2,PMAIP1,PNP,POLD2,POLR2C,POM121/POM121C,PPARG,PPIC,PPM1D,PPM1F,PPP1R7,PPP2R2A,PPP3CA,PPP3R1,PPT2,PRC1,PRDM1,PRIM1,PRPF40A,PRRC2A,PTEN,PTGFRN,PTGS2,PTPA,PTPN12,PTPN13,PTPRD,PTPRK,PTRH1,PURA,PXDN,RAB27A,RAB27B,RABGAP1L,RABL6,RAD23B,RAS,RASA1,RB1,RBL2,RBM19,RBM8A,RBMS1,RCOR1,RDH10,RELN,RERE,RFFL,RHEBL1,RHOA,RHOB,RHOG,ROBO4,RPP38,RPS6KA5,RPTOR,RRP8,RTCA,RTKN,RUNX1,RUNX2,S100A9,S1PR1,SATB2,SCD,SCYL1,SEC23A,SEC62,SGPL1,SH3BP4,SHROOM2,SIGMAR1,SLC12A4,SLC1A4,SLC25A1,SLC25A13,SLC25A24,SLC25A32,SLC38A1,SLC38A2,SLC4A10,SLC4A7,SLC7A1,SLC7A11,SLC9A3R2,SMAD1,SMAD3,SMAD4,SMAD5,SMARCA5,SMC1A,SMO,SMOX,SNAP23,SNAP25,SOX4,SOX6,SOX9,SP1,SPARC,SPCS3,SPRYD4,SPTB,SRF,SRSF10,ST18,STAT3,STK40,STRN,STX1A,STX7,SWAP70,SYPL1,SYT4,TAF9B,TAFA1,TAGLN,TBX21,TCL1A,TDG,TENM2,TET1,TGFB3,TGFBR1,TGFBR2,THBS1,THEM4,TIMP3,TJP1,TLR3,TLR4,TLR7,TMCO1,TMED10,TMED2,TMED3,TMED7,TMEM41B,TMEM59,TMEM87A,TNF,TNFAIP2,TNFAIP3,TNFRSF10B,TNRC6A,TOP2A,TOR2A,TP53,TP63,TPM2,TPM3,TRA,TRIM71,TRIM9,TRMT1,TRPS1,TPAN8,TTC9C,TUBB2A,TUSC2,TWIST1,TXNIP,TYMS,TYR,TYRP1,UAP1,UBE2I,UGT2B15,UGT2B17,UGT2B28,UGT8,UHRF1,UNG,USF2,USP46,UVRAG,VASN,VCAN,VEGFA,VIM,VPS39,VSIR,VSNL1,WASF3,WDR37,WEE1,WNT1,WNT5A,YY1,ZBTB7A,ZEB1,ZEB2,ZFP36L1,ZFPM2,ZNF385A

9. Annex IX

TABLE . Target genes for the differentially expressed miRNA classified within the 25 top pathways involved

| Function | Genes involved |
|--|--|
| T Cell Exhaustion Signaling Pathway | ACVR1,ACVR1B,ACVR2A,AKT1,BCL6,BMPR2,EOMES,FOXO1,IL10,IL6,JAK1,JUN,KRAS,MAP2K4,MAPK12,MTOR,NRAS,PIK3R1,PIK3R3,PLCG1,PPP2R2A,PRDM1,PTPA,SMAD3,STAT3,TBX21,TGFBR1,TGFBR2,TRA,VEGFA |
| Systemic Lupus Erythematosus In T Cell Signaling Pathway | AKT1,BCL6,CASP3,CASP6,CASP7,CD44,CDC42,CREB1,DNMT1,ESR1,FOXP3,GNAI2,ICOS,IL10,IL6,JUN,KRAS,MAP2K4,MAP2K7,MTOR,NRAS,PIK3R1,PIK3R3,PLCG1,PPP2R2A,PPP3CA,PPP3R1,PTPA,RHOA,RHOB,RHOG,RPTOR,SP1,STAT3,TRA |
| Senescence Pathway | ACVR1,ACVR1B,ACVR2A,AKT1,ANAPC1,BMPR2,CAPN8,CBX7,CCND1,CDC25A,CDK1,CDK4,CDK6,CDKN1A,CDKN1B,CDKN2A,CXCL8,E2F1,E2F2,E2F3,EIF4E,EZH2,HBP1,IKBKB,IL6,JUN,KRAS,MAP2K4,MAP2K7,MAPK12,MAPK14,MAPK7,MDM2,MTOR,NF1,NRAS,PCGF1,PIK3R1,PIK3R3,PPP2R2A,PPP3CA,PPP3R1,PTEN,PTPA,RB1,RBL2,RPS6KA5,SMAD1,SMAD3,SMAD4,SMAD5,TGFB3,TGFBR1,TGFBR2,TP53,ZFP36L1 |
| Regulation Of The Epithelial Mesenchymal Transition By Growth Factors Pathway | AKT1,CDC42,ERBB2,FGF16,FGFR3,FOXO1,HMGA2,ID2,IKBKB,IL6,JAK1,JUN,KRAS,LATS2,MAP2K4,MAP2K7,MAPK12,MAPK14,MET,MMP1,MMP9,MTOR,NRAS,PDGFA,PDGFB,PIK3R1,PIK3R3,RHOA,SMAD3,SMAD4,STAT3,TGFB3,TGFBR1,TGFBR2,TNF,TWIST1,VIM,ZEB1,ZEB2 |
| PTEN Signaling | AKT1,BCL2,BCL2L1,BCL2L11,BMPR1B,BMPR2,CASP3,CCND1,CDC42,CDKN1A,CDKN1B,FGFR3,FOXO1,IGF1R,IKBKB,ITGA2,ITGA5,ITGB3,KRAS,NRAS,NTRK3,PIK3R1,PIK3R3,PTEN,TGFBR1,TGFBR2 |
| Pancreatic Adenocarcinoma Signaling | AKT1,BCL2,BCL2L1,CCND1,CCNE1,CDC42,CDK4,CDKN1A,CDKN1B,CDKN2A,E2F1,E2F2,E2F3,ERBB2,HMOX1,JAK1,KRAS,MAP2K4,MAPK12,MDM2,MMP9,NOTCH1,PIK3R1,PIK3R3,PTGS2,RB1,SMAD3,SMAD4,STAT3,TGFB3,TGFBR1,TGFBR2,TP53,VEGFA |
| p53 Signaling | AKT1,APAF1,BAX,BBC3,BCL2,BCL2L1,BRCA1,CASP6,CCND1,CDK4,CDKN1A,CDKN2A,CSNK1D,E2F1,HIF1A,JUN,MAPK14,MDM2,PERP,PIK3R1,PIK3R3,PMAIP1,PTEN,RB1,THBS1,TNFRSF10B,TP53,TP63 |
| Osteoarthritis Pathway | ADAMTS5,BMPR2,CASP3,CASP6,CASP7,CASR,CREB1,CXCL8,FGFR3,GLI1,HDAC4,HIF1A,ITGA2,ITGA5,ITGB3,MMP1,MMP3,MMP9,MTOR,NOTCH1,PPARG,PTGS2,RUNX2,S100A9,SMAD1,SMAD3,SMAD4,SMAD5,SMO,SOX9,SP1,TGFBR1,T |

| | |
|--|---|
| | GFBR2,TIMP3,TLR4,TNF,VEGFA |
| Neuroinflammation Signaling Pathway | ACVR1,ACVR1B,ACVR2A,AKT1,APP,BACE1,BCL2,BMPR2,CASP3,CREB1,CRP,CXCL12,CXCL8,HMOX1,IKBKB,IL10,IL6,JAK1,JUN,KLK1,MAP2K4,MAPK12,MAPK14,MAPK7,MMP3,MMP9,MYD88,PIK3R1,PIK3R3,PLCG1,PPP3CA,PPP3R1,PTGS2,TGFB3,TGFBR1,TGFBR2,TLR3,TLR4,TLR7,TNF,WNT1 |
| Molecular Mechanisms of Cancer | AKT1,APAF1,BAK1,BAX,BBC3,BCL2,BCL2L1,BCL2L11,BMPR1B,BMPR2,BRCA1,CASP3,CASP6,CASP7,CCND1,CCNE1,CCNE2,CDC25A,CDC42,CDK1,CDK4,CDK6,CDKN1A,CDKN1B,CDKN2A,E2F1,E2F2,E2F3,FANCD2,FOXO1,GLI1,GNAI2,HIF1A,IRS1,ITGA2,ITGA5,ITGB3,JAK1,JUN,KRAS,MAP2K4,MAPK12,MAPK14,MDM2,MYC,NF1,NLK,NOTCH1,NRAS,PAK5,PIK3R1,PIK3R3,PMAIP1,RASA1,RB1,RHOA,RHOB,RHOG,SMAD1,SMAD3,SMAD4,SMAD5,SMO,TGFB3,TGFBR1,TGFBR2,TP53,WNT1,WNT5A |
| HOTAIR Regulatory Pathway | AGO1,AGO4,AKT1,AR,CD44,CDKN1A,COL1A1,COL1A2,DNMT3B,ELAVL1,ERBB2,ESR1,EZH2,H3-3A/H3-3B,HOTAIR,HOXD10,JARID2,KMT2A,MDM2,MET,MMP1,MMP14,MMP3,MMP9,MYC,PIK3R1,PIK3R3,PTEN,RCOR1,SRF,STAT3,TLR4,TWIST1,VIM,WNT1,WNT5A,YY1 |
| Hepatic Fibrosis Signaling Pathway | ACVR1,ACVR1B,ACVR2A,AKT1,BAMBI,BCL2,BMPR2,CASP3,CCN2,CCND1,CDC42,CDKN1B,COL1A1,COL1A2,COL3A1,COL5A3,CREB1,CXCL8,EZH2,FOXO1,GLI1,GNAI2,HIF1A,IKBKB,IL1RN,ITGA2,ITGA5,ITGB3,JAK1,JUN,KRAS,MAP2K4,MAP2K7,MAPK12,MAPK14,MMP1,MTOR,MYC,MYD88,NRAS,PDGFA,PDGFB,PIK3R1,PIK3R3,PLCG1,PPARG,PTEN,RHOA,RHOB,RHOG,SMAD3,SMAD4,SMO,SP1,STAT3,TGFB3,TGFBR1,TGFBR2,TLR4,TNF,VEGFA,WNT1,WNT5A |
| Hepatic Fibrosis / Hepatic Stellate Cell Activation | BAMBI,BAX,BCL2,CCN2,CCR5,COL15A1,COL1A1,COL1A2,COL3A1,COL4A1,COL4A2,COL4A5,COL5A1,COL5A2,COL5A3,COL8A1,CXCL8,IGF1R,IGFBP3,IGFBP5,IL10,IL6,MET,MMP1,MMP9,PDGFA,PDGFB,SMAD3,SMAD4,TGFB3,TGFBR1,TGFBR2,TLR4,TNF,VEGFA |
| Glucocorticoid Receptor Signaling | AKT1,ANXA1,AR,BCL2,BCL2L1,BCL2L11,BRCA1,CDKN1A,CDKN1C,CREB1,CXCL8,DUSP1,ESR1,IKBKB,IL10,IL1RN,IL2RG,IL6,JAK1,JUN,KRAS,KRT19,KRT5,KRT7,KRT85,MAP2K4,MAP2K7,MAPK12,MAPK14,MMP1,MMP3,MMP9,MYC,NCOA3,NRAS,PIK3R1,PIK3R3,POLR2C,PPARG,PPP3CA,PPP3R1,PTGS2,RPS6KA5,SMAD3,SMAD4,STAT3,TAF9B,TGFB3,TGFBR1,TGFBR2,TNF,TRA,UBE2I |
| Glioma Signaling | AKT1,CCND1,CDK4,CDK6,CDKN1A,CDKN2A,E2F1,E2F2,E2F3,IDH1,IGF1R,KRAS,MDM2,MTOR,NRAS,PDGFA,PDGFB,PIK3R1,PIK3R3,PLCG1,PTEN,RB1,RBL2,TP53 |
| Glioblastoma Multiforme Signaling | AKT1,CCND1,CCNE1,CDC42,CDK4,CDK6,CDKN1A,CDKN1B,CDKN2A,E2F1,E2F2,E2F3,FOXO1,IGF1R,KRAS,MDM2,MTOR,MYC,NF1,NF2,NRAS,PDGFA,PDGFB,PIK3R1,PIK3R3,PLCG1,PTEN,RB1,RHOA,RHOB,RHOG,SMO,TP53,WNT1,WNT5A |
| Estrogen-mediated S-phase Entry | CCNA2,CCND1,CCNE1,CCNE2,CDC25A,CDK1,CDK4,CDKN1A,CDKN1B,E2F1,E2F2,E2F3,ESR1,MYC,RB1 |

| | |
|---|---|
| Cyclins and Cell Cycle Regulation | CCNA2,CCND1,CCNE1,CCNE2,CDC25A,CDK1,CDK4,CDK6,CDKN1A,CDKN1B,CDKN2A,E2F1,E2F2,E2F3,HDAC4,PPP2R2A,PTPA,RB1,TGFB3,TP53,WEE1 |
| Coronavirus Pathogenesis Pathway | ACE2,BAX,BCL2,BCL2L11,CASP3,CCND1,CDK4,CXCL8,DDIT3,E2F1,E2F2,E2F3,EIF4E,IKBKB,IL6,JAK1,JUN,MAP2K4,MAPK12,MAPK14,PTGS2,RB1,RBL2,SMAD3,SMAD4,STAT3,TGFBR1,TGFBR2,TP53 |
| Colorectal Cancer Metastasis Signaling | AKT1,BAX,BCL2L1,CASP3,CCND1,CDC42,IL6,JAK1,JUN,KRAS,MAP2K4,MAPK12,MMP1,MMP14,MMP3,MMP9,MYC,NRAS,PIK3R1,PIK3R3,PTGS2,RHOA,RHOB,RHOG,SMAD3,SMAD4,SMO,STAT3,TGFB3,TGFBR1,TGFBR2,TLR3,TLR4,TLR7,TNF,TP53,VEGFA,WNT1,WNT5A |
| Chronic Myeloid Leukemia Signaling | AKT1,BCL2L1,CCND1,CDK4,CDK6,CDKN1A,CDKN1B,CDKN2A,E2F1,E2F2,E2F3,HDAC4,IKBKB,KRAS,MDM2,MYC,NRAS,PIK3R1,PIK3R3,RB1,RBL2,SMAD3,SMAD4,TGFB3,TGFBR1,TGFBR2,TP53 |
| Cell Cycle: G1/S Checkpoint Regulation | BMI1,CCND1,CCNE1,CCNE2,CDC25A,CDK4,CDK6,CDKN1A,CDKN1B,CDKN2A,E2F1,E2F2,E2F3,FOXO1,HDAC4,MDM2,MYC,RB1,RBL2,SMAD3,SMAD4,TGFB3,TP53 |
| Cardiac Hypertrophy Signaling | ACVR1,ACVR1B,ACVR2A,AKT1,ATP2A2,BMPR2,CXCL8,EIF4E,ENPP6,FGF16,FGFR3,GNAI2,HDAC4,IGF1R,IKBKB,IL2RG,IL6,ITGA2,ITGA5,ITGB3,JUN,KRAS,MAP2K4,MAP2K7,MAP3K12,MAPK12,MAPK14,MAPK7,MEF2D,MTOR,MYC,NRAS,PIK3R1,PIK3R3,PLCG1,PPP3CA,PPP3R1,PTEN,PTGS2,RHOA,RPS6KA5,SMO,SRF,STAT3,TGFB3,TGFBR1,TGFBR2,TNF,WNT1,WNT5A |
| Aryl Hydrocarbon Receptor Signaling | APAF1,BAX,CCNA2,CCND1,CCNE1,CCNE2,CDK4,CDK6,CDKN1A,CDKN1B,CDKN2A,CYP1A1,DHFR,E2F1,ESR1,IL6,JUN,MDM2,MYC,NCOA3,RB1,RBL2,SP1,TGFB3,TNF,TP53,TYR |

